Advancing Microbial Desalination Cell towards Practical Applications

Qingyun Ping

Dissertation Submitted to the faculty of the Virginia Polytechnic Institute and State University in partial fulfillment of the requirements for the degree of

Doctor of Philosophy in Civil Engineering

Zhen He, Chair

Marc A. Edwards

Luke E. Achenie

Olya S. Keen

October 7th, 2016

Blacksburg, VA

Keywords: Microbial Desalination Cell, Configuration, Fouling and Scaling, Back diffusion, Boron removal, Modeling and simulation

Advancing Microbial Desalination Cell towards Practical Applications

Qingyun Ping

Abstract (academic)

Conventional desalination plant, municipal water supply and wastewater treatment system are among the most electricity-intensive facilities. Microbial Desalination Cell (MDC) has emerged as a promising technique to capture the chemical energy stored in wastewater directly for desalination, which has the potential to solve the high energy consumption issue in desalination industry as well as wastewater treatment system. The MDC is composed of two critical components, the electrodes (anode and cathode), and the ion-exchange membranes separating the two electrodes which drive anions migrate towards the anode, and cations migrate towards the cathode. The multiple components allow us to manipulate the configuration to achieve most efficient desalination performance. By coupling with Donnan Dialysis or Microbial Fuel Cell, the device can effectively achieve boron removal which has been a critical issue in desalination plants. The uncertainty of water quality of the final desalinated water caused by contaminant back diffusion from the wastewater side can be theoretically explained by two mechanisms, Donnan exchange and molecule transport which are controlled by bioelectricity and concentration gradient. Scaling and fouling is also a factor needs to be taken into consideration when operating the MDC system in real world. With mathematical modeling, we can provide insight to bridge the gap between lab-scale experiments and industrial applications. This study is expected to provide guidance to enhance the efficiency as well as the reliability and controllability of MDC for desalination.

Advancing Microbial Desalination Cell towards Practical Applications

Qingyun Ping

Abstract (public)

Water and energy are the world's most valuable resources. The recent emerging technology, Microbial Desalination Cell (MDC), however, can achieve wastewater treatment, desalination for fresh water production, and energy generation simultaneously. Owing to the anodophilic microorganisms working as organic matter consumer and electron generator, the wastewater can be cleaned and the device can generate electricity through electron flow to drive ion separation for salt removal in the solution. The MDC can be constructed in versatile configurations. Decoupled configuration of anode and cathode allows flexibility of operation and maintenance. Although the MDC has wastewater adjacent to seawater which are separated by a piece of anion exchange membrane, the microorganisms and viruses are effectively blocked by the membrane which has tiny pore size around 1 nm. Back diffusion of contaminants in wastewater into the desalinated water is minimal under bioelectricity generation condition. The MDC has proved to successfully remove various inorganic ions by itself as well as remove non-dissociable boron when coupled to other devices, such as Donnan Dialysis or Microbial Fuel Cell. The water product quality can meet irrigation guideline. Through mathematical modeling tools, we can better understand the MDC process, analyze it, and make informative predictions.

ACKNOWLEDGEMENTS

All praise, honor and glory to my savior Lord Jesus Christ for the grace and blessings on the accomplishment of this thesis.

I would like to give my sincere thanks to the support I have received from many individuals right from the beginning of my PhD program. First and foremost, I am grateful for the opportunity to work under the direction of my advisor, Dr. Zhen He. I would like to thank him for the tremendous support, guidance, and insight he has offered me on my research work, and for the priceless advice on my career. Five and half years working with Dr. Zhen He has deepened and strengthened my knowledge in not only the field of bioelectrochemical system, but also the field of water and wastewater treatment. I would also like to extend my thanks to my committee members: Dr. Olya Keen, Dr. Luke Achenie, and Dr. Marc Edwards for their advice and comments on my dissertation. Additionally I would like to thank all the members of EBBL group for their laboratory assistance and friendship, and thank Jody Smiley, for her kind help with IC testing.

I would also like to thank the United States-Israel Binational Agricultural Research and Development Fund (US-4455-11) and the Qatar National Research Fund (6-289-2-125) to financially support my research.

A special thanks to my family. Words cannot express how grateful I am to my mother-in-law and my mother for taking care of my baby when I work on my PhD degree. Thanks to Charlotte, the best daughter I could ever have, for her smiles encourage me to overcome difficulties in pursuit of the PhD degree. Last but not least, to my husband for his unfailing love, and all the sacrifices

that he’s made on my behalf. The journey wouldn’t have been the same without their love and encouragement.

Table of Contents

Chapter 1 Introduction

1.1 Desalination and energy consumption issues

Water is an essential element in human life. Along with the global population growth, the issue of limited access for clean and safe fresh water is rising. Among the global water resources of 1.4 billion km^3, 2.5% of the water on the earth is potable fresh water, and 96.5% belongs to the ocean (Shiklomanov 1993). It is considered that water with more than 2,000 mg L^{-1} in the form of total dissolved solids (TDS) is too salty to drink or to grow plants (National Research Council 2008). The World Health Organization (WHO) requires the limit of salinity in drinking water is 500 mg L^{-1} and for special cases up to 1,000 mg L^{-1}. Seawater normally has a salinity in the range of 35,000–45,000 mg L^{-1} TDS, while many lakes in arid regions concentrate the inflowing salts through evaporation and has a salinity up to 10,000 mg L^{-1} TDS (Shatat and Riffat 2014). Considering the world-wide water shortage, and the fact of abundant saline water, desalination of seawater or brackish water has been increasingly considered as an option for water supply source.

One critical issue associated with desalination is the energy consumption which accounts for over one third of the total cost of desalinated water (Semiat 2008). Current commercially available and widely applied desalination technologies can be divided into two types: thermal and membrane processes. Even the representing membrane process, reverse osmosis (RO) which requires much less energy than thermal processes, have energy demand of 3.7 kW h m^{-3} (Mehanna et al. 2010a). This energy cost can contribute to approximately 30-44% of the total cost of water produced (Semiat 2008). For example, a 50 MGD Seawater Reverse Osmosis (SWRO) plant, annualized capital costs make up approximately 37% of the annual cost breakdown of the plant (Cooley, 2012). Although during the past 40 years, the energy

consumption of seawater reverse osmosis (SWRO) has been dramatically decreasing owing to technological improvements, it is approaching the theoretical minimum energy (eg. 1.7 kW h m^{-3} at 85% recovery) (Elimelech and Phillip 2011).

1.2 The intrinsic energy value in wastewater

Typical domestic wastewater has organic matter concentration of 500 mg COD L^{-1}. It is estimated that the maximum attainable energy in wastewater extracted from organic oxidation to CO_2 and H_2O is 1.93 kWh m^{-3} (Zuo et al. 2016). However, conventional aerobic treatment processes are not able to utilize the energy, but instead consume a relatively high amount of energy that accounts for about 3% of the U.S. electrical energy load (EPA 2006). Half of the required energy consumption (0.2–0.6 kWh m^{-3}) comes from electrical energy to supply air for the aeration basins (McCarty et al. 2011). Although activated sludge treatment has been very effective in achieving the goal of removing organic matters, the intrinsic energy in wastewater is either lost when the organics are decomposed into carbon dioxide by aerobic bacteria, or transformed into excess sludge. Currently anaerobic digestion process is a commonly applied technology to offset the high energy demand in wastewater treatment, by digesting the sludge to produce biogas CH_4. Through heat engine combustion, the chemical energy stored in biogas will be converted to the energy form of electricity. Based on Carnot's theorem, the most efficient heat engine can achieve 66% efficiency, which is the maximum attainable energy conversion efficiency according to the temperature difference between heat source and cold cooling water. In practice, only about 35% of the CH_4 energy might be converted into electricity, the remaining 65% is lost in waste heat (McCarty et al. 2011).

1.3 Introduction to Bioelectrochemical system

Bioelectrochemical system (BES) is a general term for a group of technologies that rely on microorganisms metabolism of organic matters to directly transfer electrons to an electrode (i.e. an anode), which are conducted over a resistance or power user towards a cathode to form a close circuit for electricity production (microbial fuel cell (MFC) (Figure 1.1)) or reduced requirement for voltage (microbial electrolysis cell (MEC)). Typical cathode reactions involve oxygen reduction reaction in MFC or hydrogen production in MEC. Equations 1.1-1.3 show the reactions at the anode and cathode:

At the anode:

$$(CH_2O)_n + nH_2O \rightarrow nCO_2 + 4ne^- + 4nH^+ \quad (1.1)$$

At the cathode:

$$O_2 + 4ne^- + 4nH^+ \rightarrow 2H_2O \text{ (oxygen reduction)} \quad (1.2)$$

$$8H^+ + 8e^- \rightarrow 4H_2 \text{ (hydrogen production)} \quad (1.3)$$

In this process, BES accomplishes direct biological conversion of organic energy into electricity (Rabaey et al. 2005). The process of transferring electrons to electrode is achieved in anaerobic bacteria respiration by a wide microbial diversity. The most frequently used model organisms are *Shewanella* and *Geobacter* genera (Yang et al. 2012). Briefly, electrons can be exchanged between microorganisms and electrode surfaces via three different pathways: (A) direct contact, (ii) mediated electron transfer, and (iii) produced nanowires (Figure 1.2).

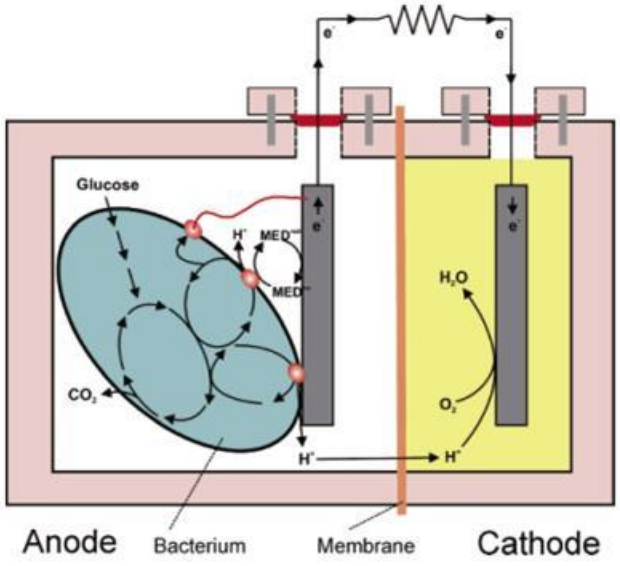

Figure 1.1 Schematic of microorganism transferring electrons to the anode and closing the electric circuit through external resistance to the cathode (Logan et al. 2006).

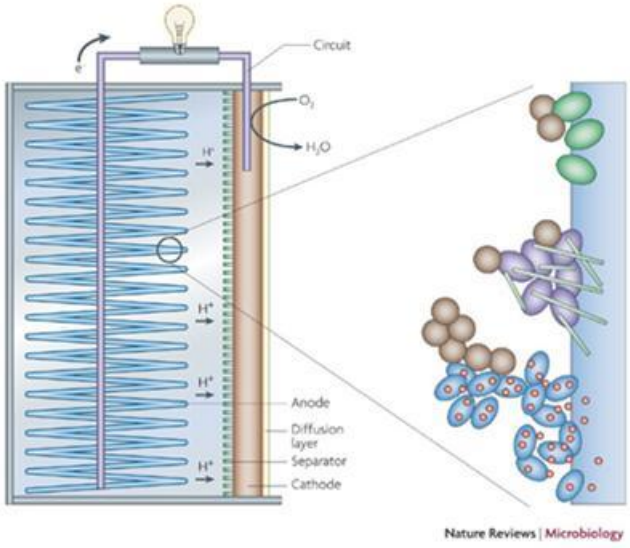

Figure 1.2 Different types of microorganisms in an anodic biofilm, including exoelectrogens that transfer electrons by direct contact (green), produce nanowires (purple) and use endogenous (and therefore self-produced) mediators (blue). Other non-exoelectrogenic

bacteria (brown) that live off the products produced by other bacteria or possibly use mediators or nanowires produced by other microorganisms can also be present (Logan 2009).

Wastewater could be used as a source of fuel for BES, with the benefit of accomplishing wastewater treatment (Liu et al. 2004). Recent years, BES has been researched on treating wastewater and extracting the waste energy extensively, with the representing technology, microbial fuel cell (MFC). For example, MFCs may produce up to 1.43 kWh m^{-3} from a primary sludge or 1.8 kWh m^{-3} from a treated effluent (Ge et al., 2013). Theoretically, BES can convert maximum 100% of chemical energy into electricity. However, there is always some energy lost through 1) coulombic loss where organics are not converted to electrical current at 100%, and 2) electrochemical potential or voltage loss. Nevertheless, the reported energy conversion efficiency for MFC can reach 80% which is much higher than 33% for typical heat engine combustion of methane gas (Rabaey et al. 2005).

From a perspective of treating primary effluent organic matters, MFCs installed in a municipal wastewater treatment facility can achieve 65–70% chemical oxygen demand (COD) removal and 50% suspended solids removal at a hydraulic retention time (HRT) of 11 h by the anode alone. Directing the anolyte flow as catholyte further reduced COD at > 90% removal with final COD concentration around 30 mg L^{-1} (Zhang et al. 2013). Thus, as a matter of fact, BES can achieve an energy-savings goal for wastewater treatment that both captures the energy potential in the dissolved organics and meets effluent standards effectively.

1.4 Introduction to Microbial Desalination Cell

1.4.1 Working principle of MDC

Microbial Desalination Cell (MDC) is one BES technology that has one adds-on benefit of desalination in addition to wastewater treatment and energy production. The recent emergence of MDC stands out as an attractive desalination alternative of traditional technologies due to its sustainable feature. The MDC converts the energy stored in the wastewater directly into electricity by microorganisms and utilizes it *in situ* to drive the desalination process. The schematic of MDC is shown in Figure 1.3. The electrons released by microorganisms on the anode of MDC move towards the cathode through external circuit. A charge balance thus needs to be reached, and the anions and cations in solution need to migrate towards the anode and the cathode respectively. By inserting ion-exchange membranes between electrodes, AEM (anion-exchange membrane) by the anode, and CEM (cation-exchange membrane) by the cathode, and creating a desalination compartment, the anions and cations will move across AEM and CEM, and the salt will be removed from the solution (Cao et al. 2009). By inserting more alternating AEM and CEM between the electrodes, concentrating and desalting compartments can be created in MDC similar to electordialysis (ED) configuration (Figure 1.4). This configuration enables more pairs of ions separated while one electron passed through the external circuit (Theoretically two NaCl molecules are removed with each transferred electron). Besides the plate configurations shown in Figure 1.3&1.4 that have one compartment for each electrode (the anode compartment and the cathode compartment), the cathode compartment can be eliminated through a tubular configuration shown in Figure 1.5. The catholyte is recirculated and dripping

from the top of the reactor to provide hydration of the cathode carbon cloth and thus make the attaching cathode conducting (Jacobson et al. 2011a).

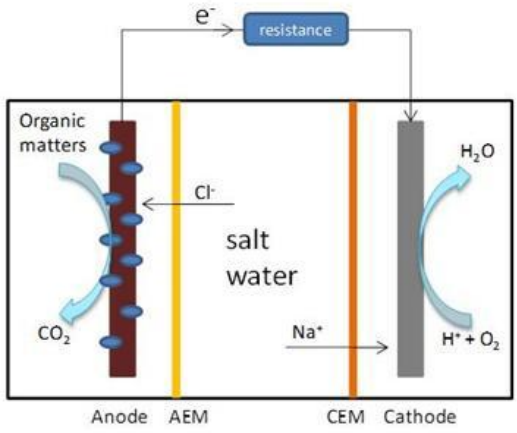

Figure 1.3 The schematic of a three-compartment plate shaped microbial desalination cell. AEM: anion exchange membrane; CEM: cation exchange membrane.

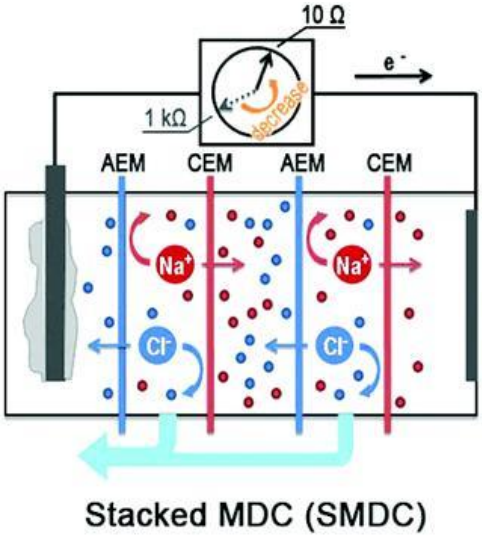

Figure 1.4 The schematic of a stack microbial desalination cell having two desalting compartments and one concentrating compartment. AEM: anion exchange membrane; CEM: cation exchange membrane (Chen et al. 2011).

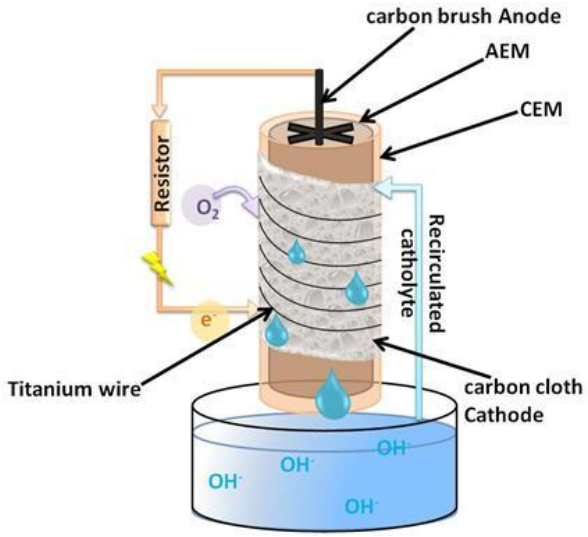

Figure 1.5 The schematic of a tubular microbial desalination cell. AEM: anion exchange membrane; CEM: cation exchange membrane.

1.4.2 Application of MDC targeting desalination

Desalination is the primary target of MDC technology. The salinity removal highly depends on the hydraulic retention time (HRT) of the salt solution in MDC. It is believed that the salinity of the desalinated product can reach drinking water standard provided with sufficient retention time. In a tubular MDC treating brackish water at an HRT of 1.7 d, the salinity was lowered to 114 mg L^{-1} , close to that of the tap water (90 mg L^{-1} TDS) collected at Virginia Tech, and lower than the requirement of potable water quality (<500 mg L^{-1} TDS) issued by US EPA (Ping et al. 2015a). With the help of ion exchange resin, the salinity can be even lowered to 7.13 mg L^{-1} (Zhang et al. 2012). A recently reported stacked microbial desalination cell (SMDC) with 10 desalination cells and cross-membrane area of 100 cm^2 has achieved the highest reported total desalination rate (TDR) of 423 mg h^{-1} (Chen et al. 2016). High salinity removals require a large volume of

wastewater. Figure 1.6 shows the amount of anolyte and catholyte needed to achieve desalination of the salt solution can reach 55 to 133 times the volumes of desalinated water depending on the initial salinity. Wastewater is needed in this process to provide organic source for microorganisms to function in the electron production process, while it also serves as a media to take away the anions. To prevent the salinity issue in wastewater and microbial inhibition of the electrogenic microorganism, a reasonable ratio of the wastewater supplied over the salt solution treated needs to be remained. Other water treatment technologies such as forward osmosis (FO) and capacitive deionization have been coupled to MDC and achieved enhanced desalination performance (Yuan et al. 2015, Wen et al. 2014, Forrestal et al. 2012). Improvement to BES materials also applies to MDC since the same redox reactions happen at the electrodes. Recently, nanostructured α-Fe_2O_3 anode has been tested in MDC which achieved improved electricity generation with 96% salt removal and effluent salinity around 1.4 mg L^{-1} (Liang et al. 2016).

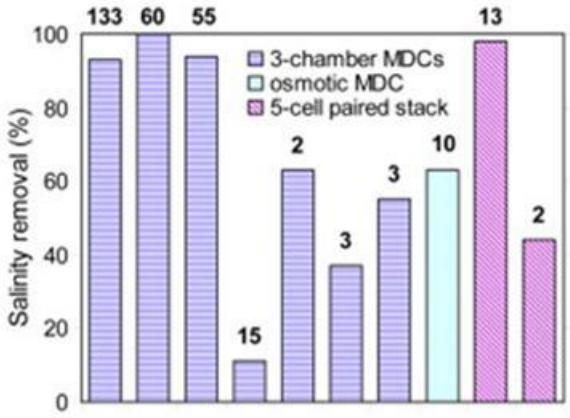

Figure 1.6 Salinity removal in MDCs from initial NaCl concentration of 20 g L^{-1} or higher. The number on the top of each bar indicates the ratio of used non-salty electrolyte solution to desalinated water volume (Kim and Logan 2013).

1.4.3 Application of MDC targeting wastewater treatment

High salinity is an issue for activated sludge process. The application of MDC for self-driven salinity removal in wastewater is promising, given the organic removal and salinity removal can be achieved in a single device without energy supply. Multiple studies have evaluated the performance of MDC treating domestic wastewater. In a multi-stage MDC (M-MDC) with two alternating anodes and cathodes, wastewater was treated by anode and cathode alternatively, the desalination, COD removal, and total nitrogen removal in domestic wastewater achieved 52.4%, 92.5% and 87.0% respectively (Zuo et al. 2016a). The MDC was also modified by incorporating nitrogen-doped carbon nanotube membranes as filtration material on the cathode to remove organics and salinity in municipal wastewater and achieved water quality for boiler or industrial cooling water supply. This filtration air cathode MDC (F-MDC) treated real wastewater first at the anode and then at the cathode, and finally in the middle membrane stack for desalination. The salinity and COD removal reached 93.6% and 97.3% respectively with final conductivity of 68 ± 12 μS cm^{-1}, and turbidity of 0.41 NTU (Zuo et al. 2016b). The pH imbalance between the anode and cathode chambers which was a common factor that hinders current generation in conventional MDC can be reduced in the operation of MDC treating wastewater through anode and cathode in a single-stream (SMDC) (Lu et al. 2016).

1.4.4 Challenges with MDC

The performance of microbial desalination cell (MDC) have been significantly improved in the past few years. Scaling up is always an interest for researchers and is an initial step for any new technology to be industrialized. From the lab scale volume of desalination compartment as small

as 3 mL, the MDC desalination volume has been scaled up to 105 L, achieving salt removal rate as high as 9.2 kg m^{-3} day^{-1} (Zhang and He 2015). So far, the MDC has been advanced through various configurations (Kim and Logan 2011, Chen et al. 2011a, Ping and He 2013b, Jacobson et al. 2011a) and operation modes (Chen et al. 2012a, Qu et al. 2012). Different strategies to achieve fabrication and operation flexibility have been evaluated. The tubular shape configuration has attracted much attention since it eliminates the cathode compartment and results in a two-layer reactor. Decoupling the anode and cathode compartments also serves as a strategy for simple construction and maintenance purpose. The microbial community in the anode of MDC (Luo et al. 2012a) as well as the mechanisms of ion transport and back-diffusion of contaminants from the wastewater into the desalinated stream were studied in depth (Luo et al. 2012a, Ping et al. 2016). Although the water quality in the aspect of salinity and multiple ion concentrations from the MDC can achieve irrigation standard, further polishing of the water product is essential. High turbidity is a problem for the desalinated water product. Although the primary barrier between wastewater and desalinated water product, a piece of anion exchange membrane, can effectively block all microorganisms in the wastewater, the back diffusion of contaminant organics as well as fouling and scaling on the membrane synergistically deteriorate the water quality. While filtration can be one potential approach to remove the trace organic matters in desalinated effluent, advanced oxidation also provides promising performance for improving water quality. Given the in-situ generation of H2O2 by the MDC cathode, it is easy to link UV which will possibly be used for polishing wastewater from the anode compartment as a disinfection method.

In the end, the goal will always be to reduce CAPEX and OPEX for the system. Although expensive catalyst can be replaced with cheap ones, the cost of electrode materials is still high. A detailed analysis for MDC was performed and it revealed the majority of the capital cost is contributed by ion-exchange membranes and electrodes construction (Figure 1.7) (Alammar 2015). This result warrants the future research focus for MDC technology in new material development and improvement. A big difference in operation cost is expected for MDC compared with traditional desalination method which was mainly contributed by energy savings. Our previous study compared MDC with ED for desalinating 6 g L^{-1} brackish water at 96% salinity removal, the energy consumption from MDC (hydraulic energy) is five times less than from ED (both electrical and hydraulic energy) (Ping et al. 2015a). The energy cost can even be further reduced by optimizing catholyte recirculation intensity. Further cost analysis integrating CAPEX and OPEX and accounting for inflation rate is needed to give guidance to policy maker.

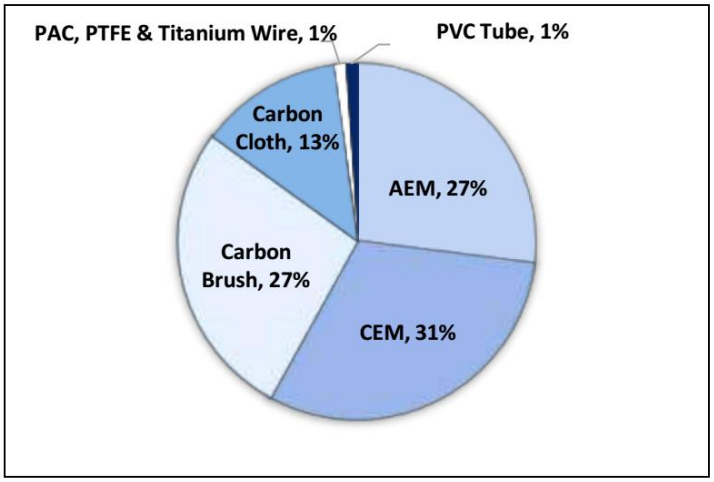

Figure 1.7 MDC Reactor Cost Breakdown Percentages (Alammar 2015).

1.5 Outline

This thesis is composed of eleven chapters. The overall goal is to identify operation problems and achieve optimal performance for advancing MDC towards practical applications. More specifically, it has the following objectives:

1) To investigate how different configurations change the desalination performance of MDC.

2) To examine the fouling and scaling issue treating real wastewater and seawater in MDC, and to evaluate and improve the desalinated water product quality.

3) To conduct mathematical modeling and simulation of MDC process and provide guidance for system operation.

The first chapter introduces the background as well as inspiration for the thesis topic. Chapter two discusses the effect of inter-membrane distance on desalination. Chapter three evaluates a novel configuration decoupling the anode and cathode in MDC. Chapter four investigates the fouling and scaling phenomenon in MDC. Chapter five studies the mechanism of contaminant back-diffusion into desalinated water product. Chapter six integrates the tool of both experiment and mathematical modeling to evaluate multiple ion removal performance. Chapter seven and Chapter eight develop two methods to remove boron from seawater and brackish water with MDC related technology. Chapter nine performs mathematical modeling and simulation for general desalination and wastewater treatment performance in MDC, and Chapter ten studies the boron removal with the mathematical modeling tool.

1.6 Attribution

Each coauthor is duly credited for his or her contribution to this work, both in their sharing of ideas and technical expertise.

Zhen He, Ph.D. Associate Professor of Civil and Environmental Engineering

(Principal Investigator)

Department of Civil and Environmental Engineering, Virginia Polytechnic Institute and State University. Blacksburg, VA 24061

Coauthor of chapters 2-10

Barak Cohen, MSc.

Faculty of Civil and Environmental Engineering, Technion - Israel Institute of Technology, Haifa 32000, Israel

Coauthor of chapter 4

Carlos Dosoretz, Ph.D. Professor of Environmental, Water and Agricultural Engineering

Faculty of Civil and Environmental Engineering, Technion - Israel Institute of Technology, Haifa 32000, Israel

Coauthor of chapter 4-6

Oded Porat, Ph.D.

Faculty of Civil and Environmental Engineering, Technion - Israel Institute of Technology, Haifa 32000, Israel

Coauthor of chapter 5

Zuyi Huang, Ph.D. Assistant Professor of Chemical Engineering

Department of Chemical Engineering, Villanova University, Villanova, PA 19085, USA

Coauthor of chapter 6, 9

Ibrahim M. Abu-Reesh, D.Sc. Professor of Chemical Engineering

Department of Chemical Engineering, College of Engineering, Qatar University, P.O. Box 2713, Doha, Qatar

Coauthor of chapter 7, 8, 10

Chenyao Zhang

Department of Chemical Engineering, Villanova University, Villanova, PA 19085, USA

Coauthor of chapter 9

Xueer Chen, M.S.

Department of Chemical Engineering, Villanova University, Villanova, PA 19085, USA

Coauthor of chapter 9

Bo Zhang, Ph.D.

Department of Civil Engineering and Mechanics, University of Wisconsin – Milwaukee,

Milwaukee, WI 53217, USA

Coauthor of chapter 9

Chapter 2 Effects of inter-membrane distance and hydraulic retention time on the desalination performance of microbial desalination cells

(This section has been published as Ping, Q. and He, Z.* (2013) Effects of inter-membrane distance and hydraulic retention time on the desalination performance of microbial desalination cells. ***Desalination and Water Treatment.*** Vol 52, pp 1324-1331.)

2.1. Introduction

Microbial desalination cell (MDC) is a novel concept of desalination technology that takes advantage of electrochemically-active microorganisms to oxidize organic compounds and accomplishes desalination without a significant requirement of external energy input (Cao et al. 2009). A typical MDC consists of three chambers, an anode, a middle (salt), and a cathode, separated by an anion exchange membrane (AEM) and a cation exchange membrane (CEM), respectively (Figure 2.1). Carbon–based materials are usually used as electrodes in the anode and the cathode. Bacteria inhabiting on the anode electrode decompose organic matters while releasing electrons and protons. Terminal electron acceptors (e.g., ferricyanide or oxygen) in the cathode are reduced by accepting those electrons through an external circuit. To achieve a charge balance in both the anode and the cathode chambers, cations like sodium ions in the middle chamber migrate into the cathode via CEM, and anions such as chloride ions move into the anode chamber through AEM. As a result, the salinity in the middle chamber is greatly reduced. MDCs can simultaneously remove organics in wastewater, conduct desalination, and produce electricity (Luo et al. 2012a).

Because of the environmental-friendly features, MDC technology has drawn increasing attention from the scientific community and has been advanced through various research. Researchers have replaced ferricyanide catholyte with oxygen that is commonly used as a terminal electron acceptor (Mehanna et al. 2010a). Continuously operated MDCs were developed in upflow configuration (Jacobson et al. 2011b), and the size of the upflow MDC was scaled up to liters (Jacobson et al. 2011a). To improve the charge transfer efficiency, stack MDCs were built by using multiple membrane pairs between the electrodes (Kim and Logan 2011, Chen et al. 2011). The use of a buffer solution has been an issue in operating bioelectrochemical systems because of the high cost and the potential environmental problems; by recirculating the electrolyte between the anode and the cathode, an MDC was operated buffer-free for a short period of time (Chen et al. 2012, Qu et al. 2012). The high cost of cathode catalysts based on noble metal hinders the future application of MDC technology; to eliminate metal catalysts, an aerobic biocathode developed by using microorganisms was found to be effective in an MDC (Wen et al. 2012). When an external voltage was applied, hydrogen gas was produced in the cathode of MDCs (Mehanna et al. 2010b, Luo et al. 2011). In addition to conventional ion-exchange membranes, a bipolar membrane was also employed in MDCs for acid and alkali production (Chen et al. 2012d). Replacing the AEM with a forward osmosis membrane resulted in an accelerated desalination because of dilution due to water extraction from wastewater (Zhang and He 2012). Recent studies applied an ion-exchange resin in the middle chamber of MDCs for treatment of a low salinity solution (Zhang et al. 2012).

MDCs are operated on a similar principle to electrodialysis (ED) (Diblíková et al. 2010, Jing et al. 2012), except that ED relies on an externally applied voltage while MDCs use the voltage produced internally. Both processes also have a similar reactor configuration. However, the membrane pairs in an ED usually have an inter-membrane distance less than 1 mm to minimize energy loss [18], while most MDCs reported in the literature have an inter-membrane distance > 5 mm. The smallest inter-membrane distance in an MDC was 1.3 mm, achieved in a stacked configuration (Kim and Logan 2011a). Although a smaller inter-membrane distance results in a lower internal resistance, it can increase the fabrication complexity and fouling problems in MDCs that contain much fewer membrane pairs than an ED. Larger desalination chambers often create greater ohmic resistance; however, larger chambers can also increase the hydraulic retention time (HRT) of the salt solution, thereby increasing the desalination time that will result in more salt removal. Small inter-membrane distances and long HRTs cannot be achieved simultaneously at a fixed water production rate. Therefore, there could be trade-offs between inter-membrane distances, HRT, and desalination efficiency.

In this study, we have investigated the relationship between the inter-membrane distance and HRT in a bench-scale MDC with different initial salinities or inter-membrane distances. At the same influent flow rate, six different inter-membrane distances ranging from 0.3 to 2.5 cm were tested, resulting in different HRTs but the same water production rate (mL/min). We also analyzed the contributions to conductivity reduction by electric current and water osmosis (water flux into the middle chamber). We studied the effect of different HRTs at the same inter-membrane distances, and the effects of different inter-membrane distances at the same HRTs.

2.2 Materials and methods

2.2.1 MDC setup

The MDC was a plate-shaped reactor, consisting of three chambers, the anode, the middle (salt), and the cathode (Figure 2.1). An anion exchange membrane (AEM, AMI-7001, Membrane International, Inc., Glen Rock, NJ, USA) was used to separate the anode and the middle chambers, while a cation exchange membrane (CEM, CMI-7000, Membrane International, Inc.) was installed between the middle and the cathode chambers, resulting in a liquid volume of 24 mL in the anode or the cathode chamber. The anode and cathode electrodes were made by wrapping carbon cloth (3.0 × 7.5 cm, Zoltek Companies, Inc., St. Louis, MO, USA) around stainless mesh (3.0 × 2.5 cm) that was connected to an external circuit via a titanium wire. The cathode electrode contained a catalyst that was prepared by applying a mixture of Pt/C powder with Nafion solution to the surface of the carbon cloth with a final Pt loading rate of 0.3 mg Pt/cm^2. Several layers of rubber gaskets between the AEM and the CEM created the middle chamber and were also used to adjust the inter-membrane distance.

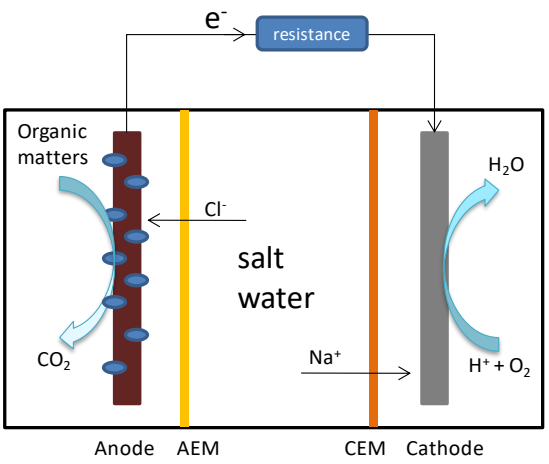

Figure 2.1 The schematic of a microbial desalination cell. AEM: anion exchange membrane; CEM: cation exchange membrane.

2.2.2 Operating conditions

The MDC was operated at a room temperature of ~ 22 ºC. The anode was inoculated with a mixture of aerobic and anaerobic sludge from local wastewater treatment plants (Jones Island and South Shore Water Reclamation Facilities, Milwaukee, WI, USA). The anode feeding solution (anolyte) was a synthetic wastewater containing acetate as an electron donor (per liter of tap water): sodium acetate, 5 g; NH_4Cl, 0.15 g; NaCl, 0.5 g; $MgSO_4$, 0.015 g; $CaCl_2$, 0.02 g; KH_2PO_4, 0.53 g; K_2HPO_4, 1.07 g; and trace element, 1 mL (Angenent and Sung 2001). The acetate was overly supplied to ensure a sufficient electron supply to drive the desalination. The catholyte was 1 mM phosphate buffer solution (Na_2HPO_4, 91.6 mg/L, and $NaH_2PO_4 \cdot H_2O$, 49.0 mg/L). The anode and the cathode chambers were linked to a 500-mL reservoir, respectively, which provided the anolyte or the catholyte that was recirculated between the anode or the

cathode chamber and the reservoir at a rate of 24 mL/min. The use of a larger size of reservoirs was to ensure a sufficient supply of the anolyte and the catholyte so that the anode and the cathode reactions would not be limiting factors to desalination. The catholyte reservoir was continuously aerated with the air to provide adequate dissolved oxygen. The middle chamber was continuously supplied with NaCl solution from a 500 mL reservoir at different flow rates controlled by a peristaltic pump. The anode and cathode electrodes were connected through an external circuit over an external resistor of 10 ohm. All tests were carried out in the same MDC by modifying the inter-membrane distance between the AEM and the CEM. The data were collected every 24 h that was designed as one operating cycle.

2.2.3 Analysis and calculation

The MDC voltage was recorded every 3 min by a digital multimeter (2700, Keithley Instruments, Inc., Cleveland, OH, USA). The pH was measured using a Benchtop pH meter (Oakton Instruments, Vernon Hills, IL, USA). The conductivity was measured by a Benchtop conductivity meter (Mettler-Toledo, Columbus, OH, USA). The polarization curve was performed by a potentiostat (Reference 600, Gamry Instruments, Warminster, PA) at a scan rate of 0.2 mV/s. The maximum power density was calculated based on the anode liquid volume. The charge transfer efficiency was calculated as the theoretical amount of coulombs required to remove NaCl divided by the coulombs harvested from the electric current, assuming that one mole of NaCl removal will require one mole of electrons. The desalination efficiency was determined as the decreased percentage of salt solution conductivity over 24 h. The specific desalination rate (SDR) was calculated as the total salt removed from the salt solution per day

per liquid volume of the middle chamber (desalination chamber) (Chen et al. 2011b). The amount of water flux due to osmosis was determined by measuring the difference of the water volume between the salt water influent and its effluent over 24 h.

2.3 Results and discussions

2.3.1 Different inter-membrane distances or HRTs at the same influent flow rate

Six inter-membrane distances, from 2.5 to 0.3 cm, were tested, resulting in decreasing the salt water HRTs from 50 to 6 h. Each distance was performed with at least three cycles. Two initial salt concentrations, 10 and 30 g NaCl/L, were examined. The desalination efficiency (conductivity reduction) exhibited a peak of ~ 40% at 0.5-1.0 cm when fed with 10 g/L (Figure 2.2A), while it decreased with the decreasing inter-membrane distance with 30 g/L (Figure 2.2B). At 10 g/L, the highest desalination efficiency of 40.7±1.0% was achieved at the inter-membrane distance of 0.5 cm (HRT 10 h), and the lowest desalination efficiency of 31.9±2.1% was obtained at 2.5 cm (HRT 50 h). When the initial salt concentration was increased to 30 g/L, the largest inter-membrane distance of 2.5 cm produced the highest desalination efficiency of 35.6±1.5%, while the smallest inter-membrane distance of 0.3 cm (HRT 6 h) resulted in the lowest desalination efficiency of 30.2±1.1%. Those results indicate that, when the water production rate (or the influent feeding rate) is kept the same, the inter-membrane distance and HRT have contradictory effects on the desalination efficiency in an MDC. The smallest distance of 0.3 cm did not perform better than larger distances in terms of overall desalination efficiency, due to a short HRT. The effect of the HRT is more significant at a higher initial salt

concentration, because more salts require more time to be removed. Therefore, it is reasonable to conclude that HRT has a greater effect than the inter-membrane distance at a higher initial salt concentration, and a larger distance will result in more salt removal at a fixed influent flow rate.

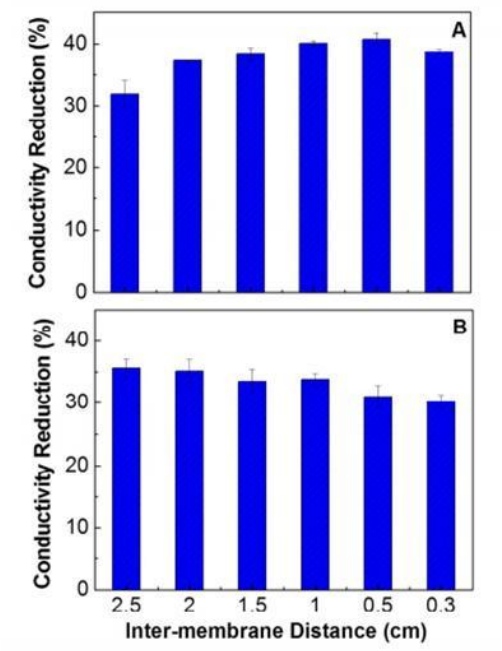

Figure 2.2 The conductivity reduction of the salt solution at different inter-membrane distances at two different initial salt concentrations: A) 10 g/L; and B) 30 g/L.

However, when we included the factor of the salt chamber volume into the evaluation by using a specific desalination rate (SDR), we observed a significantly increasing trend along the decreasing inter-membrane distance with both initial salt concentrations (Figure 2.3). At the initial salt concentration of 10 g/L, the highest SDR was 13.4±0.2 g/(d·L) at the inter-membrane distance of 0.3 cm, which was twelve times of the lowest SDR of 1.1±0.2 g/(d·L) at 2.5 cm. With 30 g/L, the highest SDR of 16.7±0.8 g/(d·L) was also obtained at the inter-membrane distance of

0.3 cm, and was about seven times of the lowest SDR, 2.6±0.4 g/(d·L) at 2.5 cm. The advantage of the 0.3-cm distance became less significant compared with the 2.5-cm distance at a higher initial salt concentration. At the same inter-membrane distance, the SDR improved by 1.1 ~ 2.3 times at 30 g/L compared with those at 10 g/L. The reduced effect of the smaller inter-membrane distance and the elevated SDR at a higher initial salt concentration were likely due to a greater conductivity of the salt solution when more salts were supplied into the middle chamber.

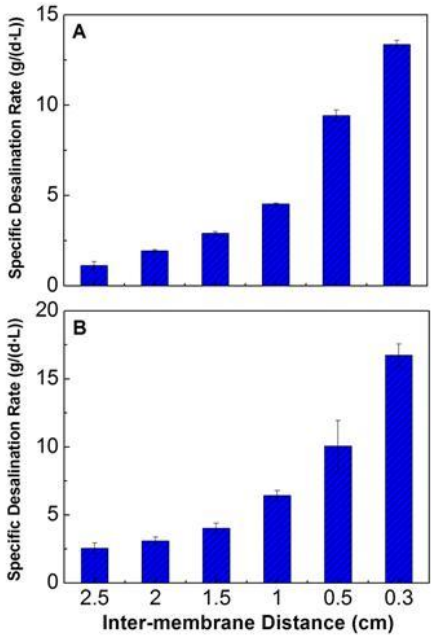

Figure 2.3 The specific desalination rate at different inter-membrane distances at two different initial salt concentrations: A) 10 g/L; and B) 30 g/L.

The calculated charge transfer efficiency (the relationship between the salt removal and the electric current) was above 100%, indicating that electric current contributed to a part of salt removal, and conductivity reduction in the middle chamber was also caused by other factors such as water osmosis, dialysis or ion exchange (Mehanna et al. 2010b, Jacobson et al. 2011c). The

theoretical analysis shows that, with the initial salinity of 10 g/L, the electric current contributed to 75.0±5.4% of the conductivity reduction at an inter-membrane distance of 0.3-2.0 cm; at 2.5 cm, we observed a higher contribution from the electric current that reduced 82.3±11.7% of the conductivity. Water osmosis was identified as another major contributor to the conductivity reduction via dilution. An inconsistent trend of the dilution effect was found; for instance, at the inter-membrane distances of 0.5, 1.0, and 1.5 cm, the dilution contributed to about 10% of the conductivity reduction, and at 0.3, 2.0, and 2.5 cm, the dilution resulted in 20.6±1.0%, 21.6±3.3%, and 33.9±15.7% of the desalination, respectively (Figure 2.4A). The higher initial salt concentration intensified the dilution effect because of the stronger water osmosis due to a higher salinity gradient between the middle chamber and the anode/cathode chambers. At an initial salt concentration of 30 g/L, it was found that over 50% of the conductivity reduction was caused by dilution; thus, the dilution became a major mechanism of desalination over the electric current that contributed to about 30% of conductivity reduction (Figure 2.4B).

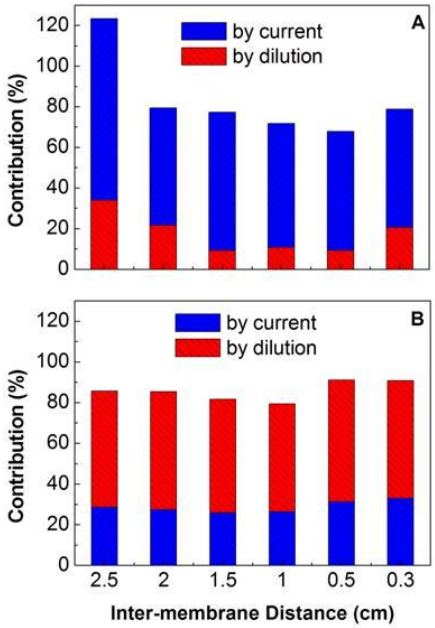

Figure 2.4 The contributions to conductivity reduction by electric current (blue) and dilution (red) at two different initial salt concentrations: A) 10 g/L; and B) 30 g/L.

The overall electricity generation was evaluated by using polarization curves. At the initial salt concentration of 10 g/L, we did not observe obvious difference in electricity generation among three inter-membrane distances of 1.5, 1.0, and 0.3 cm. The maximum power normalized by the anode chamber volume was close to 40 W/m^3 and the maximum current density was about 67 A/m^3. The indistinguishable polarization behaviors at three different distances indicated that varying inter-membrane distances within the tested range did not significantly change the internal resistance of the MDC, and thus would not affect electricity production.

2.3.2 Different inter-membrane distances at the same HRT

The previous tests contained two variables, the inter-membrane distance and the HRT. Because the HRT can greatly affect the desalination efficiency, we used a fixed HRT of 6 h and examined the influence of the inter-membrane distance on the MDC performance. Three inter-membrane distances, 1.5, 1.0, and 0.3 cm, were selected for the test and the initial salt concentration was 10 g/L NaCl. As shown in Figure 2.5A, the desalination efficiency increased with the decreasing inter-membrane distance, and the three distances (from large to small) achieved a conductivity reduction of 9.6±0.6%, 12.2±0.7% and 38.7±0.4%. The generation of electric current was similar at the three distances and varied around 1.46 mA. However, the amount of water transported into the middle chamber via osmosis became larger at a bigger distance (Figure 2.5A). When the

inter-membrane distance increased from 0.3 cm to 1.0 cm, the amount of the transported water increased from 2.5 mL to 5.8 mL. When we further increased the inter-membrane distance to 1.5 cm, there was 7.2 mL of the additional water into the middle chamber. The higher water osmosis at a larger distance was caused by the faster influent flow rate. To maintain an HRT of 6 h, the influent flow rate at the 0.3-cm distance was 0.02 mL/min, while 1.5-cm distance had a flow rate of 0.1 mL/min. The faster influent flow rate brought in more salt per unit time and thus created a larger salt gradient across the ion exchange membrane, thereby accelerating the water osmosis. The additional water contributed to conductivity reduction, and in general, the generation of electric current accounted for more than 50% of desalination at 1.0- and 1.5-cm distances, or more than 60% at 0.3-cm distance (Figure 2.5B). Although the 0.3-cm distance resulted in the best desalination performance, it produced the least amount of water because of the smallest salt chamber and the slowest influent flow rate.

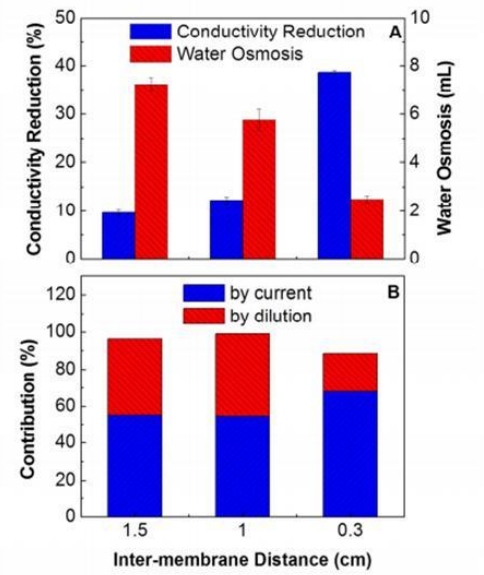

Figure 2.5 The desalination performance of the MDC with different inter-membrane distances at the same HRT of 6 h: A) conductivity reduction (blue) and the amount of

water osmosis (red); and B) The contributions to conductivity reduction by electric current (blue) and dilution (red).

2.3.3 Different HRTs at the same inter-membrane distance

We have also examined the different HRTs (6 and 20 h) at the same inter-membrane distance (1.0 cm). The results showed that the conductivity decreased by 12.2±0.7% at HRT of 6 h, and 35.2±0.1% at HRT of 20 h (Figure 2.6A), confirming that a longer HRT benefits desalination in an MDC. A shorter HRT, on the other hand, resulted in more water osmosis that had 5.8 mL additional water in the middle chamber at HRT 6 h, higher than 2.9 mL at HRT 20 h. It was found that electricity generation contributed to 68% of the desalination at HRT 20 h, higher than 55% at HRT 6 h (Figure 2.6B).

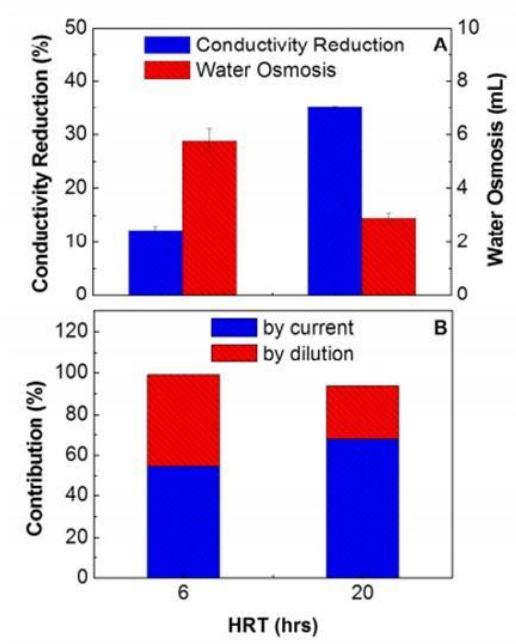

Figure 2.6 The desalination performance of the MDC with same inter-membrane distance of 1 cm at two different HRTs of 6 and 20 h: A) conductivity reduction (blue) and the amount of water osmosis (red); and B) The contributions to conductivity reduction by electric current (blue) and dilution (red).

2.3.4 SDR and inter-membrane distances

We summarized the SDR in the literature and plotted the data against the inter-membrane distance (Figure 2.7). There is not an obvious trend that SDR increases with the decreasing distance; however, the high SDRs were generally obtained with small inter-membrane distances. In addition to inter-membrane distances, factors such as the initial salt concentration, the number of desalination chambers, the electrolyte conductivity, and the reactor configuration, also affect the SDR. The highest SDR was 61.0 g/(d·L) at an inter-membrane distance of 1.0 cm and an initial salinity of 20 g/L; the SDR decreased when more desalination chambers were added in the same study (Chen et al. 2011b). The lowest SDR in the literature was 0.2 g/(d·L) with an inter-membrane distance of 1.0 cm and an initial salinity of 0.7 g/L (Zhang et al. 2012b). The significant difference in SDRs at the same inter-membrane distance between those two studies was likely due to the extremely low salt concentration in the latter, in which only a small amount of salt was provided for the ion exchange and also resulted in a very low conductivity of the electrolyte for electricity generation. The smallest inter-membrane distance that was reported was 0.13 cm, with a SDR of 4.7 g/(d·L) at an initial salinity of 35 g/L (Kim and Logan 2011a). The largest inter-membrane distance in the previous studies was 3.6 cm, and a SDR of 0.4 g/(d·L) was achieved using actual wastewater as a carbon source in the anode (Luo et al. 2012b).

Because there is limited literature on MDCs and a significant difference in MDC configuration and operation among different studies, we were not able to extract enough information to conclude a clear relationship between SDR and inter-membrane distance, but smaller distances seem to be generally beneficial. .

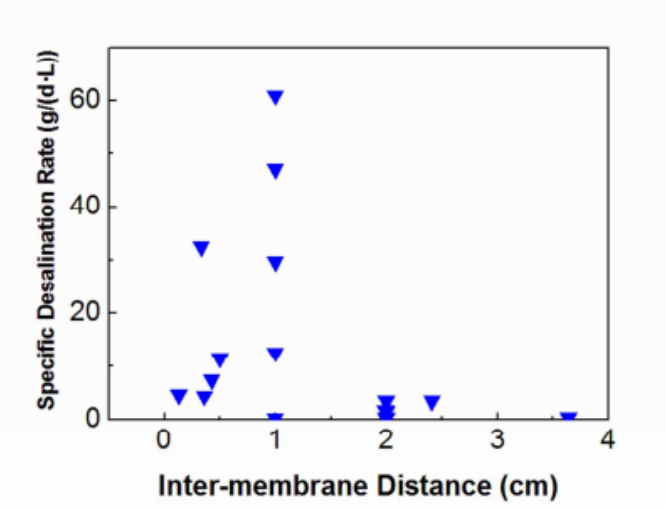

Figure 2.7 SDR vs. inter-membrane distances reported in the literature.

2.4. Conclusions

Our results show that a small inter-membrane distance results in a higher specific desalination rate; however, a larger inter-membrane distance does not negatively affect the desalination efficiency at the same influent flow rate, because the increased HRT improves the desalination performance. At the same HRT, a smaller inter-membrane distance improves the desalination efficiency, but a low water production rate remained as a drawback. In conclusion, the inter-membrane distance and the HRT have complementary effects on desalination performance in

MDCs, and future design and operation of MDCs needs to consider the tradeoff between these two factors.

Chapter 3. Improving the flexibility of microbial desalination cells through spatially decoupling anode and cathode

(This section has been published as Ping, Q. and He, Z.* (2013) Improving the flexibility of microbial desalination cells through spatially decoupling anode and cathode. ***Bioresource Technology.*** Vol 144, pp 304-310.)

Abstract

To improve the flexibility of microbial desalination cell (MDC) construction and operation, a new configuration with decoupled anode and cathode was developed and examined in this study. A higher salt concentration resulted in higher current generation, as well as a higher salt removal rate. The effect of the distance between the anode and the cathode on the MDC performance was not obvious, likely due to a sufficient conductivity in the salt solution. Because the cathode was identified as a limiting factor, adding one more cathode unit increased the current generation from 72.3 to 116.0 A/m^3, while installing additional anode units did not obviously alter the MDC current production. Changing the position of the anode/cathode units exhibited a weak influence on the MDC performance. Parallel connection of electrical circuits generally produced more current than the individual connections, and a strong competition was observed between multiple units sharing the same opposite unit.

3.1 Introduction

Desalination of sea water or brackish water is a promising method to provide fresh water for domestic, industrial, and agricultural applications. The current desalination technologies involve a large energy demand, which results in a high cost for desalinated water. Renewable energy such as solar and wind energy has been applied to drive desalination but the investment and operating expense is still high (Garcia-Rodriguez 2003, Mathioulakis et al. 2007). The recent discovery of a microbial desalination cell (MDC) provided a new approach for low-energy desalination (Kim and Logan 2013). MDCs derive from the integration of a microbial fuel cell and electrodialysis and use the microbial metabolism of organic compounds to provide a driving force for desalination (Cao et al. 2009). Several researchers have studied MDCs for salt removal from sea water, hydrogen production, desalinating low-salinity water with ion exchange resins, water softening, and production of valuable chemicals (Chen et al. 2012b). Based on this research, it is believed that MDCs are suitable for a pre-desalination process linking to conventional desalination processes such as reverse osmosis or electrodialysis (Mehanna et al. 2010a), or desalinating low-salinity water, because of the slow desalination rate resulting from a microbial process (Zhang and He 2012).

A significant challenge in MDC research is the engineering development of MDC technology; the prior research efforts have focused on MDC configuration and operation. For example, stacked MDC systems were developed by installing multiple pairs of membranes between the anode and the cathode to improve the charge transfer efficiency (Kim and Logan 2011, Chen et al. 2011). An upflow tubular MDC was constructed to eliminate the cathode “chamber” by using

a wrapped wet-cloth cathode (Jacobson et al. 2011b), and later was advanced to a liter-scale (Jacobson et al. 2011a). On the side of MDC operation, an air cathode using oxygen as an electron acceptor was studied to replace a ferricyanide catholyte for improving MDC sustainability (Mehanna et al. 2010a). A biocatalyst was applied on the cathode electrode to avoid the use of an expensive metal catalyst (Wen et al. 2012). To buffer the electrolyte pH, circulation between the anolyte and the catholyte was conducted (Chen et al. 2012, Qu et al. 2012). The long-term performance of the MDC for treating domestic wastewater was also evaluated (Luo et al. 2012b).

No matter what configuration (stacked or tubular), the MDCs are usually built with pre-designed volumes of the three compartments (anode, cathode and salt) that are fixed in a reactor. Varying the liquid volume or modifying the individual compartment, in the case of performing maintenance or overcoming limiting factors, would need to disassemble the reactor, which will create great difficulty in a future large-scale MDC system consisting of multiple MDC modules (e.g., hundreds of individual MDCs). In addition, our prior attempt to scale up MDCs encountered serious issues with a leaking reactor that could not be easily detected in the previous UMDC configuration that had the anode tube inside the cathode tube (results not shown). Therefore, to improve the flexibility of MDCs and create a simpler reactor structure that benefits future scaling up, we decoupled the anode and the cathode compartments (Figure 3.1). In this decoupled MDC, the anode unit (containing an anion exchange membrane) and the cathode unit (with a cation exchange membrane) are placed in a salt solution. Such a change makes it possible to adjust the ratio of liquid volumes between different compartments in a more convenient way

than in the previous MDCs, and more easily to repair/replace the problematic units without significantly modifying the whole MDC system.

In this study, we have examined the feasibility of the decoupled MDC and investigated the key factors such as the inter-membrane distance and the salt concentration. We have also evaluated the decoupled MDC system consisting of multiple anode and/or cathode units in terms of the number of electrodes, the installment positions, and the electrical connection. The results are expected to provide a foundation for further scaling up of the MDC system.

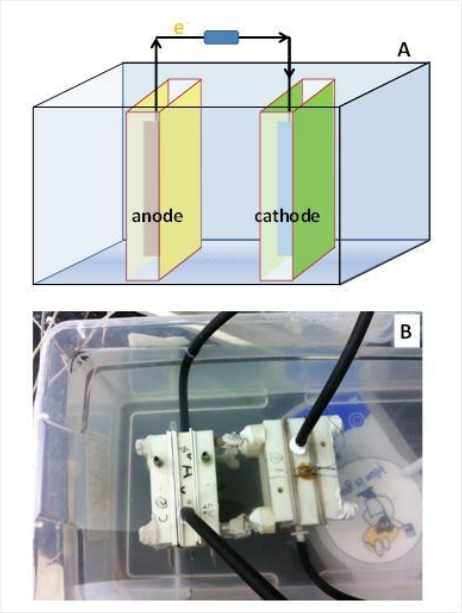

Figure 3.1 The schematic (A) and experimental setup (B) of a decoupled MDC.

3.2 Materials and methods

3.2.1 Decoupled MDC setup

The decoupled MDC system consisted of two separate units, an anode and a cathode, both of which were placed in a 4-L tank containing a salt solution (Figure 3.1). This basic configuration could be modified with the addition of more anode/cathode units. The anode unit was in a plate configuration and had an anion exchange membrane (AEM, AMI-7001, Membrane International, Inc., Glen Rock, NJ, USA) on both sides; similarly, the cathode unit had cation exchange membranes (CEM, CMI-7000, Membrane International, Inc.) on both sides. The anode and cathode electrodes were made by wrapping carbon cloth (3.0 × 7.5 cm, Zoltek Companies, Inc., St. Louis, MO, USA) around stainless mesh (3.0 × 2.5 cm) that acted as both a supporting structure and a current collector. The cathode electrode contained a catalyst prepared by applying a mixture of Pt/C powder with a Nafion solution to the surface of the carbon cloth with a final Pt loading rate of ~ 0.3 mg Pt/cm^2. The liquid volume of the anode or the cathode unit was 24 mL.

3.2.2 Operating conditions

The decoupled MDC was operated in a batch mode at a room temperature of ~ 22 ºC. The anode was inoculated with a mixture of aerobic and anaerobic sludge from local wastewater treatment plants (Jones Island and South Shore Water Reclamation Facilities, Milwaukee, WI, USA). The anode feeding solution (anolyte) was a synthetic solution containing acetate as an electron donor (per liter of DI water): sodium acetate, 2 g; NH_4Cl, 0.15 g; NaCl, 0.5 g; $MgSO_4$, 0.015 g; $CaCl_2$, 0.02 g; KH_2PO_4, 0.53 g; K_2HPO_4, 1.07 g; and trace element, 1 mL (Angenent and Sung 2001).

The catholyte was the saline water with the same salt concentration as the one in the salt solution tank prepared by dissolving NaCl in DI water. The anode compartment was linked to a 500-mL reservoir, which provided the anolyte that was recirculated between the anode and the reservoir at a rate of 24 mL/min. Likewise, the cathode compartment was connected to a 500-mL catholyte reservoir with recirculation between the two at 24 mL/min. The reservoir was continuously aerated with the air to provide adequate dissolved oxygen in the catholyte. The anode and cathode electrodes were connected through an external circuit over an external resistor of 1 Ω. The solutions (anolyte, catholyte, and salt solution) were replaced every 24 h, which was designated as one operating cycle, or when the current dropped below 1 mA for a few tests of the anolyte conductivity.

3.2.3 Analysis and calculation

The voltage of the MDC was recorded every 3 min by a digital multimeter (2700, Keithley Instruments, Inc., Cleveland, OH, USA). The pH was measured using a Benchtop pH meter (Oakton Instruments, Vernon Hills, IL, USA). The conductivity was measured by a Benchtop conductivity meter (Mettler-Toledo, Columbus, OH, USA). The polarization test was performed by a potentiostat (Reference 600, Gamry Instruments, Warminster, PA) at a scan rate of 0.1 mV/s. The densities of power and current were calculated based on the anode liquid volume. Because of a large volume of salt solution in which the anode and the cathode units were installed and a low salt removal rate in the MDC, it was very difficult to detect the conductivity change in the salt solution tank in a short period. Thus, we established a linear relationship between the charge transfer efficiency and the salt removal in a regular MDC (containing three

compartments sealed together) and used the current generation as a parameter to indicate desalination performance. Such an approach may not be very precise due to the difference between the regular and the decoupled MDCs, but we believe it could provide meaningful information to evaluate the feasibility of the decoupled MDC concept. The theoretical salt removal rate was determined as the coulombs harvested from the electric current over 24 h multiplied by the charge transfer efficiency, Faraday's constant (96485 coloumbs/mol), and the molar weight of NaCl. The charge transfer efficiency was calculated as the theoretical amount of coulombs required to remove NaCl divided by the coulombs harvested from the electric current, assuming that one mole of NaCl removal will require one mole of electrons.

3.3 Results and Discussion

3.3.1 Feasibility of the decoupled MDC

The feasibility of the decoupled MDC was examined in a system consisting of one anode unit and one cathode unit deployed in a 35 g/L salt solution with a distance of 5 cm between the anode and the cathode. The MDC produced an average current density of 67.3±3.6 A/m^3, lower than that of a regular MDC with a traditional three-compartment configuration at the inter-membrane distance of 1 cm or 2 cm (81.2±6.3 A/m^3 or 78.5±18.6 A/m^3). It was expected that with the same organic loading rate, the larger inter-membrane distance (5 cm) in the decoupled MDC would result in much less current generation, compared with a smaller inter-membrane distance of 1 cm in the regular MDC (Ping and He 2013a). The result of the (relatively) comparable current generation between the two was possibly due to a larger surface area of ion

exchange membranes: in the decoupled MDC, the anode/cathode unit had ion exchange membranes on both sides (Figure 3.1), resulting in more surface area than a regular MDC that has only a one-sided membrane for each anode or cathode. This increased membrane area may compensate for the large inter-membrane distance in the decoupled MDC. We estimated the salt removal rate of the decoupled MDC according to a linear relationship between the charge transfer efficiency and the salt removal rate developed in a regular MDC, assuming both MDCs had the same charge transfer efficiency. The decoupled MDC theoretically removed 0.073 g TDS/d, lower than 0.089 g TDS/d in the regular MDC with a 1-cm inter-membrane distance, and 0.077 g TDS/d in the regular MDC with a 2-cm inter-membrane distance. Those results demonstrate that the decoupled MDC can work like regular MDCs, although some performance was sacrificed for improving the reactor flexibility.

3.3.2 Influence factors on the decoupled MDC containing single unit

To further investigate the decoupled MDC, especially the influence factors, we examined the performance under different salt concentrations (35, 20, 5, and 1 g/L), and different inter-membrane distances (5, 10, and 20 cm). We observed a higher current generation with the increasing salt concentrations: the 35 g/L resulted in the highest current density of 67.3±3.6 A/m^3 while the 1 g/L led to the lowest of 55.6±0.1 A/m^3 (Figure 3.2A). The difference in the charge transfer efficiency (87.0% at 35 g/L and 35.5% at 1 g/L) resulted in significantly different salt removal rates, which reached the highest of 0.070-0.078 g/day at the salt concentration of 35 g/L, much higher than 0.024 g/day at 1 g/L. The conductivity increase in the anode chamber also confirmed more salt removal at a higher salt concentration (Figure 3.3). Clearly, a higher salt

loading rate helped to increase the conductivity of the salt solution and thus the current generation. On the other hand, a larger inter-membrane distance did not negatively affect the MDC performance. The current generation slightly increased with the increasing inter-membrane distance with the salt concentrations of 5-35 g/L, or remained relatively constant with 1 g/L (Figure 3.2A). With 35 g/L, the anolyte conductivity exhibited a (weak) increasing trend along the increased inter-membrane distance (Figure 3.4); this increase could be associated with water osmosis (the loss of the anolyte to the salt solution due to a salt gradient across the CEM), and we previously found that a longer distance promoted water osmosis (Ping and He 2013a). The insignificant effect of the inter-membrane distance was likely due to a sufficient conductivity of the salt solution and a low capacity of desalination in the MDC.

However, the inter-membrane distance affected the maximum power production in the decoupled MDC, especially at a low salt concentration (Figure 3.2B&C). With 1 g/L, the maximum power density decreased from 14.9 W/m^3 at 5 cm to 13.7 W/m^3 and 12.1 W/m^3 at the distances of 10 and 20 cm, respectively (Figure 3.2B). The effect of the inter-membrane distance on the maximum power density became weaker with 35 g/L (Figure 3.2C). The individual potentials of the anode and the cathode electrodes are shown in Figure 3.5. It seems that the cathode appeared to be the limiting factor, except the condition of 1 g/L at 20 cm that the anode potential increased more rapidly. In general, the anode potentials with 35 g/L (Figure 3.5B) were lower than those with 1 g/L (Figure 3.5A). The anode potential with 1 g/L - 20 cm and 35 g/L - 5 cm showed the steepest and flattest slopes, which reflected the most and the least anode overpotential.

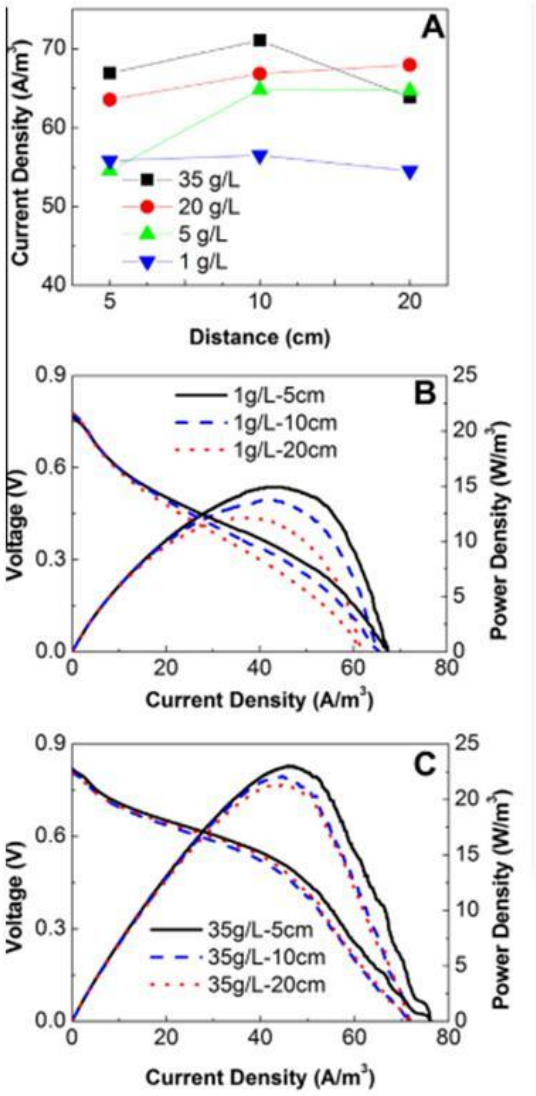

Figure 3.2 The performance of the decoupled MDC (with one anode and one cathode) at different distances (5, 10, 20 cm) between the anode and the cathode, and different salt concentrations (1, 5, 20, 35 g/L): (A) current density; (B) power and voltage in polarization tests with 1 g/L at different distances; and (C) power and voltage in polarization tests with 35 g/L at different distances.

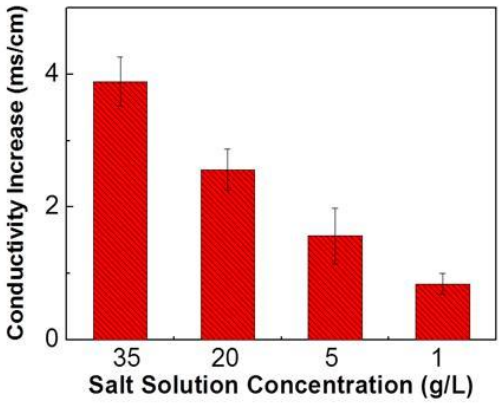

Figure 3.3 The increase in the anolyte conductivity over one operating cycle with four different salt concentrations at a distance of 5 cm.

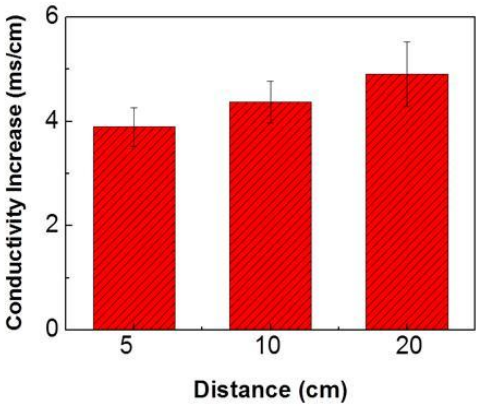

Figure 3.4 The increase in the anolyte conductivity over one cycle with 35 g/L at three different distances between the anode and the cathode.

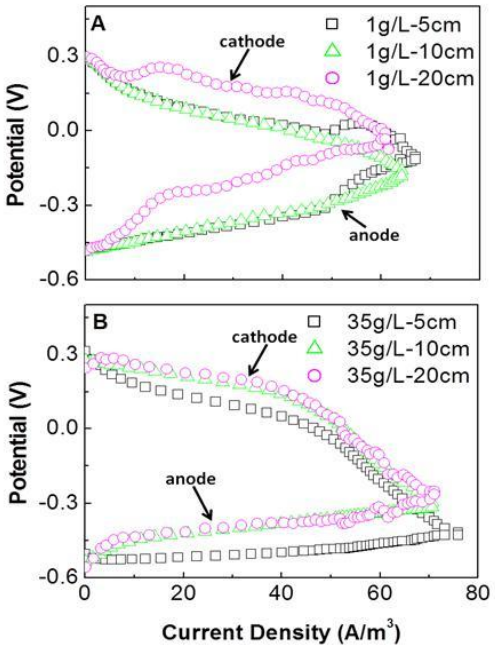

Figure 3.5 The potentials of the individual electrodes of the decoupled MDC at different distance between the anode and the cathode: (A) with 1 g/L; and (B) with 35 g/L.

3.3.3 Decoupled MDC with multiple units

A great benefit of decoupling the anode and the cathode is that we can easily adjust the number of the anode and the cathode units by adding and removing the unit. This will not only make it more convenient to construct MDC systems, but also possibly to improve MDC performance by varying the ratio between the anode and the cathode when one of them is identified as a limiting factor. However, this design also raises questions about the physical position and the electrical connections of the multiple units. Therefore, we conducted an initial investigation of the

decoupled MDC with multiple units installed in different positions and/or different electrical connections, as shown in Figures 3.6, 3.7, 3.8 and 3.9.

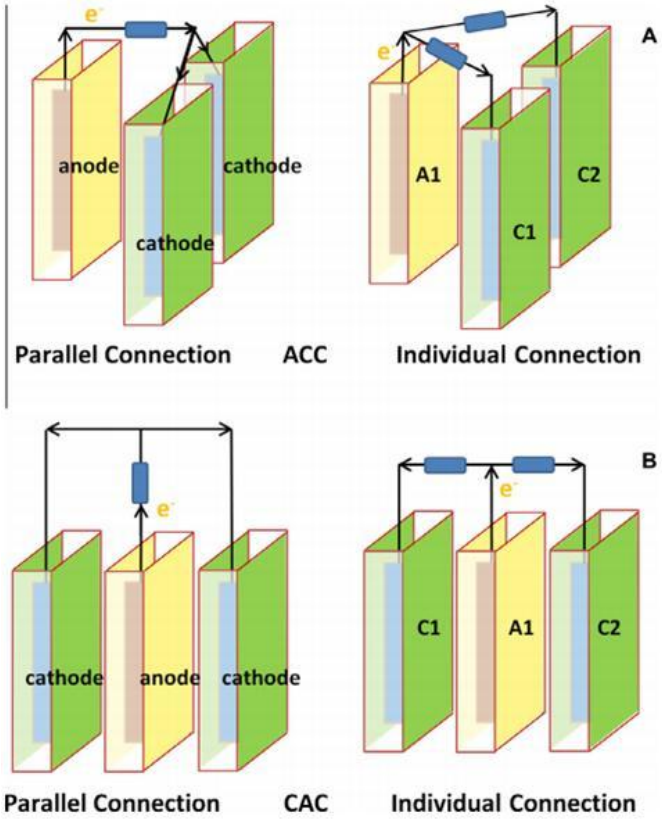

Figure 3.6 Experimental setup of the decoupled MDC with one anode and two cathode units: (A) the ACC in parallel or individual electric connections; and (B) the CAC in parallel or individual electric connections. A: anode; C: cathode.

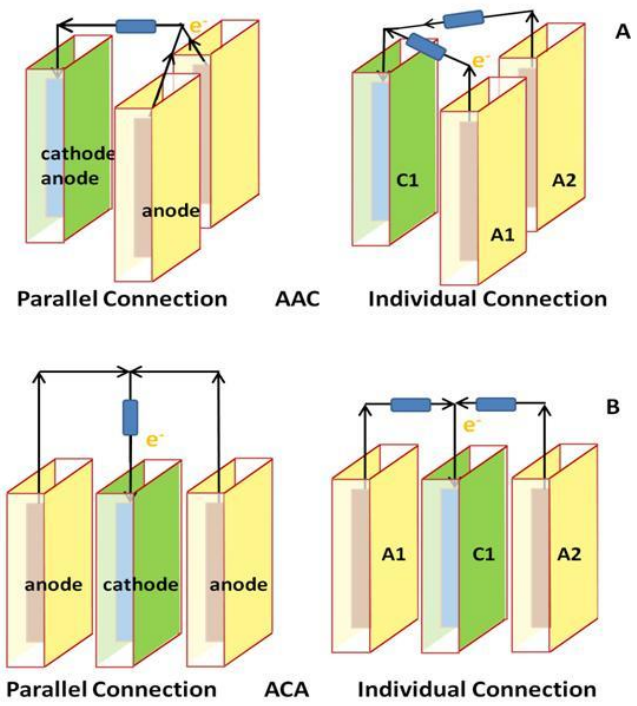

Figure 3.7 Experimental setup of the decoupled MDC with two anode and one cathode units: (A) the AAC in parallel or individual electric connections; and (B) the ACA in parallel or individual electric connections. A: anode; C: cathode.

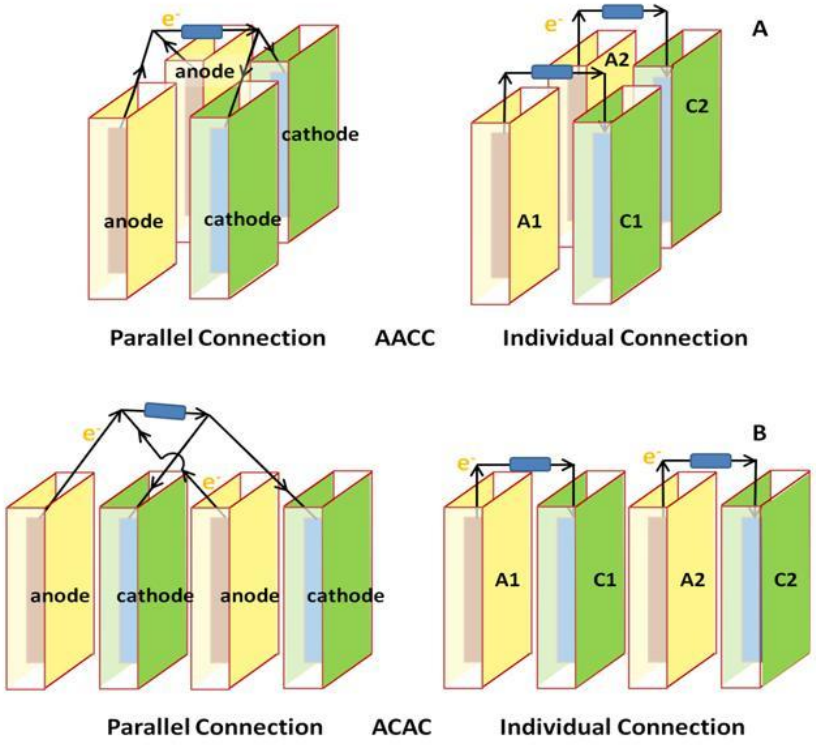

Figure 3.8 Experimental setup of the decoupled MDC with two anode and two cathode units: (A) the AACC in parallel or individual electric connections; and (B) the ACAC in parallel or individual electric connections. A: anode; C: cathode.

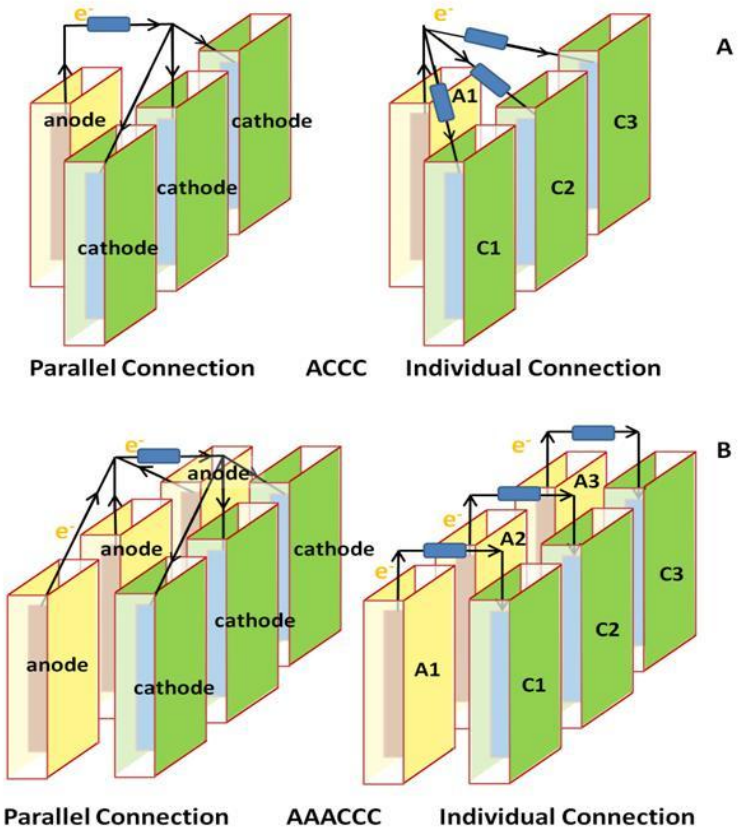

Figure 3.9 Experimental setup of the decoupled MDC with multiple anode/cathode units: (A) the ACCC in parallel or individual electric connections; and (B) the AAACCC in parallel or individual electric connections. A: anode; C: cathode.

3.3.3.1 Improving MDC performance by adding more units

As the cathode was identified as a limiting factor for the decoupled MDC consisting of one anode and one cathode, we modified the system with additional cathode units. As shown in Figure 3.10A, one more cathode unit (the ACC combination) resulted in a higher current density of 116.0 A/m^3 than 72.3 A/m^3 (the AC), while adding one more anode (the AAC) did not obviously change the current production compared with the AC combination. The limiting effect of the cathode was further demonstrated by adding one more anode to the ACC to form the AACC, which did not further improve the current generation because of an insufficient electron consumption in the cathode. Although adding cathode units benefits the MDC performance, we found that once the cathode reaction was improved sufficiently, the anode became a limiting factor in turn and the MDC performance was limited by an insufficient supply of electrons from the anode. This is supported by the fact that the ACCC did not further increase the current production compared with the ACC. At this point, adding more anode units would certainly provide more electrons, and thus the AAACCC produced the highest current density of 187.3 A/m^3 among the tested combinations. Accordingly, the AAACC combination achieved the highest salt removal rate of 0.143 g/day, which is 2.6 times of 0.055 g/day by the AC combination. The AAC slightly decreased the salt removal rate to 0.052 g/day, indicating that the competition between the anodes might result in a current loss.

In addition to the current generation from a regular operation (Figure 3.10A), the polarization tests also confirmed the effect of varying the anode/cathode units on the MDC performance (Figure 3.10B). The AAACCC combination produced the highest power density of 82.6 W/m^3, 2.5 times of that of the AC. The ACC and the AACC generated a comparable maximum power density (53.8 vs. 57.3 W/m^3). An exceptional result is that the ACCC produced a much lower

maximum power density than the ACC or the AACC, although they generated a comparable current during the regular operation, as shown in Figure 3.10A. The possible reasons for this difference might be due to the difference between the resistor-based operation and the polarization tests, the additional cathode units creating a competition of the accepting electron, and possible inter-charging among the cathodes (the stronger cathode charges the weaker one). The polarization tests also revealed that some combinations did not operate within their high current zone; for example, the maximum current densities of the ACC and the AACC were between 150 and 175 A/m^3, much higher than the current densities generated from the regular operation (resistor-based). Therefore, the MDC performance with those combinations could be further improved by reducing the external resistance for higher current generation. The potentials of individual electrodes are shown in Figure 3.10C. In general, the cathode potential dropped more steeply than the increase in the anode potentials, except that the ACCC combination had a dramatic increase in its anode potential at the high current zone, which might be caused by overdrawing the electron by the multiple cathodes but the exact reasons warrant further investigation.

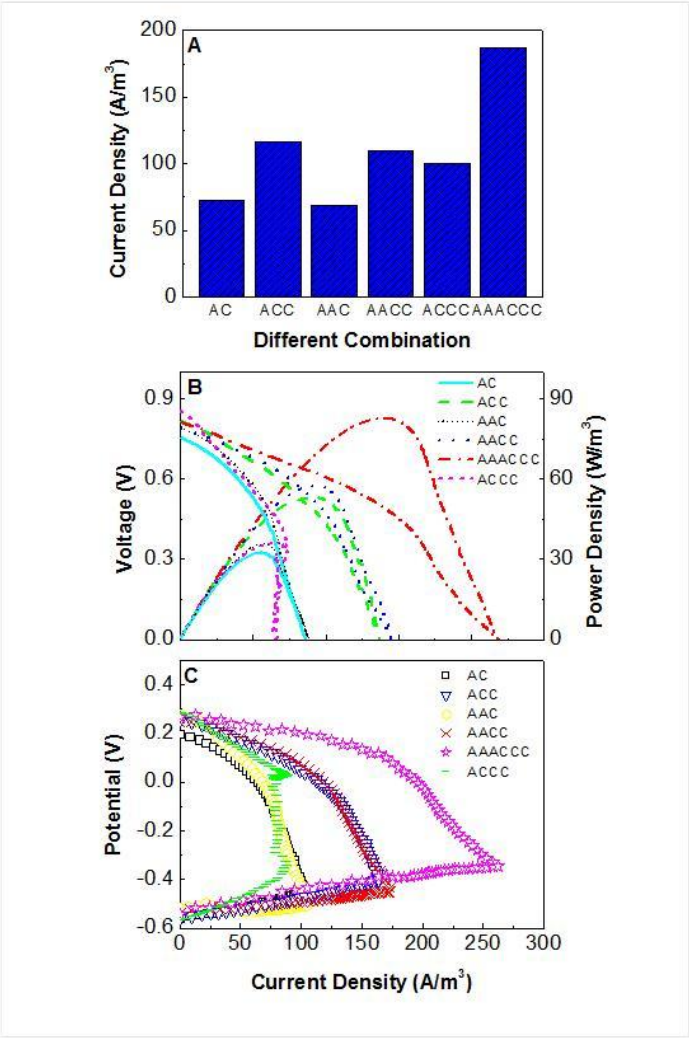

Figure 3.10 The performance of the decoupled MDC with additional cathode or anode units: (A) current density; (B) power and voltage in polarization tests; and (C) the potentials of the individual electrodes.

3.3.3.2 Effects of the unit position

The multiple units of the anode and the cathode raise questions on how to arrange the installment position and whether different positions will affect the MDC performance. Consequently we

examined three groups of the decoupled MDC system, each of which consisted of same number of units but was arranged in different ways (under parallel electrical connection): group one has one anode and two cathodes, the ACC (the cathodes on one side, Figure 3.6A) and the CAC (the cathodes on two sides, Figure 3.6B); group two has two anodes and one cathode, the AAC (the anodes on one side, Figure 3.7A), and the ACA (the anodes on two sides, Figure 3.7B); and group three has two anodes and two cathodes, the AACC (Figure 3.8A) and a staggered arrangement ACAC (Figure 3.8B). The results show that the different installment positions did not obviously change the current generation (Figure 3.11A), and this is generally supported by the polarization tests with some minor difference in the maximum power densities (Figure 3.11B). We observed higher anode potentials of the combinations with the alternative arrangement of the anode and the cathode, which increased the cathode potentials (ACA and ACAC, Figure 3.11C). The cathode reaction benefited from those arrangements likely because both sides of the cathode unit were close to an anode unit, but the effect on the anode potential is not clear at this moment.

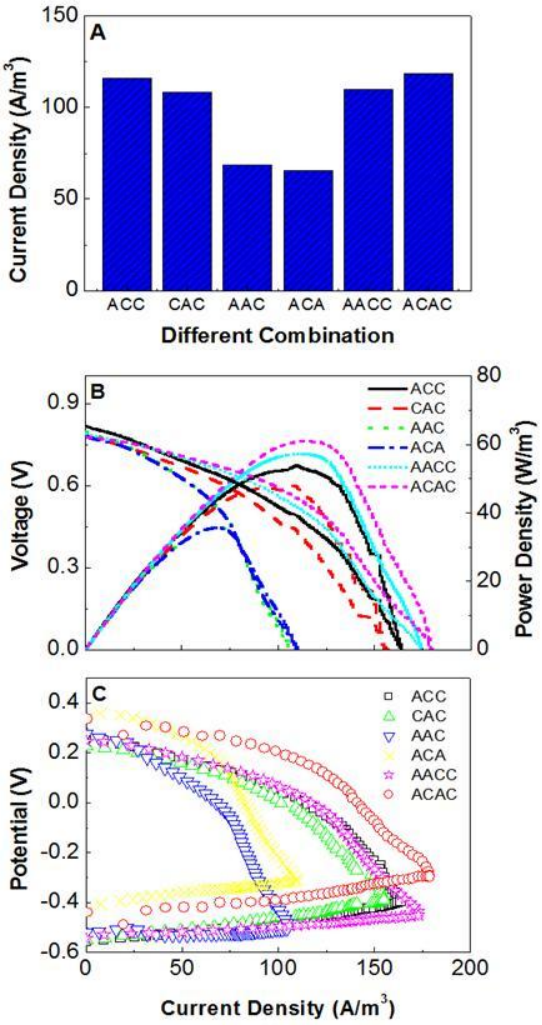

Figure 3.11 The performance of the decoupled MDC with the same number of cathode or anode units at different locations: (A) current density; (B) power and voltage in polarization tests; and (C) the potentials of the individual electrodes.

3.3.3.3 Effects of electrical connection

The above studies were conducted in a parallel electrical connection. Because all the units were in the same electrolyte (salt solution), a serial connection would not be possible. Therefore, we examined the individual connection (one anode linked to one cathode), which was compared with the parallel connection. Since the current generation is correlated to the salt removal, we simply used the sum of the current generation from multiple individual connections in an MDC system to represent its salt removal. Figures 3.12 and 3.13 show the representative current generation from the parallel and individual connections. The parallel connection resulted in more current production than the sum of the individual connections in most cases, except the AAC (Figure 3.12C) and the ACCC (Figure 3.13C): in the AAC combination, the individual connection of the A2C1 generated a higher current than the parallel connection, and in the ACCC combination, the current generation of the parallel connection exhibited a decreasing trend and was lower than the sum of the three individual connections. The current generation of the individual connection revealed strong competition, especially in the MDC system containing uneven numbers of the anode and the cathode units such as the AAC and the ACC (except the ACCC that had similar performance among the three individual connections). In the CAC and the AAC, this competition led to very low current generation (<10 A/m^3) from one of the circuits (Figure 3.12B&C).

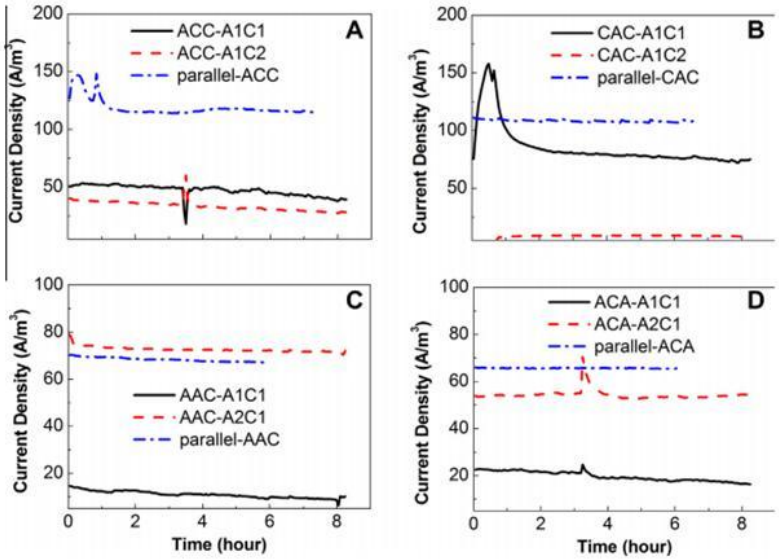

Figure 3.12 Current generation in the decoupled MDC in parallel or individual electric connection: (A) the ACC combination; (B) the CAC combination; (C) the AAC combination; and (D) the ACA combination. ‘‘ACC-A1C1’’ means the individual connection in the ACC combination between the anode (A1) and the cathode (C1) as shown in Figure 3.6A.

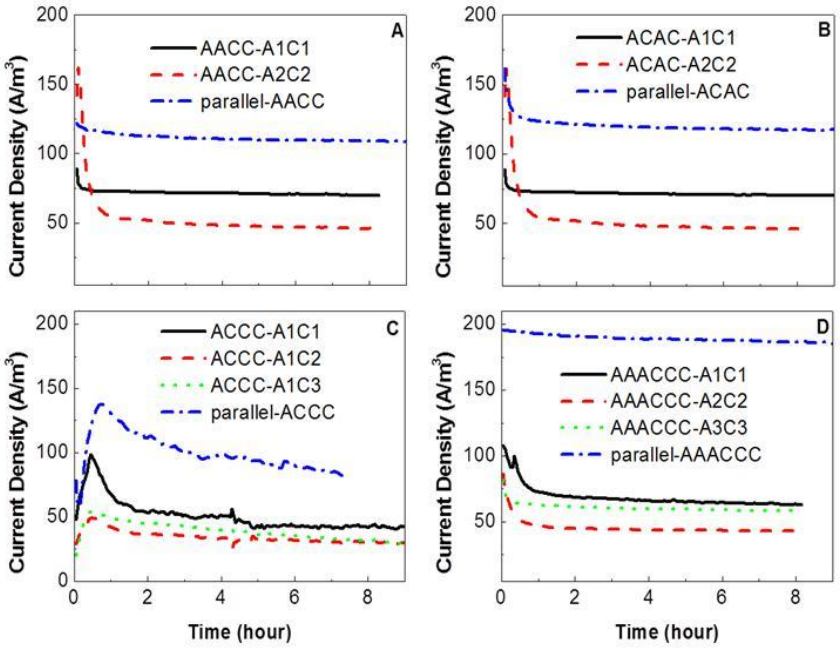

Figure 3.13 Current generation in the decoupled MDC in parallel or individual electric connection: (A) the AACC combination; (B) the ACAC combination; (C) the ACCC combination; and (D) the AAACCC combination. "AACC-A1C1" means the individual connection in the AACC combination between the anode (A1) and the cathode (C1) as shown in Figure 3.8.

Those results indicate that the parallel connection may be more suitable for the present MDC system because of the higher current generation; however, the individual connection can help to identify the "weak" unit. We envision that the future decoupled MDC system will involve both parallel and individual connections. A scaled-up decoupled MDC system will consist of many more units than those presented here, for example, multiple ACC combinations, in which a parallel connection will apply within each combination while the multiple combinations will act

as multiple individual connections. A balanced performance among different units/combination will be critical to the overall performance; thus, the careful construction and operation of individual units with uniform features (e.g., the catalyst loading rate, the electrode surface area, and the supply of organic compounds and oxygen) is important.

3.4. Conclusions

This work examined a new MDC configuration decoupling the anode and the cathode to achieve flexibility of construction and operation. The decoupled MDC could effectively produce current while conducting desalination, with some performance sacrificed for better flexibility compared with regular MDCs. The distance between the anode and the cathode exhibited some influence on the MDC performance, especially at a low initial salt concentration. The advantage of the decoupled MDC was demonstrated by varying the anode/cathode ratio to overcome the limiting factor. The arrangement of the anode/cathode physical position and the electric connection had some effects on the current generation.

Chapter 4 Long-term investigation of fouling of cation and anion exchange membranes in microbial desalination cells.

(This section has been published as Ping, Q., Cohen, B., Dosoretz, C. and He, Z.* (2013) Long-term investigation of fouling of cation and anion exchange membranes in microbial desalination cells. ***Desalination.*** Vol 325, pp 48-55.)

Abstract

The fouling of ion exchange membranes in microbial desalination cells (MDCs) was investigated through an eight-month operation. Multiple MDCs were set up by using cation (CEM), anion (AEM), and/or proton (Nafion) membranes. The MDCs exhibited relatively constant reduction of conductivity of artificial seawater during the testing period (46.3±6.3% in the CEM-MDC and 78.7±0.8% in the Nafion-MDC in an operating cycle). However, the current generation decreased from 99 to 56 A/m^3 in the CEM-MDC after 250 days, and from 97 to 46 A/m^3 in the Nafion-MDC after 130 days, indicating the presence of membrane fouling. Theoretically the MDCs removed 6.7 - 12.1 kg $TDS/m^3/d$ with a high charge transfer efficiency of 230-440%, suggesting that electric current was not the only factor to drive desalination; water dilution played an important role in conductivity reduction as well. It was observed that the AEM contained significant biofouling, resulting from wastewater and microbial growth on organic compounds migrating across the membrane, while the CEM had substantial inorganic scaling, mainly consisting of calcium and magnesium. The membrane resistance of the CEM increased

more significantly than that of the AEM, indicating that CEM needs more maintenance during MDC operation.

4.1 Introduction

A microbial desalination cell (MDC) is proposed as an alternative approach for energy-efficient desalination integrated with simultaneous wastewater treatment (Cao et al. 2009). A typical MDC consists of three chambers, an anode, middle (salt), and a cathode, separated by an anion exchange membrane (AEM, between the anode and the middle chambers) and a cation exchange membrane (CEM, between the cathode and the middle chambers), respectively (Figure 4.1). Bacteria growing on the carbon–based anode electrode break down organic matters while releasing electrons and protons in the anode chamber. Terminal electron acceptors (e.g., ferricyanide or oxygen) in the cathode chamber are reduced by accepting those electrons through an external circuit. Anions and cations are driven to migrate through AEM and CEM to balance the electric charge in the anode and the cathode chambers. Consequently, the salinity of the water in the middle chamber is greatly reduced (Luo et al. 2012a).

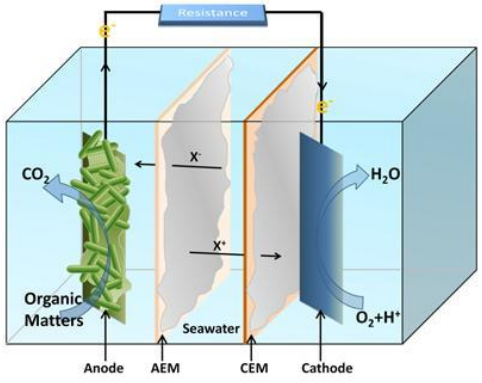

Figure 4.1 The schematic of a microbial desalination cell (MDC). AEM: anion exchange membrane; CEM: cation exchange membrane.

The MDC concept has been advanced from several aspects, including reactor architecture, operation, and functions, through various studies (Kim and Logan 2013). In most bench-scale MDCs, a synthetic solution (e.g., containing acetate) and a NaCl solution were used as the anolyte and the catholyte, respectively. While a ferricyanide catholyte remains more efficient, dissolved oxygen as a terminal electron acceptor has proved to be more applicable (Mehanna et al. 2010a). MDC configurations have been optimized through upflow tubular reactors for possible scaling up (Jacobson et al. 2011a,b), or by using stacked reactors to improve the charge transfer efficiency (Chen et al. 2011, Kim and Logan 2011). To reduce the operating cost due to the use of a buffer solution in the cathode chamber, the researchers applied recirculation to the electrolyte between the anode and the cathode to buffer the pH (Chen et al. 2012a, Qu et al. 2012). New features have been introduced to MDCs by inserting a bipolar membrane to produce acid and alkali (Chen et al. 2012b), or applying an external voltage to produce hydrogen gas in the cathode (Mehanna et al. 2010b, Luo et al. 2011). An MDC could also be modified to act as a microbial salinity-reduction electrolysis cell for saline wastewater treatment (Kim and Logan 2013). Accelerated desalination was achieved by replacing the AEM with a forward osmosis membrane to accomplish both water dilution due to water extraction from wastewater and salt removal driven by electric potential (Zhang and He 2012). Ion-exchange resins were added into an MDC for treating low-salinity solution (Zhang et al. 2012). MDCs were also studied to soften hard water by removing calcium and magnesium ions (Brastad and He 2013).

As ion exchange membranes serve a key role in creating different chambers (environments) and transporting the targeting ions, they are the critical components of an MDC system. The

performance of those membranes will largely affect the performance of an MDC (both desalination and wastewater treatment). However, a major concern of applying membranes to a bioelectrochemical treatment system is fouling, especially with actual wastewater and seawater that are much more complex than the lab-prepared solutions. Biofouling occurs because of the presence of organics and microorganisms in wastewater (Ivnitsky et al. 2005) and transparent exopolymer particles in marine water that play an important role in the initiation and development of biofilm (Berman et al. 2011). Abiotic fouling such as deposition of inorganic compounds also can form scaling.

Membrane fouling has not been well addressed in bioelectrochemical systems, and there is a lack of studies to examine fouling issues in microbial fuel cells (MFCs (Logan et al. 2006)) or MDCs. In an early study of a two-chamber MFC operated for 400 days, it was found that cation precipitation exhibited more influence on the performance of a Nafion membrane than biofouling, and periodic chemical cleaning was recommended for stable performance (Choi et al. 2011). In an MFC equipped with a proton exchange membrane (Nafion 117), physical blockage caused by cations was found to decrease the current and intensify the pH-gradient after running for 90 days (Xu et al. 2012). Thus far, the only study of membrane fouling in MDCs was conducted with domestic wastewater and salt solution (NaCl and $NaHCO_3$) in an MDC that was operated for eight months (Luo et al. 2012). Their results showed only minor scaling on the CEM; however, bio-fouling on the AEM was found to distinctly increase the MDC resistance, resulting in a decrease in both current density and desalination efficiency.

To further understand membrane behavior in MDCs, we have conducted a long-term study (over eight months) and investigated how ion-exchange membranes were deteriorated by fouling/scaling with actual wastewater and synthetic seawater (prepared with sea salts). We examined the conductivity and turbidity of treated seawater and recorded the electricity generated by the MDC during the operation. We analyzed the contribution of electric current and water osmosis to conductivity reduction, and measured the membrane resistance using electrochemical impedance spectroscopy (EIS). Using scanning electron microscopy (SEM) and X-Ray Diffraction, we also studied the fouling and scaling on the membrane surface.

4.2 Materials and methods

4.2.1 MDC setup

Multiple MDCs were established by using plate-shaped reactors, each consisting of three chambers, the anode, the middle (salt), and the cathode (Figure 4.1). An anion exchange membrane (AEM, AMI-7001, Membrane International, Inc., Glen Rock, NJ, USA) was used to separate the anode and the middle chambers, while a cation exchange membrane (CEM, CMI-7000, Membrane International, Inc.), or Nafion Membrane 117 (Fuel Cell Earth, LLC, Stoneham, MA, USA) was installed between the middle and the cathode chambers, resulting in a liquid volume of 24 mL in the anode or the cathode chamber. Several layers of rubber gaskets were installed between the AEM and the CEM with a distance of 1 cm, creating a middle chamber with a liquid volume of 24 mL. The anode and cathode electrodes were made of carbon cloth (3.0 × 7.5 cm, Zoltek Companies, Inc., St. Louis, MO, USA) attached to a piece of stainless mesh (3.0 × 2.5 cm) that acted as both a supporting structure and a current collector. The cathode

electrode contained the catalyst prepared by applying a mixture of Pt/C powder with Nafion solution to the surface of the carbon cloth with a final Pt loading rate of 0.3 mg Pt/cm^2, as described in our previous work (Xiao et al. 2012). A separate MDC with membrane surface area of 110 cm^2 was built to investigate the substrate diffusion through AEM, with each chamber volume of 60 mL.

4.2.2 MDC operating conditions

The MDCs were operated at a room temperature of ~ 22 °C. The anodes were inoculated with a mixture of aerobic and anaerobic sludge, and the feeding solution was the primary effluent of a domestic wastewater treatment plant (Jones Island and South Shore Water Reclamation Facilities, Milwaukee, WI, USA). Sodium acetate (5 g/L) was added to ensure an adequate electron supply to drive the desalination. The catholyte was tap water at pH 6.8. All the anode chambers were linked to a shared 3-L reservoir, and the cathode chambers were linked to a shared 1-L reservoir, respectively, which provided the anolyte or the catholyte that were recirculated between the anode or the cathode chambers and the reservoirs at a rate of 24 mL/min. The large-size reservoirs were used to ensure a sufficient supply of the anolyte and the catholyte so that the anode and the cathode reactions would not be limiting factors to desalination. The catholyte reservoir was continuously aerated with the air to provide dissolved oxygen. The middle chambers were supplied with seawater recirculating from a 100-mL reservoir at a flow rate of 24 mL/min. Seawater was prepared by dissolving 35 g/L sea salts (Instant Ocean, Aquarium Systems, Inc., Mentor, OH, USA) in DI water. The anode and cathode electrodes were connected through an external circuit over an external resistor of 10 ohm. The

solutions in the reservoirs were replaced once a week, a period that was designed as one operating cycle.

An additional MDC was operated for a short term (33 days) with a synthetic solution in the anode chamber and 10 g NaCl/L in the middle chamber; the anode inocula were MFC-enriched culture obtained from Emefcy (Israel). The MDC for the substrate diffusion test was operated abiotically at a fixed voltage of 1 V using an external power supply. Both the anode and the cathode chambers were supplied with the model organic compounds (glucose, ethylene glycol, and sodium acetate, respectively) at the concentration of 20 mg/L (as in C), or the mixture of three organic compounds (10 mg C/L, each). The middle chamber was supplied with a 15 g/L NaCl solution. All solutions were recirculated from external 180 mL-reservoirs at the flow rate of 0.75-1.0 mL/min.

4.2.3 MDC analysis

The MDC voltage was recorded every 3 min by a digital multimeter (2700, Keithley Instruments, Inc., Cleveland, OH, USA). The pH was measured using a Benchtop pH meter (Oakton Instruments, Vernon Hills, IL, USA). The conductivity was measured by a Benchtop conductivity meter (Mettler-Toledo, Columbus, OH, USA). The desalination efficiency was determined as the decreased percentage of salt solution conductivity over an operating cycle. The charge transfer efficiency was calculated as the theoretical amount of coulombs from the removed NaCl divided by the coulombs harvested from the electric current, assuming that one mole of NaCl removal will require one mole of electrons. The contribution of electric current to

conductivity reduction was calculated as the theoretical salt removal by coulombs harvested from the electric current divided by the actual salt removal determined by the conductivity decrease. The amount of water flux due to osmosis was determined by measuring the difference of the water volume between the salt water influent and its effluent over 24 h. The contribution of dilution to conductivity reduction was estimated as the theoretically reduced conductivity by sole dilution divided by the actually reduced conductivity in the MDC.

4.2.4 Analysis of ion exchange membranes

The membrane resistance was determined by using electrochemical impedance spectroscopy (EIS) that was performed in a cell consisting of two chambers separated by the testing membrane. The impedance across the membrane was measured by using a potentiostat (Gamry reference 600) in a four-electrode mode, which included two platinum electrodes as the working electrode and the counter electrode, and two Ag/AgCl reference electrodes as the reference electrodes (according to Gamry technical notes). The frequency was set at the range of 0.01 Hz~100 kHz. The electrolyte was a NaCl solution of 35g/L. The resistance measured at high frequency represented the combined solution and membrane resistance, R_{m+s}. To obtain the pure membrane resistance R_m, the combined resistance was deducted by the solution resistance, R_s, which was obtained from a blank experiment without the membrane over the same frequency range (Dlugolecki et al. 2010).

The morphology of microorganisms on the membranes and the fouling/scaling layer were examined by using scanning electron microscopy (SEM) (S-4800 Hitachi, Japan). The samples for SEM analysis were prepared by the following procedures: after fixation with 2.5% glutaraldehyde, the samples were dehydrated with a graded ethanol series: 20%, 40%, 60%, 80%, 100%, 100% and 100%; then, the samples were critical-point dried in liquid CO_2 in a Balzers CPD 020 critical point drying apparatus (Balzers Union, Liechtenstein); after drying, the samples were coated with 5.0 nm Iridium in the Emitech K575X Sputter Coater (Emitech, Polaron, Britain). X-Ray Diffraction (XRD, Scintag XDS 2000) tests were performed for inorganic scaling on the membranes.

4.3. Results and discussion

4.3.1 MDC performance

4.3.1.1 Electricity generation

Four identical MDCs with CEM were operated for different lengths of time with the longest one for about 250 days, and one MDC with Nafion membrane was operated for approximately 130 days. The electricity generation exhibited a batch profile affected by the organic substrate in the anodes. At the initial period, the CEM-MDCs produced an average current density of 99 A/m^3 when the organic supply was sufficient. After 80 days of operation, the current density decreased to 83 A/m^3, and after 250 days of operation, the current density dropped down to 56 A/m^3 (Figure 4.2A). In the Nafion-MDC, the current density varied between 67 and 97 A/m^3 upon a sufficient supply of organic contents and decreased to 46 A/m^3 after 130 days (Figure 4.2B). The

decrease in current generation over time in both types of the MDCs indicates the presence of factors such as membrane fouling and scaling that restricted the current-generating process.

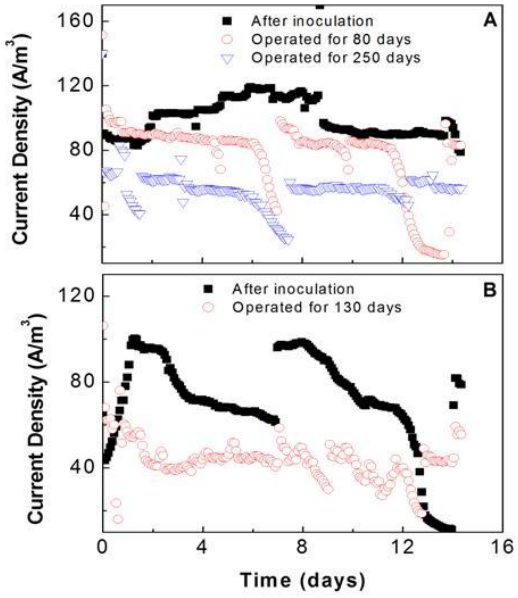

Figure 4.2 Current generation by the MDCs with (A) CEM, and (B) Nafion membrane.

4.3.1.2 Desalination

The conductivity of the seawater in the MDCs was measured once a week. The four CEM-MDCs achieved a similar reduction of conductivity at 46.3±6.3% and the Nafion-MDC achieved a conductivity reduction of 78.7±0.8% (Figure 4.3A). The long-term operation did not significantly decrease the efficiency of the conductivity reduction in both the CEM- and the Nafion-MDCs, although we observed fluctuation in reduction efficiency. When we translated the conductivity reduction into the salt removal rate by assuming NaCl as the only salt in the

seawater, we found that the CEM-MDCs theoretically removed 6.7±1.1 kg TDS/m^3/d, while the Nafion-MDC removed 12.1±0.5 kg TDS/m^3/d.

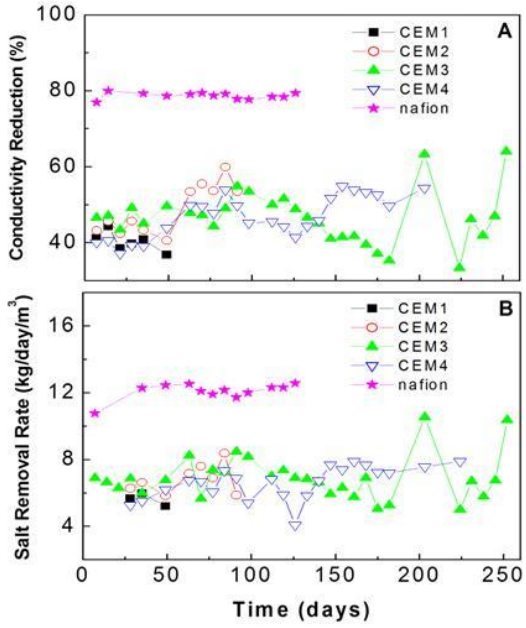

Figure 4.3 Desalination performance of the MDCs with different membranes: (A) conductivity reduction in an operating cycle; and (B) (theoretical) salt removal rate.

Charge transfer efficiency was 229.9±49.9% and 441.4±101.7% for the CEM-MDCs and the Nafion-MDC, respectively. Those high charge transfer efficiencies suggest that current generation contributed to part of the salt removal (in fact, conductivity reduction) and that there were other factors causing conductivity reduction. According to the principle of an MDC, electric current is expected to be the driving force of desalination. However, the previous studies found that dilution due to water osmosis caused by the salt gradient across the membrane played an important role in the conductivity reduction (Jacobson et al. 2011e). Herein we analyzed the

theoretic contributions of electric current and dilution to conductivity reduction. In general, we observed a weaker effect of dilution in the CEM-MDCs than that in the Nafion-MDC (Figure 4.4). In the CEM-MDCs, electric current contributed to 61.0±5.2% of the conductivity reduction during the first 50 days' operation; this contribution decreased to 45.6±4.3% during days 50-100 and further down to 39.9±6.7 % in days 100-250 (Figure 4.4A). Water osmosis was clearly observed with more water moving into the salt chamber of the Nafion-MDC than that of the CEM-MDCs (Figure 4.5). Consequently, the dilution effect resulted in 28.8±9.1% of conductivity reduction in the Nafion-MDC. Likewise, the conductivity reduction in the Nafion-MDC was also mainly due to the electric current (23.0±5.0%) and the dilution effect (34.0±2.2%) (Figure 4.4B). There were unaccounted contributions that might be caused by ion exchange and other unknown effects (Mehanna et al. 2010a).

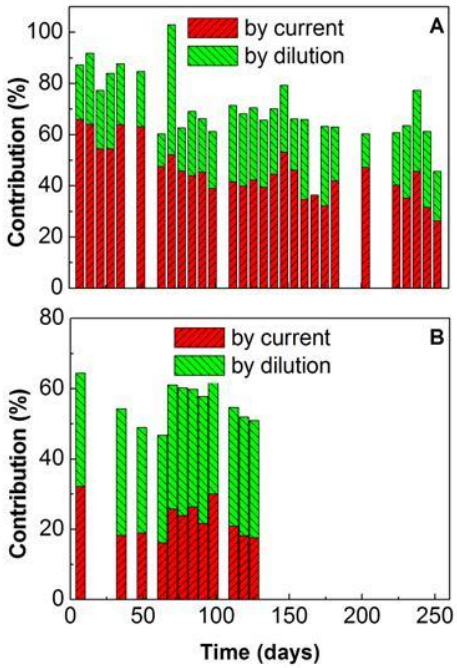

Figure 4.4 Contributions to conductivity reduction by electricity current and water dilution in the MDCs with (A) CEM, and (B) Nafion membrane.

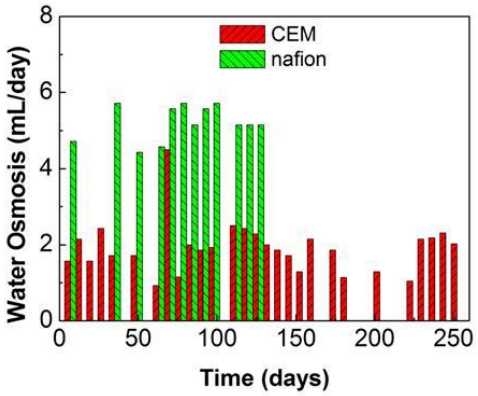

Figure 4.5 The amount of water osmosis per day into the middle chamber of the MDCs with CEM or Nafion membrane.

The decreasing contribution of the electric current to the conductivity reduction in MDCs indicated the effect of fouling. In addition, the turbidity of the desalinated seawater increased to 5~10 NTU from 1.6 NTU of the untreated seawater; the high turbidity of the treated seawater effluent was probably caused by both organic substances and microbial growth.

4.3.2 Membrane fouling

4.3.2.1 Biofouling

Biofouling of ion exchange membranes, especially the AEM that was in contact with the anolyte, was expected. Through visual inspection, we observed that the surface of the AEM turned black and was covered with a fungi-like deposit. Analysis of SEM images provided more detailed information about the conditions of the membrane surface and clearly showed the difference between a raw membrane (unused) and the fouled membranes (Figure 4.6). The raw membranes of both the AEM and the CEM exhibited a slightly cracked surface (Figure 4.6A and 6D) as observed by a previous study (Wang et al. 2011). There were microorganisms, probably the mixture of bacteria and fungi, on the surfaces of both the AEM and the CEM facing the middle chamber (containing seawater) (Figure 4.6B&E). Although microbial analysis was not performed, we could identify diverse microbial morphology such as rod shape, spheral shape, and filamentous shape, in the size of 1 to 2 μm. The existence of numerous fungi was further confirmed with a light microscope by identifying hyphae that were partitioned by septa. On the AEM facing the anode, microorganisms and particles were oberved, likely due to the presence of microorganisms in the wastewater (Figure 4.6C); on the CEM facing the cathode, particle deposits were presented and a few microorganisms were found (Figure 4.6F). Similarly, we observed biofouling of both membranes in an MDC operated for 33 days with different anode inocula and containing NaCl solution in the middle chamber (Figure 4.7); interestingly, it appears that filamentous organisms (which might be fungi) tend to be on the CEM side facing the saline water (Figure 4.7D), different from that in the long-term study, and the exact reasons warrant further investigation.

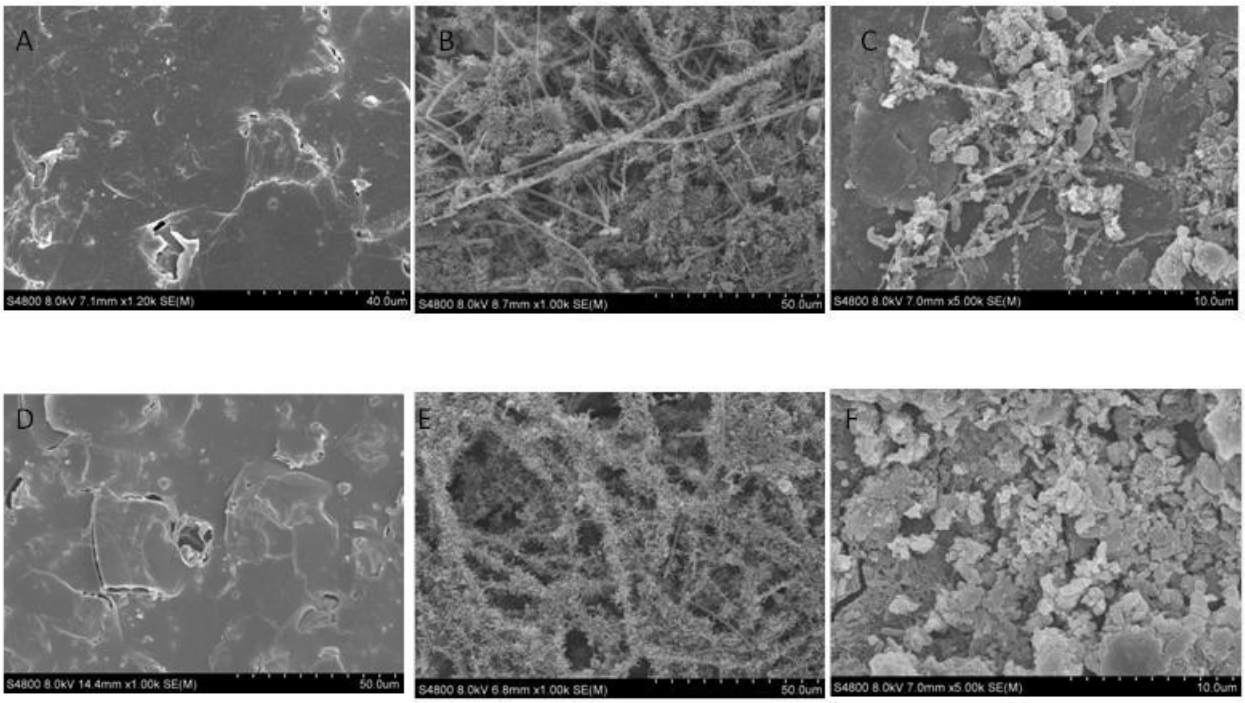

Figure 4.6 SEM images of the ion exchange membranes: (A) raw AEM; (B) AEM facing seawater; (C) AEM facing the anode after 250 days; (D) raw CEM; (E) CEM facing seawater; and (F) CEM facing the cathode after 250 days.

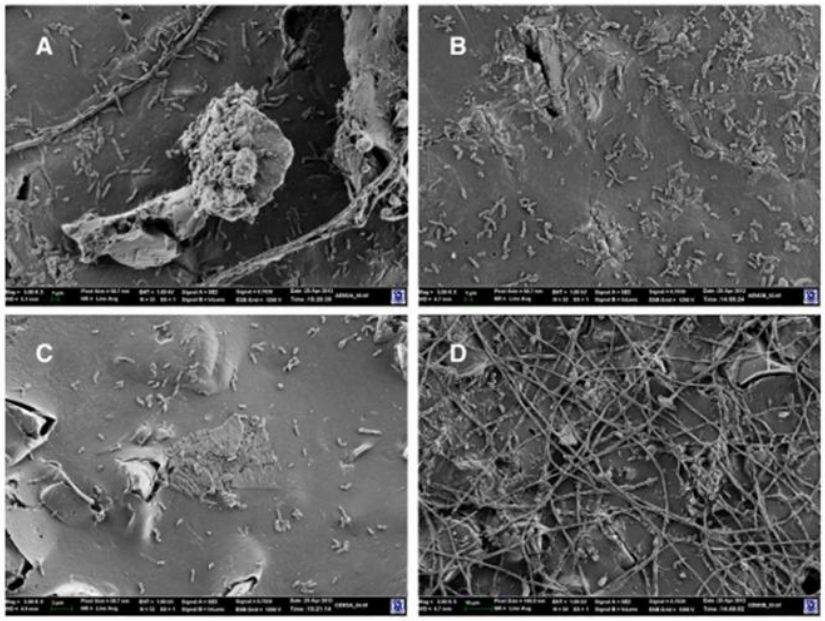

Figure 4.7 SEM images of the ion exchange membranes after a short-term test (33 days): (A) AEM facing the anode; (B) AEM facing saline water; (C) CEM facing the cathode; and (D) CEM facing saline water.

Biofouling of the ion exchange membranes facing the middle chamber (seawater) could generate potential concerns of deteriorating the quality of desalinated water and causing biofouling of the downstream desalination processes. Ion exchange membranes are expected to block the transport of microorganisms; thus, the source of microbial contamination was possibly from the feeding seawater. The AEM is known for transporting ionic organic compounds such as acetate ions (Kim et al. 2007); those organic compounds supported the growth of microorganisms in the middle chamber, resulting in biofouling of both the AEM and the CEM.

To further confirm the transport of organic compounds across the AEM or the CEM in the MDC, we conducted tests in an abiotic MDC under 1 V controlled by a power supply. The transport of organic compounds into the middle chamber was observed with all the tested compounds (Figure 4.8). The individual organic compound resulted in a higher increase in the TOC (total organic carbon) concentration in the middle chamber, and sodium acetate led to the highest increase in TOC, likely due to its ionic charge of the acetate group. A blank experiment was carried out in the MDC without organic matters in the anolyte or catholyte and it achieved a salt removal rate of 3.2 kg TDS/m^3/d. When 20 mg/L glucose, ethylene glycol, or sodium acetate was added into both the anolyte and the catholyte, the salt removal rate decreased to 2.5, 2.4, or 2.4 kg

TDS/m^3/d., respectively. With the mixture of organics, the salt removal rate was about 2.3 kg TDS/m^3/d. The decreased salt removal rate in the presence of organic compounds was possibly because of the competition in the ion migration between the salt ions and the organic compounds driven by electricity. Although the fouling effect may not occur in this short-term abiotic test, its results demonstrate the movement of organic compounds into the middle chamber, which can cause biofouling with microorganisms in a long-term operation.

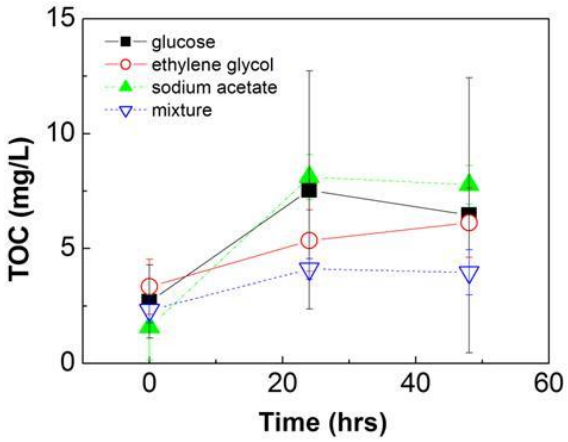

Figure 4.8 The change in TOC concentrations in the middle chamber of the abiotic MDC supplied with glucose, ethylene, sodium acetate, or the mixture of the three organics.

4.3.2.2 Inorganic scaling

The scaling on ion exchange membranes is mainly caused by the precipitation of various inorganic compounds such as calcium carbonate and magnesium hydroxide. We observed a layer of whitish crystals and deposits formed on the CEM (both sides); after 180 days of operation, the

middle chamber was filled with these deposits. Because of the relatively higher concentrations of calcium and magnesium ions in seawater than other scaling ions, we chose those two as representative compounds and examined their atomic percentage in the scaling at days 40 and 250. Calcium was found to be the main element in the scaling on both sides of the CEM at day 40 (Figure 4.9A). The side of the CEM facing the seawater contained 52.4% of calcium, while the other side facing the cathode had a higher percentage of calcium (66.7%). The amount of magnesium was insignificant. Both compounds had a very low presence on the AEM (the side facing seawater) at this time. After operating for 250 days, the atomic percentage of those compounds significantly changed. The atomic percentage of magnesium increased to 4.8% and 12.5% on the sides of the CEM facing the seawater and the cathode, respectively (Figure 4.9B). Meanwhile, calcium and magnesium on the AEM increased to 26.5% and 8.1% (Figure 4.9B). The XRD analysis showed that the scaling layer was composed mainly of calcium carbonate.

The variation in the atomic percentage of calcium and magnesium on the different sides of the CEM over the time suggests different scaling mechanisms. The scaling of the CEM on the side facing seawater developed much faster than the other side facing the cathode, because of the direct exposure of this side to the scaling compounds in the seawater. Calcium precipitation occurred more quickly than magnesium. The existence of bacteria in the middle chamber also helped the precipitation of calcium carbonate (Rivadeneyra Torres et al. 2013, Chu et al. 2012). During the operation, both the calcium and the magnesium ions migrated across the CEM into the cathode chamber as a result of the electricity generation. Magnesium precipitated on the CEM likely due to the high pH (~10.2) of the catholyte, while calcium had less precipitation

because of the lack of a source of carbonate ions in the catholyte. The scaling on the AEM (the side facing seawater) was less serious than that of the CEM, and the fouling was dominated by biofouling. The proton diffusion through the AEM from the anode (lower pH) into the middle chamber (higher pH ~ 8.9) might have alleviated the scaling on the AEM surface, but further evidence is required.

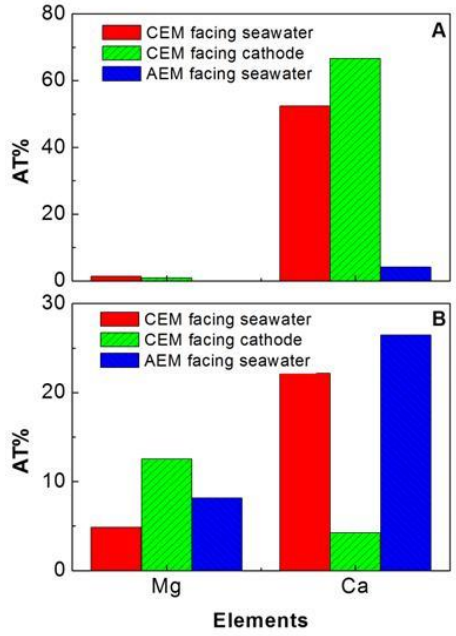

Figure 4.9 Atomic percentages of calcium and magnesium in the fouling layer from EDS analysis after (A) 40 days, and (B) 250 days.

4.3.2.3 Membrane resistance

The membrane resistance is an indicator of membrane properties and is affected by the fouling condition. In an MDC it is also interesting to know which ion exchange membrane, the CEM or

the AME, will have more serious fouling, which is related to MDC maintenance, membrane replacement, and related expense. We monitored the resistance of both the CEM and the AEM and observed obvious differences between the two. The AEM showed a relatively constant membrane resistance with some increase at the end of the testing period, while the CEM exhibited a trend of increasing with a significantly higher resistance at the end (almost three times higher than that of an unused CEM) (Figure 4.10). The Nafion membrane had a slight increase of its resistance (by 0.32 ohm) after the 130-day operation. That does not mean the Nafion membrane is more resistant to fouling; it is probably that the operating time was not long enough to develop significant fouling that changed the membrane resistance, like those of the CEM or the AEM that had not exhibit much change in their resistances at day 130.

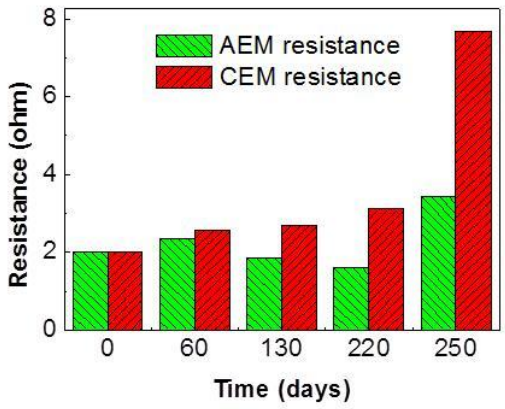

Figure 4.10 The membrane resistance of the AEM and the CEM over time.

Those results indicate that the inorganic scaling had a more serious effect on the membrane resistance of a CEM than organic fouling of an AEM, and this effect took a long time (> 220

days) to significantly increase the membrane resistance. Our findings are different from a previous long-term MDC study that concluded that the declined current generation and desalination rate was mainly caused by biofouling on the AEM (Luo et al. 2012b); the use of a ferricyanide catholyte and a non-calcium/magnesium salt solution in their experiments may result in different fouling effects from what is shown in the present study with a tap-water catholyte and seawater. In this study we intentionally created a "tough" condition for membranes by using seawater without any pretreatment; appropriate pretreatment before desalination will greatly slow down membrane fouling and thus extend the membrane lifetime (Kim et al. 2013, Van der Bruggen and Vandecasteele 2002). However, fouling still needs to be properly controlled. Although biofouling might not significantly change the membrane properties, the presence of microorganisms in the middle chamber would deteriorate the quality of the desalinated water and also introduce organisms to cause biofouling in the downstream desalination units. It is difficult to control the microorganisms in the feed water due to the available nutrients; either a disinfection practice (Kim et al. 2009) or using anti-microbial materials (Kugel et al. 2011) may be considered. The inorganic scaling may be alleviated by reducing the pH of the catholyte, for example, by using an acidified catholyte that can also improve the electricity generation and thus the desalination efficiency in an MDC (Jacobson et al. 2011e).

4. Conclusions

This study demonstrates the long-term performance of MDCs and ion exchange membranes in the presence of both biofouling and scaling. The mechanisms of fouling on both sides of the

membranes may be different due to the contact of different solutions (in different chambers). The membrane resistance of the CEM increased more significantly because of scaling than that of the AEM with biofouling, suggesting that the CEM will require more maintenance than the AEM during the MDC operation. Biofouling can have a greater effect on the quality of the desalinated water. Although membrane fouling did not significantly decrease the rate of conductivity reduction within the testing period, the negative effect of fouling in a longer period of operation will be expected, and thus proper control of fouling should be considered.

Chapter 5 Bioelectricity inhibits back diffusion from the anolyte into the desalinated streams in microbial desalination cells

(This section has been published as Ping, Q., Porat, O., Dosoretz, C. and He, Z.* (2016) Bioelectricity inhibits back diffusion from the anolyte into the desalinated streams in microbial desalination cells. ***Water Research.*** Vol 88, pp 266-273.)

Abstract

Microbial desalination cells (MDCs) taking advantage of energy in wastewater to drive desalination represent a promising approach for energy-efficient desalination, but concerns arise whether contaminants in wastewater could enter the desalinated stream across ion exchange membranes. Such back diffusion of contaminants from the anolyte into the desalinated stream could be controlled by two mechanisms, Donnan effect and molecule transport. This study attempted to understand those mechanisms for inorganic and organic compounds in MDCs through two independently conducted experiments. Donnan effect was found to be the dominant mechanism under the condition without current generation. Under open circuit condition, the MDC fed with 5 g L^{-1} salt solution exhibited 1.9 ± 0.7%, 10.3 ± 1.3%, and 1.8 ± 1.2% back diffusion of acetic, phosphate, and sulfate ions, respectively. Current generation effectively suppressed Donnan effect from 68.2% to 7.2%, and then molecule transport became more responsible for back diffusion. A higher initial salt concentration (35 g L^{-1}) and a shorter HRT (1.0 d) led to the highest concentration gradient, resulting in the most back diffusion of 7.1 ± 1.2% and 6.8 ± 3.1% of phosphate and sulfate ions, respectively. Three representative organic

compounds were selected for test, and it was found that organic back diffusion was intensified with a higher salt concentration gradient and molecular weight played an important role in compound movement. Principal component analysis confirmed the negative correlation between Donnan effect and current, and the positive correlation between molecule transport and concentration gradient related conditions.

5.1 Introduction

Microbial desalination cell (MDC) is a promising bioelectrochemical system for water supply with simultaneous wastewater treatment and saline water desalination. With anion exchange membrane (AEM) and cation exchange membrane (CEM) installed between the anode and the cathode, an MDC takes advantage of the electrical field generated by anode microbial metabolism and cathode (oxygen) reduction reaction to separate ions in salt solution between the two ion-exchange membranes (Cao et al. 2009). The mechanism of ion separation in an MDC is similar to that of electrodialysis (ED), but its driving force is the energy extracted from organic matters in wastewater by microorganism in the anode. Therefore, an MDC does not require external electrical energy but generates electricity during desalination. As a result, energy consumption by desalination can potentially be low, compared with ED or other industrialized desalination technologies.

MDCs have been developed in two major configurations, cubic shape (Mehanna et al. 2010a, Ping and He 2013b) and tubular shape (Jacobson et al. 2011a, Jacobson et al. 2011b). The desalination can be enhanced through stacked cells (Chen et al. 2011, Kim and Logan 2011), electrolyte recirculation (Qu et al. 2012, Chen et al. 2012), applying small external voltage (Ge et al. 2014), incorporating forward osmosis membrane in situ (Zhang and He 2012) or ex situ (Yuan et al. 2015), adding ion exchange resin (Zhang et al. 2012), or integrating capacitive adsorption (Forrestal et al. 2012). Hydrogen and other chemicals can be produced by combining electrolysis with an MDC (Chen et al. 2012b, Luo et al. 2011). The scale of MDCs has been advanced from milliliters to over 100 liters (Zhang and He 2015). In addition to engineering

development, MDCs have also been investigated with fundamental studies on muti-ion transport behavior from the salt solution (Chen et al. 2012b, Zuo et al. 2013), inter-membrane distance (Ping and He 2014), microbial community in MDC (Luo et al. 2012a), and mathematical modeling (Ping et al. 2014).

Having the adjacent anode compartment containing wastewater separated from salt solution by one piece of AEM, MDCs generate concerns of the crossover of organic and inorganic contaminants from wastewater into the desalinated stream. Our previous study of an MDC operated with a high acetate concentration discovered extensive back diffusion of acetic ions from the anolyte into the salt solution opposite the electrical field, thereby lowering the effluent quality and causing bio-fouling (Ping et al. 2013). We also observed that an MDC fed with wastewater (~260 mg L^{-1} total organic carbon) exhibited mild organic back diffusion (~7 mg L^{-1}) in the desalinated effluent (Ping et al. 2015a). It is reported that substances with negative or neutral charge and with molecular weight less than 350 Da can be transported through AEM (Kim and Logan 2013). Most inorganic anions can freely cross AEM, and thus back diffusion of anions from the anolyte into the salt solution against the electrical field is expected to occur to some degree. Industrialized AEMs usually do not have an ideal 100% permselectivity, and would allow co-ions (cations) to pass through (Kim and Logan 2013). As a result, there is a great possibility that cationic contaminants may be found in the desalinated stream. MDCs are proposed as a pre-desalination process for seawater desalination, or desalinating brackish water; in either application, back diffusion of inorganic ions and organic substances could deteriorate the quality of the desalinated water and create requirement for additional treatment at an expense

of cost and time. Therefore, understanding the process of back diffusion is of great importance for the development of MDC technology. So far there has not been any research focusing on the issue of back diffusion of contaminants in an MDC, which warrants our motivation of this study.

Herein, we proposed two mechanisms of back diffusion in an MDC: first, simple anion exchange (Donnan effect) through AEM with chloride ion in the salt solution moving towards the anolyte by a concentration gradient while forcing anion or negatively charged organics in the anolyte moving into the desalinated stream to balance the charge; and second, molecule transport of equally charged anion and cation or neutral charged organics from the anolyte into the desalinated stream through AEM. Water transport (driven by a concentration gradient) from the anolyte to the salt solution could promote molecule transport, and a high concentration of chloride ion in the salt solution will benefit the Donnan effect. However, current generation would inhibit the Donnan effect. To understand above mechanisms and their effects on back diffusion, we have conducted the MDC experiments fed with synthetic wastewater by 1) manipulating the electric current, an opposing force of back diffusion, 2) altering the salt concentration gradient, a key factor for back diffusion, and 3) varying the salt solution retention time, which is related to salt solution-anolyte interaction time.

5.2 Materials and Methods

5.2.1 MDC setup and operation

The study of inorganic back diffusion was conducted with an MDC that was assembled in a tubular shape similarly to the one in the previous study (Ping et al. 2014), which consisted of two layers of ion exchange membranes (IEM): the inner anion exchange membrane (AEM, AMI-7001, Membrane International, Inc., Glen Rock, NJ, USA) forming the anode compartment (300 mL, diameter of 3.8 cm) with a 20-cm long carbon fiber brush anode electrode inserted inside, and the outer cation exchange membrane (CEM, diameter of 5 cm, CMI-7000, Membrane International, Inc.) wrapped by a piece of carbon cloth coated with activated carbon supported platinum (Pt/C) catalyst (loading rate of 0.2 mg Pt cm^{-2}) as the cathode electrode. The space between those membranes formed a desalination compartment (150 mL). The two ion exchange membrane tubes were sealed at both ends to PVC caps with robust epoxy glue. An external resistor was applied by connecting the two electrodes with titanium wire. The anode feed solution was a synthetic solution containing (per L of tap water): NaAc, 0.5 or 1 g; NH_4Cl, 0.15 g; NaCl, 0.5 g; $MgSO_4$, 0.015 g; $CaCl_2$, 0.02 g; KH_2PO_4, 0.53 g; and K_2HPO_4, 1.07 g. The phosphate concentration was higher than that of a typical domestic wastewater, because of the need for buffering the anolyte. The salt solution in the desalination compartment was prepared by dissolving NaCl in tap water. The catholyte was tap water (to ensure that the anolyte was the only source responsible for back diffusion), dripping from the top to the bottom of the outer (CEM) tube for rinsing the cathode electrode, and recirculated at a rate of 35 mL min^{-1} from a 9-L reservoir. The anolyte had a feeding rate of 0.5 mL min^{-1}, resulting in a hydraulic retention

time (HRT) of 10 h, and was recirculated at 100 mL min^{-1}. The salt solution had a feeding rate of 0.06 or 0.1 mL min^{-1} that had HRT of 1.7 or 1.0 day.

The MDC for characterization of organic back diffusion was set up in a biotic or abiotic environment with an anode volume of 1000 mL and a desalination compartment volume of 250 mL. Three organics were tested, acetate, Paracetamol (PCM) and Ibuprofen (IBP). Acetate represents a small, negatively charged and hydrophilic organic compounds in wastewater. PCM and IBP represent neutral and negatively charged micro-pollutants in municipal wastewater, respectively, of relatively low hydrophobicity. The anode feed solution contained (per L of tap water): (in biotic MDC) NaAc, 1000 mg; PCM, 10 mg; IBP, 10 mg; KH_2PO_4, 2.6 g; K_2HPO_4, 5.4g; NH_4Cl, 0.04 g; NaCl, 0.45 g; $MgSO_4$, 0.2 g; $CaCl_2$, 0.015 g and $NaHCO_3$, 2 g; and Sigma solution (Kim and Logan 2013b), 5 mL; or (in abiotic MDC) each representative organics, 100 mg; NaN_3 (biocide), 100 mg; KH_2PO_4, 2.6 g and K_2HPO_4, 5.4 g. The salt solution in the desalination compartment was prepared with 10 g L^{-1} NaCl in tap water in biotic MDC, or in abiotic MDC with: NaN_3 (biocide), 100 mg; KH_2PO_4, 2.6 g; K_2HPO_4, 5.4g; with or without NaCl, 10 g. The cathode for biotic MDC was rinsed with solution from a 500 mL container containing (per L of tap water) KH_2PO_4, 2.6 g and K_2HPO_4, 5.4g, at recirculation rate of 60 mL min^{-1}. The abiotic MDC was operated with a dry cathode to avoid complications. Both MDCs were operated in a batch mode and solution samples were collected after 2 d of retention time.

5.2.2 Measurement and calculations

The MDC voltage was recorded every 3 min using a digital multimeter (Keithley Instruments, Inc., Cleveland, OH, USA). The conductivity of the salt solution was measured using a benchtop conductivity meter (Mettler-Toledo, Columbus, OH, USA). The chemical oxygen demand (COD) was measured using a colorimeter according to the manufacture manual (Hach Company, Loveland, CO USA). The ion compositions in the solution were measured using ion chromatography (Dionex DX-500) with suppressed conductivity detection. The column used for cations was a CS-16 with a CSRS-300 suppressor and for anions was an AS-9HC with an ASRS-300 suppressor. The concentrations of pharmaceuticals were tracked by liquid chromatography-multiple stage/mass spectrometry (LCMS/MS) (Kim and Logan 2013b). Injections were performed on an Agilent 1200 HPLC (Hewllet Packard) system coupled with an ion spray interface to an API 3200 triple quadropole mass spectrometer (Applied Biosystems). A LiChroCART Purospher STAR RP-18 (Merck) end capped column (4.6 mm × 15 cm, 5 μm pore size) was used with a binary gradient of 0.1% (v/v) formic acid in water and HPLC grade methanol. Electrospray ionization was used in positive ion mode for PCM, and in negative ion mode for IBP with the limit of quantification of 5 μg L^{-1}. The compounds were detected in multiple-reaction monitoring (MRM) mode. Acetate concentration was measured in an 881 compact IC Pro ion chromatograph (Metrohm), equipped with Metrohm A supp 5–150 (with 4 μm pore size) column, and the limit of quantification was 1 mg L^{-1}. A solution of 3.2 mM sodium carbonate and 1.0 mM sodium bicarbonate in 5% acetonitrile was used as eluent. The back diffusion percentage for each ion in continuous operated MDC was calculated by excluding

tap water ion concentration as shown in equation (1). It is worth noting that current-driven ion migration and back diffusion are in opposite directions, and back-diffused ions can also be removed from the desalination compartment by current. These two processes are happening simultaneously. Here we quantified the back diffusion as the result of the two mixed effects which is directly observable:

$$\text{Back diffusion } \% = \frac{(C_{salt,out} - C_{tap})Q_{salt}}{C_{anode,in}Q_{anode}} \quad (1)$$

where $C_{salt,out}$ is the ion concentration in the desalinated stream, C_{tap} is the ion concentration in the tap water, $C_{anode,in}$ is the ion concentration in the anolyte influent, Q_{salt} is the salt solution flow rate, and Q_{anode} is the anolyte flow rate.

The back diffusion percentage and adsorption percentage on the AEM for each organic compound in the batch mode MDC was calculated by equation (2) and (3):

$$\text{Back diffusion } \% = \frac{C_{salt,t}V_{salt,t}}{C_{anode,0}V_{anode,0}} \quad (2)$$

$$\text{Adsorption } \% = \frac{C_{anode,0}V_{anode,0} - (C_{anode,t}V_{anode,t} + C_{salt,t}V_{salt,t})}{C_{anode,0}V_{anode,0}} \quad (3)$$

where $C_{anode,0}$ is the initial organic compound concentration in the anolyte, $C_{salt,t}$ and $C_{anode,t}$ are the organic compound concentrations at time t (2 d in this study) in the salt solution and anolyte, $V_{anode,0}$ is the initial volume of the solution in the anode compartment, $V_{salt,t}$ and $V_{anode,t}$ are the volumes of the solution in desalination and anode compartments at time t.

The percentage of back diffusion contributed by molecule transport and Donnan effect were calculated by equation (4) and (5), respectively. The back-diffused cations were caused by molecule transport from the anolyte, while the back-diffused anions were a work of both molecule transport and Donnan effect:

$$\text{Molecule transport}\,\% = \frac{q_{\text{cation ,total}}}{q_{\text{anion ,total}}} \quad (4)$$

$$\text{Donnan effect}\,\% = \frac{(q_{\text{anion ,total}} - q_{\text{cation ,total}})}{q_{\text{anion ,total}}} \quad (5)$$

where $q_{cation,total}$ is the total charge of contaminant cations in the desalinated stream, and $q_{anion,total}$ is the total charge of contaminant anions in the desalinated stream. Based on the pH value of the salt solution, the hydrolytic equilibrium of phosphate ion was applied in determining its form (hydrogen phosphate ion or dihydrogen phosphate ion), which affects the calculation of total charge of anions.

The osmotic water flux from the anolyte to the salt solution was calculated according to Van't Hoff's equation as in equation (6):

$$Q_{\text{osmosis}} = A_{\text{AEM}}\, RTi\left(C_{\text{salt ,out ,total}} - C_{\text{anode ,out ,total}}\right) \quad (6)$$

where A_{AEM} is the water permeability of AEM, R is the gas constant, T is the temperature, i is the Van't Hoff factor, and the last part of the equation is the total mole concentration difference between the desalinated stream and anolyte effluent.

Principal component analysis (PCA) as a multivariate statistical tool was performed in R to determine the key factors causing back diffusion. The data matrix was scaled to have a mean of 0 and standard deviation of 1 to ensure equal weights of all variables before singular value decomposition was done. PCA transforms original variables into new uncorrelated variables called principal components. The first component (PC1) contains the highest variance, and the second component (PC2) has the second highest variance. Biplot displays the loadings (for the variables) and scores (for the samples) generated from PCA to visualize the similarity or difference between samples.

5.3 Results and Discussion

5.3.1 Effect of current generation on inorganic back diffusion

Theoretically, current generation drives anion movement from the deasalination compartment to the anode compartment, against back diffusion. The actual effect of current generation on back diffusion of inorganic ions was investigated by varying external resistance loading (which changed current generation) with an initial salt solution concentration of 5 or 35 g L^{-1}. By examining the anolyte composition, three anions (acetic, phosphate, and sulfate ions) and three cations (magnesium, potassium, and calcium ions) were selected as dominant back diffusion ionic species for study. Acetic ion is listed here because acetate was the substrate for microorganism growth, and contributed to total back diffusion. Sodium and chloride ions were excluded from back diffusion ions, because they were the native ions in the salt solution with significantly high concentrations. There is a clear trend that with the increased current the back

diffusion of anions was suppressed under both initial salt concentrations (Figure 5.1). At 0 current generation (open circuit-OC with no current-driven anion movement from the desalination compartment to the anolyte) with an initial salt of 5 g L^{-1}, the back diffusion percentages of acetic, phosphate, and sulfate ions were 1.9 ± 0.7%, 10.3 ± 1.3%, and 1.8 ± 1.2%, respectively. When an external resistor of 100 Ω was applied to increase the current generation to 13.0 A m^{-3} (desalination efficiency of 41.3 ± 1.9 % with current-driven anion movement (mostly chloride ion) from the desalination compartment to the anolyte at the rate of 23.2 mmol L^{-1} d^{-1}), the back diffusion percentages of those three anions decreased to 0.3 ± 0.1%, 4 ± 0.7%, and 0%, respectively. Further increasing current production to 26.7 A m^{-3} by reducing external resistance to 0.1 Ω (desalination efficiency of 79.2 ± 4.7 % with current-driven anion movement at the rate of 47.8 mmol L^{-1} d^{-1}) almost inhibited the crossover of acetic and sulfate ions completely, and reduced the back diffusion percentage of phosphate ions to 2.3 ± 0.4% (Figure 5.1A). The experiment with 35 g L^{-1} of the initial salt concentration showed the same trend for individual back diffusion due to current effect, with the back diffusion percentages of acetic, phosphate, and sulfate ions at 4.7 ± 0.2%, 17.5 ± 4.4%, and 11.8 ± 1.4% at zero current, which decreased to 2.0 ± 2.8%, 5.7 ± 1.9%, and 4.6 ± 4.3%, respectively, at current generation of 34.2 A m^{-3} (desalination efficiency of 49.0 ± 0.4 % with current-driven anion movement at the rate of 61.2 mmol L^{-1} d^{-1}) (Figure 5.1B). There is no notable trend in the back diffusion of cations under different current generation (Figure 5.2); however, the data provide useful information in obtaining the molecule transport and Donnan effect percentage (equation (4) and (5)).

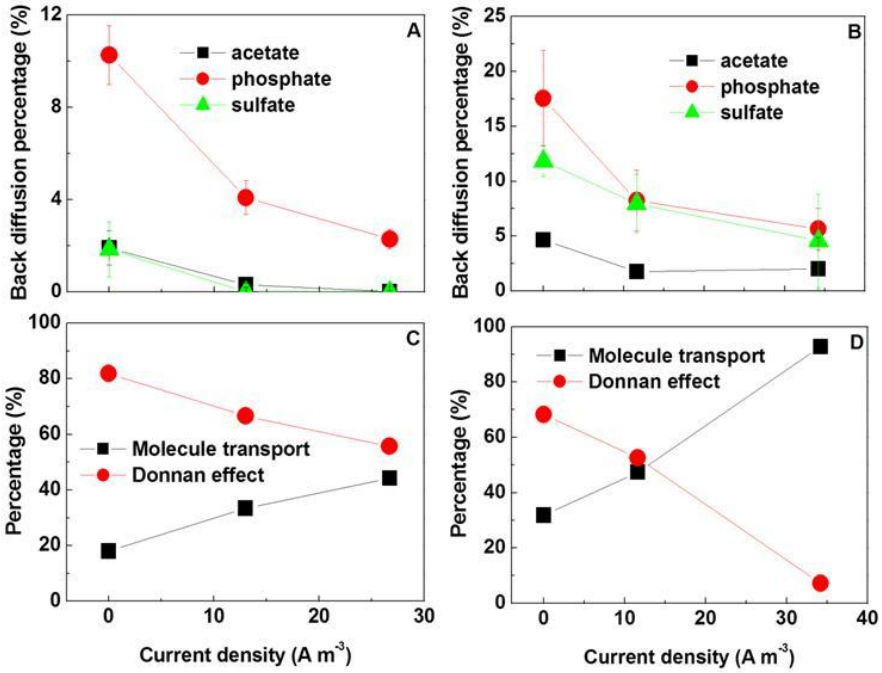

Figure 5.1 Back diffusion of anions and contribution of each mechanism to back diffusion affected by current generation: (A) anion back diffusion at an initial salt concentration of 5 g L^{-1} ; (B) anion back diffusion at an initial salt concentration of 35 g L^{-1}; (C) contribution of each mechanism to back diffusion at an initial salt concentration of 5 g L^{-1}; and (D) contribution of each mechanism to back diffusion at an initial salt concentration of 35 g L^{-1}.

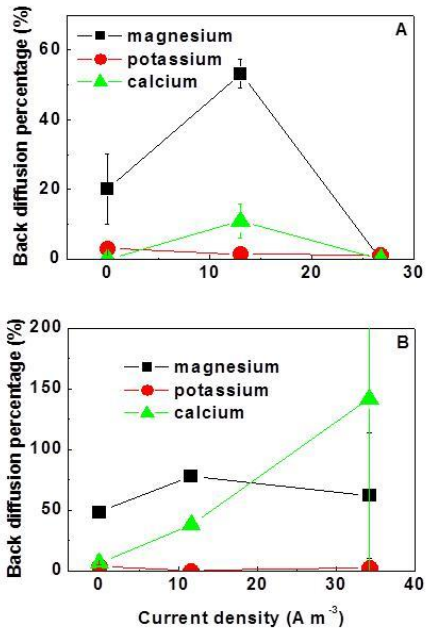

Figure 5.2 Back diffusion percentage of different cations in MDC at different current generation with initial salt concentration of A) 5 g L^{-1} and B) 35 g L^{-1}.

The high salinity in the salt solution and low salinity in the anolyte creates a concentration gradient, which may play different roles in the two back-diffusion mechanisms. In the Donnan effect, the abundant chloride ions in the salt solution move through AEM to the anolyte due to the chloride concentration difference and this movement forces other anions in the anolyte to migrate into the salt solution. Because the concentration gradient is mainly caused by NaCl in the salt solution, the higher initial salt concentration would lead to a greater Donnan effect. In the molecule transport, a higher concentration gradient leads to a higher osmotic pressure and thus more water transport from the anolyte to the salt solution, which drives more molecules to transfer to the salt solution. Current generation results in a lower salinity in the salt solution, and

decreased the concentration gradient between the anolyte and the salt solution. Therefore, current and concentration gradient have contradictory effects on back diffusion.

In the test with 5 g L^{-1} initial salt concentration, higher current and resulted smaller concentration gradient between the salt solution and the anolyte (-1.9 mS cm^{-1} at 26.7 A m^{-3} compared with 1.2 mS cm^{-1} at 13.0 A m^{-3}, and 4.6 mS cm^{-1} at 0 A m^{-3}) both led to less back diffusion. Having the same concentration gradient variation trend caused by current generation, the test with 35 g L^{-1} initial salt concentration had approximately two times the back diffusion percentage compared with 5 g L^{-1} at each current generation condition (Figure 5.1A&B). The cause of more severe back diffusion was the higher concentration gradient which increased from -1.9~4.6 mS cm^{-1} with 5 g L^{-1} to 28.0~35.4 mS cm^{-1} with 35 g L^{-1}. The effect of different initial salt concentrations on back diffusion will be discussed in details in the next section.

The Donnan effect was more influential than the molecule transport at no current generation. The molecule transport accounted for 18.0% (or 31.8%) of the total back diffusion at 5g L^{-1} (or 35 g L^{-1}), and Donnan effect accounted for 82.0% (or 68.2%) (Figure 5.1C&D). Current generation suppressed the relative Donnan effect, and led to higher relative molecule transport. At 26.7 A m^{-3}, the two mechanisms accounted nearly 50% each for the back diffusion at 5 g L^{-1} initial salt concentration. Increasing the salt concentration to 35 g L^{-1} decreased the Donnan effect generally, likely because of stronger molecule transport due to higher concentration gradient. The molecule transport accounted for 92.8% of the total back diffusion, and Donnan effect accounted for 7.2%

at current generation of 34.2 A m^{-3}, indicating that Donnan effect was almost inhibited due to strong anion movement from the salt solution to the anolyte driven by current, and molecule transport was most responsible for the back diffusion (Figure 5.1D).

5.3.2 Effect of initial salt concentration and salt retention time on inorganic back diffusion

The experiments were conducted at external resistance of 0.1 Ω (for high current generation) under two sets of conditions, a flow rate of 0.06 or 0.1 mL min^{-1} (HRT of 1.7 and 1.0 d) and the initial salt concentration of 5 or 35 g L^{-1}. The desalination efficiency ranged from 25.4 to 79.2 %, and a longer HRT or a lower initial salt concentration resulted in higher desalination efficiency.

A higher initial salt concentration promoted back diffusion. For example, the initial salt concentration of 35 g L^{-1} resulted in 4.2 ± 2.0% and 7.1 ± 1.2% of phosphate back diffusion at HRT 1.7 and 1.0 d, respectively, much higher than 2.3 ± 0.4% and 6.6 ± 0.6% with 5 g L^{-1}. Similar results were obtained with sulfate back diffusion that had 2.2 ± 0.4% and 6.8 ± 3.1% with 35 g L^{-1} under two HRTs, and there was no observable back diffusion with 5 g L^{-1}. Almost no acetic ions were found in the salt solution under these testing conditions (Figure 5.3A), likely due to the high current generation at 26.7~28.2 A m^{-3}. Higher initial salt concentration also brought in more back diffusion of cations (magnesium and calcium) with 35 g L^{-1}, of which the greater than 100% back diffusion was due to the extreme small concentration of magnesium and calcium in the anolyte (less than 10 mg L^{-1}), and even a little residual in the desalination compartment or desorption from the ion exchange membranes could raise the percentage

dramatically. There was no observable back diffusion of magnesium and calcium with 5 g L^{-1}. The change of the back diffusion of potassium due to initial salt concentration was not distinct (Figure 5.3B).

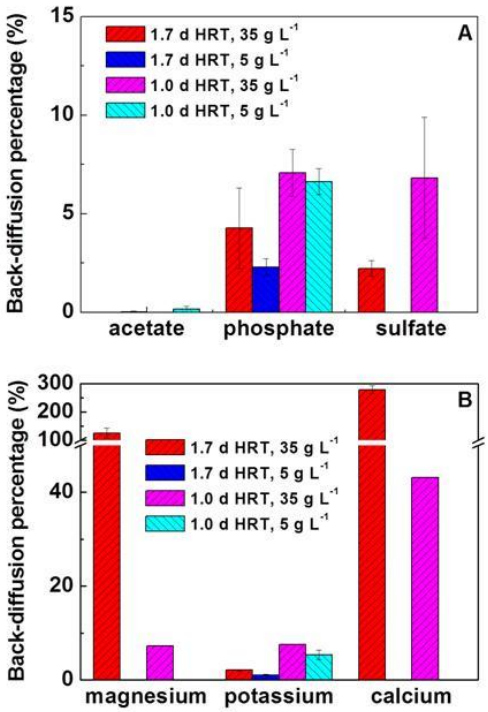

Figure 5.3 Back diffusion affected by HRTs and initial salt concentrations: (A) anion back diffusion; (B) cation back diffusion.

A higher salt concentration in the salt solution is expected to have a greater Donnan effect, considering that more chloride ions would exchange more anions in the anolyte. However, that was not supported by the experimental results shown in Figure 5.4A, which exhibits stronger effect of molecule transport on back diffusion when the salt concentration gradient was high. Donnan effect was inhibited under high current generation, and the high salt concentration in the salt solution mainly contributed to molecule transport back diffusion. Molecule transport was

severe at high salt initial concentrations, the greater concentration gradient between the anolyte and the salt solution (32.3 and 39.6 mS cm^{-1} at 35 g L^{-1} (Figure 5.4B)) led to more water transport across the AEM towards the salt solution (0.009 and 0.010 mL min^{-1} at 35 g L^{-1}), and as expected brought more back-diffused salts into the salt solution. The negative value of Donnan effect or the > 100% molecule transport was due to the fact that back-diffused cations were more than anions, probably because back-diffused anions were removed out of the salt solution by current.

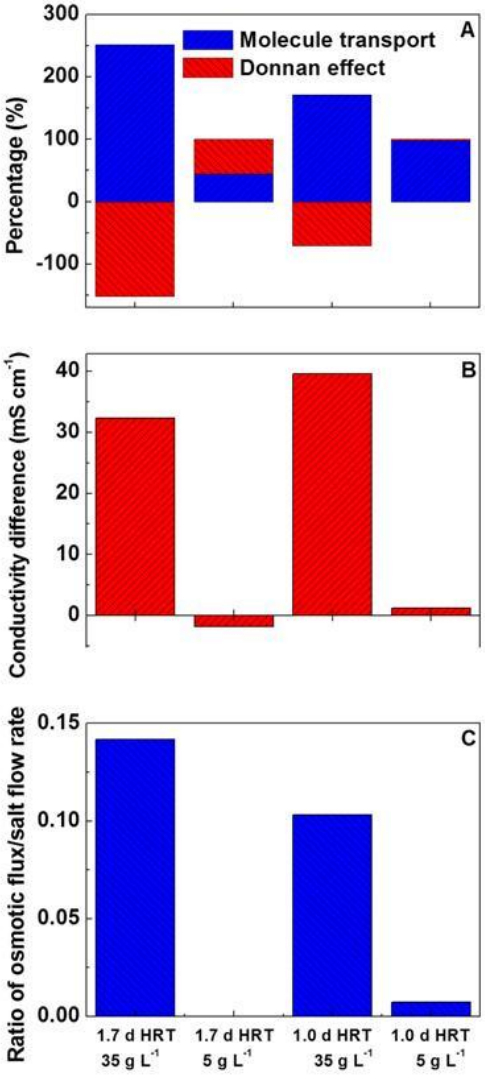

Figure 5.4 Back diffusion affected by HRTs and initial salt concentrations: (A) contribution of Donnan effect and molecule transport attribution to back diffusion; (B) concentration gradient between the anolyte and the salt solution; and (C) the ratio between osmotic water flux and salt solution flow rate.

A shorter HRT accelerated the back diffusion due to a greater overall concentration gradient that enhanced both the Donnan effect and molecule transport. While the ratio of osmotic water flux over salt solution flow rate that determined the severity of molecule transport was lower at longer HRT with 5 g L^{-1}, and higher at longer HRT with 35 g L^{-1}. With 5 g L^{-1}, the molecule transport effect was much greater (97.2%) than Donnan effect (2.8%) at HRT 1.0 d, while the two mechanisms had comparative effect at HRT 1.7 d. The ratio of osmotic water flux over salt solution flow rate indicated an insignificant amount of water was transported from the salt solution to the anolyte (opposite direction of osmotic water flux) at 1.7 d HRT, while at HRT 1.0 d water was transported from the anolyte to the salt solution at a flow rate ratio of 0.007 (Figure 5.4C). When the osmotic water flux exhibited opposite direction, the molecule transport of other anions from the anolyte to the salt solution was only caused by the individual anion concentration differences between the anolyte and the salt solution, and thus molecule transport was not significant at 1.7 d HRT. The osmotic water flux was more significant with a higher initial salt concentration of 35 g L^{-1}. Despite the comparably lower concentration gradient at longer HRT (32.3 mS cm^{-1} at 1.7 d compared with 39.6 mS cm^{-1} at 1.0 d) (Figure 5.4B), the effect of molecule transport was greater (2.52% at 1.7 d compared with 1.71% at 1.0 d). The higher ratio between the osmotic water flux and salt solution flow rate (0.14 at 1.7 d HRT, higher than 0.10 at 1.0 d HRT) explained the elevated molecule transport (Figure 5.4C). With high

current generation, the osmotic water flux that led to molecule transport played an important role in back diffusion.

Those results suggest that back diffusion of inorganic ions under electricity generation could be minor. A longer salt retention time does not lead to more back diffusion as a consequence of the smaller concentration gradient as well as the resulted lower osmotic water flux, especially for desalinating brackish water. However, using MDCs as a pretreatment desalination process of seawater is more likely to cause more back diffusion contamination due to a higher concentration gradient (higher osmotic water flux) between the anolyte and salt solution. The ratio between osmotic water flux and salt solution flow rate needs to be precisely designed in real application to minimize back diffusion.

5.3.3 Organic back diffusion

Three organics were tested in the anode of MDC, NaAc, paracetamol and ibuprofen with molecular weight of 82, 151, and 206 Da, respectively. The open circuit test showed back diffusion percentage of 16 ± 0.5%, 1.3 ± 0.8%, and 2.8 ± 1.1% for acetate, PCM, and IBP, respectively. Applying an external resistor of 10 Ω with a current generation of 1.2 ± 0.5A m^{-3} reduced the back diffusion of acetate and IBP slightly to 12.1 ± 3.2% and 2.1 ± 1.5%, whereas no reduction was observed with PCM (2.9 ± 1.7%) due to its neutral charge and negligible biological degradation in the presence of acetate (more readily degradable) (Figure 5.5A). High back diffusion of acetate in this batch mode MDC was due to the limitation of low bacteria

consumption rate/low current generation that led to a high acetate concentration gradient between the anolyte and desalinated stream throughout the test period in both OC and current modes. The high acetate concentration left in the anolyte (1600 mg L^{-1} with OC and 1300 mg L^{-1} with current at the end of the 48-h batch test) and the salt concentration gradient (10 g L^{-1} at 0-h and 6 ± 1 g L^{-1} at 48-h) that would lead to a considerable amount of osmotic water flux likely determined that the dominant mechanism of acetate back diffusion was molecule transport, and current generation (reduced Donnan effect) had relatively less impact on back diffusion. Back diffusion of PCM and IBP was very low, probably because of their higher molecular size.

To eliminate the factor of bacterial degradation of organics, experiments were carried out in an abiotic MDC to examine the effect of salt concentration in desalination compartment on back diffusion of three representative organics with the same initial concentration 100 mg L^{-1}. Results were compared under two conditions, with 0 or 10 g L^{-1} NaCl solution in the desalination compartment, which resulted in 15.6 ± 2.8% or 20.7 ± 6.9% back diffusion of acetate, 3.1 ± 0.3% or 2.3 ± 1.0% back diffusion of PCM, 0.7 ± 0.7% or 1.3 ± 0.8% back diffusion of IBP (Figure 5.5B). Control experiments conducted with equal concentrations of organics in both anode and desalination compartment (no organic concentration gradient or salt concentration gradient) showed no back diffusion. With 0 g L^{-1} NaCl in the desalination compartment, no salt concentration gradient was present between the anode and desalination compartments, and molecule transport due to organic concentration gradient was the sole driving force for back diffusion. Acetate was most prone to back diffusion followed by PCM and IBP, and the trend is relevant to their molecular weight (NaAc < PCM < IBP) that leads to diffusion coefficient

(NaAc > PCM > IBP), which is in accordance with Fick's law stating that under the same concentration gradient, the molecules with the larger diffusion coefficient will have greater flux. Under the influence of additional 10 g L^{-1} salt concentration in the desalination compartment, both Donnan effect and intensified molecule transport (due to osmotic water flux of 9 ± 3 mL from the anolyte to the salt solution) enhanced the back diffusion of acetate, while the effect on IBP and PCM was not notable. It is worth noting that PCM was only subjected to molecule transport because of its neutral charge. The large molecular weight and hydrophobicity of PCM and IBP possibly hindered their crossing over the AEM, and ended up trapped in the hydrophobic AEM (contact angle of 87.0 ± 3.5). The adsorption of organics on the AEM was 32.6 ± 1.1% under salt effect (30.2 ± 1.2% under no salt effect) for acetate, 37.7 ± 14.7% (44.3 ± 1.5%) for PCM and 62.5 ± 3.1% (74.9 ± 8.6%) for IBP (Figure 5.5C). The larger amount of organics trapped in the AEM with additional salt present in the desalination compartment clearly demonstrates the more intense movement of organics towards the desalination compartment under effect of osmotic water flux (and Donnan effect for charged organics). The absorption intensity order was IBP > PCM > NaAc, which is closely correlated to their molecular weight and hydrophobicity (IBP>PCM>NaAc). The larger molecular weight and greater hydrophobicity, the more likely the compound would be trapped by the AEM, and not cause back diffusion in the salt solution.

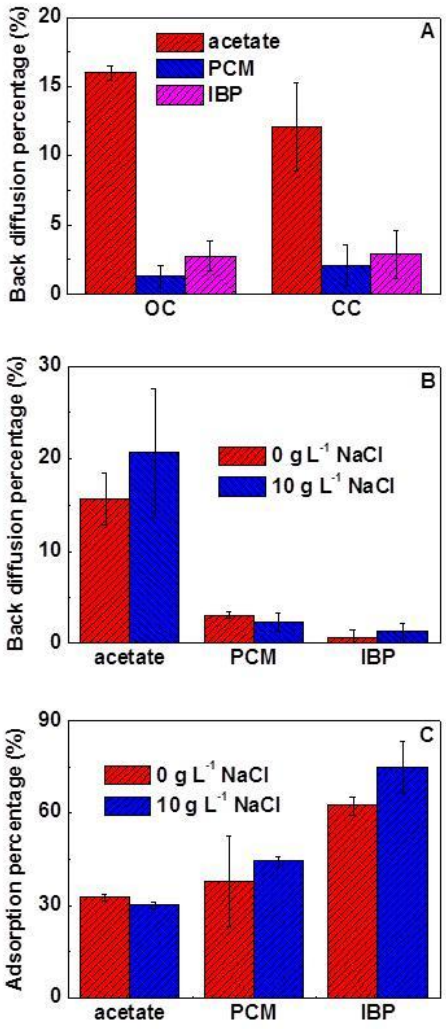

Figure 5.5 Back diffusion of selected organic compounds: (A) back diffusion in an MDC under open and closed circuit conditions; (B) back diffusion in an abiotic MDC with 0 g L^{-1} and 10 g L^{-1} NaCl in the desalination compartment; and (C) adsorption of three organic compounds on the AEM in abiotic MDC with 0 g L^{-1} and 10 g L^{-1} NaCl in the desalination compartment.

5.3.4 Principal Component Analysis

To further analyze the key factors affecting back diffusion (continuous mode), variables such as current, concentration difference between the salt solution and the anolyte, osmotic water flux, as well as the ratio between osmosis flux and salt flow rate were taken into account and processed through principal component analysis (PCA). The PCA biplot mainly separated the MDC performance into two major groups associated with different initial salt concentrations of 5 g L^{-1} and 35 g L^{-1}, with Principal Component 1 (PC1) and Principal Component 2 (PC2) picking up 52.1% and 37.4% of the variation of the data, respectively, and 89.5% in total (Figure 5.6). A close positive correlation between concentration gradient related variables and molecule transport was shown, as well as a negative correlation between current and Donnan effect, supporting our conclusion that a higher concentration gradient promotes molecule transport, and higher current inhibits Donnan effect. The scree plot with parallel analysis shows the eigenvalues of two components are above 1 suggesting that appropriate number of principal components is two, and thus a rotation method "varimax" with two components were performed in order to clarify the structure of the loadings matrix. The off diagonal fitting was achieved at 99%. The first rotated component heavily loaded on molecule transport, the concentration gradient, osmotic water flux, as well as the ratio between osmosis flux and salt flow rate (0.81~0.97), which further confirmed the close association between the four variables, indicating that molecule transport back diffusion increases with a higher concentration gradient/osmotic water flux. The second rotated component is strongly associated with Donnan effect (0.96), and negatively loaded on current (-0.92), which suggests the negative correlation between the two variables and that Donnan effect decreases with stronger current. The variable back diffusion of anions was heavily loaded on the second rotated component (0.93), which explains the effect of

current was more potent than concentration gradient on back diffusion (Table 5.1). It can be concluded that with high current generation, concentration gradient will be diminished and thus molecule transport can be minimized.

Table 5.1 Standardized loadings based upon correlation matrix (Principal Components Method with rotation)

	RC1	**RC2**	**h2**	**u2**
Jw	0.97	0.05	0.94	0.057
F_ratio	0.97	0.14	0.96	0.037
deltaC	0.97	0.05	0.94	0.057
current	-0.01	-0.92	0.85	0.150
BD_anion	0.27	0.93	0.93	0.067
MT	0.81	-0.11	0.68	0.323
DE	-0.16	0.96	0.95	0.049

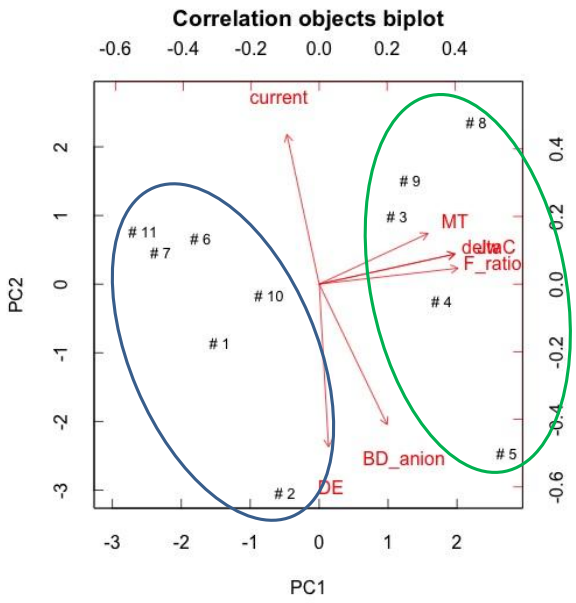

Figure 5.6 PCA bipolot with scores and loadings for MDC plotted on the first two components, where the number labeled points are the MDC with different operation conditions (in terms of initial salt concentration and external resistance), MT is the molecule transport, DE is the Donnan effect, BD_anion is the back diffusion of anions, deltaC is the concentration difference between the anolyte and the salt solution, Jw is the osmotic water flux, and F_ratio is the ratio of osmotic water flux over salt flow rate.

5.4 Conclusions

This study has presented two mechanisms for contaminant back diffusion from the anolyte into the desalinated stream in an MDC, Donnan effect for negatively charged ion exchange and molecule transport driven by osmotic water flux. Current generation could inhibit Donnan effect and result in relatively higher percentage of molecule transport. Organic matters with a larger

molecular weight and greater hydrophobicity could be retained by the AEM resulting in less back diffusion. Desalinating a higher-salinity stream (e.g., seawater) will likely cause more back diffusion than that with a low-salinity stream (e.g., brackish water), because of a higher osmotic water flux resulted from a greater concentration gradient between the anolyte and salt solution. The ratio between osmotic water flux and salt solution flow rate was found to be a critical design criterion for MDC development. These findings have enhanced our understanding of back diffusion in MDCs and provide useful information for the further development.

Chapter 6 Integrated Experimental Investigation and Mathematical Modeling of Brackish Water Desalination and Wastewater Treatment in Microbial Desalination Cells

(This section has been published as Ping, Q., Huang, Z., Dosoretz, C. and He, Z.* (2015) Integrated experimental investigation and mathematical modeling of brackish water desalination and wastewater treatment in microbial desalination cells. ***Water Research.*** Vol 77, pp 13-23.)

Abstract

Desalination of brackish water can provide freshwater for potable use or non potable applications such as agricultural irrigation. Brackish water desalination is especially attractive to microbial desalination cells (MDCs) because of its low salinity, but this has not been well studied before. Herein, three brackish waters prepared according to the compositions of actual brackish water in three locations in Israel were examined with domestic wastewater as an electron source in a bench-scale MDC. All three brackish waters could be effectively desalinated with simultaneous wastewater treatment. The MDC achieved the highest salt removal rate of 1.2 g L^{-1} d^{-1} with an initial salinity of 5.9 g L^{-1} and a hydraulic retention time (HRT) of 0.8 d. The desalinated brackish water could meet the irrigation standard of both salinity (450 mg L^{-1} TDS) and the concentrations of major ionic species, given a sufficient HRT. The MDC also accomplished nearly 70% removal of organic compounds in wastewater with Coulombic efficiency varied between 5-10%. A previously developed MDC model was improved for brackish water

desalination, and could well predict salinity variation and the concentrations of individual ions. The model also simulated a staged operation mode with improved desalination performance. This integrated experiment and mathematical modeling approach provides an effective method to understand the key factors in brackish water desalination by MDCs towards further system development.

6.1 Introduction

Because of the world-wide water shortage and local water scarcity, desalination has been increasingly considered as a viable approach for freshwater supply (National Research Council 2008). The recently emerged microbial desalination cell (MDC) appears to be a promising alternative or supplement for traditional desalination technologies. An MDC converts the energy stored in wastewater directly into electricity by microorganisms and utilizes it *in situ* to drive desalination in a process similar to electrodialysis (ED) (Cao et al. 2009). The difference between MDC and ED is the source of electrons and energy consumption: an MDC uses the electrons released by microbial oxidation of organic compounds, while an ED is driven by electrons from water oxidation; as a result, an MDC does not necessarily require external voltage, but an ED must be applied with a high external voltage or current. The MDC has been advanced with reactor configurations, such as stacked reactor (Kim and Logan 2011, Chen et al. 2011a), decoupled reactor (Ping and He 2013b), and upflow tubular reactor that has demonstrated a salt removal efficiency > 99% (Jacobson et al. 2011a). Optimized operation through recirculation between the anode and the cathode compartments could achieve pH balance without the addition of costly buffer (Chen et al. 2012a, Qu et al. 2012). Fundamental studies have also been conducted to reveal the diverse microbial community in the anode of MDC (Luo et al. 2012a). Recently, MDCs have been scaled up to a total liquid volume of 105 L, which encourages further development of this technology (Zhang and He 2015).

Although MDCs can achieve desalination without external voltage applied, its desalination requires a fairly long time because of slow microbial oxidation, compared with electrochemical

oxidation of water in ED. The low desalination rate of MDCs indicates that this technology may be more suitable for application as a pre-desalination process for conventional desalination such as RO (reverse osmosis) or ED (Zhang and He 2012). Another potential application of MDC technology is to desalinate low-salinity water, such as brackish water that has TDS (total dissolved solids) in the range of 1,000 to 10,000 ppm (Levite 1972), or the treated wastewater. In many arid parts of the world, the local aquifers that contain brackish water are the main source of freshwater. It is of great importance to desalinate brackish water for municipal or agricultural applications. ED and EDR (electrodialysis reversal) are the current technologies for treating brackish water with TDS up to 3,500 mg L^{-1}; a higher salinity significantly increases the energy consumption compared with RO (USBR 2003). The salinity in brackish water comes from two sources: dissolution of minerals, and natural mixing of seawater with groundwater in coastal aquifers (Zhang and He 2012d). Most brackish water cannot be directly used for drinking purpose or irrigation due to the high salinity, and specific ion toxicity for plants or the possibility of deteriorating soil conditions (Rhoads et al. 1992). There have been several MDC studies that examined desalination of synthetic salt solution with salinity similar to brackish water (Zuo et al. 2013, Luo et al. 2012e). The study of actual brackish water was reported only in a previous work that focused on the softening of hardness in several groundwater samples (Brastad and He 2013). The transport behavior of multiple ions across ion-exchange membranes were studied at the same initial molar concentration with only one kind of counter ion (anion/cation) (Luo et al. 2012c); however the results cannot be applied to predict the ion composition in the actual brackish water desalination where the individual ion has different concentration. The transport rate of individual ions is a product of mobility (affected by hydrated radius and ionic charge) and ion concentration (Strathmann 2004), while the previous study only considered hydrated radius

as influencer. Clearly, there is a lack of detailed analysis and understanding of removal of different ionic species during desalinating actual brackish water or saline water with more complicated composition than NaCl solution in MDCs.

To assist the interpretation of the data obtained from the bench studies and to provide guidance for system operation, mathematical models of MDCs treating brackish water will be very valuable. Recently, the first MDC model was reported and it could effectively predict MDC performance under different operating conditions (Ping et al. 2014). However, the model did not well predict the change in salt concentration, likely related to that the low current efficiency, which mostly occurs when maximum current is not reached, was neglected in the model development. Desalinating brackish water in an MDC by using the energy obtained from domestic wastewater comes with two issues: low organic strength in the anode compartment, and low salinity in the desalination compartment, both of which will lead to current deviating from normal values and the low current efficiency due to low current generation. In addition, diffusion element in the previous model might not work for brackish water considering the difference in salt concentration across ion exchange membranes. Therefore, the previously developed MDC model must be improved with new information obtained from brackish water desalination.

In this study, we have adopted an integrated approach of experimental investigation and mathematical modeling to study brackish water desalination in bench scale MDCs. Three synthetic brackish waters were prepared with the recipes to mimic actual brackish water in three

locations in Israel. Actual domestic wastewater (primary effluent) was used as an anode substrate to provide driving force for desalination. The objectives of this study were: (1) to demonstrate the MDC performance treating brackish water and actual wastewater; (2) to understand the removal of different ionic species during desalination; and (3) to improve the MDC model for brackish water desalination by incorporating junction potential, current efficiency, restricted diffusion, and osmotic flux. The model was calibrated with steady state values and validated by experimental data of both dynamic and steady state conditions.

6.2 Materials and Methods

6.2.1 MDC setup and operation

The MDC was constructed as a tubular reactor similarly to the one in the previous study (Brastad and He 2013b), consisting of two layers of ion exchange membranes (IEM): anion exchange membrane (AEM, AMI-7001, Membrane International, Inc., Glen Rock, NJ, USA) with a 3.8-cm diameter and 20-cm length formed the anode compartment (300 mL), and cation exchange membrane (CEM, CMI-7000, Membrane International, Inc.) that had a diameter of 5 cm and a length of 20 cm wrapped the AEM tube and created a space between the two membrane tubes forming a desalination compartment (150 mL) (Figure 6.1). The distance between the AEM and the CEM was 0.6 cm. The anode electrode was a 20-cm long carbon fiber brush, and the cathode electrode was a piece of carbon cloth coated with activated carbon supported platinum (Pt/C) as a catalyst at a loading rate of 0.2 mg Pt cm^{-2}. An external resistor of 0.1 Ω connected the two electrodes by using titanium wire. The anode feed solution was the primary effluent from a local

wastewater treatment plant (Peppers Ferry, Radford, VA, USA), and amended with 500 mg L^{-1} of glucose. The modified wastewater contained a COD (chemical oxygen demand) concentration varying between 500~650 mg L^{-1}. Three brackish waters were prepared by dissolving different salt compounds into tap water according to the composition shown in Table 6.1. The catholyte was prepared same as the brackish water used in the desalination compartment, dripping from the top to the bottom of the outer (CEM) tube for rinsing the cathode electrode and recirculated from a 9-L reservoir at a recirculation rate of 35 mL min^{-1}. The anolyte had a feeding rate of 0.5 mL min^{-1}, resulting in a hydraulic retention time (HRT) of 10 h, and was recirculated at 100 mL min^{-1}. The brackish water was fed into the desalination compartment without recirculation at three flow rates, 0.015 mL min^{-1} (HRT of 6.9 d), 0.06 mL min^{-1} (HRT of 1.7 d), and 0.13 mL min^{-1} (HRT of 0.8 d) for the brackish water A, or 0.06 mL min^{-1} (HRT of 1.7 d), 0.13 mL min^{-1} (HRT of 0.8 d), and 0.3 mL min^{-1} (HRT of 0.35 d) for the brackish waters B & C.

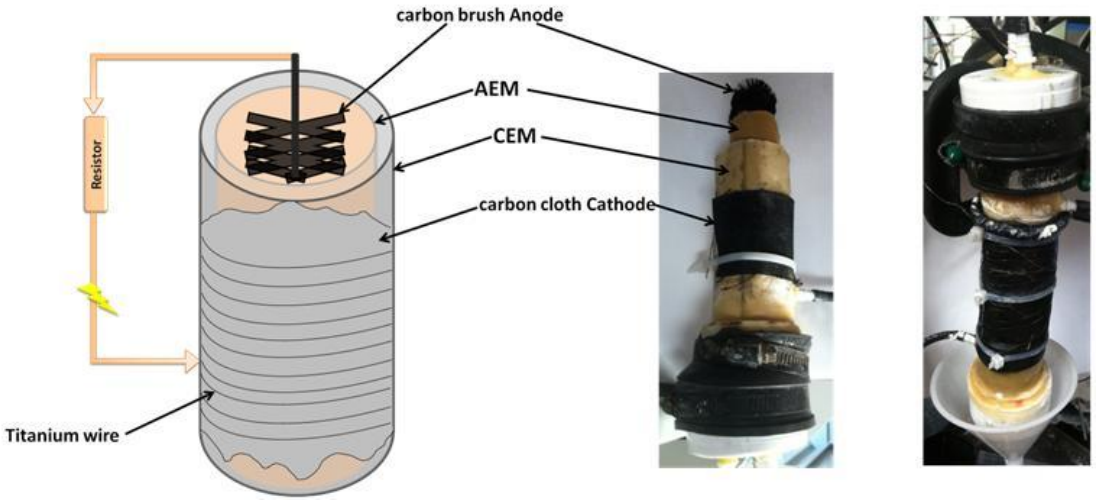

Figure 6.1 Schematic of a tubular MDC

Table 6.1 The concentrations of major ions (mg L^{-1}) in three brackish waters

Brackish water composition	A	B	C
Ca^{2+}	742	105	71.7
Mg^{2+}	207	78	56.1
Na^{+}	1054	364.5	235
K^{+}	26	5.3	3.7
NH_4^{+}	0.0	0.0	0.0
HCO_3^{-}	92	405	369.4
SO_4^{2-}	781	88	68
Cl^{-}	2942	620.3	366
NO_3^{-}	3.5	65.6	50
TDS	5887.7	1540	1068

6.2.2 Measurement and analysis

The MDC voltage was recorded every 3 min using a digital multimeter (Keithley Instruments, Inc., Cleveland, OH, USA). The conductivity of the salt solution was measured using a benchtop conductivity meter (Mettler-Toledo, Columbus, OH, USA). The chemical oxygen demand (COD) was measured using a colorimeter according to the manufacture manual (Hach Company, Loveland, CO USA). The ion compositions in the solution were measured using ion chromatography (Dionex DX-500) with suppressed conductivity detection. The column used for

cations was a CS-16 with a CSRS-300 suppressor and for anions was an AS-9HC with an ASRS-300 suppressor. The TOC (total organic carbon) of the samples was measured by Shimadzu Scientific Instruments TOC-VCP with combustion catalytic oxidation/NDIR detection method. The salt removal rate was calculated as the removed salt concentration divided by HRT.

6.3 Model Improvement

6.3.1 Electricity generation

Junction potential created by concentration gradient across the IEM is an additional potential source responsible for the ion-separation besides the potential difference created by electrode reactions. In an MDC treating wastewater and seawater, the junction potential is up to 0.2 V. For brackish water desalination, when the salt concentration in the desalination compartment is reduced lower than in the anolyte or catholyte, the junction potential poses a negative effect on the current generation, In this updated model, the junction potential is defined as (Kim and Logan 2013):

$$V_{jct} = \frac{RT}{F}\left|\sum_{ion}\frac{t_{AEM,ion}}{z_{ion}}ln\left(\frac{a_{ion,m}}{a_{ion,a}}\right)\right| + \frac{RT}{F}\left|\sum_{ion}\frac{t_{CEM,ion}}{z_{ion}}ln\left(\frac{a_{ion,m}}{a_{ion,c}}\right)\right| \quad (1)$$

where $t_{AEM,ion}$ and $t_{CEM,ion}$ are the transport number of ionic species in AEM and CEM, z_{ion} is the ionic charge, $a_{ion,m}$, $a_{ion,a}$, and $a_{ion,c}$ are the ionic activity in the desalination, anode, and cathode compartments, F is the Faraday constant (96,485 A s mole^{-1}), R is the ideal gas constant (8.31 J K^{-1} mol^{-1}), and T is the MDC temperature (298.15 K). In an MDC, the junction potential can be

roughly estimated by assuming that the activity ratio equals the total dissolved solids ratio. The ideal t_{Na+} and t_{Cl-} will be 0 and 1 for AEM, and 1 and 0 for CEM.

The MDC current is then calculated as:

$$I_{MDC} = \frac{V_{\mathrm{OC}} - OP_{\mathrm{conc}} + V_{jct}}{(R_{\mathrm{ext}} + R_{\mathrm{int}})} \quad (2)$$

where V_{OC} is the open circuit cell voltage that depends on the anodophilic microorganism concentration, OP_{conc} is the concentration overpotential and R_{int} is the internal resistance of the MDC, which were defined in the previous study (Ping et al. 2014). R_{ext} is the applied external resistance.

6.3.2 Mass balance of salt in MDCs

To better show the removal of individual ions in brackish water, the present model takes milliequivalent ions per liter (meq L^{-1} = mg L^{-1} ÷ equivalent weight) as the unit for salt concentration instead of mol L^{-1} in the previous model. We incorporate in the present model the current efficiency α, which shows the ratio between the coulombs harvested from the movement of salt ions and the coulombs harvested from electrical circuit. The ideal situation is that one mole of electrons would take away two molar-equivalents of ions, which means that α is equal to 1. However, it was observed in our previous study that an MDC usually exhibits low current efficiency when the maximum current is not reached. Thus, we proposed an inverse tangent function to present the relationship between current and α. α begins with a zero value, increases

sharply, and levels off upon the increase of I_{MDC} from zero. The small value of α for a low I_{MDC} is able to relax the assumption made in the previous model in which α was always equal to 1.

$$\alpha = \frac{arctan\left(I_{MDC} * 1000 - I_{r\alpha,max} * 1000\right) + arctan\left(I_{r\alpha,max} * 1000\right)}{arctan\left(I_{\alpha=1} * 1000 - I_{r\alpha,max} * 1000\right) + arctan\left(I_{r\alpha,max} * 1000\right)} \qquad (3)$$

where I_{MDC} is the current generated by the MDC, $I_{r\alpha,max}$ is the current when $d\alpha/dI$ is the greatest and needs to be estimated from experimental data, and $I_{\alpha=1}$ is the current when α = 1. A profile of α is shown in Figure 6.2

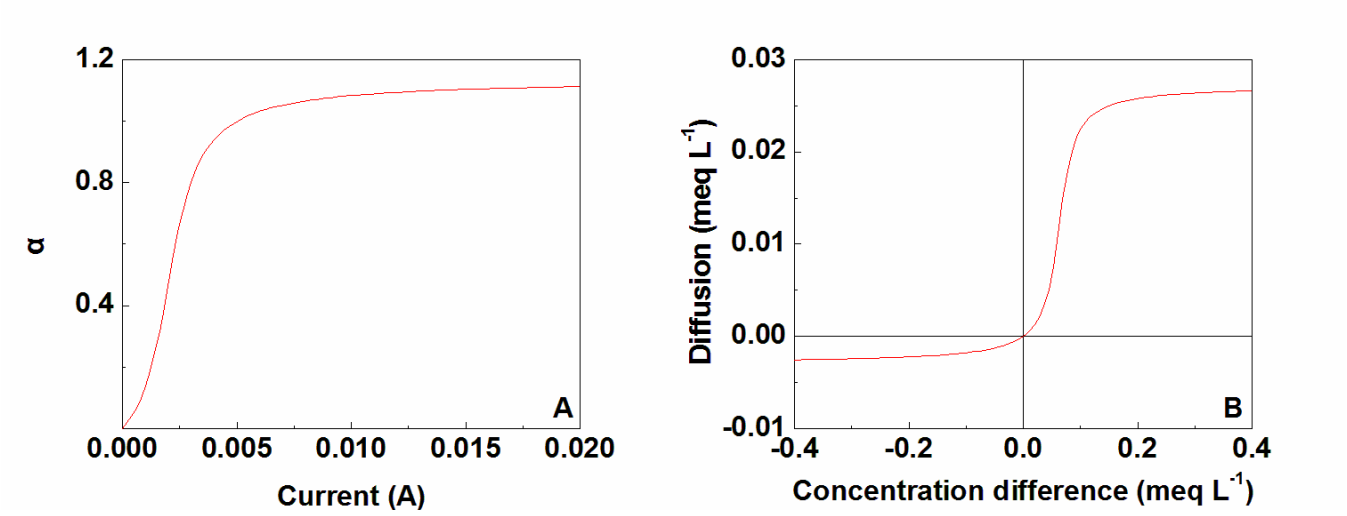

Figure 6.2 (A) The profile of α with $I_{\alpha=1}$ =5, and $I_{r\alpha,max}$ = 2; (B) The profile of Diffusion with d = 0.0096.

.

The water transport across an IEM is another important factor that contributes to the reduced salt concentration in the desalination compartment. The water flux between the desalination compartment and the anode and cathode compartments is represented by an osmotic pressure

model, and the osmotic pressures in the solutions were calculated in accordance with the Van't Hoff's equation:

$$J_{w,a} = A_{AEM} \cdot RTi\left(C_{salt,m} - C_{salt,a}\right)/2 \quad (4)$$

$$J_{w,c} = A_{CEM} \cdot RTi\left(C_{salt,m} - C_{salt,c}\right)/2 \quad (5)$$

where, $C_{salt,m}$, $C_{salt,a}$, and $C_{salt,c}$ are the salt concentrations in the desalination, anode, and cathode compartments (meq L^{-1}), respectively. A_{AEM} and A_{CEM} stand for the water permeability of anion and cation exchange membranes (L day^{-1} atm^{-1}), respectively. *i* is the Van't Hoff factor that reflects the number of discrete ions when compounds dissolve in water and was approximated to be 2 for salt NaCl in the present study.

Diffusion of salt molecules from high concentration to low concentration is greatly smaller in the opposite direction of current-driven ion movement and does not follow a linear relationship of the salt concentration difference as defined by the previous model. Therefore, to make concentration difference less influential when the salt concentration in the desalination compartment is less than in the anode or cathode compartment, the diffusion was modified to restricted diffusion functions $D_{res,a}$ and $D_{res,c}$ by an inverse tangent function. The profile of diffusion is shown in Figure 6.2.

$$D_{res,a} = \left[\arctan\left(\left(C_{salt,m} - C_{salt,a}\right)/2 \cdot 50 - pi\right) + \arctan(pi)\right] \quad (6)$$

$$D_{res,c} = \left[\arctan\left(\left(C_{salt,m} - C_{salt,c}\right)/2 \cdot 50 - pi\right) + \arctan(pi)\right] \quad (7)$$

The previous model assumed that only NaCl will cause concentration-gradient-driven-diffusion of salt, and excluded the contribution of current-driven movement of ions to the salt

concentration change in the anode and cathode compartments. In the case of brackish water desalination, where the concentration difference could be very small and even negative, it causes large discrepancy from the experimental data. Concerning the above facts, the updated equations for concentration change in the desalination compartment, the anode, and the cathode compartments were modified as equations (8), (9), and (10):

$$\frac{dC_{salt,m}}{dt} = D_{salt} \cdot C_{salt,in} - \frac{Q_{salt} + J_{w,a} + J_{w,c}}{V_{salt}} \cdot C_{salt,m} - 2 \cdot \frac{I_{MDC}}{F \cdot V_{salt}} \cdot \alpha - 2d \cdot D_{res,a} - 2d \cdot D_{res,c} \quad (8)$$

$$\frac{dC_{salt,a}}{dt} = D_{anode} \cdot C_{salt,a,in} - \frac{(Q_{anode} - J_{w,a})}{V_{anode}} \cdot C_{salt,a} + 2 \cdot \frac{I_{MDC}}{F \cdot V_{anode}} \cdot \alpha + 2d \cdot D_{res,a} \cdot \frac{V_{salt}}{V_{anode}} \quad (9)$$

$$\frac{dC_{salt,c}}{dt} = 2 \cdot \frac{I_{MDC}}{F \cdot V_{cathode}} \cdot \alpha + 2d \cdot D_{res,c} \cdot \frac{V_{salt}}{V_{cathode}} \quad (10)$$

where Q_{salt} and Q_{anode} are the flow rates (L day^{-1}) of the salt solution in desalination compartment and of anolyte in the anode compartment. V_{salt}, V_{anode}, and $V_{cathode}$ are the volumes of the desalination, anode, and cathode compartments. $C_{salt,in}$ and $C_{salt,a,in}$ are the salt concentration in the salt influent and anolyte influent (meq L^{-1}). D_{salt} and D_{anode} are the dilution rates (day^{-1}) in the desalination compartment and anode compartment defined in the previous model quantified by the ratio of the flow rate over the volume of the compartment. d is the membrane salt transfer ability (g L^{-1} day^{-1}). The first and second terms of equation (8) and (9) represent the cause of concentration change by inflow and outflow of solutions. The third term in equation (8) and (9), and the first term in equation (10) represent the current-driven movement of ions. The last two

terms in equation (8) and the last terms in equation (9) and (10) show the diffusion between the three compartments. The volume ratios of desalination compartment to anode or cathode compartment were considered for the rate change of $C_{salt,a}$, and $C_{salt,c}$.

To show the individual ion concentration in the salt solution, such as Na^+, K^+, Mg^{2+}, Ca^{2+}, Cl^-, NO_3^-, SO_4^{2-}, the following equations are needed.

$$\frac{dC_{ion,m}}{dt} = D_{salt} \cdot C_{ion,in} - \frac{Q_{salt} + J_{w,a} + J_{w,c}}{V_{salt}} \cdot C_{ion,m} - \varphi_{ion} \cdot \left\{ \frac{I_{MDC}}{F \cdot V_{salt}} \cdot \alpha + d \cdot D_{res,a} + d \cdot D_{res,c} \right\} \quad (11)$$

where $C_{ion,in}$, and $C_{ion,m}$ are the individual ion concentration in the salt influent and desalination compartment, and *ion* refers to any anion or cation according to the ion composition in the salt influent.

φ_{ion} is the ratio defined as

$$\varphi_{anion} = \frac{u \cdot C_{anion,m}}{\sum u \cdot C_{anion,m}} \quad (12a)$$

Or

$$\varphi_{cation} = \frac{u \cdot C_{cation,m}}{\sum u \cdot C_{cation,m}} \quad (12b)$$

Where u is the mobility of ions in solution (Vanysek 2002).

Equation (8) is then modified to Equation (13) by summing up the individual ion concentration in the salt solution according to the relationship $\sum C_{ion,m} = C_{salt,m}$, and $\sum C_{ion,in} = C_{salt,in}$.

$$\frac{dC_{salt,m}}{dt} = \sum \frac{dC_{ion,m}}{dt} \quad (13)$$

6.3.3 Parameter Estimation

Parameter estimation was performed with *fmincon* subroutine in Matlab to search a local minimum of objective function defined as normalized room-mean-square-error (RMSE) for dynamic data:

$$RMSE = \frac{\sqrt{\frac{\sum_{i=1}^{N}(y_i - \hat{y}_i)^2}{N}}}{\max(\hat{y})} \tag{14}$$

Or squared error (SE) for steady sate data:

$$SE = \sqrt{\left(\frac{y_i - \hat{y}_i}{\hat{y}}\right)^2} \tag{15}$$

Where $\hat{y}_i$ and y_i represent experimental data and model predicted values at t_j or at steady state. Constraints were set to satisfy the true yield range for anodophilic microorganisms between 0.027 and 0.054 mg-Biomass mg-COD^{-1} (Marcus et al. 2007).

6.4 Results and Discussion

6.4.1 Wastewater Treatment

The MDC effectively treated wastewater with little influence from the different salinity of brackish waters or current generation. With the initial COD concentration of 500 ~ 650 mg L^{-1} (varied due to variation of organic concentration in actual wastewater), the MDC removed the

COD of 421 ± 85 mg/L, resulting in a final COD concentration of 80 ~ 262 mg L^{-1} and the COD removal rate of 68.9 ± 10.7%. Current generation was affected by the salinity (or conductivity) of the brackish water. The MDC generated 12.3 ± 2.4 A m^{-3} when treating the brackish water A, which had the highest initial salinity of 5.9 g L^{-1} of TDS among the three brackish waters. Consequently, higher Coulombic efficiency (of 10.9 ± 0.9%) was observed with the brackish water A. For comparison, the brackish waters B (1.5 g TDS L^{-1}) and C (1.1 g TDS L^{-1}) resulted in lower current generation of 8.1 ± 0.5 A m^{-3} and 7.5 ± 1.0 A m^{-3}, respectively; they also had lower Coulombic efficiency of 5.7 ± 0.6% and 5.6 ± 1.2%, respectively (Figure 6.3). The lower Coulombic efficiency with treating the brackish waters B and C, along with similar COD removal performance (to that with the brackish water A) indicated that, with decreased conductivity in the desalination compartment, the portion of COD used for electricity generation also decreased. Non-anodophilic microorganism played an important role in removing COD, especially when the current generation was suppressed, thereby maintaining a comparable COD concentration in the final effluent. When the initial organic strength in wastewater was increased to ~1162 mg L^{-1} by adding more glucose for desalinating the brackish water A, the current was not improved. In fact, it was observed that the increased COD strength lowered Coulombic efficiency to 5.8% (Figure 6.3) and resulted in a higher effluent COD of 524 mg L^{-1}. Those results suggest that the present MDC system was not limited by the anode activity and electron source; instead, the limiting factors that resulted in low CE might come from the low conductivity in both the wastewater and the desalination compartment, and complex substrates that led to competing electron sinks (Lee et al. 2008).

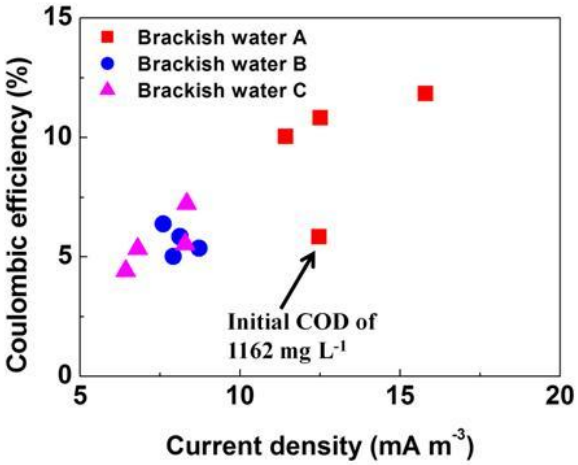

Figure 6.3 Coulombic efficiency of the MDC at different current densities when desalinating three types of brackish waters.

6.4.2 Brackish Water Desalination

6.4.2.1 General desalination performance

The MDC accomplished desalination of the tested brackish waters, affected by both salinity and HRT of brackish water. At the same HRT of 0.8 d (salt flow rate of 0.13 mL min^{-1}), the MDC decreased the conductivity by 19.6 % in the brackish water A, while the conductivity reduction in the brackish waters B and C was much higher at 43.4 and 57.4%, respectively (Figure 6.4A). Increasing the HRT to 1.7 d (salt flow rate of 0.06 mL min^{-1}) significantly improved the conductivity reduction to 33.3 ± 7.2% for the brackish water A; meanwhile, the MDC further improved the desalination of the brackish waters B and C to 82.5 ± 5.0 and 88.1 ± 0.9%, respectively. To achieve desalination of >90% for the brackish water A, the HRT must be

increased to 7 d. It was observed that higher desalination efficiency was obtained at a longer HRT and the trend became more distinct as the initial salinity decreased (Figure 6.4A), suggesting that the treatment time had a greater influence on desalination because of the limited desalination capacity of the present MDC. Salt removal rate, on the other hand, exhibited a different trend from desalination efficiency (or conductivity decrease) (Figure 6.4B). At the HRT of 0.8 or 1.7 d, the salt removal rate increased for brackish waters C, B, and A (0.75, 0.80, and 1.2 g L^{-1} day^{-1}; or 0.52, 0.74, and 1.1 g L^{-1} day^{-1}) as the initial salinity increased (C<B<A). Relatively higher salt removal rate was also observed with a shorter HRT (Figure 6.4B). The accelerated desalination with higher initial salinity or shorter HRT was because of the resulted higher conductivity in the desalination compartment (as well as the salt effluent) that led to a lower internal resistance and thus higher current generation that drove desalination. The slightly lower salt removal rate of treating brackish water C at HRT of 0.35 d than that at 0.8 d was likely due to the low current of 6.4 A m^{-3} compared with 7.5 A m^{-3}. The higher conductivity of 1.2 mS cm^{-1} (0.35 d) compared with 0.7 mS cm^{-1} (0.8 d) did not lead to higher current generation, indicating that some factors other than electrolyte conductivity (resistance) limited the MDC performance.

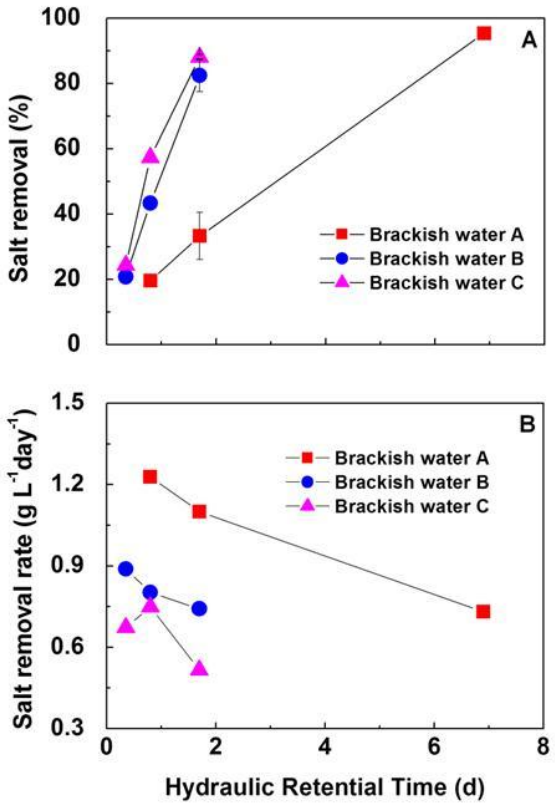

Figure 6.4 The effect of hydraulic retention time on the brackish water desalination: (A) salt removal efficiency, and (B) salt removal rate.

Given sufficient retention time, the MDC could reduce the salinity to a very low level. For example, at the HRT of 1.7 d, the TDS of the brackish water C was decreased to 114 mg L^{-1} , close to that of the tap water (90 mg L^{-1} TDS) collected at Virginia Tech, and lower than the requirement of potable water quality (<500 mg L^{-1} TDS) issued by US EPA (EPA 816-F-09-0004, May 2009). The concentrations of major ionic species in the desalinated brackish water were also comparable to those in the tap water sample and the influent brackish water (Figure 6.5). It should be noted that MDCs do not intend to produce directly potable water. Although the

ion-exchange membranes can block bacteria and virus (Strathmann 2004), concerns would still arise because of the wastewater adjacent the desalination compartment and potential biofouling due to the transport of small organic ions or molecules into the desalination compartment. For non-portable application such as agricultural irrigation, MDCs may deliver satisfactory water quality. The salinity level of irrigation water is the primary concern for plant growth, because the available water for plant in the soil decreases dramatically as salinity increases. Crops also suffer from yield reduction if being irrigated with high salinity water (Ayres and Westcot 1985). At an HRT of 1.7 d, the desalinated water of the brackish waters B (0.37 mS cm^{-1}) and C (0.19 mS cm^{-1}) meets the "none restriction irrigation guideline" of ECw (Electrical conductivity) < 0.7 mS cm^{-1}. However, considering the potential water infiltration problem that will be discussed in the following section, low salinity (ECw less than 0.2 mS cm^{-1}) does not always mean a better quality. A reduced HRT of 0.8 d yields the ECw of 1.4 mS cm^{-1} for the brackish water B, and 0.74 mS cm^{-1} for the brackish water C, which is in the range of "slight to moderate restriction". For the brackish water A, the present MDC would need an HRT of 7 d to decrease its conductivity to 0.41 mS cm^{-1}, which made it qualify the non-restricted standard for agricultural application.

The above results demonstrate that, compared with ED, the MDC could achieve satisfactory performance of brackish water desalination, though with a longer HRT. As stated before, the major advantage of MDC technology lies in less energy consumption. The present MDC was estimated to consume 1.27 kWh m^{-3} (hydraulic energy) for a 96% salinity removal of 6 g L^{-1} brackish water, significantly lower than 7 kWh m^{-3} (including electrical and hydraulic energy) in a bench-scale ED desalinating brackish water (Walker et al. 2014). Meanwhile, the same energy consumed by the MDC desalination was also used for wastewater treatment in 0.038 kWh m^{-3}

(based on the volume of treated wastewater). Therefore, MDCs may be applied when energy requirement is a bigger concern than water production rate, with simultaneous wastewater treatment.

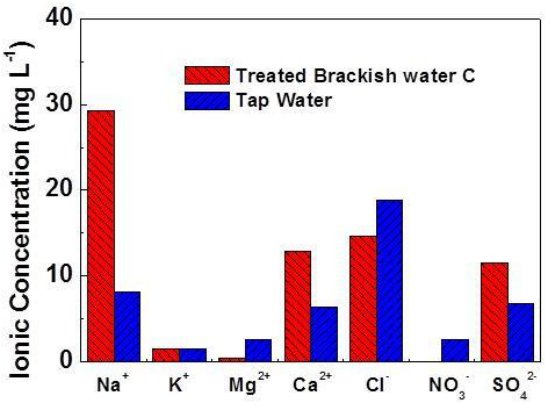

Figure 6.5 Comparison of individual ion concentrations between the brackish water C (untreated and treated), and tap water sampled at Virginia Tech.

6.4.2.2 Removal of individual ionic species

Because of complex composition of brackish water (compared with synthetic saline water containing only NaCl for many lab tests) and potential effects of some ions on plants that should receive specific care during desalination, we investigated the removal of major ions in a greater detail. Theoretically, the removal rate of specific ions in the desalination compartment of an MDC is determined by its concentration and mobility. The mobility of major cations are in the order of $K^+ > Na^+ > Ca^{2+} > Mg^{2+}$, and the anions are in the order of $Cl^- > NO_3^- > SO_4^{2-}$ (Vanysek 2002). As shown in Figure 6.6, Na^+ and Cl^- had the highest removal rates among cations and anions,

because of their large abundance and strong mobility. The removal rates of K^+, Ca^{2+}, and Mg^{2+} were relatively low, likely related to their initial low concentrations, except that the initial concentration of Ca^{2+} in the brackish water A was as high as 18.6 mmole L^{-1} (742.0 mg L^{-1}). The removal rate of NO_3^- was higher than SO_4^{2-} in the brackish waters B and C, owing to the higher mobility of NO_3^- as well as the comparable concentrations of the two ions (1.1 and 0.9 mmole L^{-1}, or 65.6 and 88 mg L^{-1} in the brackish water B, and 0.8 and 0.7 mmole L^{-1}, or 50 and 68 mg L^{-1} in the brackish water C). The removal rate of NO_3^- was considerably slow in the brackish water A, possibly related to its low concentration of 0.06 mmole L^{-1} (or 3.5 mg L^{-1}). It was observed that a higher salt flow rate (or lower HRT) generally resulted in a higher ionic removal rate, which was consistent with overall salt removal rate discussed in the previous section.

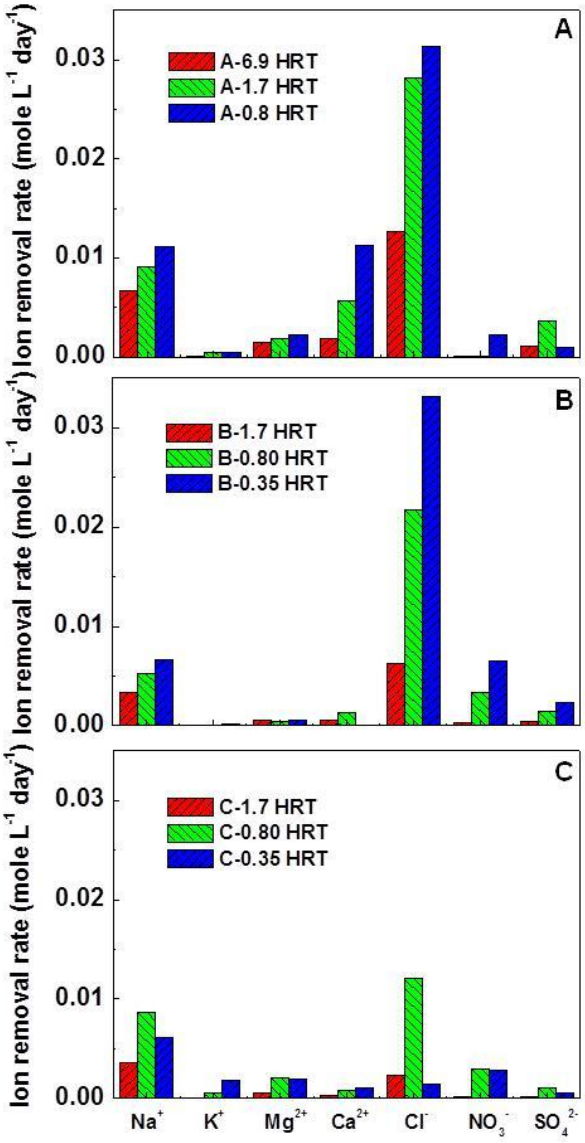

Figure 6.6 The removal rates of major ions at three HRT (d) (A) brackish water A; (B) brackish water B; and (C) brackish water C.

Chloride is the most common cause of toxicity in irrigation water due to its ability to accumulate in plant leaves. Leaf tissue will be severely injured if the chloride concentration exceeds the tolerance (Tak et al. 2012). At HRT of 1.7 d, the MDC decreased the chloride concentrations in

brackish waters B and C to 36.3 and 14.7 mg L^{-1}, respectively, below the guidelines of "non-restriction" for sprinkler (106.5 mg L^{-1}) and surface (142 mg L^{-1}) irrigation. The desalinated brackish water A could meet the guideline only when treated with the seven-day HRT. When the HRT was shortened to 0.8 days, the chloride concentrations increased to 307.9 and 270.0 mg L^{-1} for B and C. Cautions need to be taken because these are in the range of "slight to moderate restriction on use" of 142~350 mg L^{-1}.

High sodium content in irrigation water relative to the calcium and magnesium contents, also known as sodium hazard, will cause infiltration reduction in the plant and reduce crop yield. The Sodium Adsorption Ratio (SAR) is an important parameter to access this tendency, calculated as (Miller and Gardiner 2007):

$$SAR = \frac{Na^{+}\ meq/L}{\sqrt{\frac{(Ca^{++}\ meq/L) + (Mg^{++}\ meq/L)}{2}}} \quad (16)$$

The SAR of the three brackish waters, treated and untreated, all oscillated between the "low sodium hazard" and "medium sodium hazard" standard of 1~18 (Fipps 1996). The measurement of SAR together with salinity also provides the evaluation of the sodium hazard problem. With the best salinity quality at HRT of 1.7 d, treated brackish water C had SAR of 2.1 in the range of "slight to moderate restriction on use". Desalinated brackish water B at HRT 1.7 d resulted in a high SAR of 7.5, indicating that the produced water would bring forth severe infiltration problem. If the "none-restriction" of salinity is met, the SAR should always be maintained below 6 (Ayres and Westcot 1985). Chemical amendments of the treated brackish water, such as addition of Gypsum, needs to be taken into consideration before applying the treated water to irrigation.

Other inorganic ions that contribute to salinity also play important roles in plant and crop growth, such as sulfate and nitrate that benefit fertility of crops (Tak et al. 2012). At HRT of less than 2 d, the brackish water B and C both fall in the “low” to “normal” nutrient concentrations range. Brackish water A was enriched in sulfate and maintained excessive sulfate in its effluent at a short HRT. At seven-day HRT, the sulfate concentration was reduced to 33.0 mg L^{-1} and met the “normal nutrient concentration”.

The commercial ion exchange membranes usually have a pore size of 1 nm Strathmann 2004), and do not block molecules or ions that have a molecular weight less than 350 Da (Kim and Logan 2013). The common inorganic ions in the wastewater, Ca^{2+}, Mg^{2+}, Na^{+}, K^{+}, NH_4^{+}, $SO4^{2-}$, and Cl^{-}, which originally exist in brackish water as well, may not be a major concern if they move across the ion exchange membranes from wastewater into brackish water, because they will contribute to the nutrient concentrations for irrigation. When treating wastewater with high phosphate content in the anode of an MDC (which is not a case in the present study), the back-diffused phosphate will cause potential problem in irrigation process because of phosphate-related precipitation in irrigation pipe and emitters. This issue can be prevented by adjusting the pH of the desalinated water (Rauschkolb et al. 1976).

Organics in wastewater exist in complex forms, and the back-diffusion of small-size organic compounds might lead to microorganism contamination of the desalinated brackish water and

biofouling of the ion-exchange membranes (Ping et al. 2013). The wastewater used in this study had an initial acetate (60 Da) concentration of 0 ~ 20 mg L^{-1} and a glucose (180 Da) concentration of ~500 mg L^{-1}. The concentrations of glucose and short chain fatty acids could increase through decomposition of large organic compounds by bacteria in the anode. The back-diffused organics during the MDC operation resulted in a TOC concentration of 2~7 mg L^{-1} in the desalinated brackish water. We hypothesized that there could be two driving forces causing back-diffusion: the osmotic water movement from the anode to the desalination compartment, and the organics gradient between the wastewater and the brackish water. At an HRT of 1.7 d when desalinating brackish waters B and C, the osmotic pressure across the AEM dropped to -0.38, and -0.53 atm due to the lower salinity in the desalination compartment than the anode compartment (the anolyte of ~1.4 mS cm^{-1}), which meant the water moved from the desalination compartment to the anode compartment and thus water movement would not cause back-diffusion of organics. For the brackish water A, an osmotic pressure of 1.83 atm was presented between the desalination compartment (5.0 mS cm^{-1}) and anode compartment (1.4 mS cm^{-1}), and possibly organics were transported across the AEM from the anode to the desalination compartment with water as the carrier. However, the TOC in the three treated brackish waters showed undistinguishable concentrations of 6.9, 5.1, and 6.6 mg L^{-1} for A, B, and C, respectively. Unlike seawater desalination in an MDC, in which osmotic pressure could reach as high as 10 atm, the back-diffusion of organics during desalinating brackish water was not affected by osmotic pressure severely. The organic gradient across the AEM were similar at about 70 mg L^{-1} TOC when treating the three brackish waters, and this similar organic gradient was likely the major reason for the similar degree of organic contamination in the treated brackish waters.

6.4.3 Model fitting and validation

To better understand the desalination behavior of brackish water in the MDC and to provide guidance for system operation, the MDC model was updated and implemented in MATLAB using ODE 23tb solver for solving stiff differential equations. The diffusion constant *d* was calibrated as 0.0096 mole L^{-1} day^{-1} with the steady state $C_{salt,m}$ by an open circuit (OC) experiment (the performance was not subject to current generation, but only salt diffusion or water permeate) operated with the same MDC reactor fed with acetate as the substrate and salt solution of 5 g L^{-1} NaCl. With initial salt concentration of 35 g L^{-1} and external resistance of 0.1 ohm, the steady state $C_{salt,m}$ along with the maximum water permeability (86 mL $h^{-1}m^{-2}$ for AEM and 32 mL $h^{-1}m^{-2}$ for CEM at 5 psi) provided by the manufacture (Membrane International, Inc.), were then used to estimate the water permeability of the ion exchange membranes used in this study. Figure 6.7A shows the measured and simulated salt effluent conductivity in the MDC fed with acetate, and with 5 g L^{-1} or 35 g L^{-1} NaCl as the initial salt concentration at different external resistance loads. The two different salt concentrations were selected to represent the brackish water and seawater salinity (seawater was studied here for comparison purpose). The different external resistance loads allowed the evaluation of the model performance affected by current variation, as well as the concentration difference between different compartments which lead to salt diffusion and water permeation. At both initial salt concentrations, the salt effluent conductivity decreased as the external resistance load decreased which led to enhancement of the current generation. The rapid reduction in conductivity (with 35 g L^{-1} as the initial salt concentration) when external resistance was changed from 100 ohm to 0.1 ohm was because of the dramatically increased current (increment of 6.7 mA), much higher than that from OC to 100 ohm (3.5 mA). The current change was slow with 5 g L^{-1} as the initial salt concentration (4 mA

increment for every resistance change), and so resulted in a gradual conductivity reduction. The simulated salt effluent conductivity shows strong agreement with the measured value, with SE less than 0.8% for the initial salt concentration of 35g L^{-1}, and SE less than 2.9% for 5 g L^{-1}, except for the case of 5 g L^{-1} NaCl operated with 0.1 ohm, which has a calculated SE of 14.5%. These results indicate excellent accuracy of the improved model for both high and low salinity desalination in MDC. With the improved mathematical model, the RMSE of the dynamic salt concentration from the previous MDC with dynamic anolyte flow rates was improved from 12.12% to 5.32% of their maximum values, and from 17.57% to 13.09% when changing the external resistances (Figure 6.8&6.9) (Ping et al. 2013).

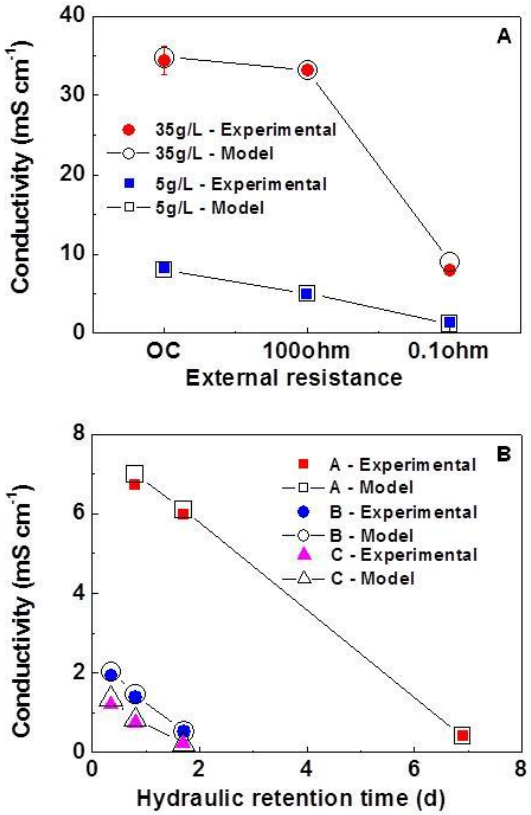

Figure 6.7 Experimental data and model prediction of the MDC performance: (A) synthetic NaCl solution at two different salinities with different applied external resistance; and (B) three brackish waters at different HRT.

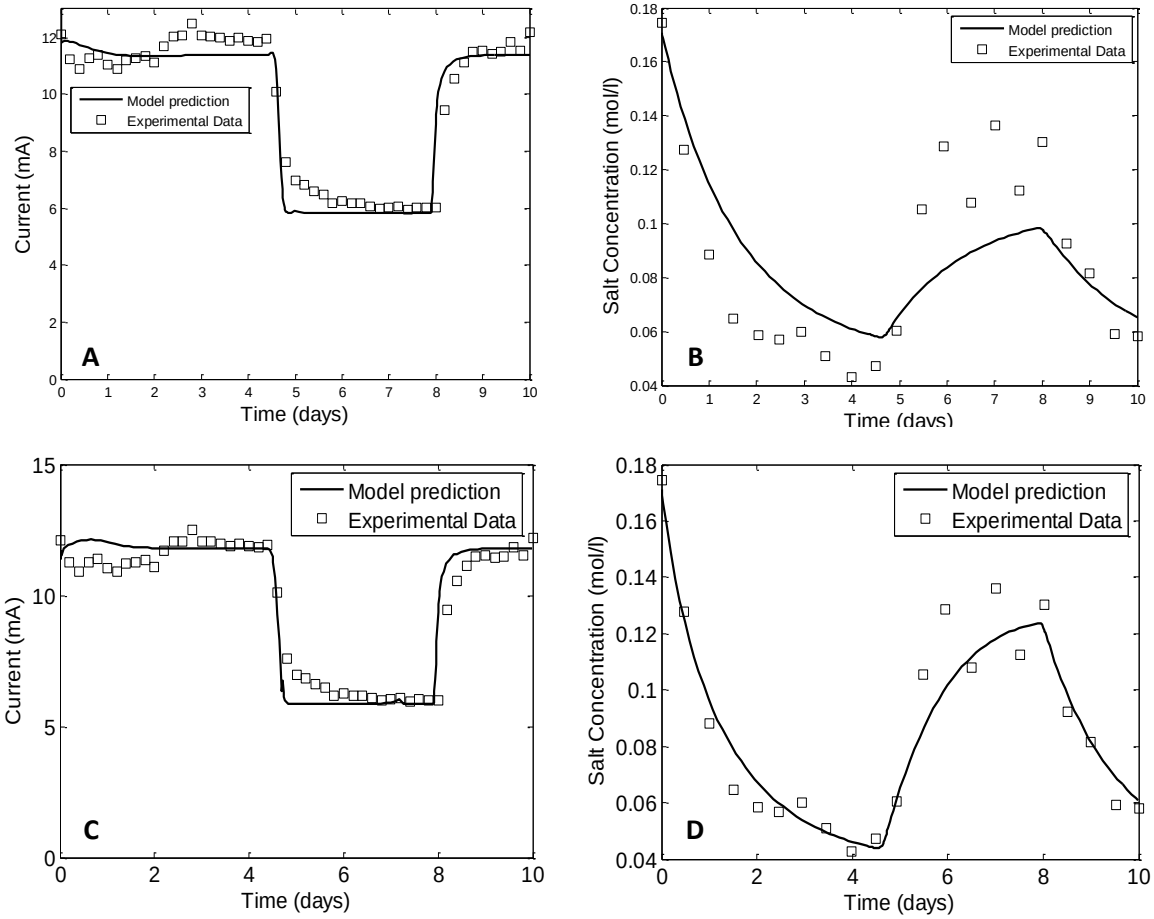

Figure 6.8 Experimental data and model simulation when the anode influent feeding rate was changed from 0.5 to 0.2, and then back to 0.5 mL·min^{-1}: (A) & (B) the results from the previous model; (C) & (D) the results from the updated model.

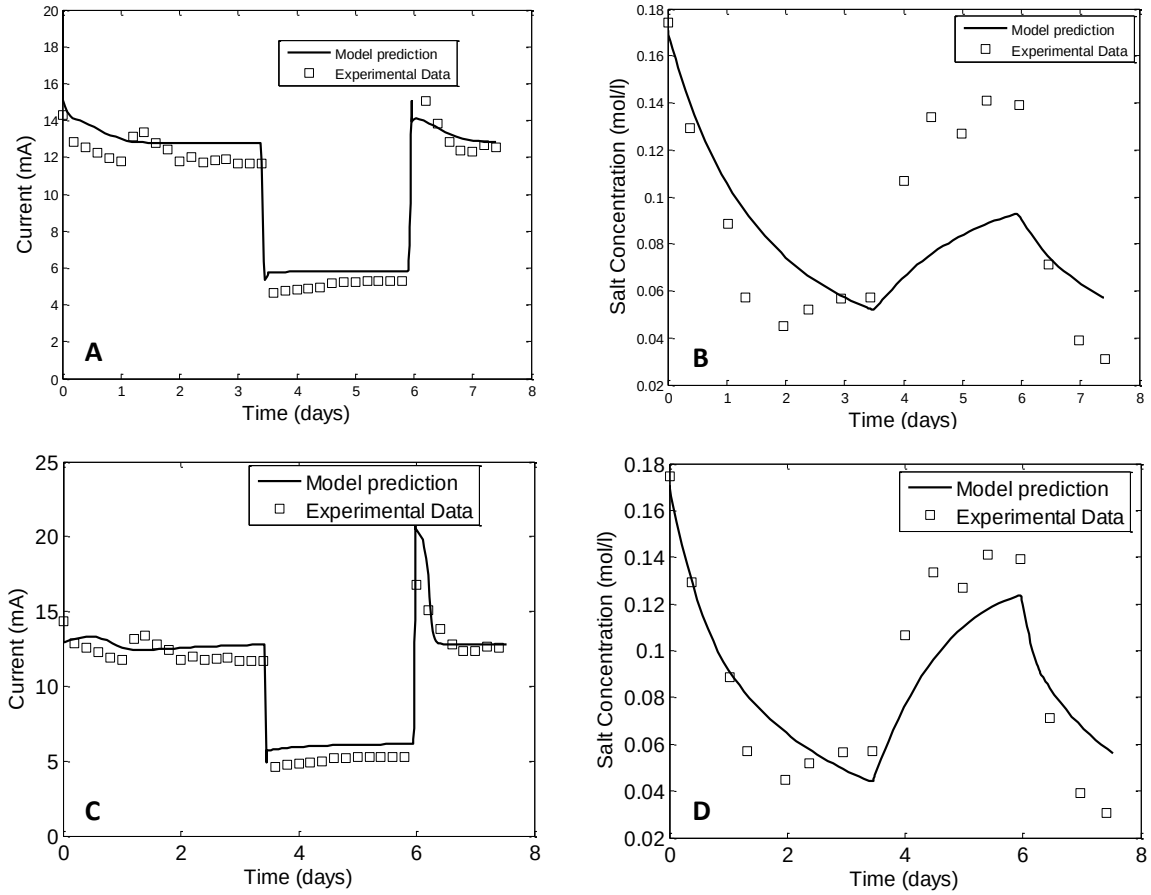

Figure 6.9 Experimental data and model simulation when the external resistance was changed from 0.1 to 100, and then back to 0.1 Ω: (A) & (B) the results from the previous model; (C) & (D) the results from the updated model.

For actual brackish water desalination operated with domestic wastewater in this study, the parameters related to anodophilic and methanogenic miroorganisms were adopted from the previous model, and then adjusted with the experimental results obtained in this study. The maximum attainable current was estimated to be 5 mA by both the microbial growth mode in

domestic wastewater and the low conductivity of wastewater (1 mS cm^{-1}) and brackish water. Given the weaker activity of anodophilic microorganisms in domestic wastewater, the parameter values of maximum substrate consumption rate by anodophilic microorganisms $k_{s,a,max}$, half-saturation concentrations for the anodophillic microorganism K_a, half-saturation concentrations for the methanogenic microorganism K_m, maximum anodophilic microorganism growth rate $k_{a,max}$, and mediator yield Y_M were modified to 3.06 mg-S mg-a^{-1} day^{-1}, 80 mg-S L^{-1}, 100 mg-S L^{-1}, 0.164 d^{-1},2.83 mg-M mg-S^{-1}. The steady state performance at the longest HRT (the brackish water A at HRT of 6.9 d and brackish waters B&C at HRT of 1.7 d) was used to estimate model parameters (mainly transfer coefficient factor α), while other HRTs were for model validation (Figure 6.7B). As discussed previously, longer HRT provided more treatment time, and thus resulted in lower effluent salt conductivity. The results showed excellent agreement between measured and simulated salt effluent conductivity (Figure 6.7B), with the highest SE of 3.82% for the brackish water A, 4.96% for the brackish water B, and 10.7% for the brackish water C.

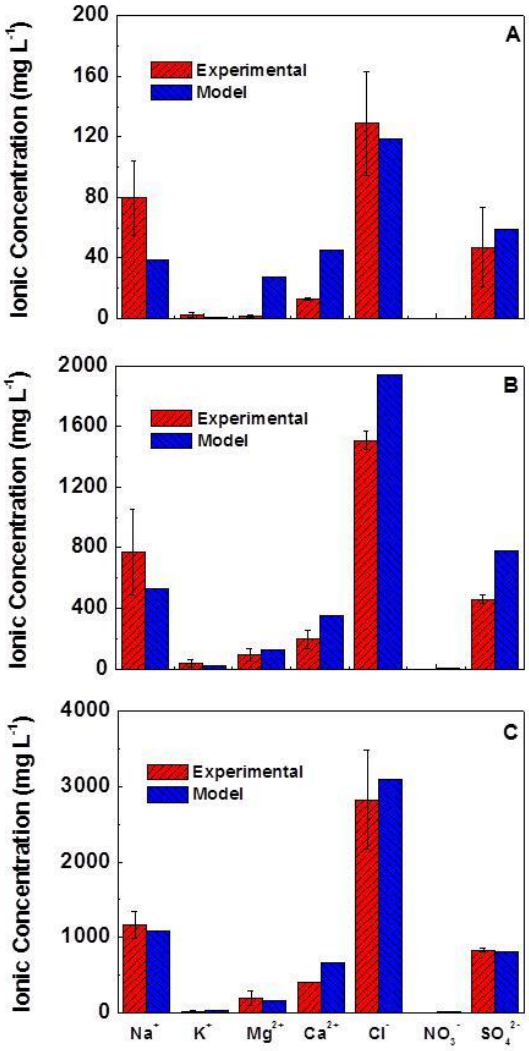

Figure 6.10 Experimental data and model prediction of the concentration of major ions in the desalinated brackish water A at HRT (A) 6.9 d, (B) 1.7 d, and (C) 0.8 d.

The ionic composition was also well predicted by the model. Using the brackish water A as an example, its ionic composition in the desalinated effluent showed normalized RMSE of 5.21% (at HRT of 0.8 d), 15.2% (1.7 d), and 17.7% (6.9 d). The predicted concentrations of Ca^{2+}, Mg^{2+}, and SO_4^{2-} were relatively higher than the measured values at HRTs of 6.9 d and 1.7 d, and the discrepancy might be related to the factors of pH and precipitation or absorption rate of hardness

ions onto the membrane (Figure 6.10A&B), which phenomenon was also observed in the previous study (Luo et al. 2012b). The pH of the brackish water A ranged from 7.49 to 8.51, and the higher pH in that range could accelerate the precipitation of those ions on the membrane, which was a complicated process that could not be predicted by the present model. The scaling on the ion-exchange membrane probably reduced the transport ability of other ions, so that the measured Na^+ concentration was higher than predicted values. However, the reason for measured Cl^- concentration to be lower than predicted value at HRT of 1.7 d was not clear, and it is possible the initial input Cl^- concentration in MATLAB was overestimated from IC result. At a shorter HRT of 0.8 d, the measured concentrations of Mg^{2+} and SO_4^{2-} were close to the predicted values (Figure 6.10C), probably because that the high flow rate did not allow enough time for $MgSO_4$ to precipitate, which has a slower precipitation rate compared with $CaCO_3$ (Ping et al. 2013).

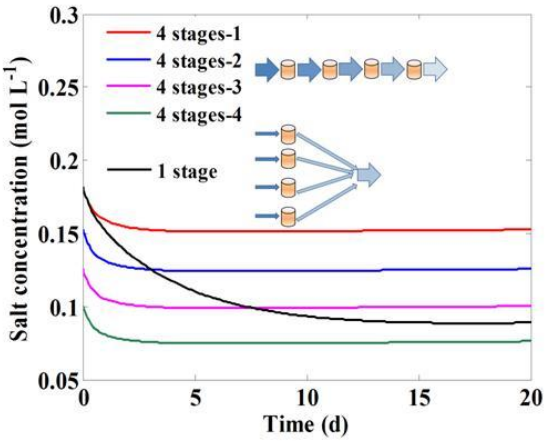

Figure 6.11 The salt concentration in the desalinated effluent in two simulated operations, four-stage, and one-stage operation, both at HRT 4 d.

Inspired by the fact that a lower HRT in a single reactor results in a higher salt removal rate, the model simulated and compared two operational modes to identify an optimal mode for better desalination: the four-stage operation has a single feed of salt solution flowing through four MDCs in series with HRT of 1 day in each reactor, and the one-stage operation has four feed streams in parallel to four MDCs with HRT of 4 days in each reactor, respectively (Figure 6.11; inset shows two operational modes); both systems will desalinate the same amount of salt water within the same time period. The salt concentration in the effluent decreases with the stages in the four-stage operation, while it decreases with time in the one-stage operation (Figure 6.11). The four-stage operation achieves 14% improvement in salinity reduction compared with the one-stage operation. It is worth noting that more stages could exhibit better improvement, but not intensively. For example, a simulated ten-stage operation further improves the desalination by another 4%, compared with the four-stage operation. The model assumes same microorganism population and growth mode in the four reactors of both operations; however, actual application of the staging operation might result in different microorganism activities in different reactors. For example, the earlier stage will most likely have stronger anodophilic activities, because of sufficient uptake of electrons. . Thus, the identified optimal operation mode will also need to be experimentally verified.

6.5 Conclusions

This study has demonstrated the effective desalination of brackish water and treatment of municipal wastewater in MDCs, through integrated experiments and mathematical modeling. Given sufficient HRT, the desalinated brackish water could meet the none-restriction irrigation

standard in terms of both salinity and composition of individual ions. A small amount of back diffused organics might lead to microbial contamination of the desalinated water, and post-disinfection may be required to inhibit bacteria growth. The improved mathematical model fit the experimental data fairly well, and was able to provide useful information for operation optimization. Those results encourage further investigation and development of MDC technology for combined wastewater and brackish water treatment.

Chapter 7 Boron Removal from Saline Water by a Microbial Desalination Cell Integrated with Donnan Dialysis

(This section has been published as Ping, Q., Abu-Reesh, I. and He, Z. (2015) Boron removal from saline water by a microbial desalination cell integrated with Donnan dialysis. ***Desalination*****.** Vol 376, pp 55-61.)

Abstract

Boron has potentially toxic effects on plant growth and thus its removal is necessary from desalination of saline water for irrigation application. Microbial desalination cells (MDCs) are a new approach for effective desalination but boron removal has not been addressed. Herein, MDCs were studied for boron removal with aid of Donnan Dialysis (DD). The alkaline solution generated by the MDC cathode was used to ionize boric acid to facilitate boron removal. An MDC system with DD pretreatment removed 60 or 52% of boron with the initial boron concentration of 5 or 20 mg L-1. In the absence of DD, direct cathodic alkalinization of boron in an MDC was not effective in terms of boron removal and had serious issue of salt accumulation. The MDC with DD post-treatment could reduce the boron concentration below 2 mg L-1, although the high pH of its final effluent needs to be further addressed. Further investigation will consider an MDC system with both DD pre-treatment and post-treatment for improving boron removal.

7.1 Introduction

Boron is a common element in brackish water having a concentration up to 40 mg L^{-1} and in seawater around 5 mg L^{-1} (Guler et al. 2015, Melnik et al. 1999). Boron is an essential element for plant growth, but the high-concentration boron in the irrigation water could damage plants. Many plants encounter toxicity problems when the concentration of boron exceeds 2 mg L^{-1}, and some sensitive plants cannot tolerate a boron concentration greater than 0.3 mg L^{-1} (Guler et al. 2015). Thus, when desalinating saline water for irrigation use, boron removal will be necessary. The world's largest desalination plant, the Ashkelon Seawater Reverse Osmosis (SWRO) plant in Israel, has incorporated boron removal as post-treatment after the multi-stage RO. Boron exists in water in the form of boric acid, and because of boric acid's non-dissociative character, pH amendment must be applied according to the pKa value of boric acid (9.14) to ionize boric acid before treating boron-containing water (as shown in Equation (1)). Effective removal of boron has been accomplished by electro-flocculation, ED, or RO, and no matter which method is applied, the key is to raise pH and ionizing boric acid to the charged form (borate) (Guler et al. 2015, Ofir et al. 2011, Kabay et al. 2008). The pH adjustment is usually conducted by adding sodium hydroxide, thereby increasing the operating cost and thus the price of the desalinated water.

$$B(OH)_3 + H_2O \Leftrightarrow B(OH)_4^- + H^+ \qquad (1)$$

High-pH solution is a side product of desalination by microbial desalination cells (MDCs), and this feature may be used to facilitate boron removal. MDCs are bioelectrochemical systems

through integrating electrodialysis into microbial fuel cells (MFCs) (Cao et al. 2009), and the overview of this technology can be found in the recent review papers (Kim and Logan 2013, Sevda et al. 2015, Saeed et al. 2015). Although still at an early stage of development, the MDC technology has been advanced with improved desalination through optimizing reactor configurations (Kim and Logan 2011, Chen et al. 2011a, Jacobson et al. 2011a, Ge et al. 2014), applying resin in the desalination compartment to reduce internal resistance (Zhang et al. 2012, Zuo et al. 2013), or adjusting pH with electrolyte recirculation (Chen et al. 2012a, Qu et al. 2012). Fundamental studies have revealed the diverse microbial community in the anode of an MDC (Luo et al. 2012a, Mehanna et al. 2010b), and mathematical modeling has helped explicitly analyze the desalination process (Ping et al. 2014, Ping et al. 2015a). In a recent study, an MDC system with a total liquid volume of 105 L was developed with a desalination rate up to 9.2±0.2 kg TDS m^{-3} d^{-1} by applying an additional external voltage (Zhang and He 2015). Considering the low desalination rate, MDCs may be applied for 1) desalinating seawater as pretreatment followed by conventional desalination methods and offsetting energy consumption extracting bioenergy from wastewater; and 2) desalinating brackish water for irrigation application. MDCs have been demonstrated for successful removal of multiple ions from brackish water, such as sodium, calcium, magnesium, chloride and sulfate, to meet irrigation guidelines (Ping et al. 2015a). However, boron removal has not been studied in MDCs. If MDCs will be applied for desalination, boron issues must be properly addressed.

Oxygen reduction reaction on the cathode of an MDC accumulates hydroxide ions (POpat et al. 2012) with a side product of alkaline solution:

$$O_2 + 2H_2O + 4e^- \rightarrow 4OH^-$$

(2)

This hydroxide-ion abundant catholyte from an MDC can serve as an alkaline solution in Donnan Dialysis (DD) that may be used to produce dissolved borate for boron removal in the MDC and/or through ion exchange. DD is a pH modifying treatment process that the pH of the target solution can be elevated without raising conductivity. When an alkaline solution is used as the stripping solution and a target solution as the feed solution in a DD device equipped with AEM (anion exchange membrane), the difference in chemical potential of hydroxide ions drives the diffusion of hydroxide ions from the stripping solution into the feed solution, and meanwhile extracts negative ions from the target solution. In the case of pretreatment of boron containing saline solution, anions such as chloride ions will likely compete with borate ions for extraction because of its abundance.

In this study, we have proposed and investigated an MDC system integrated with DD to treat boron-containing saline water. In the system where DD acts as a pre-treatment process (Figure 7.1), the saline water is firstly treated in the DD device that uses the catholyte of the MDC as a stripping solution and converts boric acid to borate; then, the DD feed effluent is desalinated in the MDC for boron removal that has borate moving from the desalination compartment into the anode effluent. Such a process takes advantage of ion separate and accumulation of hydroxide ions in an MDC and ion exchange in the DD. The objectives of this study were to: (1) examine the feasibility of the system; (2) study the effect of pH in DD stripping solution and salt loading on boron removal; and (3) examine different integration approaches including direct cathodic

alkalinization of the salt solution, DD as pretreatment before MDC, and DD as post-treatment after MDC.

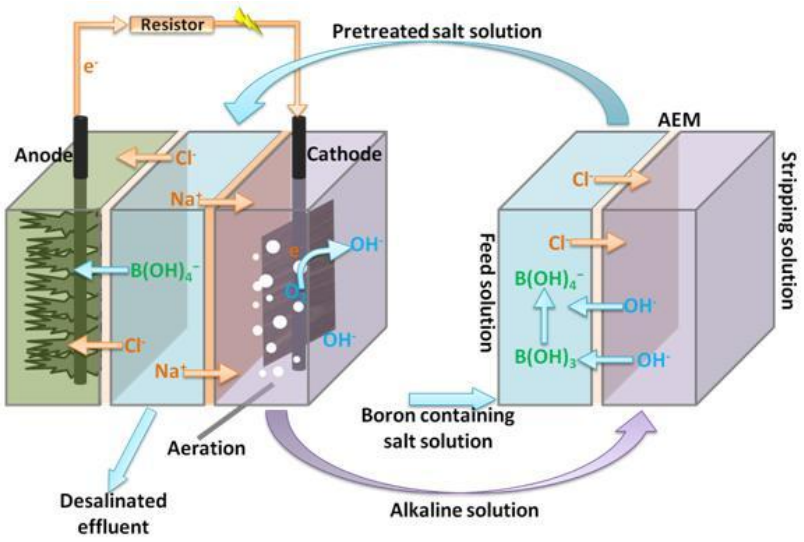

Figure 7.1 Schematic of a microbial desalination cell system integrated with Donnan Dialysis as the pretreatment process.

7.2 Materials and Methods

7.2.1 MDC setup and operation

The MDC was constructed as a tubular reactor similarly to the one in a previous study (Ping et al. 2014, Ping et al. 2015a), consisting of two layers of ion exchange membranes (IEM): anion exchange membrane (AEM, AMI-7001, Membrane International, Inc., Glen Rock, NJ, USA) with a 3.8-cm diameter and a 20-cm length forming the anode compartment (300 mL), and cation exchange membrane (CEM, CMI-7000, Membrane International, Inc.) that had a diameter

of 5 cm and a length of 20 cm wrapping the AEM tube and creating a space between the two membrane tubes that formed a desalination compartment (150 mL) . The distance between the AEM and the CEM was 0.6 cm. The anode electrode was a 20-cm long carbon fiber brush, and the cathode electrode was a piece of carbon cloth coated with activated carbon supported platinum (Pt/C) as a catalyst at a loading rate of 0.2 mg Pt cm^{-2}. An external resistor of 0.1 Ω connected the two electrodes by using titanium wire. The anode feed solution contained (per L of tap water): NaAc, 3 g (to ensure sufficient substrate supply); NH_4Cl, 0.15 g; NaCl, 0.5 g; $MgSO_4$, 0.015 g; $CaCl_2$, 0.02 g; KH_2PO_4, 0.53 g; and K_2HPO_4, 1.07 g. The anolyte was fed at a rate of 0.5 $mL \cdot min^{-1}$ (HRT of 10 h), unless elsewhere stated, and was recirculated at 100 $mL \cdot min^{-1}$. The salt solution (saline water) was prepared to mimic brackish water, and contained (per L of tap water): NaCl, 3g; and H_3BO_3, 0.028 or 0.112 g. The catholyte was either tap water or prepared by dissolving NaOH in tap water, dripping from the top to the bottom of the outer tube for rinsing the cathode electrode at a recirculation rate of 35 $mL \cdot min^{-1}$.

7.2.2 Donnan Dialysis

The DD device was an AEM tube with the volume of 300 mL submerged in a 1 L container. The tube was filled with salt solution (feed solution) recirculated at 35 $mL \cdot min^{-1}$, and the container was filled with alkaline solution (stripping solution) either from the MDC catholyte or prepared by dissolving NaOH in tap water.

7.2.3 Measurement and analysis

The MDC voltage was recorded every 3 min using a digital multimeter (Keithley Instruments, Inc., Cleveland, OH, USA). The conductivity of the salt solution was measured using a benchtop conductivity meter (Mettler-Toledo, Columbus, OH, USA). The pH was measured by a benchtop pH meter (Oakton Instruments, USA). The boron concentration was measured by using the Carmine method (HACH Co., Ltd., USA, method 10252).

7.3 Results and Discussion

7.3.1 Feasibility of boron removal

The feasibility of boron removal was examined by using an additional alkaline solution as a stripping solution in the DD. The MDC system was operated in a batch mode DD with a synthetic stripping solution prepared by dissolving sodium hydroxide in tap water. The reason why a synthetic alkaline solution was applied instead of the MDC catholyte was to achieve better manipulation of the pH. A control experiment without the DD pretreatment was conducted to evaluate the treatment performance of an MDC alone. At the flow rate of 0.06 mL min^{-1} (HRT of 41.7 h), the salt solution was desalinated from 5.2 mS cm^{-1} to lower than 0.5 mS cm^{-1} by the MDC alone. The MDC removed 20 ~ 25% of boron, decreasing its concentration from 20 to 15 mg L^{-1} B, or 5 to 4 mg L^{-1} B (Figure 7.2A). Such a removal was likely caused by a concentration gradient driven Fick's diffusion in the MDC, because the low pH of the salt solution (7.79±0.09

in the MDC salt influent and 8.03±0.03 in the MDC salt effluent) allowed the boron stay in the form of non-charged boric acid; even though the pH of the MDC catholyte (preconditioned) was as high as 12.66, the amount of hydroxide ions migrating through the CEM into the desalination compartment was not enough to raise the pH of the salt solution above 9.14 to dissociate boric acid. In the presence of the DD pretreatment with the stripping solution at pH 11 or 13, the boron concentration in the MDC salt effluent was reduced to 11 or 7 mg L^{-1} from initially 20 mg L^{-1}, or 3 or 2 mg L^{-1} from 5 mg L^{-1} (Figure 7.2A). Those results have demonstrated that the DD pretreatment could function to enhance boron removal with an MDC system, and higher pH in the stripping solution would better dissociate boric acid and thus improve the boron removal.

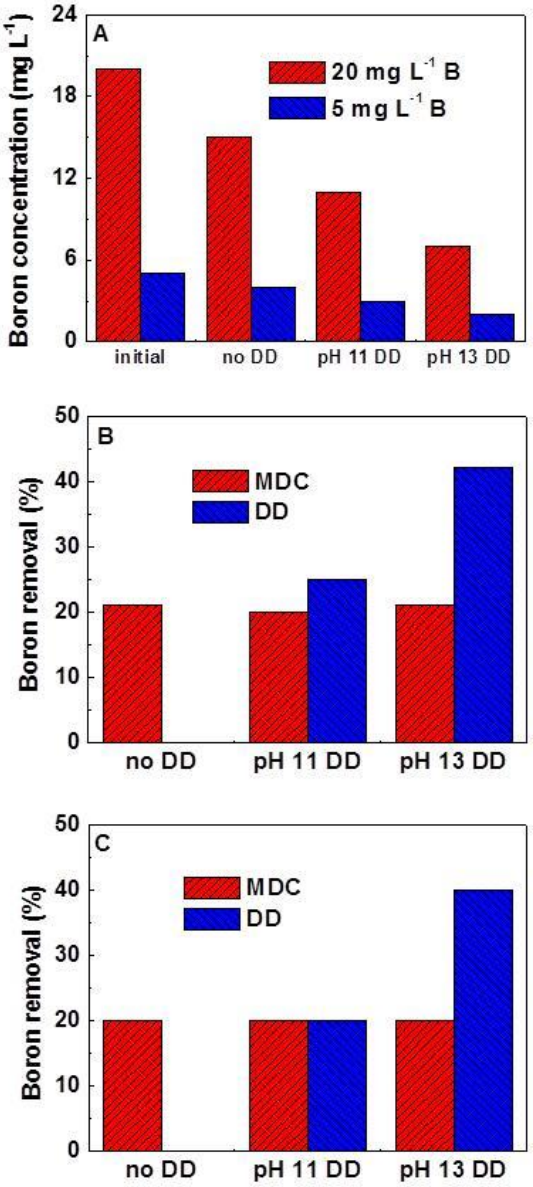

Figure 2. The Effects of pH of the DD stripping solution on boron removal: (A) Boron concentration in the MDC salt effluent; (B) removal efficiency with the initial 20 mg L^{-1}; and (C) removal efficiency with the initial 5 mg L^{-1}.

The improvement with the DD pretreatment was further analyzed. Increasing pH of the stripping solution from 11 to 13 improved the boron transport in the DD (from the feed solution into the

stripping solution), resulting in the enhanced boron removal by the DD from 25 to 42% or 20 to 40% with the initial 20 or 5 mg L^{-1} B (Figures 7.2B&C). The remaining boron in the feed (salt) solution dropped from 15 to 11 mg L^{-1} or 4 to 3 mg L^{-1}, and the boron transport rate in the DD increased from 0.21 to 0.34 μg m^{-2} s^{-1} with the initial 20 mg L^{-1} B, or 0.042 to 0.084 μg m^{-2} s^{-1} with the initial 5 mg L^{-1} B. The transport of boron in DD was contributed by hydroxide ions in a two-step process. First, the migrated hydroxide ions from the stripping solution raised the feed solution pH from 7.79±0.07 to 10.00±0.23 with pH 11 treatment, or to 12.39± 0.04 with pH 13 treatment, which completely dissociated the boric acid into borate ions. In the second step, negatively charged borate ions in the feed solution were forced to exchange with hydroxide ions in the stripping solution. Greater hydroxide concentration gradient exhibit stronger force of ion-exchange and promoted borate ion transport. However, the boron removal by the MDC was not affected by the different pH of the DD feed solution (pretreated salt solution), and remained at 20% (Figures 7.2B&C). The boron transport rate in the MDC was also stable at 0.17 or 0.042 μg m^{-2} s^{-1} with the initial 20 or 5 mg L^{-1} B. After the MDC treatment, the pH of the MDC salt effluent dropped to 7.11±0.68 or 9.09±0.30, indicating that the remaining borate in the DD effluent might be mostly converted to boric acid when it entered the MDC desalination compartment. This pH change was caused by two factors: first, driven by electricity generation, hydroxide ions could migrate faster than borate into the anode compartment (Dydo and Turek 2013), and second, protons in the anolyte could diffuse into the desalination compartment neutralizing the salt solution. However, borate ions could still exist in the MDC because of high pH zone in microenvironment inside the desalination compartment.

7.3.2 Effect of salt competition on boron removal

In an MDC, competition for ionic migration exists between borate ions and other anions (such as chloride). Because of the strong competition, borate could not be removed out of the MDC system until the concentration of chloride ions is reduced to a certain level (e.g., comparable to the concentration of borate). Thus, it is important to examine the effect of salt competition on boron removal, and this was conducted by varying hydraulic retention time (HRT) of the salt solution in the MDC at three levels, 20.8, 12.5, and 6.3 h, which resulted in different salt loading rates. To accelerate the desalination and alkaline production processes, an external voltage of 1 V was applied to the MDC. A batch MDC catholyte with pH of 10.78±0.20 and conductivity of 2.74±0.36 mS cm^{-1} (initially tap water) was used as the stripping solution in the DD device for a batch pretreatment before the salt solution was fed into the MDC.

Reducing HRT increased the salt loading rate and thus the current density of the MDC from 34.9 to 60.7 A m^{-3}. Although the longest HRT 20.8 h resulted in the conductivity of salt effluent as low as 0.066 mS cm^{-1}, in the absence of the DD pretreatment, the boron concentration remained high at 4 mg L^{-1} in the MDC salt effluent, slightly reduced from 5 mg L^{-1} B. When the DD pretreatment was linked to the MDC, the pH of the salt solution was raised from 7.77±0.10 to 10.43±0.15, while the conductivity was reduced from 5.29±0.15 to 4.38±0.09 mS cm^{-1} after the pretreatment. Despite the increased molar conductivity by exchange of chloride ion (76.2 S cm^2 mol^{-1}) with hydroxide ion (197.9 S cm^2 mol^{-1}), dilution of the feed solution due to water osmosis from the stripping solution (initial stripping solution conductivity was at 2.74±0.36 mS cm^{-1} and the difference between the stripping and the feed solutions was 2.55 mS cm^{-1}) has more impact

on the feed solution and caused the decrease in conductivity. Consequently, the MDC achieved a final boron concentration of 9.67±0.58 or 2.00±0.00 mg L^{-1} B, with removal efficiency of 51.7 or 60.0% at initial 20 or 5 mg L^{-1} B; the salt effluent had conductivity less than 0.067 mS cm^{-1}. It was found that, even with the DD pretreatment, the boron concentration in the MDC salt effluent remained high and boron removal efficiency remained below 50% until the salt solution was desalinated to conductivity lower than 0.3 mS cm^{-1}. At a lower HRT of 6.3 h that had a higher salt loading rate, the conductivity of the salt effluent was above 2 mS cm^{-1}, and the boron remained in the salt effluent increased to 12.50±0.71 and 3.00±0.00 mg L^{-1} at two initial concentrations with removal efficiency around 40% (Table 7.1; Figures 7.3A&B).

Table 7.1 Boron removal vs. conductivity of the desalinated salt effluent in the MDC system with DD pretreatment

	Boron removal (%)	Conductivity of the MDC salt effluent (mS cm^{-1})
Initial 5 mg L^{-1} B	60.0	0.07
	50.0	0.32
	40.0	2.02
Initial 20 mg L^{-1} B	51.7	0.07
	37.5	0.79
	37.5	2.73

Further analysis reveals that with a lower salt loading rate, boron removal by the MDC could become higher up to 40%, and when the salt loading rate increases, the MDC removal of boron greatly decreased (Figure 7.3C). The DD pretreatment could improve the removal efficiency of the MDC by about 15%, which further confirmed that the ionized form of boron could benefit its removal in the MDC. We observed that at the longest HRT of 20.8 h (salt loading rate of 3.03 kg m^{-3} d^{-1}) with initial 20 mg L^{-1} B, the MDC removed 11.7% of boron, less than 17.5% at a shorter HRT of 12.5 h (salt loading rate of 5.24 kg m^{-3} d^{-1}), likely related to better boron removal by the DD pretreatment (40% compared with 20%) that suppressed the following MDC treatment. The reason for variation in the DD contribution to boron removal (20 to 40%) was not clear, and it did not seem to be directly related to the pH of the stripping solution that ranged from 10.58 to 11.12. Those results collectively demonstrate that boron removal can be improved with the DD pretreatment and lower salt loading rate benefits the boron removal in the MDC.

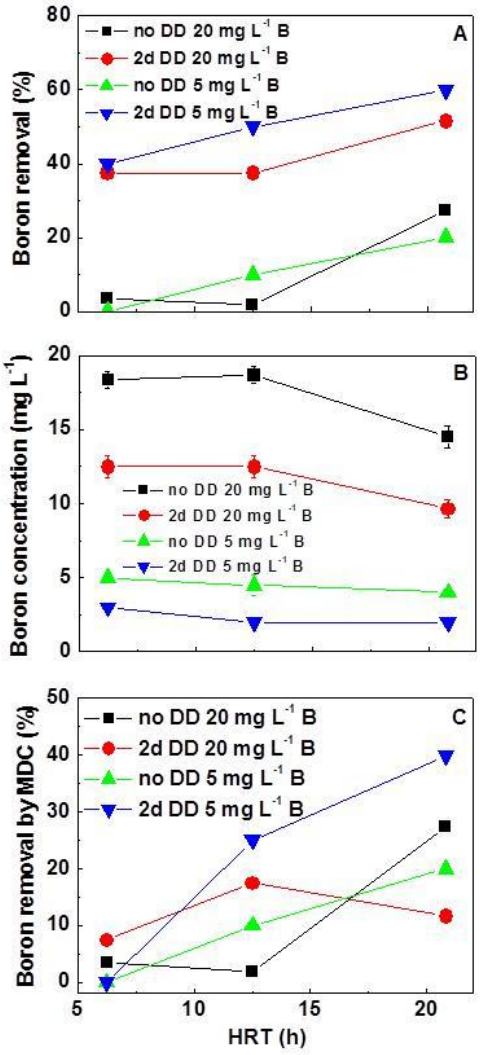

Figure 7.3 The effects of HRT (and thus salt loading rate) on boron removal with two different initial boron concentration: A) overall removal efficiency; B) boron concentration in the MDC salt effluent; and C) boron removal efficiency of the MDC.

7.3.3 Different treatment strategies

In addition to the DD pretreatment, two additional treatment strategies were investigated and compared with the DD pretreatment. First, direct alkalinization pretreatment in the MDC cathode was conducted by flowing the salt solution into the cathode first and then the desalination chamber (Figure 7.4A); in that way, the pH of the salt solution could be directly increased and thus a DD component was not needed. Second, the DD post-treatment was examined with the salt solution treated in the MDC first and then the MDC salt effluent acted as the feed solution for the DD (Figure 7.4B); such arrangement was to reduce the competition between chloride ions and borate ions in DD through removing chloride ions by the MDC. An external voltage of 1 V was applied to accelerate alkaline solution production and desalination rate in all three systems, and they were continuously operated for comparison. When the system contained a DD component (for either pre- or post-treatment), the stripping solution was recirculated through the MDC cathode.

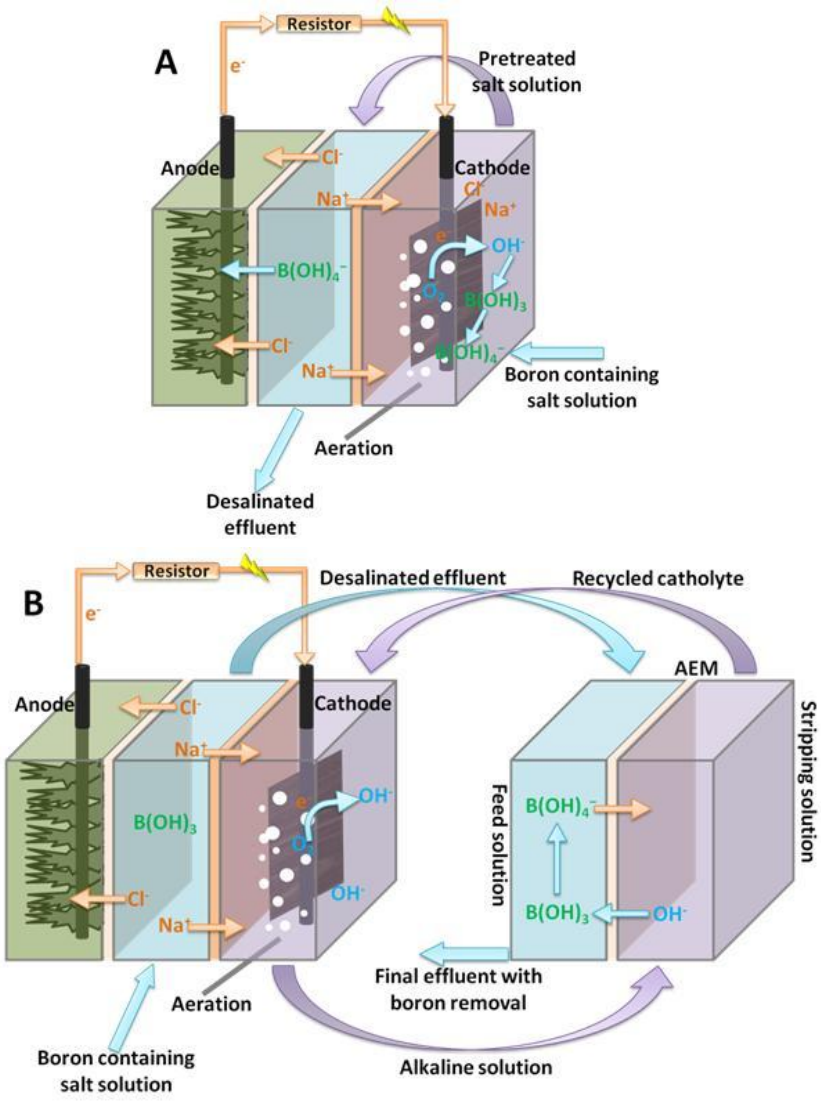

Figure 7.4 Two additional treatment strategies: (A) cathodic alkalinization system; and B) MDC with DD as a post-treatment process.

Both cathodic alkalinization and the DD pretreatment system could reduce the boron concentration in the salt solution from 5 to around 3 mg L^{-1} (Figures 7.5A&D). The DD post-treatment system was able to decrease the boron concentration from 5 to 2 mg L^{-1} with 20~30% removal of boric acid by the MDC and 30~40% by ion exchange removal in the DD (Figure

7.5G). All three systems achieved conductivity lower than 0.07 mS cm^{-1} in the final effluent, although in cathodic alkalinization the conductivity of the MDC salt effluent did not reach a steady state (for example, it kept increasing from 0.06 mS cm^{-1} to above 0.50 mS cm^{-1} at the salt solution flow rate of 0.08 mL min^{-1}) as a result of the rising salinity of the MDC salt influent (catholyte) (Figures 7.5B&E&H). In the cathodic alkalinization approach, increased salinity in the MDC salt influent (from 5.26 mS cm^{-1} in the catholyte influent to 11.73 mS cm^{-1} in the catholyte effluent) would create challenges for long-term operation. When the salinity of the salt solution was reduced to a very low level (e.g., 0.3 mS cm^{-1}), the current was mostly used to drive the migration of hydroxide ions rather than borate. Thus, it is conjectured that chloride ions are the major competitor to borate with the salinity of salt solution above 0.30 mS cm^{-1}, and when the salinity is further reduced, hydroxide ions become a competitor to borate and migrate into the anolyte before borate ions do. The DD post-treatment system had the best performance of boron removal, benefited from two factors: (1) unlike an MDC that had the loss of hydroxide ions, hydroxide ions in the DD migrated from the stripping solution into the feed solution and were kept there to maintain the ionized form of boron; and (2) the MDC (before the DD post-treatment) removed chloride ions through desalination and thus resulted in weak competition between chloride ions and borate ions.

A major drawback of the DD post-treatment system is the high pH of the final desalinated solution (DD effluent) and the associated risk for irrigation application. Affected by the stripping solution (pH above 10), the final effluent of the salt solution (DD effluent) had pH around 8.7, higher than the normal pH range for irrigation water at 6.5~8, and further improving the DD

performance (and thus the exchange with hydroxide ions) could result in even higher pH. Reducing the HRT of the salt solution in the DD by increasing the salt flow rate from 0.12 to 0.16 mL min^{-1} allowed hydroxide ions less time to migrate into the feed solution; however, it did not alleviate the high pH issue in the final salt effluent (DD effluent) (Figure 7.5I). When we removed the external power supply from the MDC and reduced the salt flow rate to 0.04 mL min^{-1}, the current generation decreased to12 A m^{-3} with catholyte pH of 9.7; then, the final salt solution achieved a boron concentration of 1 mg L^{-1} with conductivity of 0.21 mS cm^{-1} and pH of 8.0, within range of the irrigation guideline.

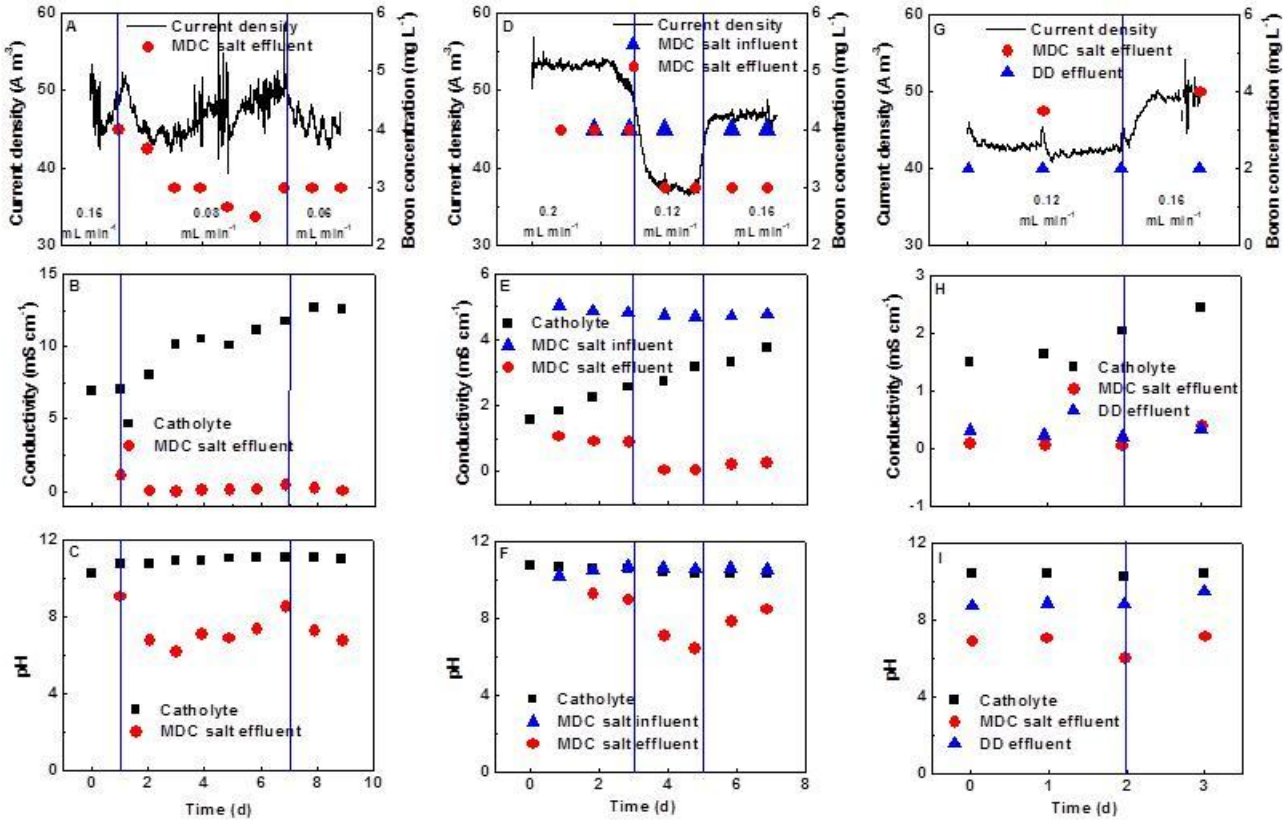

Figure 7.5 Comparison among three treatment strategies (continuous operation), cathodic alkalinization (A-C), Donnan Dialysis pretreatment (D-F) and Donnan Dialysis post-

treatment (G-I): (A, D, and G) current generation and boron concentration; (B, E, and H) solution conductivity; and (C, F, and I) solution pH.

Among all three systems, cathodic alkalinization had the highest catholyte conductivity above 7 mS cm^{-1}, which ensured a fast electron transfer in the cathode, and thus the current (varied mostly between 45 and 50 A m^{-3}) was not interrupted dramatically by the conductivity change in the desalinated solution. However, it did not seem to be sustainable in terms of the constantly increasing catholyte conductivity with influence on the MDC salt influent as previously discussed. In the presence of a DD treatment (either pre or post), the catholyte conductivity remained relatively low. It increased from 1.59 to 3.77 mS cm^{-1} over 7 days in the DD pretreatment system (Figure 7.5E), or 1.50 to 2.43 mS cm^{-1} over 3 days in the DD post-treatment system (Figure 7.5H). A salinity increase rate of 0.31 mS cm^{-1} per day was observed in both systems and was unavoidable because the exchange of hydroxide ions with chloride ions. If the catholyte conductivity rises to a high level (through long-term accumulation of salts), then it could negatively affect the exchange of hydroxide ions because of anion competition. Thus, replacement of catholyte at that time will be necessary.

7.4 Conclusions

This study has presented simultaneous desalination and boron removal through integrating microbial desalination cells and Donnan dialysis. The alkaline solution generated by the MDC can be used to ionize boric acid to borate and serve as a stripping solution in the DD treatment.

Higher pH of the stripping solution in DD pretreatment promotes the boron removal from the feed solution. A lower salt loading rate ensures less competition between chloride ions and borate in the MDC and thus benefits boron removal. Loss of hydroxide ions into the anolyte in the MDC negatively affects boron removal but helps maintain neural pH for the final effluent. Three treatment strategies are investigated and compared, and the results show that a system with DD post-treatment can achieve the best performance of boron removal, but the high pH of the final effluent needs to be further addressed. Cathodic alkalinization (without DD treatment) seems to be the least sustainable strategy due to salinity increase and unsatisfied boron removal performance. Given the advantages and disadvantages of each strategy, future study will investigate an MDC treatment system with both DD pre-treatment and post-treatment.

Chapter 8 Enhanced boron removal by electricity generation in a microbial fuel cell

(This section has been published as Ping, Q., Abu-Reesh, I.M. and He, Z. (2016) Enhanced boron removal by electricity generation in a microbial fuel cell. ***Desalination***. Vol 398, pp 165-170.)

Abstract

Boron needs to be removed during desalination, because excessive boron in the product water for irrigation can deteriorate plant growth. In this study, a microbial fuel cell (MFC) equipped with anion exchange membrane (AEM) was proposed and investigated to remove boron via two successive steps: boric acid is ionized to borate ions in the presence of high pH as a result of cathode reaction, and borate ions are transported across AEM driven by electricity generation. Two scenarios were examined, the MFC as a pretreatment process and the MFC as a post-treatment step in connection with conventional desalination. In the pretreatment mode, the MFC achieved 40-50% boron removal and the high pH condition could benefit downstream desalination or other methods for further boron removal. In the post-treatment mode, the MFC removed 80-90% of boron and decreased the boron concentration from 20 to 2 mg L^{-1} or from 5 to 1 mg L^{-1}, which meets the irrigation water requirement. The removal rate in this MFC was much higher than that of a previously reported microbial desalination cell coupled with Donnan Dialysis system. Those results have demonstrated the potential of using MFCs for boron removal with benefits of conductivity reduction and electricity generation.

8.1 Introduction

Desalination of seawater or brackish water has become an important process to obtain clean water worldwide due to the limited freshwater sources (Mathioulakis et al. 2007). One of the problems for desalination is the remaining trace elements in the product water, such as boron. Boron exists in natural water in the form of boric acid, which is a non-dissociable compound. Seawater usually has a boron concentration of ~ 5 mg L^{-1}, while brackish water contains boron up to 40 mg L^{-1} (Melnik et al. 1999). Despite the fact that boron is an essential element for plant growth, when its concentration in the irrigation water exceeds 2 mg L^{-1}, many plants would exhibit toxicity symptoms (Guler et al. 2015). Boron can also be detrimental to animals and humans when being exposed to excessively. The World Health Organization (WHO) recommends the boron limit in drinking water to be as low as 0.5 mg L^{-1}, while the Drinking-Water Quality Committee revised the boron guideline value to 2.4 mg L^{-1} in 2011 (Kabay and Bryjak 2015).

Although conventional reverse osmosis (RO) technologies can remove anions and cations at almost 100% rejection rate, the rejection of boron by RO in the uncharged form, boric acid, is low at ~ 70% (Guler et al. 2010). The low-pressure brackish water RO membranes may have the boron rejection as low as 40% [6]. To ensure adequate removal of boron from permeate, it will be necessary to raise the pH of the feed solution above the pKa value of 9.14 where the dominant boron is transformed to charged borate species (Eq. 1) (Kabay and Bryjak 2015, Guler et al. 2009). Other methods such as electrodialysis and electro-flocculation also require high pH to ionize boric acid to the charged form - borate (Ofir et al. 2011, Kabay et al. 2008, Kijanski et al.

2013). The need for high pH in the feed solution will increase the consumption of chemicals such as sodium hydroxide, resulting in higher operating costs (Guler et al. 2015).

$$B(OH)_3 + H_2O \Leftrightarrow B(OH)_4^- + H^+ \qquad (1)$$

Elevation of pH is a phenomenon in the cathode of bioelectrochemical systems (BES) as a result of reduction reactions. BESs are emerging technologies that can convert chemical energy stored in wastewater directly into electrical energy with the help of microorganisms (Ge et al. 2014, Rozendal et al. 2008). They have been demonstrated to efficiently remove organics from wastewater in the anode compartment of microbial fuel cells (MFCs) (Ge and He 2016), desalinate seawater or brackish water in microbial desalination cells (MDCs) (Jacobson et al. 2011a, Ping et al. 2015a), produce hydrogen gas on the cathode of microbial electrolysis cells (MECs) with reduced external power supply (Logan et al. 2008), or conduct groundwater remediation (Tong and He 2013, Li et al. 2016, Wu et al. 2016). Under an anoxic condition, the anodic microorganisms release electrons while oxidizing organic matters and then transfer the electrons from inside the cells to the anode resulting in a negative anode potential [20]. The reduction of a terminal electron acceptor such as oxygen on the cathode is driven to produce hydroxide ions (Eq. 2) and complete the electric circuit (Popat et al. 2012). This feature of the cathode was employed in a previous study that accomplished boron removal by a system coupling MDCs with Donnan Dialysis (DD) (Ping et al. 2015b). Although the coupled system achieved effective boron removal, the higher mobility of hydroxide ions over borate ions in the MDC resulted in loss of hydroxide ions from the desalination compartment into the anode compartment and those hydroxide ions outcompeted borate ions, thereby limiting the removal

efficiency. The DD as post-treatment proved to have the most effective boron removal due to the trapped hydroxide ions in the feed solution allowing boron to remain the negatively charged form and be transferred out of the feed solution through anion exchange membrane (AEM) (Ping et al. 2015b). However, the boron removal in DD is generally slow, limited by a driving force of concentration gradient.

$$O_2 + 2H_2O + 4e^- \rightarrow 4OH^- \qquad (2)$$

To overcome the limitation of concentration-gradient driven boron removal, a new strategy was proposed in this study to remove boron driven by electrical field in an MFC with AEM separating its anode and cathode compartments. In such an MFC, the oxygen reduction reaction on its cathode produces hydroxide ions, resulting in high pH that transforms boric acid into borate ions. The electrical field drives the movement of chloride ions, borate ions, or other abundant anions in the catholyte across the AEM into the anode compartment (Figure 8.1). Such current driven borate removal is expected to surpass the passive movement of borate in the previously reported MDC-Donnan Dialysis system. The objectives of this study were to 1) examine the feasibility of using an MFC to remove boron under either the pretreatment or post-treatment mode; 2) evaluate the effect of current generation on boron removal; and 3) investigate the salinity change during boron removal.

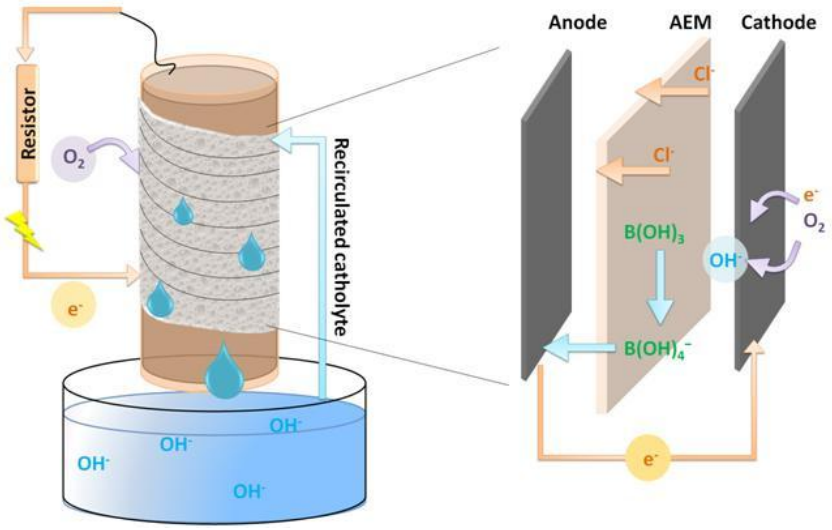

Figure 8.1 Schematic of a microbial fuel cell treating boron containing salt solution.

8.2. Materials and Methods

8.2.1 MFC setup

The MFC was constructed as a tubular reactor consisting of one layer of anion exchange membrane (AEM, AMI-7001, Membrane International, Inc., Glen Rock, NJ, USA) with a diameter of 3.8 cm and a length of 32 cm, making the anode compartment volume of 350 mL. The top and bottom of the reactor were sealed by PVC caps, on which the effluent and influent connectors were installed. The anode electrode was a piece of carbon cloth (with effective surface dimensions of 22 cm-long and 2.9 cm-diameter) installed alongside the inner surface of the AEM tube and supported by a plastic mesh. The cathode electrode was a piece of carbon cloth that was coated with activated carbon supported platinum (Pt/C) as a catalyst at a loading

rate of 0.3 mg Pt cm^{-2} and wrapped outside of the AEM tube. An external resistor of 10 or 1 Ω connected the two electrodes by using titanium wire.

8.2.2 MFC operation

The MFC was operated at a room temperature of ~ 22 ºC. The anode was inoculated with a mixture of aerobic and anaerobic sludge from the Peppers Ferry Regional Wastewater Treatment Plant (Radford, VA, USA). The anode feed solution was fed in a continuous mode at a rate of 0.13 mL min^{-1} (HRT of 1.9 d), containing (per L of tap water): NaAc, 3 g (to ensure sufficient substrate supply); NH_4Cl, 0.15 g; NaCl, 0.500 g; $MgSO_4$, 0.015 g; $CaCl_2$, 0.02 g; KH_2PO_4, 0.53 g; and K_2HPO_4, 1.07 g. The catholyte was recirculated from a container that had a volume of 200 mL, and was dripping from the top to the bottom of the tube for rinsing the cathode electrode at a recirculation rate of 35 mL min^{-1}. The catholyte was prepared by dissolving sodium chloride and boric acid in tap water to represent four types of solutions: seawater in the pretreatment mode contained (per L of tap water) NaCl, 35 g and H_3BO_3, 28 mg; seawater in the post-treatment mode contained (per L of tap water) H_3BO_3, 28 mg; brackish water in the pretreatment mode contained (per L of tap water) NaCl, 6 g and H_3BO_3, 28 or 112 mg; and brackish water in the post-treatment mode contained (per L of tap water) H_3BO_3, 28 or 112 mg. The prepared solutions have 5 mg L^{-1} B in seawater and 5 or 20 mg L^{-1} B in brackish water.

8.2.3 Measurement and analysis

The MFC voltage was recorded every 3 min using a digital multimeter (Keithley Instruments, Inc., Cleveland, OH, USA). The conductivity of the salt solution was measured using a benchtop conductivity meter (Mettler-Toledo, Columbus, OH, USA). The pH was measured by a benchtop pH meter (Oakton Instruments, USA). The boron concentration was measured by using the Carmine method (HACH Co., Ltd., USA, method 10252). The ion compositions in the solution were measured using ion chromatography (Dionex DX-500) with suppressed conductivity detection. The column used for cations was a CS-16 with a CSRS-300 suppressor and for anions was an AS-9HC with an ASRS-300 suppressor. The current density was normalized by the volume of the anode compartment. The boron removal rate was calculated as the amount of boron removed from the catholyte within the treatment time normalized by the AEM area:

$$r_B = \frac{(C_0 - C_t) * V}{A * t} \qquad (3)$$

where C_0 is the initial boron concentration in the catholyte, C_t is the boron concentration at time t, V is the volume of the catholyte, A is the membrane surface area of the AEM, and t is the time length of the treatment.

8.3 Results and Discussion

8.3.1 Boron removal from seawater

The feasibility of boron removal by the MFC was firstly examined with artificial seawater that contained 5 mg B L^{-1}. The experiments were conducted under two scenarios: the pretreatment

mode that the MFC is assumed to treat original seawater followed by further desalination (which was not included in this study), and the post-treatment mode that the MFC receives the desalinated seawater. Meanwhile, the effect of current generation on boron removal was investigated by adjusting the external resistance load (10 and 1 ohm). In both modes, the pH of the catholyte was increased higher than 9.14 within 4 h due to oxygen reduction reaction, which rendered borate ions to be the dominant boron species. In the pretreatment mode, the MFC reduced the boron concentration from 5 to 3 mg B L^{-1}(Figure 8.2A), which is above the irrigation standard or the WHO guideline value. Higher current generation at 1 ohm (67.8 ± 33.2 A m^{-3}) than that at 10 ohm (45.5 ± 14.0 A m^{-3}) did not obviously improve boron removal, likely because that the high concentration of chloride ions in the catholyte outcompeted the borate ions during anion transport across the AEM. On the other hand, the post-treatment mode exhibited effective removal of boron. At 10 ohm, the MFC generated 48.7 ± 1.1 A m^{-3} (Figure 8.2B), slightly higher than that of the pretreatment mode, and decreased the boron concentration from 5 to 2 mg L^{-1}. Decreasing the external resistance to 1 ohm improved the current generation to 81.0 ± 1.2 A m^{-3}, resulting in an even lower boron concentration of 1 mg L^{-1}(Figure 8.2A). The boron removal rate of 0.31 μg m^{-2} s^{-1} was observed during the first 8 h with 10 ohm. When switching to 1 ohm, because of a stronger driving force due to higher current generation, the borate removal rate across the AEM was improved to a higher level, resulting in a much higher boron removal rate of 0.98 μg m^{-2} s^{-1} during the first 8 h.

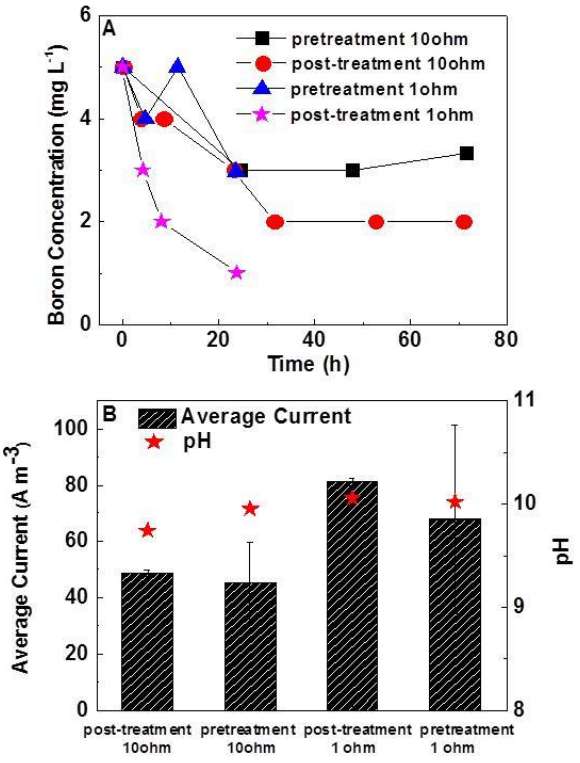

Figure 8.2 The MFC performance of treating boron containing seawater: (A) boron concentration in the catholyte; and (B) The average current densities and the pH of the catholyte after one day's treatment.

It is worth noting that the migration of chloride ions from the catholyte into the anolyte largely influenced the microbial community and thus the current generation in the pretreatment mode. Upon supplying the synthetic seawater to the MFC cathode, an instant current increase to 72 A m^{-3} was observed due to the reduced electrolyte resistance (seawater conductivity of 51.60 mS cm^{-1} compared with tap water at 0.15 mS cm^{-1}) and followed by constant current decrease to around 30 A m^{-3}, lower than 49 A m^{-3} from the MFC with the tap water catholyte (Figure 8.3).

Because the MFC was inoculated with nonhalophile bacteria from wastewater, which would survive with a NaCl concentration lower than 12.9 g L^{-1} (Wang et al. 2011, Liu et al. 2005), intrusion of chloride ions from the catholyte into the anolyte could damage the anode microbial activity, thereby affecting electricity generation. Such an inhibitory effect could be alleviated by decreasing the salt input to the catholyte (e.g., slow down its flow rate), or increasing the anolyte flow rate for more dilution effect. The detailed analysis of transport of chloride ions will be discussed in section 3.3. Despite higher current generation of the pretreatment mode in the first few hours, the total electrical charge (coulomb) of the pretreatment mode within one day was lower than that of the post-treatment mode. However, the pH of the catholyte under the pretreatment mode was comparable or even higher than that in the post-treatment mode (Figure 8.2B). By dividing the amount of retained hydroxide ions in the catholyte (converted from pH value) over the theoretical production of hydroxide ions based on current generation, a ratio of

0.0007 or 0.0018 was obtained for the pretreatment mode with 10 ohm or 1 ohm, higher than 0.0004 or 0.0007 in the post-treatment mode, indicating that the extent of hydroxide ion migration across the AEM in the post-treatment mode could be greater than that in the pretreatment mode. Because the ionic transport rate is closely correlated with ion concentration [25], chloride ions were most responsible for the ionic transport across the AEM in the pretreatment mode due to its greater concentration, and hindered the transport of both hydroxide and borate ions.

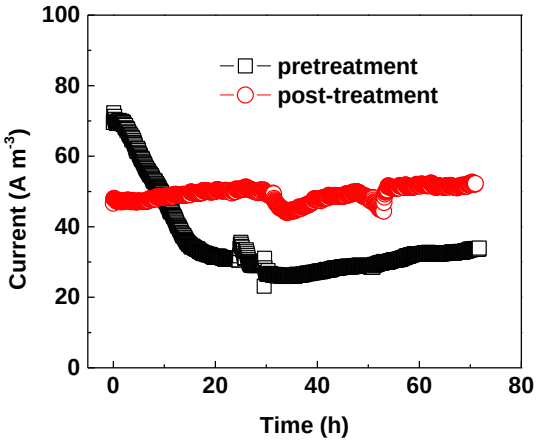

Figure 8.3 The current generation by the MFC in the pretreatment and post-treatment modes.

8.3.2 Boron removal from brackish water

Boron removal by the MFC was further investigated with brackish water containing either 5 or 20 mg L^{-1} of boron (28 or 113 mg L^{-1} boric acid); 1-ohm external resistance was used in the electrical circuit for high current generation. Like the seawater experiments, the post-treatment mode achieved better boron removal than the pretreatment mode. When operated in the pretreatment mode, the MFC reduced the boron concentration from 19 to 10 mg L^{-1} at a removal rate of 4.40 μg m^{-2} s^{-1} or from 4.0 to 2.3 mg L^{-1} at a rate of 0.73 μg m^{-2} s^{-1} during the first 3~5 h; no further removal was observed afterwards (Figure 8.4A). In the post-treatment mode, the MFC decreased the boron from 20 to 2 mg L^{-1}, or 5 to 1 mg L^{-1} within one day, both of which were below the required concentration for irrigation or WHO (World Health Organization) regulation. The post-treatment mode also achieved a high removal rate of 6.25 μg m^{-2} s^{-1} during

the first 4 h with an initial 20 mg L^{-1}. The MFC generated a much higher current density of 115.6 ± 3.7 A m^{-3} in the pretreatment mode than that of the post-treatment mode (84.0 ± 4.4 A m^{-3}), due to the higher catholyte conductivity (6.18 ± 0.18 mS cm^{-1} vs. 0.27 ± 0.03 mS cm^{-1}); however, the hindrance of the high salinity in the pretreatment mode towards the removal of borate ions was also obvious. Higher current generation led to higher pH of 10.58 ± 0.08 in the salt solution in the pretreatment mode compared with 10.10 ± 0.08 of the post-treatment mode (Figure 8.4B). The ratio between the amount of retained hydroxide ions in the catholyte (converted from pH value) and the calculated production of hydroxide ions based on current generation was 0.0038 for the pretreatment mode, which is higher than 0.0018 in the post-treatment mode, suggesting that the extent of hydroxide ions migration was lower in the pretreatment mode due to the competitor ions such as chloride ions. However, the microbial community on the anode might not be negatively affected by the migrated chloride ions from the catholyte, indicated by the stable current generation of 115.6 ± 3.7 A m^{-3}. This was likely due to the lower salinity of the brackish water.

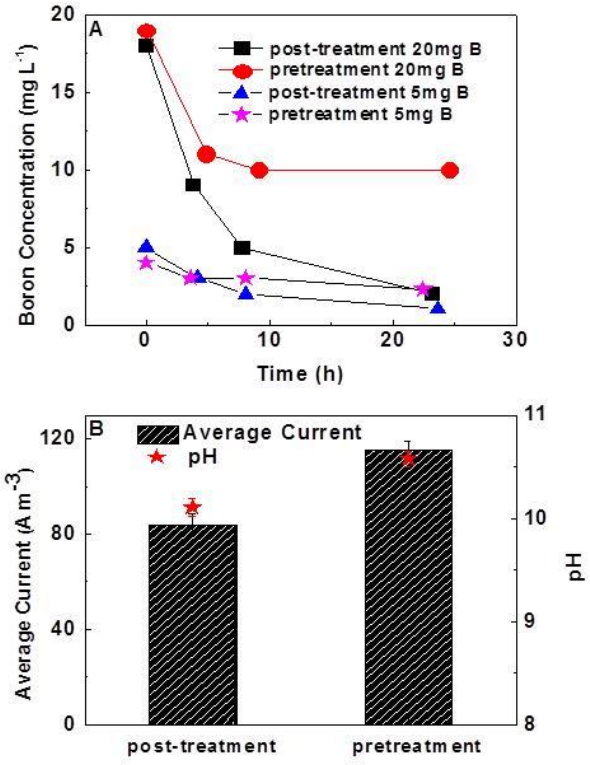

Figure 8.4 The MFC performance of treating boron containing brackish: (A) boron concentration in the catholyte; and (B) the average current densities and pH of the catholyte after the treatment in pretreatment and post-treatment modes.

To further understand the contribution of boric acid diffusion and current-driven migration of borate ions to boral removal, the control experiments operated with open circuit (OC) were conducted for the post-treatment mode. The MFC with OC achieved 55~60% boron removal for initial 20 or 5 mg B L^{-1} in 24 h, while the similar removal efficiency was obtained in the MFC with electricity generation (1 ohm external resistance) in 4 or 8 h. The removal rate of the MFC under OC was 1.13 or 0.36 μg m^{-2} s^{-1}, much lower than 6.25 or 0.98 μg m^{-2} s^{-1} with 1 ohm

electrical connection (Figure 8.5). In the absence of electricity generation, there was no production of hydroxide ions in the catholyte, and as a result, the pH of the catholyte was around 8.32 ± 0.01, below the pKa value of boric acid. With electricity generation, the pH of the catholyte could reach 9.55~10.16. It was conjectured that the water movement dragged boric acid out of the catholyte via convective transport, based on the facts that 1) the majority of boron remained in the uncharged form during the OC operation and thus ion exchange would not be effective; 2) water osmosis from the catholyte into the anolyte reached approximately 10 mL within one day; and 3) the trigonal structured boric acid has a small size close to water molecule. This presumption was confirmed with the experiments conducted in a Donnan Dialysis device equipped with AEM and neutral pH of the feed and strip solutions, where strong osmosis from the boron containing solution led to boron movement in the same direction (50 mL water movement coupled with 31 mg boric acid).

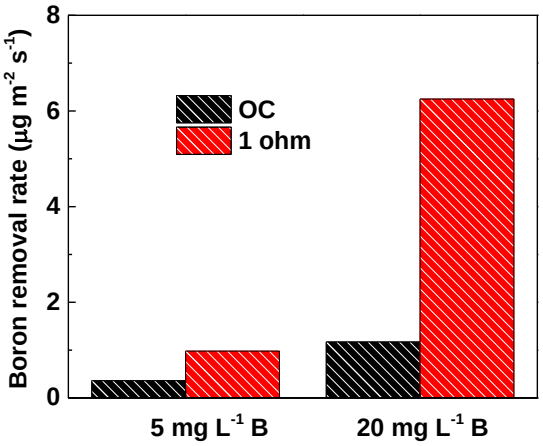

Figure 8.5 The boron removal rate under the open circuit (OC) condition and electricity-generating condition (with 1ohm external resistance) in the post-treatment mode.

8.3.3 Conductivity variation

The conductivity of the catholyte exhibited different profiles under the two operational modes. In the post-treatment mode, the catholyte conductivity increased from 0.15 to 0.31 mS cm^{-1} with 10 ohm, or to 0.27 mS cm^{-1} with 1 ohm (Figure 8.6A). Despite this increase, the final conductivity of the catholyte (or the product water) is still below the non-restriction guideline for surface irrigation [26]. The increase was mainly caused by diffusion of Na^+, K^+, and PO_4^{3-} from the anolyte and the generated OH^-. At 1 ohm, the highest concentration of Na^+ in the catholyte was 46.1 mg L^{-1} followed by K^+ of 7.0 mg L^{-1} and PO_4^{3-} of 2.1 mg L^{-1} (Figure 8.6B). Because the industrially manufactured AEM usually does not have 100% permselectivity, it is possible that Na^+ ions were driven by an electrical field to cross AEM and make up for the slow anion transport due to insufficient anion supply in the catholyte. The reduction of Cl^-, NO_3^-, and SO_4^{2-} from 24.8, 1.0, and 5.4 mg L^{-1} to 12.0, 0.0, and 0.0 mg L^{-1} was observed in the post-treatment mode, possibly being transported into the anolyte driven by the electrical field (Figure 8.6C). The disappearance of 3.7 mg L^{-1} Ca^{2+} was likely due to precipitation of $Ca(OH)_2$.

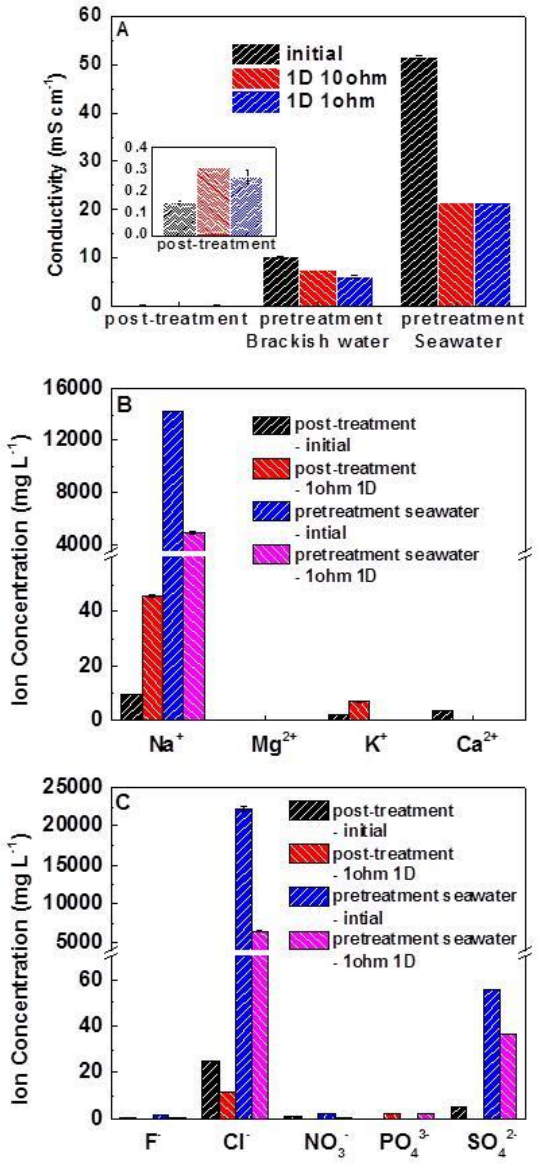

Figure 8.6 Conducitivity change in the MFC cathode:(A) the conductivity of product water; (B) the concentrations of cations; and (C) the concentrations of anions in the product water.

In the pretreatment mode, the salinity of the product water (catholyte) decreased from 10.14 ± 0.13 to 6.18 ± 0.18 mS cm^{-1} for brackish water, and more dramatically from 51.60 ± 0.28 to

21.30 ± 0.00 mS cm^{-1} for seawater (Figure 8.6A). According to the results of the IC test for ion concentrations, the declined salinity was mainly caused by the reduction of both Na^+ and Cl^- concentrations. For example, when seawater was used as a catholyte, 80.7 mmole of Na^+ and 88.5 mmole of Cl^- were transported from the catholyte into the anolyte within one day, reducing the Na^+ and Cl^- concentrations in the catholyte from 14.2 to 5.0 g L^{-1} and 22.2 to 6.5 g L^{-1}, respectively (Figure 8.6B&C); the migrated Na^+ and Cl^- raised the anolyte conductivity from 6.31 to 7.28 mS cm^{-1}. It is unusual that the Na^+ ions were transported across the AEM at such a high level, which could be related to the non-ideal permselectivity of the particular AEM used in this study. The appearance of PO_4^{3-} in the product water in both the pretreatment and the post-treatment modes was due to the diffusion of phosphate ions from the anolyte that had a high concentration of phosphate buffer (95 mg P L^{-1}); this would not be an issue for real-world practice because the phosphate is typically below 10 mg P L^{-1} in domestic wastewater and many industrial wastewater (Yuan and Pratt 2012).

8.3.4 Perspectives

The MFC with AEM as a separator between the anode and the cathode compartments could be a promising approach to treat boron containing saline water and reduce the boron concentration for irrigation purpose. The simple one-membrane tubular MFC is easy to construct and maintain compared with the MDC which has two membranes. In addition to that, the MFC has achieved much higher boron removal rates than that of a previously reported MDC-DD system (0.34 μg m^{-2} s^{-1} at 1.7 d HRT) (Ping et al. 2015b). In the post-treatment mode, the MFC achieved a boron removal rate as high as 6.25 μg m^{-2} s^{-1} (within 4 h), 10 times higher than that of the MDC-DD.

Such improvement was benefited from active transport of borate ions driven by current generation, rather than the passive movement depending on the hydroxide migration in the DD to achieve charge balance. The boron concentration in the product water could meet the irrigation requirement as well as the WHO standards. One potential problem of this approach is the high pH of the product water, which would require further adjustment.

Although the pretreatment mode did not achieve a low concentration of boron with either brackish water or seawater, the MFC raised the pH of seawater or brackish water up to 10.60, which could potentially improve boron removal in the following desalination (e.g., by RO). In addition, the MFC greatly reduced the conductivity of saline water through electricity-driven transport of Cl^- and diffusion of Na^+ across the AEM, which could benefit the following desalination. The intense salt/ion transport could lead to inhibition on the anodic bacteria, but the problem can be alleviated by adapting microbial community in response to increased salinity and/or by adjusting the anolyte retention time. The pH increase in the MFC avoids addition of chemicals, which will benefit the downstream desalination and save the operating expense.

8.4 Conclusions

This study has demonstrated the feasibility of using MFC to enhance boron removal by electricity generation. The oxygen reduction reaction serves as an effective method to raise the pH of saline solution and ionize boric acid to borate ions. Both pretreatment and post-treatment modes achieved boron removal while the post-treatment mode was able to reduce boron

concentration to meet requirement for irrigation or municipal use. In addition to the electrical current driving force exerted on borate ions, convective transport of boric acid with water osmosis also contributed to the migration of boron species. During boron removal, the MFC greatly decreased the conductivity of artificial seawater through both current-driven migration of chloride ions and diffusion of salt. Further development of MFCs for boron removal will need to consider continuous operation and examine long term performance.

Chapter 9 Mathematical model of dynamic behavior of microbial desalination cells for simultaneous wastewater treatment and water desalination

(This section has been published as Ping, Q., Zhang, C., Chen, X., Zhang, B., Huang, Z. and He, Z.(2014) Mathematical model of dynamic behavior of microbial desalination cells for simultaneous wastewater treatment and water desalination. ***Environmental Science & Technology.*** Vol 48, pp 13010-13019.)

9.1 Introduction

Water shortage is a global issue that influences a large population, especially in the developing nations.(Onda et al. 2012) To alleviate this problem, desalinating seawater or brackish water appears to be an effective approach to provide alternative source of fresh water. However, high energy consumption associated with desalination processes makes desalinated water prohibitively expensive. For example, reverse osmosis (RO), which is the most widely applied desalination technology, requires 3-7 kWh of energy to produce 1 m^3 of freshwater.(Semiat 2008) Recent development of microbial desalination cell (MDC) provides a potentially energy-efficient desalination method.(Cao et al. 2009, Jacobson et al. 2011), MDCs use electricity generated from low-grade substrates such as wastewater to drive desalination process so that it requires little external energy input (e.g., to drive pumping systems). Therefore, it holds great promise to significantly reduce energy consumption in the desalination processes. The MDC research is still in an early stage, and the studies have been carried out to improve the understanding of MDCs by investigating the key factors such as the anode organic loading rates,[5]

salt loading rates,[6,7] external resistance,[8,9] hydraulic retention time,[9] new functions,[10,11] membrane fouling,[12,13] inter-membrane distance,[14] and system configuration.[15]

Given complex desalination processes and strong interactions between biological, electrochemical, and engineering factors in MDCs, a proper mathematic model will be essential for the optimization and the scaling up of MDCs. MDCs derive from microbial fuel cells (MFCs) by adding a third compartment between the anode and the cathode, separated by anion or cation exchange membranes for a new function of desalination. While several mathematical models exist for MFCs or microbial electrolysis cells (MECs) (Pinto et al. 2010, Pinto et al. 2011), no model has been developed for MDCs. Most MFC/MEC models are based on the Nernst-Monod type of equations to quantify substrate consumption and bacterial growth.(Pinto et al. 2010, Pinto et al. 2011) When it comes to mass transfer in an anode compartment, two types of approaches are usually employed. The first approach is based on the assumption of heterogeneous spatial distribution of substrates and microorganisms in both bulk liquid and biofilm, and quantified by using partial differential equations. (Picioreanu et al. 2010) The second approach employs simplified ordinary differential equations, based on continuous stirred tank reactor (CSTR) model assuming ideal mixing in the anodic compartment and ignoring the concentration gradient within biofilm.(Pinto et al. 2010, Pinto et al. 2011)

Based on the MFC models, a mathematic MDC model was developed here. The model was calibrated using experimental data obtained from a lab-scale MDC upon the change of substrate

flowrates, and validated by the data from the experimental conditions with different substrate concentrations, salt concentrations, and external electrical resistance. The validated model was then used to predict the performance of the MDC affected by either single or multiple operating parameters. The model was also verified by the experimental data from a large-scale MDC system (total liquid volume of 105 L). To the best of our knowledge, this is the first mathematic model for MDCs.

9.2Materials and Methods

9.2.1MDC setup and operation

The MDC reactor was constructed in tubular configuration similar to that in the previous study.(Jacobson et al. 2011b) It consisted of an inner tube made with anion exchange membrane (AEM, AMI-7001, Membrane International, Inc., Glen Rock, NJ) and an outer tube made of cation exchange membrane (CEM, CMI-7000, Membrane International, Inc.) The diameters of the AEM and the CEM tubes were 3.8 and 5.0 cm, respectively, and the effective lengths of both tubes were 20 cm, resulting in an anode liquid volume of 300 mL (including the liquid in the PVC caps and connectors) and a saline water volume of 150 mL. The anode electrode was a 20-cm long carbon fiber brush, and the cathode electrode was a piece of carbon cloth coated with activated carbon supported platinum (Pt/C) as a catalyst at a loading rate of 0.2 mg Pt cm^{-2}. (Xiao et al. 2012) Both electrodes were connected to an external circuit using titanium wire across 0.1 Ω unless indicated elsewhere. The anode feed solution contained (per L of tap water): sodium acetate, 1 g (unless stated otherwise); NH_4Cl, 0.15 g; NaCl, 0.5 g; $MgSO_4$, 0.015 g; $CaCl_2$, 0.02

g; KH_2PO_4, 0.53 g; K_2HPO_4, 1.07 g; and trace element, 1 mL.[26] The salt solution was prepared by dissolving NaCl into tap water. The catholyte was 50 mM phosphate buffer solution, dripping from the top to the bottom of the outer tube for rinsing the cathode electrode at a recirculation rate of 35 $mL \cdot min^{-1}$. The feeding rates of the anolyte and the salt solution were 0.5 $mL \cdot min^{-1}$ (HRT of 10 h) and 0.06 $mL \cdot min^{-1}$ (HRT of 1.7 d), respectively (unless stated otherwise). In addition, the anolyte was recirculated at 100 $mL \cdot min^{-1}$.

9.2.2Measurement and analysis

The MDC voltage was recorded every 3 min using a digital multimeter (Keithley Instruments, Inc., Cleveland, OH, USA). The conductivity of the salt solution was measured using a benchtop conductivity meter (Mettler-Toledo, Columbus, OH, USA). The chemical oxygen demand (COD) was measured using a colorimeter according to the manufacture manual (Hach Company, Loveland, CO USA). According to an established linear relationship between conductivity and NaCl concentration, the concentration of NaCl was calculated based on the measured conductivity.

9.3 Model Formulation

9.3.1Mass balances for substrate, microorganisms, and electron mediators in the anode

The mass balance was established based on the assumption that microbial growth follows the multiplicative Monod kinetics.(Marcus et al. 2007, Pinto et al. 2010) In addition, an intracellular

redox mediator was assumed to be generated by anodophillic bacteria to aid the transfer of the electrons produced by the bacteria from the substrate, as suggested by a previous work of an MFC model.(Pinto et al. 2010) Ideal mixing in all three compartments of MDCs was assumed, thus ordinary differential equations could be used to quantify the concentrations of the substrate, anodophillic, and methanogenic microorganisms in the anode compartment. These differential equations were based on or modified from the previous study.(Pinto et al. 2010)

The mass balance for the substrate is shown in Equation (1):

$$\frac{dS}{dt} = D_{anode}\,(S_{in} - S) - k_{s,a,max}\,\frac{S}{K_a + S}\frac{M_{OX}}{K_M + M_{OX}}C_a - k_{s,m,max}\,\frac{S}{K_m + S}C_m \qquad (1)$$

where S is the concentration of the substrate (mg-S·L^{-1}); S_{in} is the concentration of the influent substrate (mg-S·L^{-1}); C_a and C_m are the concentrations of anodophilic and methanogenic microorganisms (mg-C·L^{-1}), respectively; $k_{s,a,max}$ and $k_{s,m,max}$ are the maximum substrate consumption rates by anodophilic and methanogenic microorganisms (mg-S·mg-a^{-1}·day^{-1}), respectively; M_{OX} is the oxidized mediator fraction per anodophillic microorganism (mg-M·mg-a^{-1}); K_a, K_m, and K_M are the half-saturation concentrations for the anodophillic microorganisms, methanogenic microorganisms, and the redox mediator (mg-S·L^{-1}, mg-S·L^{-1}, and mg-M·mg-a^{-1}), respectively. The growth of anodophillic bacteria, represented by the second term of Equation (1), was assumed to be limited by both substrate (i.e., acetate in this work) concentration and the oxidized form of the mediator, while the growth of methanogenic microorganisms , i.e., the last term of Equation (1), was assumed to be limited only by the substrate concentration.(Pinto et al. 2010) D_{anode} is the dilution rate (day^{-1}) as defined in Equation (2).

$$D_{anode} = \frac{Q_{in}}{V_{anode}} \quad (2)$$

where Q_{in} is the influent flow rate of the substrate (L·day^{-1}), and V_{anode} is the volume of the anode compartment (L).

The differential equations for the concentrations of anodophilic and methanogenic microorganisms in the anode compartment are shown below:

$$\frac{dC_a}{dt} = k_a C_a - k_{d,a} C_a - D_{anode} \frac{1 + \tanh(k_{a,x}(C_a + C_m - C_{a,max}))}{2} C_a \quad (3)$$

$$\frac{dC_m}{dt} = k_m C_m - k_{d,m} C_m - D_{anode} \frac{1 + \tanh(k_{m,x}(C_a + C_m - C_{m,max}))}{2} C_m \quad (4)$$

where $k_{d,a}$ and $k_{d,m}$ are the decay rates of the microorganisms (day^{-1}); $k_{a,x}$ and $k_{m,x}$ are the steepness factors for anodophillic microorganism (L·mg-a^{-1}) and methanogenic microorganisms (L·mg-m^{-1}) for the biofilm retention; $C_{a,\max}$ and $C_{m,\max}$ are the maximum attainable concentrations for anodophillic microorganism (mg-a·L^{-1}) and methanogenic microorganisms (mg-m·L^{-1}); k_a and k_m are the growth rates of the microorganisms (day^{-1}) calculated by the Equations (5) and (6):

$$k_a = \mathrm{k}_{a,max} \frac{S}{K_a + S} \frac{M_{OX}}{K_M + M_{OX}} \quad (5)$$

$$k_m = \mathrm{k}_{m,max} \frac{S}{K_m + S} \quad (6)$$

where $k_{a,max}$ and $k_{m,max}$ are the maximum microorganism growth rates (day^{-1}) ;

The intracellular material balance for the oxidized mediator can be described as:

$$\frac{dM_{ox}}{dt} = -Y_M k_{s,a} + \frac{\gamma}{V_{anode}\, C_a} \frac{I_{MDC}}{n_e \mathrm{F}} \tag{7}$$

$$M_{total} = M_{ox} + M_{red} \tag{8}$$

where M_{total} is the total mediator fraction per microorganisms (mg-M·mg-a^{-1}); M_{red} is the reduced mediator fraction per microorganisms (mg-M·mg-a^{-1}); Y_M stands for the mediator yield (mg-M·mg-S^{-1}); γ is the mediator molar mass (mg-M·mole-M^{-1}); I_{MDC} is the current through the circuit of MDCs (A); F is the Faraday constant (A·day·mole^{-1}); and n_e is number of electrons transferred per mole of mediator (mole-e·mole-M^{-1}).

9.3.2 Mass balance of salt

Salt is removed from the saline solution mainly by ionic current between the anode and cathode of MDCs. In addition, salt diffuses into other compartments due to the concentration gradient. Ordinary differential equations shown below are developed to quantify the salt concentration during the desalination process:

$$\frac{dC_{salt,m}}{dt} = D_{salt} \cdot \left(C_{salt,in} - C_{salt,m}\right) - d \cdot \left(C_{salt,m} - C_{salt,a}\right) - d \cdot \left(C_{salt,m} - C_{salt,c}\right) - \frac{I_{MDC}}{F \cdot V_{salt}} \tag{9}$$

$$\frac{dC_{salt,a}}{dt} = d \cdot \left(C_{salt,m} - C_{salt,a}\right) - D_{anode} \cdot C_{salt,a} \tag{10}$$

$$\frac{dC_{salt,c}}{dt} = d \cdot \left(C_{salt,m} - C_{salt,c}\right) \tag{11}$$

where $C_{salt,a}$, $C_{salt,m}$, $C_{salt,m}$ and are the salt concentrations in the anode, the salt, and the cathode compartments (mg-salt·L^{-1}), respectively; D_{salt} is the dilution rate (day^{-1}) in the salt compartment that is quantified by the ratio of the salt flow rate (Q_{salt}) over the volume of the salt compartment (V_{salt}); d is a membrane salt transfer coefficient that is equal to the ratio between the product of diffusion coefficient and membrane surface area and the product of the membrane thickness and the anode volume (day^{-1}).

The first term on the right hand side of Equation (9) represents the salt concentration retained in the middle compartment. The second and third term represents the desalination due to the concentration-gradient driven diffusion from the salt compartment through ion exchange membranes to the anode and cathode respectively, which can be described by the Fick's Laws. The last term of Equation (9) quantifies the desalination via the salt ion migration driven by the ionic current and charge balance, which is described by the Faraday's law. Equation (10) describes the salt balance in the anode compartment in which the second term describes the salt lost in the anode effluent flow. Equation (11) quantifies the salt concentration in the cathode compartment. The change in the salt concentration due to water osmosis (dilution effect) was not considered in this model.

9.3.3 Current generation

The overall cell voltage in MDCs is modeled by the following equation:

$$I_{\mathrm{MDC}}\, R_{\mathrm{ext}} = V_{\mathrm{OC}} - OP_{\mathrm{anode}} - OP_{\mathrm{cathode}} - OP_{\mathrm{conc}} - I_{\mathrm{MDC}}\, R_{\mathrm{int}} \quad (12)$$

Where R_{ext} is the external resistance (Ω); V_{oc} is the open circuit voltage (V); OP_{anode} is the anode overpotential (V); $OP_{cathode}$ is the cathode overpotential (V), OP_{conc} is the concentration overpotential (V); R_{int} is the internal resistance of the cell (Ω) that is given in Equation (13) and made up of mass transfer resistance, the ohmic resistance, and activation resistance. In particular, mass transfer resistance through the exchange membrane R_{membrane} is estimated from experiment as 2.0 Ω for our MDC system.[12] The ohmic resistance includes the resistance of anolyte solution R_{anolyte} (0.28 Ω in this work), and the resistance of salt solution R_{salt} (Ω) that is quantified by Equation (14) which were obtained from integration according to the MDC's tubular configuration. The last two terms of Equation (13) describe other internal resistance sources that are related to the bacterial growth (e.g., activation resistance).

$$R_{int} = R_{\text{membrane}} + R_{\text{anolyte}} + R_{\text{salt}} + R_{min} + (R_{max} - R_{min}) \cdot e^{-k_r \cdot C_a} \quad (13)$$

$$R_{\text{salt}} = \frac{1.2 \times 10^{-3}}{C_{\text{salt,m}}} \quad (14)$$

where R_{min} is the minimum internal resistance (Ω), R_{max} is the maximum internal resistance (Ω), and k_r is the constant that determines the how fast the internal resistance and the open circuit voltage respond to the change in microorganism concentration C_a (L·mg-a^{-1}).

The dependence of cell voltage on the catalyst load suggests the exponential relationship between anodophilic microorganism concentration and the open circuit voltage:(Pinto et al. 2010)9

$$V_{oc} = V_{min} + (V_{max} - V_{min}) \cdot e^{-1/(k_r \cdot C_a)} \quad (15)$$

where V_{min} and V_{max} are the lowest and highest observed V_{oc} values (V).

The open circuit potential of the MDC used in the model was ~1.2 V according to the previous studies.[3,8] It was assumed in this study that the anode overpotential and the cathode overpotential could be neglected based on the following two factors: sufficient buffer solutions were used for both the anode and cathode, which eliminated the effect of the most influential parameter (pH) on overpotential;(Stein et al. 2010) and a cathode catalyst Pt/C was used to ensure an efficient cathode reaction. Using this assumption and Equation (12), the MDC current is calculated as:

$$I_{MDC} = \frac{V_{\mathrm{OC}} - OP_{\mathrm{conc}}}{(R_{\mathrm{ext}} + R_{\mathrm{int}} + R_{\mathrm{salt}})} \tag{16}$$

The concentration overpotential was assumed to be associated with electron mediators and could be modeled as:(Pinto et al. 2010)

$$OP_{\mathrm{conc}} = \frac{RT}{\mathrm{F}} \ln\left(\frac{M_{\mathrm{total}}}{M_{\mathrm{red}}}\right) \tag{17}$$

9.3.4 Sensitivity analysis

Most model parameters in this study were based on the previous work.(Pinto et al. 2010) Parameter $k_{\mathrm{a,max}}$ was estimated to 0.197 according to the average value of maximum growth rate of anaerobic culture.[28] The most influencing ones among the 24 parameters have the priority to be re-estimated. Thus, sensitivity analysis, one of the most commonly used technique for parameter selection,(Huang et al. 2010) was conducted to quantify the influence of each model parameter on the dynamics of the MDC current and the salt concentration.

In the sensitivity analysis, the values of parameters deviate from their nominal values, and the changes of the outputs are quantified. The sensitivity measure $s_{i,j}$ is typically defined by Equation (18), in which the partial derivative of the output y_j over parameter p_i is normalized by the nominal values of p_i and y_j (i.e., p_i^0 and y_j^0 respectively).

$$s_{i,j} = \frac{p_i^0 \partial y_j}{y_j^0 \partial p_i}\Big|_{\mathbf{P}_0} \tag{18}$$

where the vector P_0 is a vector of nominal values of all the parameters in the model.

This work employed local sensitivity analysis, in which only one parameter is changed at one time while other parameters are fixed at their nominal values. The steady states of current and salt concentration were defined as the output vector, i.e., $Y = [I_{MDC}\ C_{salt,m}]$. Parameter p_i was changed to $p_i^0 + \Delta p_i$, and the steady states of I_{MDC} and $C_{salt,m}$ were quantified from the simulation and used to construct the output vector Y, which was compared to its nominal value Y^0. Equation (18) is reorganized as

$$s_{i,j} = \frac{p_i^0[\mathrm{norm}(Y) - \mathrm{norm}(Y^0)]}{\mathrm{norm}(Y^0)\Delta p_i}\Big|_{P_0} \tag{19}$$

Equation (19) was applied to quantify another sensitivity measure $s_{i,j}$ for the scenario where parameter p_i was changed to $p_i^0 - \Delta p_i$. In this sensitivity analysis, each parameter was increased or decreased by one magnitude. The sum of the absolute values of the two sensitivity values $s_{i,j}$ for parameter p_i (i.e., decreased and increased by Δp_i) was used to present the impact of this parameter on the change of current and salt concentration.

9.3.5 Parameter estimation

The parameters selected by sensitivity analysis were further re-estimated from experimental data. Genetic algorithm routine in MATLAB was used for parameter estimation to minimize the relative root-mean-square error (Equation (20) between the predicted value and the experimental data. Unlike typical nonlinear least squares approaches, which generally return local optimal solutions, genetic algorithm can find the global optimal solution that minimizes the relative error shown in Equation (20) with moderate searching efficiency. This method mimics the natural processes of fitness-based selection for the best-adapted individuals and species from among their competitors.

$$RMSR = \frac{\sqrt{\frac{\sum_{i=1}^{N}(y_i - \hat{y}_i)^2}{N}}}{\max(\hat{y})} \tag{20}$$

Where N is the total sampling time points in the simulation; $\hat{y}_i$ and y_i represent experimental data and model predicted values at t_j, respectively. The maximum value of the experimental data for the current and the salt concentration were used to normalize the error in Equation (20) such that the relative root-mean-square error (RMSR) is a direct measure of the discrepancy between the experimental data and the estimated value. A small RMSR indicates a good fit of the model to the data.

9.4 Results and Discussion

9.4.1 Model Fitting

All the parameters were tested in the sensitivity analysis, and the parameters were ranked on the basis of their sensitivity measure values. The impact from the initial values of the two microorganism concentrations was also evaluated. Thus, those two initial values were also regarded as changeable parameters. The parameters with the top 10 sensitivity values are listed in a descending order (Table 9.1). The sensitivity measures were normalized by the largest sensitivity value (i.e. the value for parameter k_r) to show the relative difference among these values. It was found that parameter k_r had a much larger impact on the MDC current and the salt concentration than other parameters. This can be explained by Equations (13) and (15) in which k_r is an important parameter that correlates the anodophilic microorganism concentration with the internal electrical resistance and the open circuit voltage. The sensitivity measures for other parameters are relatively small, possibly because of the fact that sensitivity analysis heavily depends on the initial guessed values of parameters, and the selected nominal values of model parameters constrain the MDC performance from variation with those parameters other than k_r. In other words, the sensitivity measure can be changed if the nominal values of model parameters change, which was confirmed by multiple simulates. Interestingly, the parameters listed in Table 9.1 were still ranked top for their influence on the MDC current and salt concentration. Therefore, these parameters were good candidates for re-estimation. Among these parameters, V_{min} and R_{max} were determined directly from experiment measure. Other than these two, the five most important parameters, including k_r, the membrane salt transfer coefficient d, the mediator yield Y_M, the maximum microorganism growth rate $k_{a,max}$, and the initial

concentration of anodophilic microorganism $C_a(0)$, were selected for re-estimation. Using the genetic algorism estimation, the five parameters selected by sensitivity analysis, i.e., k_r , d, Y_M, $k_{a,max}$, and $C_a(0)$ were estimated to be 0.082 L·mg-a^{-1}, 0.029 day^{-1}, 6.14 mg-M·mg-S^{-1}, 5.32 day^{-1}, and 465.30 mg-a·L^{-1} respectively. The values of other parameters are listed in Table 9.2.

Table 9.1 Sensitivity measure of the top 10 ranked parameters

Rank	**Parameters**	**Descriptions**	**Sensitivity measure**
1	k_r	Parameter in Eq.17 & 18	1
2	d	Diffusion coefficient of salt in Eq. 13.	0.045
3	V_{min}	Minimum V_{oc}	0.0067
4	R_{max}	Maximum internal resistance	0.0046
5	Y_M	Mediator yield in Eq.11	0.0038
6	$k_{a,max}$	Maximum microorganism growth rate in Eq. 9	0.0038
7	$C_a(0)$	Initial concentration of anodophilic microorganism	0.0037
8	n	Electrons transferred per mol of mediator	0.0017
9	$C_{a,max}$	Maximum attainable concentrations for anodophillic microorganism	0.00028
10	M_{total}	Total mediator fraction	0.00014

Table 9.2 Parameters used in the model.

Parameters	**Description**	**Values**
$k_{s,a,max}$	Maximum substrate consumption rates by	5.32 mg-S·mg-a^{-1}·day^{-1}

	anodophilic microorganisms	
$k_{s,m,max}$	Maximum substrate consumption rates by methanogenic microorganisms	8.20 mg-S·mg-a^{-1}·day^{-1}
K_a	half-saturation concentrations for the anodophillic microorganism	20 mg-S·L^{-1}
K_m	half-saturation concentrations for the methanogenic microorganism	80 mg-S·L^{-1}
K_M	half-saturation concentrations for the redox mediator	0.2* M_{total} mg-M·mg-a^{-1}
$k_{\alpha,x}$	the steepness factors for anodophillic microorganism	0.04 L·mg-a^{-1}
$k_{m,x}$	the steepness factors for methanogenic microorganism	0.04 L·mg-m^{-1}
$C_{\alpha,max}$	maximum attainable concentrations for anodophillic microorganism	512.5 mg-a·L^{-1}
$C_{m,max}$	maximum attainable concentrations for methanogenic microorganism	525 mg-m·L^{-1}
$k_{a,max}$	maximum microorganism growth rates for anodophillic microorganism	0.197 day^{-1}
$k_{m,max}$	maximum microorganism growth rates for methanogenic microorganism	0.10 day^{-1}
M_{total}	Mediator fraction	0.05 mg-M·mg-x^{-1}
Y_M	the mediator yield	6.14 mg-M·mg-S^{-1}

γ	Mediator molar mass	663,400 mg-M·$mol_{mediator}^{-1}$
n_e	Electrons transferred per mol of mediator	2 $mole^{-1}$·$mol_{mediator}^{-1}$
F	Faraday constant	96,485 A·s·$mole^{-1}$
d	the membrane salt transfer coefficient	0.029 day^{-1}
k_r	Parameter in Eq.17 & 18	0.082 L·mg-a^{-1}
R	Ideal gas constant	8.314472 J·K^{-1}·mol^{-1}
T	MDC temperature	298.15 K

The data used for parameter estimation were obtained by the following experimental conditions: the MDC was operated under a dynamic anolyte influent flow rate, which was changed from 0.5 to 0.2, and then back to 0.5 mL·min^{-1}. During the experiment, the change of each influent flow rate was made after the system had reached steady state. The predicted current and salt concentration was plotted along with the experimental data in Figure 9.1A&B, which shows that the electrical current decreased from 12 to 6 mA when the influent acetate rate was reduced from 0.5 to 0.2 mL·min^{-1}, and once the influent flow rate was increased back to 0.5 mL·min^{-1} the current increased close to the previous level (around 11 mA). The initial salt solution (0.170 mol·L^{-1}) was gradually desalinated to 0.060 mol·L^{-1} in four days. When the anode influent flow rate decreased, the resulted low current weakened the desalination efficacy, and caused the effluent $C_{salt,m}$ increasing to 0.120 mol·L^{-1}. However, the efficient desalination was restored within two days when the anode influent rate was increased back to 0.5 mL·min^{-1}. The model output of current value shows satisfactory agreement with the experimental measurement, and the relative root-mean-square error (RMSE) shows that the mean error for the current and salt

concentration were within 6.97% and 12.12% of their maximum values. On the other hand, some overestimation/underestimation can be seen from the modeled variation trend of the effluent salt concentration as shown in Figure 9.1B. The predicted salt profile matches the experimental data better when the current was of a large value, despite some underestimation of salt removal. The overestimation of the salt removal mainly happens for the low current region (low anode influent rate). In the model, it was assumed that every electron would pull out a salt ion, but in reality it might not happen ideally, thereby resulting in the overestimation of the desalination efficiency.

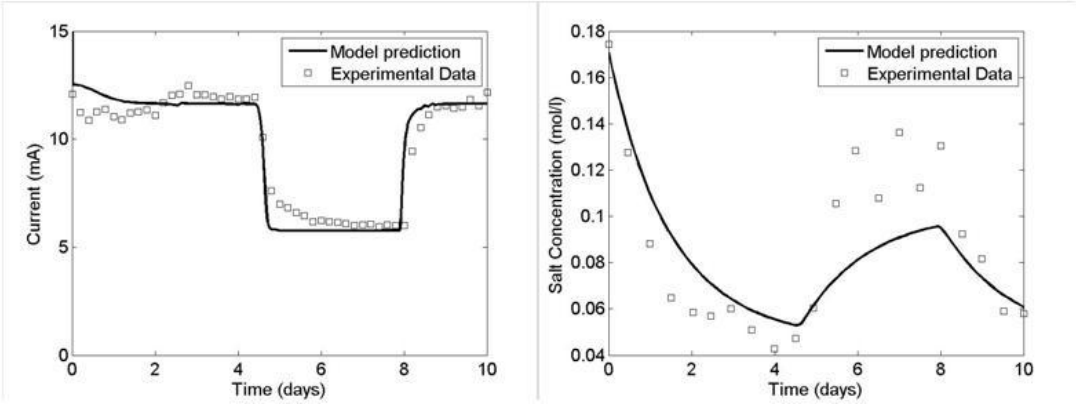

Figure 9.1 Experimental data and model simulation when the anode influent feeding rate was changed from 0.5 to 0.2, and then back to 0.5 mL·min^{-1}: A) current generation, and B) effluent salt concentration.

The model is also able to predict the dynamics of the other outputs, i.e., the anode effluent acetate concentration (S), the concentration of anodophilic microorganisms (Ca), the concentration of methanogenic microorganisms (Cm) and the oxidized mediator fraction (Mox) (Figure 9.2). The substrate concentration in the effluent was clearly affected by the anolyte influent rate, which also influenced the concentration of anodophilic microorganisms. When the

remained acetate in the anode drops to 16 mg L^{-1} due to microbial consumption, which is much lower than the half-saturation concentrations for the methanogenic microorganisms (80 mg L^{-1}), the concentration of methanogenic microorganisms began to decrease. The oxidized mediator fraction remained stable. It should be noted those simulated results provide some implication about the dynamics within the MDC and should be experimentally verified for more accurate prediction.

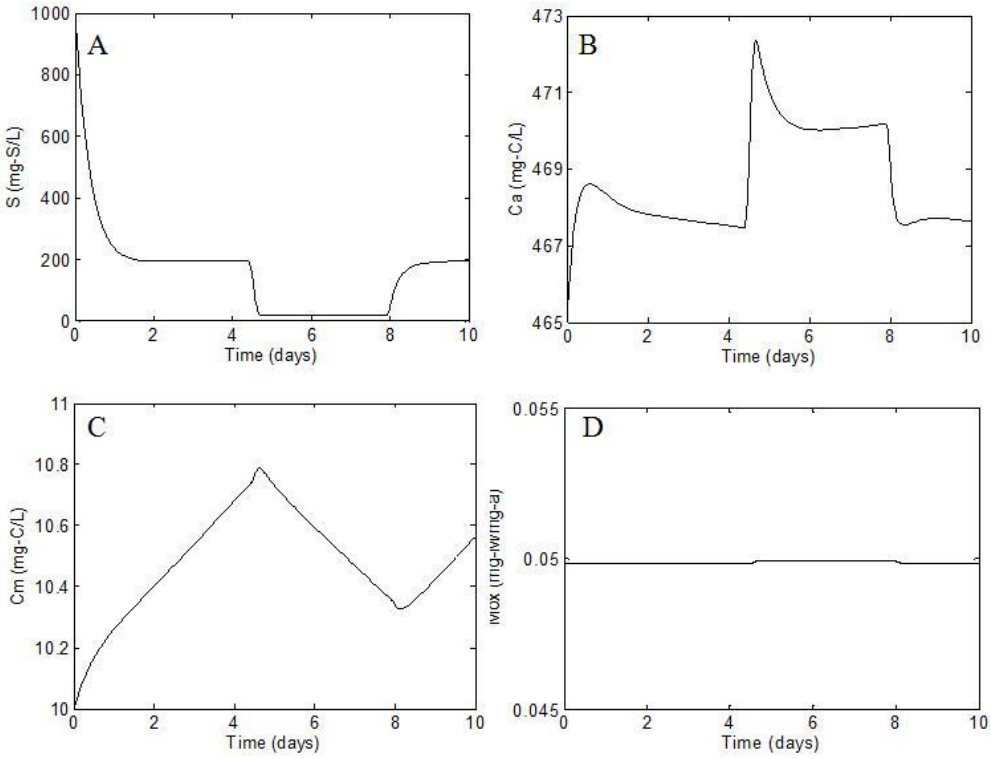

Figure 9.2 The simulation results when the anode influent feeding rate was changed from 0.5 to 0.2, and then back to 0.5 mL·min^{-1}: A) substrate concentration, B) the concentration of anodophillic microorganisms, C) the concentration of methanogenic microorganisms, and D) the oxidized mediator fraction per anodophillic microorganism.

9.4.2 Model validation

Three independent operation tests were carried out to evaluate the prediction capability of the developed MDC model for the change in the influent concentration of acetate, the external resistance, and the concentration of the salt solution. The operating parameters were kept the same except for the target parameter being studied in each test.

The first set of tests was performed by changing the influent concentration of acetate from 1 to 0.6, to 0.2, then back to 1 $g \cdot L^{-1}$. In response to the changes, the electrical current decreased from 12 to 10, to 6 and then back to around 11 mA, and the model give a good fit for most part with some deviation for the acetate concentration 0.2 $g \cdot L^{-1}$ (Figure 9.3A). Meanwhile, the experimental salt concentration decreased significantly from initial 0.175 to around 0.055 $mol \cdot L^{-1}$ when operated at the acetate concentration of 1 $g \cdot L^{-1}$ (Figure 9.3B). As the acetate concentration underwent two-step decrease, the salt concentration first increased slightly to 0.075 $mol \cdot L^{-1}$ and then jumped up to about 0.130 $mol \cdot L^{-1}$. The salt concentration resumed to 0.055 $mol \cdot L^{-1}$ as the acetate concentration was increased back to 1 $g \cdot L^{-1}$. The salt concentrations predicted by the model in response to this test generally followed the trend of experimental salt concentrations, with some underestimation for the first period of desalination and slight overestimation of salt removal ability at the low substrate supply period. The relative RMSE for the current and salt profiles were 12.08 % and 9.01 %, respectively.

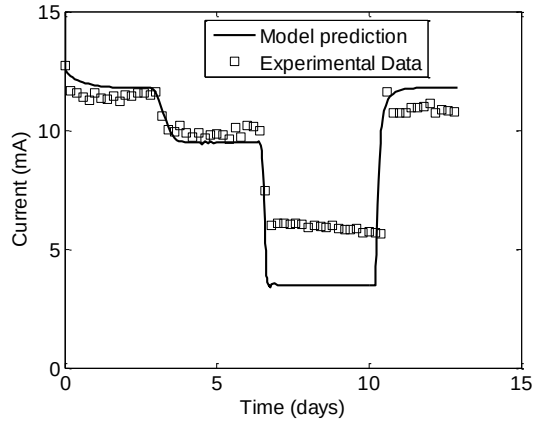

(A)

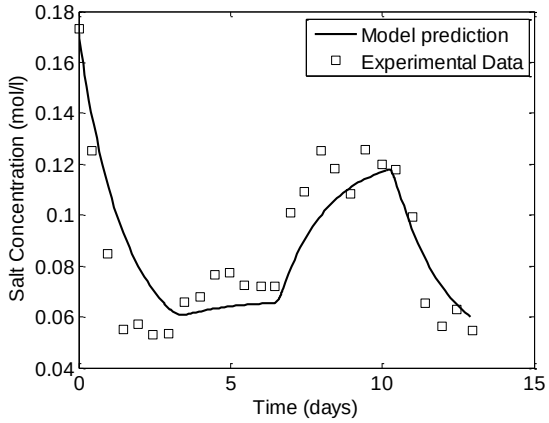

(B)

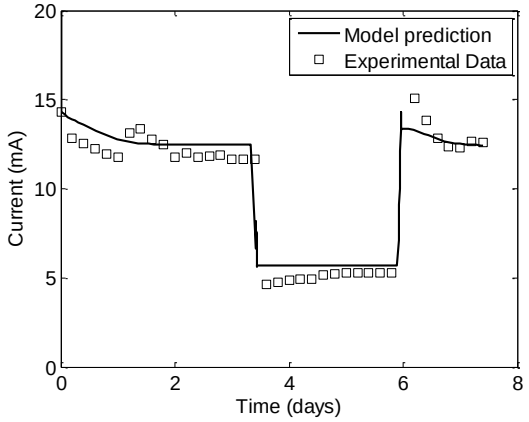

(C)

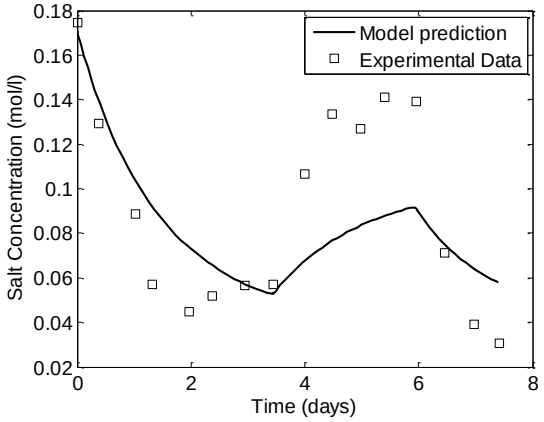

(D)

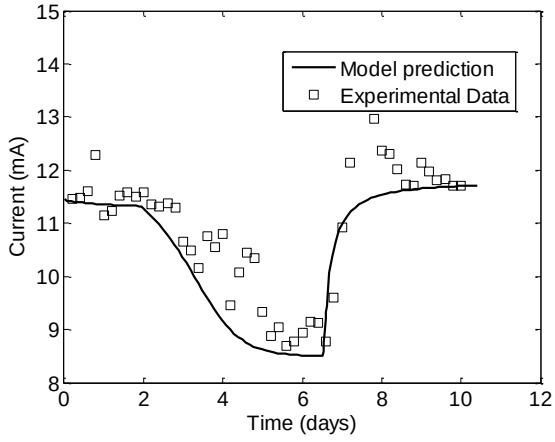

(E)

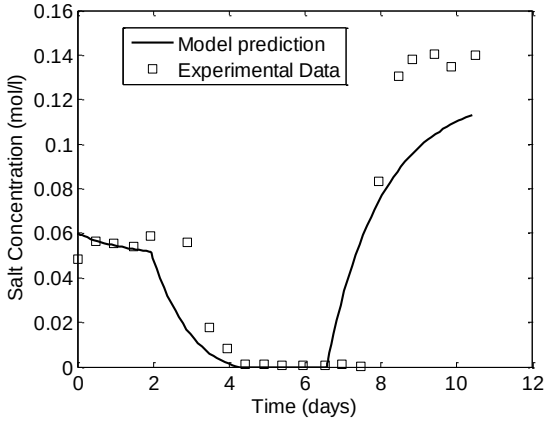

(F)

Figure 9.3 Model fitting under three different testing conditions: A) current generation, and B)

effluent salt concentrations, when the concentration of acetate was changed from 1 to 0.6, 0.2 and then back to 1 g·L^{-1}; C) current generation, and D) effluent salt concentrations, when the external resistances was changed from 0.1 to 100, and then back to 0.1 Ω; E) current generation, and F) effluent salt concentrations, when the salt concentration was changed from 10 to 5, and then back to 15 g·L^{-1}.

The second dynamic test was performed by varying the external resistance from 0.1 to 100 and then back to 0.1 Ω (Figure 9.3C&D). The experimental current responded rapidly and decreased significantly as the external resistance was increased to 100 Ω. The model predicted the current values fairly well with slight overestimation and a low relative RMSE of 8.87 %. The experimental salt concentration responded to the decreased current within a day and increased gradually. When the external resistance was decreased to 0.1 Ω again, the salt concentration started to decrease. Although the model-predicted salt profile showed similar dynamic trend as the experimental data, the relative RMSE showed a high error of 17.57 % for the salt profile, which mainly came from the low current region (high external resistance) where the assumption that one electron pulls out one salt ion might fail.

The third dynamic test was performed by varying the influent salt concentration from 10 to 5 and then up to 15 g·L^{-1}**.** Both current generation and final salt concentration responded to the variation of initial salt concentration (Figure 9.3E&F). In general, the model presented a tight fit to the current data with a relative RMSE of 5.81 %. The model also predicted fairly accurate steady state salt concentration, with some overestimation of salt removal at the very beginning of

each change. The relative RMSE for the salt profile was 16.14%, which mainly came from the mismatch with the salt concentration in the last few time points. The delay for the modeled salt concentration to reach steady state might be responsible for the discrepancy.

9.4.3 Model prediction: one parameter variation

The validated MDC model can predict the dynamics of current and salt concentration with reasonable accuracy for three different experimental conditions and is of great value as an *in silico* platform to investigate optimal operation parameters. Herein, the effectiveness of desalination in the MDC, which is defined as the difference of salt concentration between the influent and the effluent normalized by the influent salt concentration, is evaluated for various values of operating parameters including influent acetate concentrations and flow rates, influent salt concentrations and flow rates, external electrical resistance, and volumes of the anode and salt compartments.

In this section, only one design parameter is changed at each time to determine the parameter value that optimizes the desalination performance of the MDC. Figure 9.4A shows the effectiveness of desalination affected by acetate concentration that is gradually changed from 10 to 2900 $mg \cdot L^{-1}$. The inflection point, below which corresponds to the largest slope in the curve, suggesting that the effectiveness has limited increase after the acetate concentration increases above 950 $mg \cdot L^{-1}$. Similarly, the acetate flow rate is varied from 0.1 to 15 $mL \cdot min^{-1}$, as shown in Figure 9.4B. The optimal acetate flow rate is determined to be 0.8 $mL \cdot min^{-1}$ based on the

inflection point. Excessive acetate cannot be further oxidized by microorganisms and thus cannot contribute to improving desalination. Increasing acetate flow rate above 0.8 $mL \cdot min^{-1}$ has a slightly reducing effect to desalination effectiveness. It is expected that as the acetate flow rate keeps increasing, it will reach a so called cell-washout point eventually, where no bacteria activity exists in the anode leading to no electrical-driven desalination.

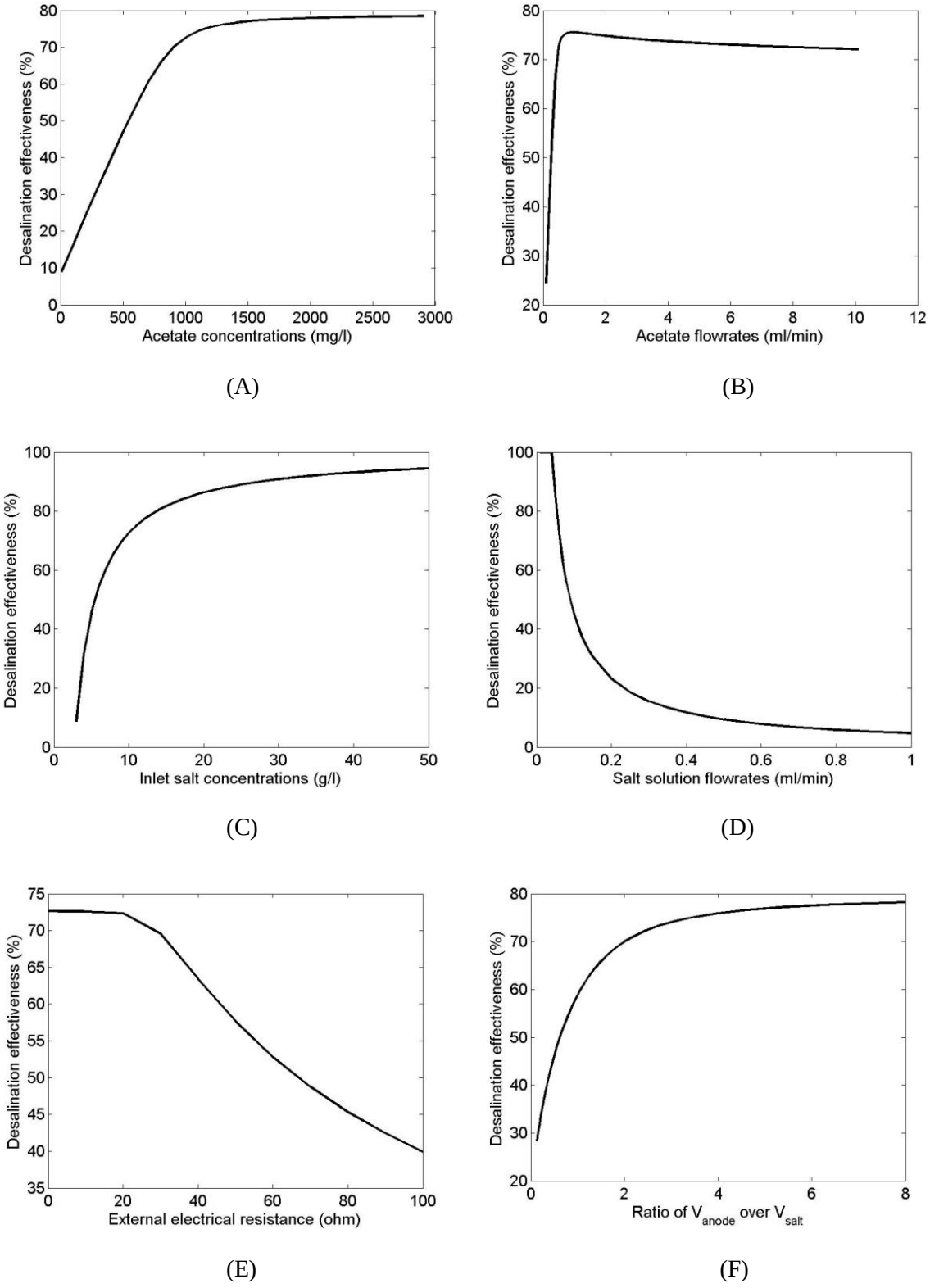

Figure 9.4 Model prediction with one variable parameter: A) acetate concentrations; B) acetate

flow-rates; C) influent salt concentrations; D) salt solution flowrates; E) external electrical resistance; F) ratios of volumes V_{anode} and V_{salt} in the MDC.

The optimal salt influent concentration and influent is evaluated as shown in Figure 9.4C&D. The influent salt concentration is gradually changed from 3 to 50 $g \cdot L^{-1}$, and the desalination effectiveness increases until the inflection point, suggesting that the optimal influent salt concentration is around 13 $g \cdot L^{-1}$ (Figure 9.4C). The increased salt concentrations provide more ions to the solution thus to make it more conductive and also increase the concentration gradient that facilitates the salt diffusion to other compartments. Further increasing influent salt concentration still improves the desalination effectiveness, but very slowly, as the capacity of an MDC to remove salt reaches a limit at this setting. The flow rate of saline water is varied from 0.01 to 1 $mL \cdot min^{-1}$ (Figure 9.4D). The desalination effectiveness reaches 100% if the saline water flow rate is less than 0.04 $mL \cdot min^{-1}$, and increasing influent salt flow rate tends to reduce the desalination effectiveness. A faster salt influent flow rate leads to a shorter hydraulic retention time which in turn limits the desalination time of a certain amount of saline water.

The external electrical resistance is evaluated from 0.01 to 100 Ω, and the desalination effectiveness is graphed in Figure 9.4E. The trend in the figure suggests that when the external resistance is higher than 30 Ω, the effectiveness starts to decrease significantly, because that larger external electrical resistance leads to smaller current in the MDC, and thus a lower driving force for the ion migration from the saline solution into other compartments. Reducing external

resistance lower than 30 Ω does not significantly change the current generated by the MDC, and thus maintains the desalination effectiveness around 70%.

The optimal volume distribution in the anode and salt compartments is studied upon the constraint that the total volume of the anode compartment (V_{anode}) and the middle desalination compartment (V_{salt}) is kept constant at 450 mL. The simulation is performed as the ratio of V_{anode} over V_{salt} increases from 0.125 to 8 (Figure 9.4F). Higher V_{anode} to V_{salt} ratios result in better desalination effectiveness. The inflection point in this curve indicates the optimal ratio of 2.5, which corresponds to an anode compartment volume of 321 mL. Further increasing the ratio of V_{anode} over V_{salt} does not further improve desalination. A larger anode compartment benefits the desalination, likely because of more current generation as a result of stronger anode microbial activities, and this was also demonstrated by the previous studies. For example, in a rectangular MDC the desalination effectiveness exhibited a decreasing trend as the desalination compartment was enlarged and the optimal ratio of V_{anode} over V_{salt} was obtained around 2.[14] The change in V_{anode} and V_{salt} may lead to the change in the areas of ion exchange membranes and the distance between the two ion exchange membranes. These changes can influence the amount of bacteria in the anode but also the solution resistance, and the mass transfer in the anode and desalination chambers. In order to take into account the change especially regarding membrane area in the simulation for Figure 9.4F, substantial experiments need to perform to calibrate the change in the value of model parameters with the change in V_{anode} and V_{salt}. This is an interesting problem for future investigation. Nevertheless, the developed model is able to predict the desalination of a

scaled up MDC (100L) developed at Virginia Tech with a small relative error (i.e., 1.2%). Interested readers can refer to the supplemental document for more detail on this.

9.4.4 Model prediction: combined parameters variation

The combined effects were studied focusing on acetate flow rates, saline water flow rates, and external electrical resistance, where two design parameters were changed simultaneously for evaluating the desalination effectiveness. The simulation performed by varying different combinations of acetate flow rates and external electrical resistance shows that: 1) for a fixed external electrical resistance, the desalination effectiveness increases upon the increase of acetate flow rate up to 0.8 $mL \cdot min^{-1}$; 2) for a fixed acetate flow rate (lower than 0.8 $mL \cdot min^{-1}$), the desalination effectiveness increases upon the decrease of the external electrical resistance (Figure 9.5A). These observations are consistent with the profiles shown in Figure 9.4B&E. For the region where the external resistance is lower than 30 Ω and the acetate flow rate rises higher than 0.8 $mL \cdot min^{-1}$, nearly constant high desalination effectiveness is observed, suggesting the optimum operation.

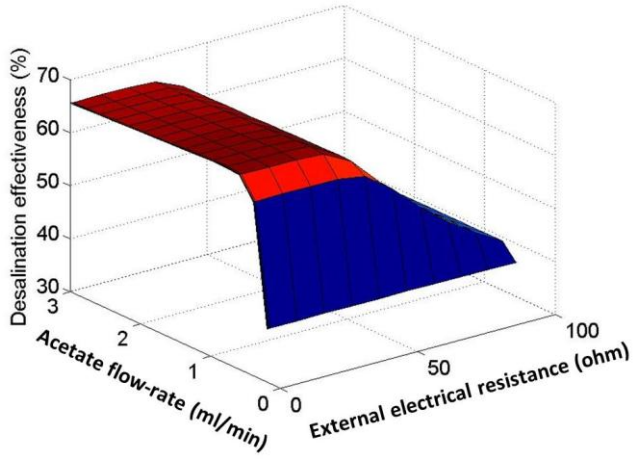
Desalination effectiveness (%)
70
60
50
40
30
3
2
1
0
Acetate flow-rate (ml/min)
0
50
100
External electrical resistance (ohm)

(A)

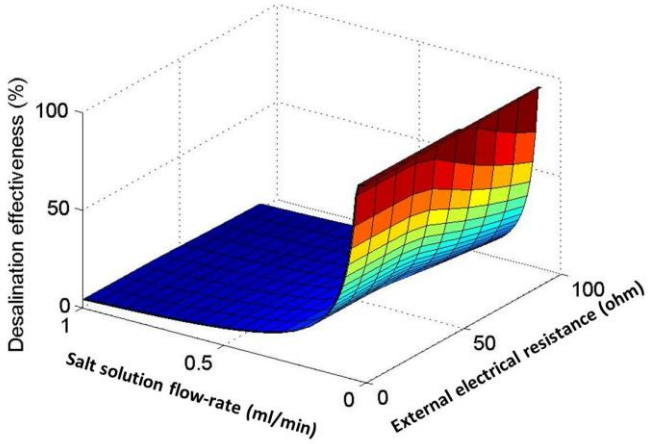
Desalination effectiveness (%)
100
50
0
1
0.5
0
Salt solution flow-rate (ml/min)
0
50
100
External electrical resistance (ohm)

(B)

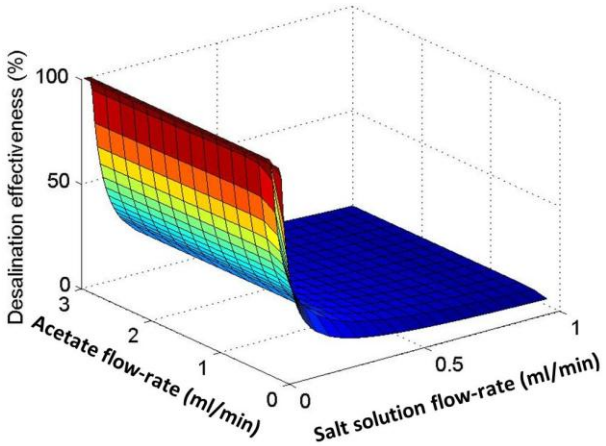
Desalination effectiveness (%)
100
50
0
3
2
1
0
Acetate flow-rate (ml/min)
0
0.5
1
Salt solution flow-rate (ml/min)

(C)

Figure 9.5 Model prediction with two variable parameters: A) the combination of varying both acetate flow rate and external electrical resistance; B) the combination of varying both salt solution flow rate and external electrical resistance; and C) the combination of varying both acetate and salt solution flow rates.

The effects of different combinations of salt flow rates and external electrical resistance is shown in Figure 9.5B. A higher salt solution flow rate (within the range of ~0.2 $mL \cdot min^{-1}$) can be compensated by reducing external resistance. While as the salt solution flow rate gets very close to 0 $mL \cdot min^{-1}$, the external resistance has much smaller effect on desalination effectiveness because a long hydraulic retention time makes it possible for all the ions to be removed out of salt solution as long as the system is under a closed-circuit condition. The salt solution flow rate higher than 0.2 $mL \cdot min^{-1}$ results in overall low desalination effectiveness, and the effect of reducing external resistance is indistinguishable, because the increase in salt removal is negligible in comparison to the large amount of salt in the solution.

The simulation was also performed by varying different combinations of acetate flow rates and salt solution flow rates (Figure 9.5C). In the region of acetate flow rate lower than 0.8 $mL \cdot min^{-1}$, the desalination effectiveness can be improved by reducing salt solution flow rate. Slower acetate supply leads to lower bacterial activity and thus less electron generation to produce current. Reducing the amount of salt addition in a specific amount of time is able to compensate for the low current and still keeps relatively high desalination effectiveness. The remarkable increment in desalination effectiveness by reducing slat solution flow rate is not observed if the salt

solution flow rate is higher than 0.2 $mL \cdot min^{-1}$. Increasing acetate flow rate higher than 0.8 $mL \cdot min^{-1}$ does not help improve desalination effectiveness at a higher salt solution flow rate, possibly because no further improvement in microorganism-driven current generation occurs.

9.5 Perspectives

This work represents the first attempt to model the desalination process in MDCs, and the results have some important implications to MDC development and encourage further development of the MDC model. According to the simulation data, we have developed our next-stage MDC system (105 L) with a ratio of 3:1 between the anode and the salt compartments (the performance data of the scaled MDC system will be presented in a separate publication). The model was able to well predict the current generation, organic concentration and salt removal rate in the large-scale MDC system. However, as the first MDC model, we expect limitations (e.g., the model may be limited by the present MDC configuration) and problems (e.g., discrepancy of salinity between simulated and experimental data), which will be addressed in further development.

The present model was based on a number of assumptions, which simplified model and avoided the intense computational load of the simulations, which makes it more suitable for real-time process control and optimization of MDC systems when compared to more complicated models that consider spatial heterogeneity. However, the simplification on the anode biofilm, such as that substrate concentration gradient and heterogeneous spatial distribution of microorganisms across the anode biofilm were not considered, does limit the model's ability in predicting the

desalination behavior of MDCs when external resistances and salt concentrations deviate from their nominal values. Further improvement will consider both discretized biofilm and bulk liquid regions. The assumption that every electron would pull out a salt ion is a possible factor that may lead to discrepancies in predicting salt removal. Having a current-dependent factor (which needs to be experimentally determined) and considering dilution effects may improve the model prediction for salt removal.

A mathematical model has its boundary, because of conditions that the data were obtained for determining the key parameters. The present model was developed based on the data from a bench-scale tubular MDC system, but it can also be adapted to describe other MDC systems through re-estimating some important model parameters that are listed in Table 9.1 and 9.2. Those parameters include k_r, which correlates the internal resistance with the growth rate of anodophilic microorganisms that may change for different microorganism species and anolyte compositions used in the MDC system, and the membrane salt transfer coefficient d, which is related to the diffusion coefficient, the membrane surface area, the membrane thickness, and the anode volume. Other parameters, such as the maximum growth rate of anodophilic microorganism (i.e., $k_{a,max}$), the initial concentration of anodophilic microorganism (i.e., $C_a(0)$) and the maximum attainable concentrations for anodophillic microorganism (i.e., $C_{a,max}$), may be adjusted depending on the specific microbial community.

Chapter 10 Mathematical Modeling based Evaluation and Simulation of Boron Removal in Bioelectrochemical Systems

(This section has been published as Ping, Q., Abu-Reesh, I.M. and He, Z. (2016) Mathematical modeling based evaluation and simulation of boron removal in bioelectrochemical systems. ***Science of the Total Environment***. Vol 569-570, pp 1380-1389.)

10.1 Introduction

With the global population growth, the issue of limited access for clean and safe freshwater has resulted in increasing attention on desalination of seawater or brackish water as an alternative source of freshwater. Despite the high energy cost, the installed desalination capacity worldwide has reached 74.8 million $m^3 d^{-1}$ (in 2012) and continues to increase (Bennett 2013). Reverse osmosis (RO) is used as the desalination technology in 63% of the current desalination industry (Gude 2016). Although conventional RO technologies can achieve almost 100% rejection of salt, the rejection of boron by RO is low at 40 ~ 70% and often requires post-treatment (Guler et al. 2010).

The removal of boron is essential due to its toxic effects on plants, animals, and human beings (Guler et al. 2015). The World Health Organization (WHO) recommends the boron limit in drinking water to be as low as 2.4 mg L^{-1} (Kabay and Bryjak 2015), while seawater contains ~ 5 mg L^{-1} and brackish water has up to 40 mg L^{-1} of boron. The common form of boron in natural

water is non-dissociable boric acid, which is non-charged and very small in size (Melnik et al. 1999). It is critical to raise pH above pKa value of 9.14 in order to improve rejection of boron in RO; in that way, boron transforms to borate ions with larger hydrated radius and negative charge (Eq. 1) (Kabay and Bryjak 2015, Guler et al. 2009). However, the alkalization process will increase the consumption of chemicals such as sodium hydroxide, and result in higher cost of desalinated water (Guler et al. 2015).

$$B(OH)_3 + H_2O \Leftrightarrow B(OH)_4^- + H^+ \qquad (1)$$

Bioelectrochemical systems (BES) are an emerging technology that takes advantage of microbial interaction with solid electron acceptors/donors (Wang and Ren 2013). As a representative BES, microbial fuel cells (MFCs) can transform chemical energy stored in waste into electrical energy with the benefit of removing the intrinsic organics in wastewater (Li et al. 2014) (Venkidusamy et al. 2016). The concept of BES is also applied to desalination of seawater or brackish water in microbial desalination cell (MDCs) driven by *in-situ* electricity production (Cao et al. 2009, Sevda et al. 2015). With electrons released from the oxidation of organic matters in an anode, the reduction of a terminal electron acceptor such as oxygen in a cathode is driven to produce hydroxide ions (Eq. 2) (Popat et al. 2012). This special feature has been employed to accomplish boron removal with the transformation of boric acid to borate ions in BES, and both the MDC-Donnan Dialysis (DD) coupled system and an MFC have been demonstrated to achieve effective boron removal (Ping et al. 2015b). Although the application of BES in boron removal is promising, the mechanism of boron transport is not fully understood and this could mislead the operational strategies. For example, the loss of high-mobility hydroxide ions in the desalination

compartment of an MDC can lead to reduced alkalinity, which challenges the stability of borate ion electromigration. In particular, it is important to further understand the transport of boron in solution with neutral pH and evaluate the contribution of different driving forces.

$$O_2 + 2H_2O + 4e^- \rightarrow 4OH^- \qquad (2)$$

Mathematical modeling can provide useful insight into the boron transport processes in BES. Owing to the multiple processes of microbiology, chemistry and electrochemistry, the parameters in BES are dynamically linked (Luo et al. 2016), and most BES models that focused on the fate of solute did not deal with non-dissociable compounds (Ping et al. 2015a, Harnisch et al. 2009, Picioreanu et al. 2010). Therefore, it is essential to develop BES models for evaluation of the boron removal process and predication of the performance affected by operational factors. Herein, mathematical models were developed based on our previous BES models and the experimental data from the MDC-DD and MFC systems (Ping et al. 2015b). The models focused on the factors that could contribute to boron transformation and transport, such as pH change, diffusion, electromigration, ion-exchange and convective transport. The results were expected to help design suitable BES configuration and optimize operation for boron removal.

10.2 Methods

10.2.1 Bioelectrochemical systems

The mathematical models developed in this study were based on the experimental data of two BES systems from our previous studies, the MDC-DD system and the MFC system (Ping et al. 2015b). The MDC-DD system recycles the alkaline catholyte from the MDC to the stripping side of the DD, and treats the boron-containing salt solution at the feed side of the DD that acts as the pretreatment (or post-treatment) before (or after) it is desalinated in the desalination compartment of the MDC. In the DD pretreatment, the salt solution at the feed side is alkalized without salinity increase, owing to the exchange of hydroxide ions in the stripping solution with anions in the feed solution across the anion exchange membrane (AEM) in the DD. The alkalized solution with boric acid transformed into borate ions is then treated in the desalination compartment of the MDC (Figure 10.1A) (Ping et al. 2015b). In the DD post-treatment system, the transported hydroxide ions from the stripping solution to the feed solution are trapped which allow boron to remain borate ions to be transferred out of the feed solution through AEM to balance the charge. Since the feed solution is pre-desalinated in MDC, the concentrations of other anions (eg. Cl^-) are very low and have little competition to cross AEM (Figure 10.1B) (Ping et al. 2015b). The MFC cathodic treatment of the boron-containing salt solution effectively raises the pH and transports borate ions (transformed from boric acid) out of the salt solution (catholyte) through the AEM (Figure 10.1C) (Ping et al. 2016).

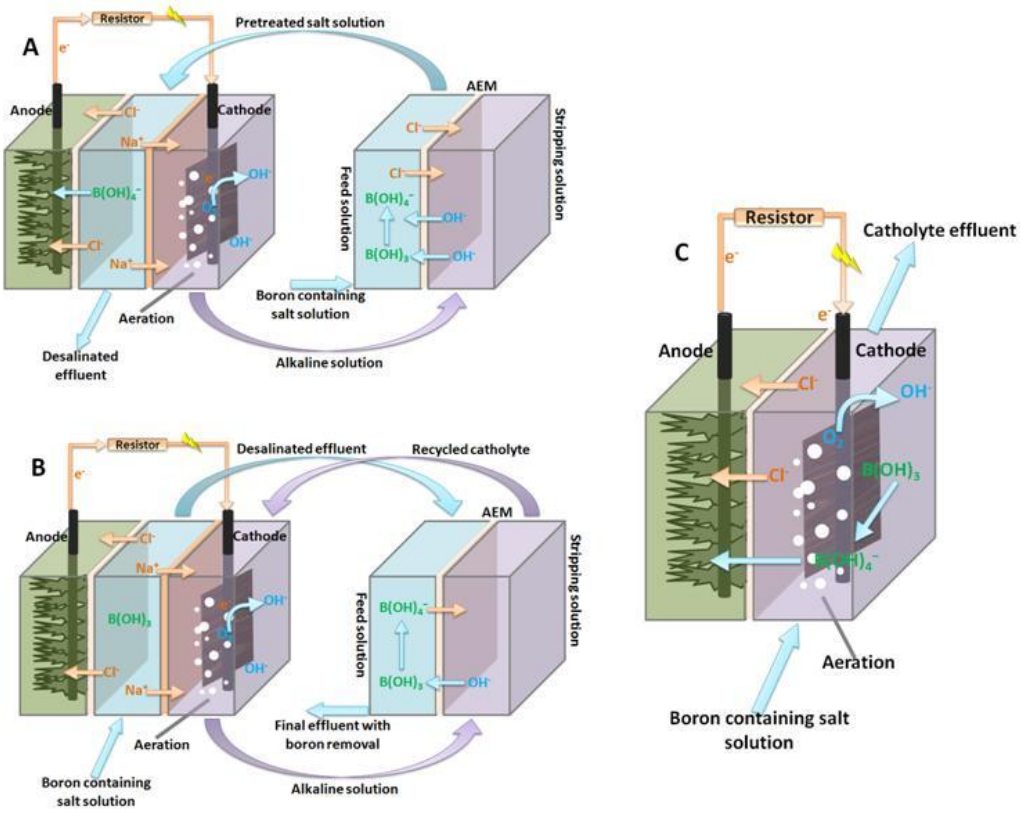

Figure 10.1 The schematic illustration of BES treating boron containing salt solution: (A) MDC with DD-pretreatment; (B) MDC with DD-post-treatment; and (C) MFC cathodic treatment.

10.2.2. Numerical methods and calculations

An integrated macro-scale time-dependent model was implemented in a combination of MATLAB code (2014b, The Mathworks Inc., Natick, MA) for solving stiff differential equations (ODE 23tb). The MATLAB code defines (1) model input parameters; (2) initial biomass concentrations, substrate concentrations, salt concentrations, hydroxide concentrations and boron concentrations in the system; and (3) ODE system of mass balances. Parameter estimation was

carried out by minimizing the objective function defined as relative root-mean-square error (RMSE).

$$RMSR = \frac{\sqrt{\sum_{i=1}^{N}(y_i - \hat{y}_i)^2}}{\max(\hat{y})} \qquad (3)$$

where N is the total sampling time point in the simulation; $\hat{y}_i$ and y_i represent experimental data and model predicted values at t_i, respectively. The maximum values of the experimental data for the current and the salt concentration were used to normalize the error in Eq. 3. To equalize the number of sampling time points in the experimental and simulation data, interpolation of both data sources was applied using "spline", which is a cubic interpolation of the values at neighboring grid points. The RMSE calculation of boron concentration used rounded values of the simulation data in accordance to the experimental measurement limitation where only integer values can be obtained. FMINCON subroutine of the MATLAB Optimization Toolbox was used to solve the optimization problem with several parameters starting at an initial estimate.

10.2.3 Model formulation

10.2.3.1. MDC-DD system

The MDC model was developed for three continuous operation modes, direct cathodic alkalization, DD as pretreatment, and DD as post-treatment for brackish water desalination and boron removal. The mass balances for substrates, microorganisms, and electron mediators in the MDC were adopted from a previous study based on the multiplicative Monod kinetics (Ping et al. 2014). The current generation was calculated by the cell voltage divided by the sum of internal

resistance and external resistance. The cell voltage was calculated as the experimentally measured open circuit voltage (~0.8 V) subtracting concentration overpotential (Ping et al. 2014). The membrane and electrolyte resistance that can contribute to the internal resistance of BES was calculated according to a previous study (Qin et al. 2015). The electrolytes in the BES were assumed to be completely mixed so that the concentrations of all soluble chemical and microbial species are uniform in each compartment. In the MDC, the mass balance of salt is governed by diffusion and electromigration that was adopted from the previous model (Ping et al. 2014). The mass balance of salt in the DD is governed by diffusion and reflected by the following equations:

$$\frac{dC_{salt,feed}}{dt} = D_{feed} \cdot \left(C_{salt,feed,in} - C_{salt,feed}\right) - D_{salt,feed} \qquad (4)$$

$$\frac{dC_{salt,strip}}{dt} = D_{strip} \cdot \left(C_{salt,strip,in} - C_{salt,strip}\right) - D_{salt,strip} \qquad (5)$$

where D_x is the dilution rate (day^{-1}) defined by the flow rate (L day^{-1}) divided by the volume of the compartment x (L); $C_{salt,x,in}$ is the influent concentration (mol L^{-1}) of the compartment x, and $C_{salt,x}$ is the effluent concentration of the compartment x (mol L^{-1}); and $D_{salt,x}$ is the diffusion term that will be discussed in later section (Eq. 26).

10.2.3.2. MFC system

In the MFC model, it is important to incorporate a noncompetitive inhibition term to regulate anodophillic microorganism growth, which thereby governs the response of current generation to a shock load of salt in the catholyte that can diffuse across AEM into the anolyte. Noncompetitive inhibition term was added to the microorganism kinetics that can decrease the

microbial growth rate, but do not affect *Ks*, the half saturation constant (Grady et al. 2011). The anodophilic growth rate was modified as:

$$k_a = k_{a,max} \frac{S}{K_a + S} \frac{M_{OX}}{K_M + M_{OX}} \frac{K_I}{K_I + \left(C_{salt,anode} - C_{salt,anode,0}\right)} \qquad (6)$$

where $k_{a,max}$ is the maximum anodophilic microorganism growth rates (day^{-1}); S is the concentration of the substrate (mg-S L^{-1}); K_a and K_M are the half-saturation concentrations for the anodophillic microorganisms (mg-S L^{-1}) and the redox mediator (mg-M mg-a^{-1}), respectively; M_{OX} is the oxidized mediator fraction per anodophillic microorganism (mg-M mg-a^{-1}); K_I is the inhibition coefficient; and ($C_{salt, anode}$ - $C_{salt, anode,0}$) is the term representing the salt concentration increase in the anolyte.

For the salt solution to be treated in the MFC cathode compartment, an ideal situation would be that anion electromigration across AEM from the catholyte to the anolyte reaches a balance with the cathodic hydroxide generation and thus the salinity remains same. However, when the balance is not achieved with strong anion migration and weak hydroxide production, positively charged cations will be forced to migrate across AEM along with negatively charged anions to reach charge balance, resulting in decreased salinity in the catholyte. It was assumed in the model that two factors contribute to the catholyte salinity variation: the difference between the generated hydroxide ions and electro-migrated anions across AEM, and the salt diffusion caused by a concentration gradient between the anode and cathode compartments. The equations showing the mass balance of salt in the catholyte and the anolyte are as following:

$$\frac{dC_{salt,cathode}}{dt} = D_{cathode} \cdot \left(C_{salt,cathode,in} - C_{salt,cathode}\right) + \left(G_{cathode} - M_{salt,cathode}\right) - D_{salt,cathode} \qquad (7)$$

$$\frac{dC_{salt,anode}}{dt} = D_{anode} \cdot \left(C_{salt,anode,in} - C_{salt,anode}\right) - \left(G_{anode} - M_{salt,anode}\right) + D_{salt,anode}$$

(8)

where G_x is the generation of hydroxide ions, and $M_{salt,x}$ is the electromigration of anions from the catholyte into the anolyte that is explained in Eq. 24&25. The difference between them contributes to the cation migration and leads to salt concentration variation. $D_{salt,x}$ is the diffusion of salt between the catholyte and anolyte caused by concentration gradient, which is explained in Eq. 26.

10.2.3.3. Solute components

In this study, we focus on two components in the solution, hydroxide ions and boron (boric acid and borate ions). In an MFC, both of hydroxide ions and boron species are subject to diffusion and electromigration (boron in the form of borate ion), while additionally boron is subject to convective transport by an electrical field (Nikonenko et al. 2010) and water osmosis (Dydo and Turek 2013). The current-driven electromigration is constrained by the possibility of each anion to be transported in relation to the product of ion concentration and mobility (Eq. 9) (Ping et al. 2015a):

$$\varphi_{i,x} = \frac{u_i \cdot C_{i,x}}{\sum u_i \cdot C_{i,x}} \quad (9)$$

where u_i ($m^2 s^{-1} V^{-1}$) is the mobility of the anion i in the solution.

The convective drag transport of boron can be explained by the coupling effect between boric acid molecules and ions or water molecules. As the electric current expedites ions movement or

the osmotic pressure promotes water molecules movement, they drag an additional amount of boric acid (Dydo and Turek 2013).

The equations of mass balance of hydroxide ions and boron in the MFC are as following:

$$\frac{dC_{OH,cathode}}{dt} = D_{cathode} \cdot \left(C_{OH,cathode,in} - C_{OH,cathode}\right) + G_{cathode} - M_{OH,cathode} - D_{OH,cathode} \quad (10)$$

$$\frac{dC_{B,cathode}}{dt} = D_{cathode} \cdot \left(C_{B,cathode,in} - C_{B,cathode}\right) - M_{borate,cathode} - D_{B,cathode} - Conv_{B,cathode,current} + Conv_{B,cathode,osmosis} \quad (11)$$

$$\frac{dC_{B,anode}}{dt} = D_{anode} \cdot \left(0 - C_{B,anode}\right) + M_{borate,anode} - D_{B,anode} + Conv_{B,anode,current} - Conv_{B,anode,osmosis} \quad (12)$$

where $Conv_{B,x,current}$ and $Conv_{B,x,osmosis}$ are the current-induced convection and water transport-induced convection, respectively, as explained in Eq. 27&28.

In the MDC-DD system, the mass balance of hydroxide ions in the catholyte of the MDC is not subject to electromigration (blocked by cation exchange membrane - CEM), and thus the term is eliminated. The mass balance of hydroxide ions is expressed in the following equations:

$$\frac{dC_{OH,cathode}}{dt} = D_{cathode} \cdot \left(C_{OH,cathode,in} - C_{OH,cathode}\right) + G_{cathode} - D_{OH,cathode} \quad (13)$$

$$\frac{dC_{OH,salt}}{dt} = D_{salt} \cdot \left(C_{OH,salt,in} - C_{OH,salt}\right) - \varphi_{OH,salt} \cdot \frac{I_{MDC}}{F \cdot V_{salt}} - D_{OH,salt-anode} - D_{OH,salt-cathode} \quad (14)$$

$$\frac{dC_{OH,feed}}{dt} = D_{feed} \cdot \left(C_{OH,feed,in} - C_{salt,feed}\right) - D_{OH,feed} - E_{OH,feed} \quad (15)$$

$$\frac{dC_{OH,strip}}{dt} = D_{strip} \cdot \left(C_{OH,strip,in} - C_{salt,strip}\right) - D_{OH,strip} + E_{OH,strip} \quad (16)$$

The mass balance of boron species is expressed as:

$$\frac{dC_{B,salt}}{dt} = D_{salt} \cdot \left(C_{B,salt,in} - C_{B,salt}\right) - \varphi_{Borate,salt} \cdot \frac{I_{MDC}}{F \cdot V_{salt}} - D_{B,salt-anode} - D_{B,salt-cathode} \quad (17)$$

$$\frac{dC_{B,anode}}{dt} = D_{anode} \cdot \left(C_{B,anode,in} - C_{B,anode}\right) - \varphi_{Borate,salt} \cdot \frac{I_{MDC}}{F \cdot V_{anode}} - D_{B,anode} \quad (18)$$

$$\frac{dC_{B,cathode}}{dt} = D_{cathode} \cdot \left(C_{B,cathode,in} - C_{B,cathode}\right) - \varphi_{Borate,salt} \cdot \frac{I_{MDC}}{F \cdot V_{cathode}} - D_{B,cathode} \quad (19)$$

$$\frac{dC_{B,feed}}{dt} = D_{feed} \cdot \left(C_{B,feed,in} - C_{B,feed}\right) - D_{B,feed} - E_{B,feed} + E_{B,strip} - Conv_{B,feed,osmosis} \quad (20)$$

$$\frac{dC_{B,strip}}{dt} = D_{strip} \cdot \left(C_{B,strip,in} - C_{B,strip}\right) - D_{B,strip} - E_{B,strip} + E_{B,feed} + Conv_{B,strip,osmosis} \quad (21)$$

where $E_{i,x}$ is the ion-exchange term in the DD limited by the lower salt concentration of either side:

$$E_{i,x} = \varphi_{i,x} \cdot \frac{a_{ex} \cdot min\left(C_{salt,feed}, C_{salt,strip}\right)}{V_x} \quad (22)$$

where a_{ex} is the ion-exchange coefficient (L d^{-1}).

The pH is then calculated using the expression:

$$pH = 14 + \log[OH^-] \quad (23)$$

A constant pH was assumed in the anolyte of BES considering the buffer effect.

The hydroxide ion generation, migration of ions, and diffusion of ions are formulated in the following equations:

$$G_c = \frac{I_{BES}}{F \cdot V_x} \cdot a_{OH}$$

(24)

$$M_{i,x} = \varphi_{i,x} \cdot \frac{I_{BES}}{F \cdot V_x} \cdot C_{\text{salt ,x}} \cdot a_e \quad (25)$$

$$D_{i,x} = \frac{A_{membrane}}{V_x} \cdot \left(C_{i,x} - C_{i,y}\right) \cdot a_d \quad (26)$$

where I_{BES} (A) is the current generated by BES reactor; F is the Faraday constant (A day mole^{-1}); V_x is the volume of the target compartment (L); a_{OH} is the hydroxide ion generation efficiency; φ_i is the possibility of each anion to be transported across AEM driven by current (Eq. 12); a_e (L mol^{-1}) is the general anion electromigration coefficient; $A_{membrane}$ is the membrane surface area (m^2); a_d (m d^{-1}) is the diffusion coefficient; y is the adjacent compartment to x with the membrane separating them. $\varphi_{salt,x}$ is equal to 1 in the case of $M_{salt,x}$.

The current-induced convection and water transport-induced convection are expressed in the following equations:

$$Conv_{B,x,current} = \frac{I_{BES}}{F \cdot V_x} \cdot C_{\text{B,cathode}} \cdot a_c \quad (27)$$

$$Conv_{B,x,osmosis} = \frac{Osmosis}{V_x} \cdot C_{\text{B,O}} \cdot a_o \quad (28)$$

$$C_{\text{B,O}} = \begin{cases} C_{\text{B,anode}} & \text{if } C_{\text{salt ,cathode}} < C_{\text{salt ,anode}} \\ C_{\text{B,cathode}} & \text{if } C_{\text{salt ,cathode}} \geq C_{\text{salt ,anode}} \end{cases} \text{ in MFC} \quad (29)$$

$$\text{or } \begin{cases} C_{\text{B,feed}} & \text{if } C_{\text{salt,feed}} < C_{\text{salt,strip}} \\ C_{\text{B,strip}} & \text{if } C_{\text{salt,feed}} \geq C_{\text{salt,strip}} \end{cases} \text{ in DD} \quad (30)$$

where a_c (L mol^{-1}) is the current-induced convection coefficient, and a_o (d^{-1}) is the osmosis-induced convection coefficient. Both convection type transports are constricted by boron concentration in the source (the compartment from which the boron transports out).

10.3 Results and Discussion

10.3.1 Model fitting

10.3.1.1 The MDC-DD system

The model was fitted with the experimental conditions of varying salt solution flow rate, 0.16 – 0.08 – 0.06 mL min^{-1} in the MDC cathodic alkalization, 0.2 – 0.12 – 0.16 mL min^{-1} in the DD-pretreatment system, and 0.12 – 0.16 mL min^{-1} in the DD-post-treatment system. The parameters that were slightly adjusted during simulation included the mediator yield (*Y*) related to current production, initial anodophilic microorganism concentration (*xa*), and alkali production efficiency (a_{OH}) by the cathode; while other parameters were kept the same during all simulations. A list of the parameters is shown in Table 10.1. The osmosis-induced convection coefficient a_o was estimated according to the post-DD experiments where the pH of the feed solution was below 9.14 and boron was in the form of non-charged boric acid and thus not subject to ion exchange ($E_{i,x}$ in Eq. 20&21) (Figure 10.2F). Incorporating concentration-gradient-driven diffusion ($D_{i,x}$) alone in the boron mass balance equations was not able to achieve satisfactory fitting results. Thus, the osmosis-driven convection term ($Conv_{B,x,osmosis}$) was added in Eq. 20&21 and successfully improved the fitting results of the DD-feed boron concentration with RMSE decreased from 42.45% (Figure 10.2) to 0.00% (Figure 10.3A). u_{borate} and u_{OH} were

kept the same (5.33 and 45.72 $10^{-8}m^2s^{-1}V^{-1}$) under most conditions except in the MDC desalination compartment where they were multiplied with the factor $e^{-300C_{Cl,salt}}$ and $15e^{-300C_{Cl,salt}}$ considering the strong competition of anions (e.g., chloride ions). This adjustment improved the fitting of pH in the salt solution with RMSE decreased from 11.59% to 6.68%, and the RMSE of the boron concentration fitting decreased from 50.75% to 1.44% in the MDC-DD pretreatment system (Figure 10.4A&B and Figure 10.5A&B). In the MDC cathodic alkalization system, the fitting of pH in the salt solution was improved with RMSE decreased from 15.79% to 8.93%, and the RMSE of the boron concentration fitting decreased from 52.00% to 11.25% (Figure 10.4C&D and Figure 10.6B&D).

Table 10.1 Parameters used in the model.

Parameters	Description	Values
$k_{a,max}$	maximum microorganism growth rates for anodophillic microorganism	0.197 day^{-1}
K_a	half-saturation concentrations for the anodophillic microorganism	20 mg-S L^{-1}
K_M	half-saturation concentrations for the redox mediator	0.2 M_{total} mg-M·mg-a^{-1}
M_{total}	Mediator fraction	0.05 mg-M·mg-x^{-1}
K_I	Inhibition coefficient for anodophilic microorganism	0.04 mol L^{-1}
u_{borate}	Mobility of borate ion	5.33 $10^{-8}m^2s^{-1}V^{-1}$
u_{Cl}	Mobility of chloride ion	7.92 $10^{-8}m^2s^{-1}V^{-1}$
u_{OH}	Mobility of hydroxide ion	45.72 $10^{-8}m^2s^{-1}V^{-1}$

a_{ex}	ion-exchange coefficient in DD	0.32 L d^{-1}
a_{OH}	hydroxide ion generation efficiency	0.02 (in MFC pretreatment of seawater)
a_e	general anion electromigration coefficient	10 L mol^{-1} (in MFC pretreatment of seawater)
a_d	diffusion coefficient across membrane	0.74 m d^{-1}
a_c	current-induced convection coefficient	3.35 L mol^{-1}
a_o	osmosis-induced convection coefficient	3000 d^{-1}
Y_M	the mediator yield	24.46 mg-M·mg-S^{-1} (in MFC pretreatment of seawater)
F	Faraday constant	96,485 A s $mole^{-1}$
R	Ideal gas constant	8.314472 J K^{-1} mol^{-1}
T	MDC temperature	298.15 K

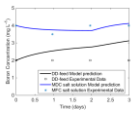

Figure 10.2 Model fitting of boron concentration in DD-feed solution and MDC salt effluent in MDC-DD as post-treatment system, without osmosis-driven convection term (ConvB,x,osmosis) in Eq. 20&21.

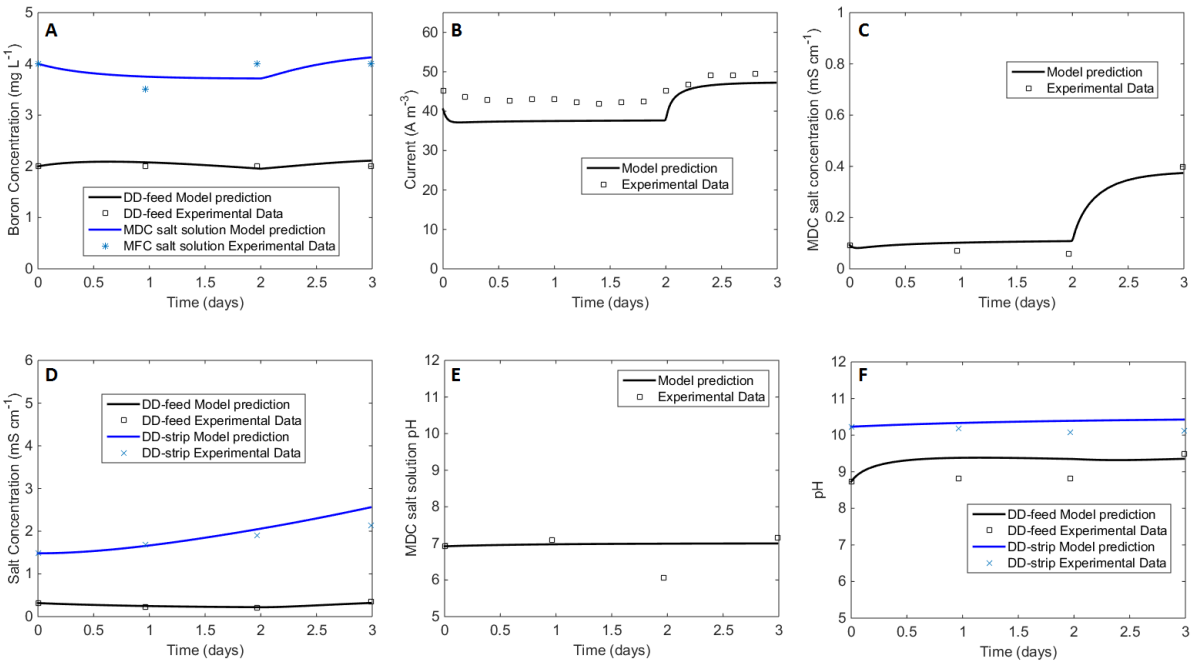

Figure 10.3 Model fitting of the MDC-DD as post-treatment system. (A) Boron concentration in the DD-feed solution and MDC salt effluent; (B) Current generation; (C) MDC salt effluent conductivity; (D) DD-feed and strip solution conductivity; (E) MDC salt effluent pH; (F) pH of DD-feed and stripping solutions.

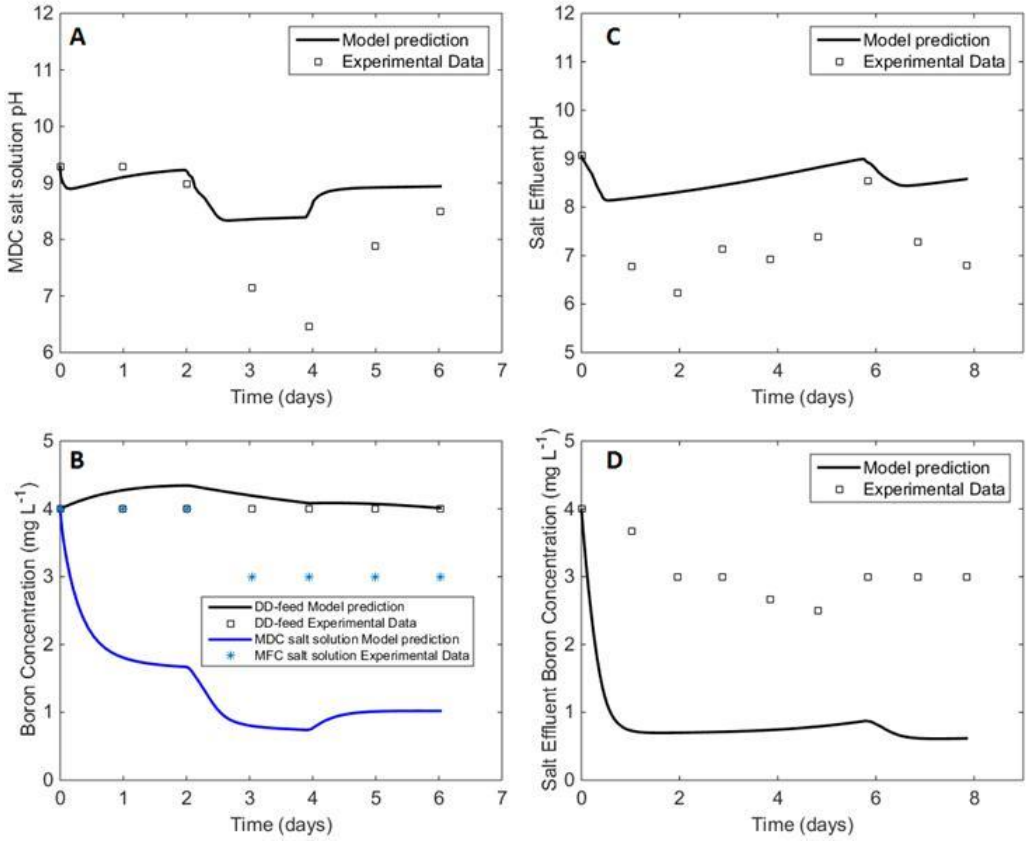

Figure 10.4 Model fitting without ion mobility adjustment. (A) MDC salt effluent pH; (B) boron concentration in the DD-feed solution and MDC salt effluent in the MDC-DD as pretreatment system; (C) MDC salt effluent pH; (D) MDC salt effluent boron concentration in direct cathodic alkalization system.

After calibration, the variation of current generation, salinity and solute concentration in response to the salt solution flow rates in the three operations was fitted by the model with small discrepancy. For example, in the DD pretreatment system, the model accurately simulated the MDC boron concentration and salt solution pH variation trend (Figure 10.5A&B). It should be noted that the experimental measurement of the boron concentration can only be precise to integers, and thus even the modeled data deviated slightly from the experimental data, it was still

considered a good fit. Slight overestimation of the salt concentration in the MDC salt solution was observed at day 4-6 when the MDC recovered from low current generation, which was regulated by salt solution HRT (longer HRT resulted in a lower salt concentration and greater internal resistance, and vice versa) (Figure 10.5C). This discrepancy could be possibly caused by the fact that the MDC salt influent concentration (DD-feed salt concentration in Figure 10.5D) was affected by slight variation in the prepared solution while the model assumed constant salt solution input. In Figure 10.5D, underestimation of the salt concentration in the stripping solution was observed; however, the simulation agreed well with the trend of the experimental data. This discrepancy was probably caused by the inadequate mixing under the experimental conditions, while the model assumed complete mixing of the liquid. The RMSE values between the experimental data and modeled results were mostly less than 10%, except the relative higher discrepancy for the salt concentration in the MDC up to 22.67% with the DD as post-treatment (Table 10.2). The high RMSE of the salt concentration was caused by the limitation of interpolation of the experimental data and the inadequate data points.

Table 10.2 The RMSE between the experimental data and modeled values of continuous MDC-DD systems.

		Direct cathodic alkalization	DD as pretreatment	DD as post-treatment
Boron Concentration	MDC Salt solution	11.25%	1.44%	8.77%
	DD-feed	-	0.00%	0.00%
Salt	MDC Catholyte	5.12%	-	-

Concentration	MDC Salt solution	17.16%	13.44%	22.67%
	DD-feed	-	3.95%	4.99%
	DD-strip	-	10.39%	8.24%
pH	MDC Catholyte	0.97%	-	-
	MDC Salt solution	8.93%	6.68%	8.14%
	DD-feed	-	1.27%	4.89%
	DD-strip	-	1.75%	2.42%
Current		8.66%	2.67%	9.63%

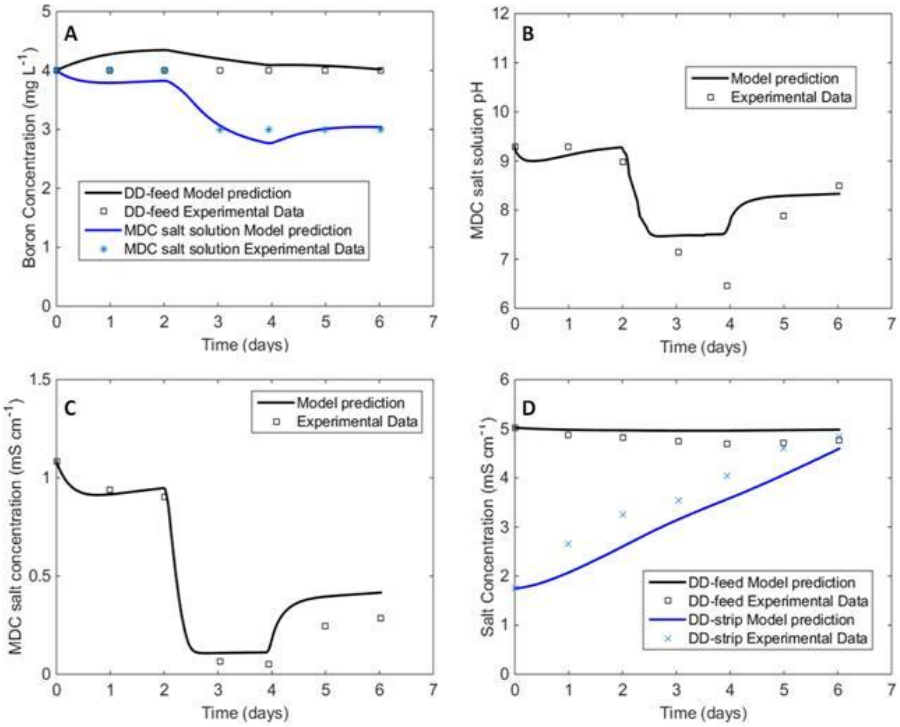

Figure 10.5 Model fitting of the MDC-DD system with DD as pretreatment: (A) boron concentration in the DD-feed solution and the MDC salt effluent; (B) MDC salt effluent pH; (C) MDC salt effluent conductivity; and (D) DD-feed and strip solution conductivity.

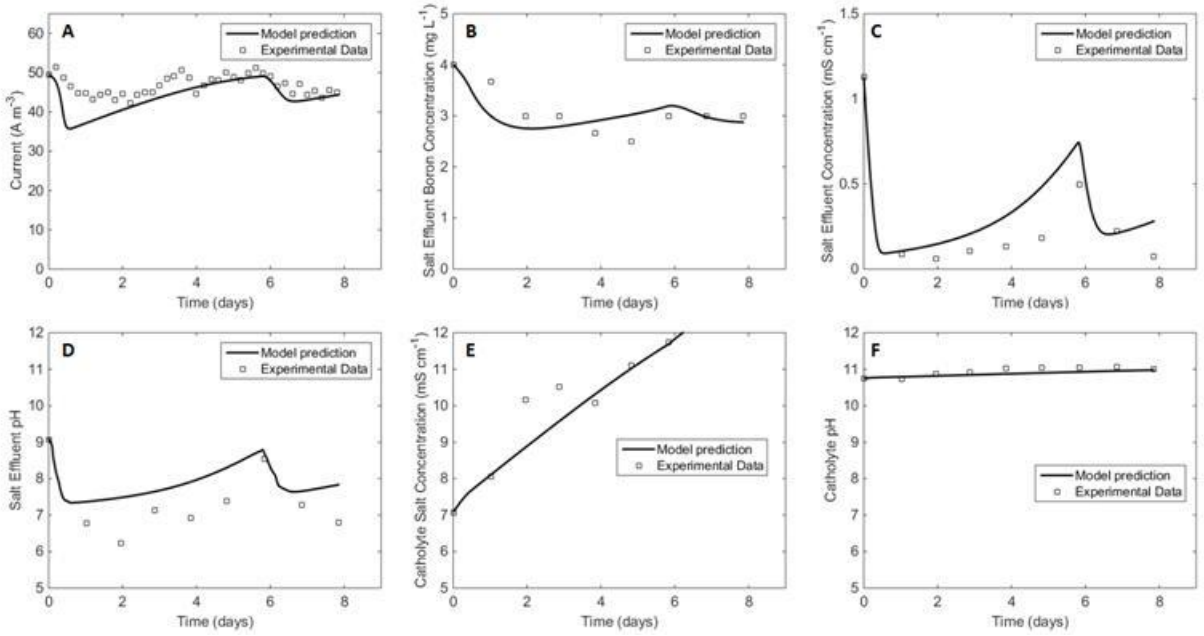

Figure 10.6 Model fitting of the MDC direct cathodic alkalization system. (A) Current generation; (B) Boron concentration in the MDC salt effluent; (C) MDC salt effluent conductivity; (D) MDC salt effluent pH; (E) MDC catholyte conductivity; (F) MDC catholyte pH.

10.3.1.2 The MFC system

The mass balance of batch operation was formulated by eliminating the dilution term D_x (related to flow rates) in the existing continuous operation model. Both pretreatment and post-treatment

of seawater or brackish water were simulated. In the MFC system, previously determined a_o fitted well under the open circuit condition where the pH of the catholyte was not raised and boron was not subject to electromigration or current-induced convection (data not shown). The parameter a_c was then calibrated under the condition of close circuit with the optimization tool, where the boron removal was contributed by the four forces $M_{borate,cathode}$, $D_{B,cathode}$, $Conv_{B,cathode,current}$, $Conv_{B,cathode,osmosis}$. In addition to the parameters related to anodophilic microorganism kinetics (Y and x_a), the alkali production efficiency (a_{OH}) and anion electromigration efficiency (a_e) were also slightly adjusted during simulation.

The model results of current generation, catholyte salinity, pH and boron concentration generally followed the experimental data (Figure 10.7), with some overestimation of the boron concentration (Figure 10.7A and Figure 10.9B&10.10B). The mismatch of the boron concentration in the first 0.4 d is probably due to the batch operation where the reactor might encounter an impulse response at the beginning and thus was not simulated by the model. The minimal removal of boron simulated by the model during pretreatment of seawater agreed with the experimental data with a small RMSE value of 5.62% (Figure 10.7D). The stable current generation in the MFC post-treatment of seawater system was fitted well by the model with RMSE of 6.1% (Figure 10.7B). By adding the inhibition term in the microbial kinetics, which is governed by salt intrusion into the anolyte, the model can achieve satisfactory prediction of the declining current generation in the MFC pretreatment of seawater system (RMSE of 11.6%) (Figure 10.7E). The catholyte salt concentration under both post-treatment and pretreatment conditions was fitted well, although the model did not reflect the initial impulse response before

0.4 d in the batch operation (Figure 10.7 C&F and Figure 10.9D&10.10D). The RMSE values for the MFC system are shown in Table 10.3. As explained previously, the higher RMSE values of salt concentration could be caused by the limitation of interpolation.

Table 10.3 The RMSE between the experimental data and modeled values of batch MFC system.

	MFC pretreatment of seawater	MFC post-treatment of seawater	MFC pretreatment of brackish water	MFC post-treatment of brackish water
Catholyte Boron Concentration	5.62%	13.03%	18.55%	15.55%
Catholyte Salt Concentration	13.93%	17.29%	22.45%	21.58%
Catholyte pH	6.90%	13.71%	9.78%	7.63%
Current	11.60%	6.1%	5.06%	11.47%

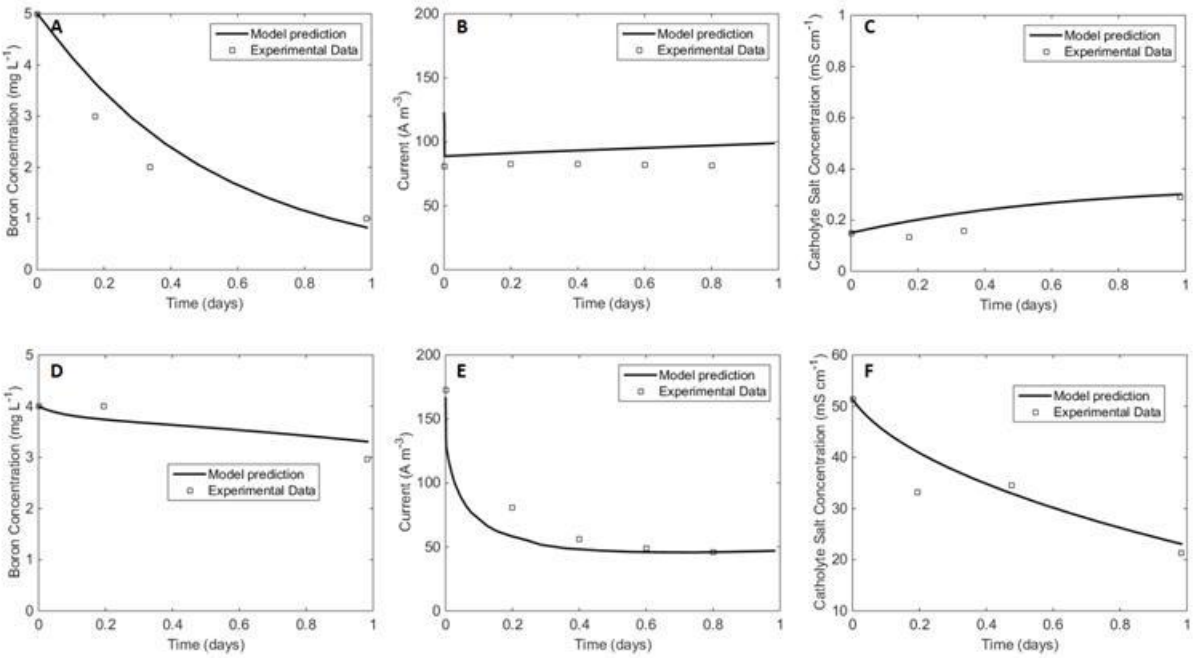

Figure 10.7 Model fitting of the MFC as post-treatment or pretreatment of seawater. Post-treatment: (A) boron concentration in the MFC catholyte; (B) current generation; and (C) MFC catholyte conductivity. Pretreatment: (D) boron concentration in the MFC catholyte; (E) current generation; and (F) MFC catholyte conductivity.

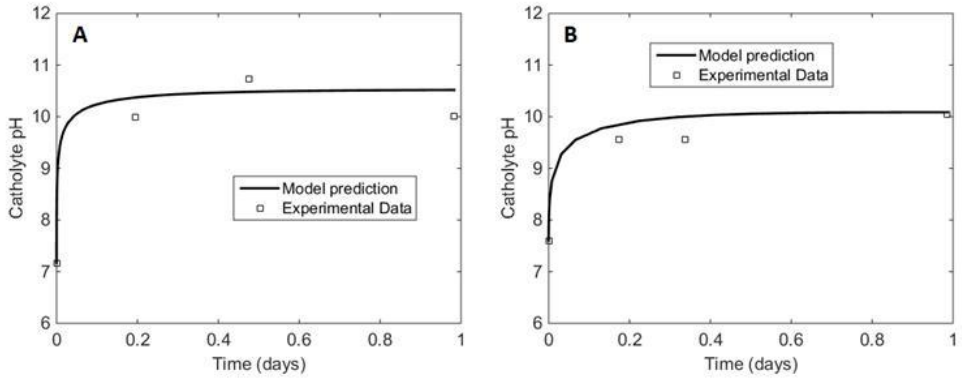

Figure 10.8 Model fitting of the catholyte pH in MFC as (A) pretreatment and (B) post-treatment.

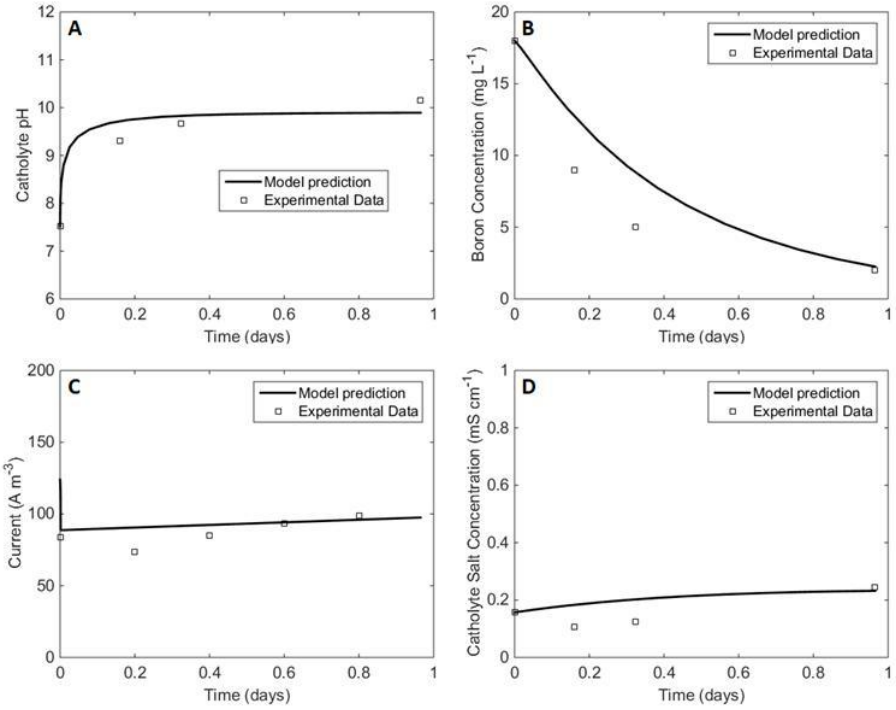

Figure 10.9 Model fitting of the MFC as post-treatment of brackish water. (A) MFC catholyte pH; (B) Boron concentration in the MFC catholyte; (C) Current generation; (D) MFC catholyte conductivity.

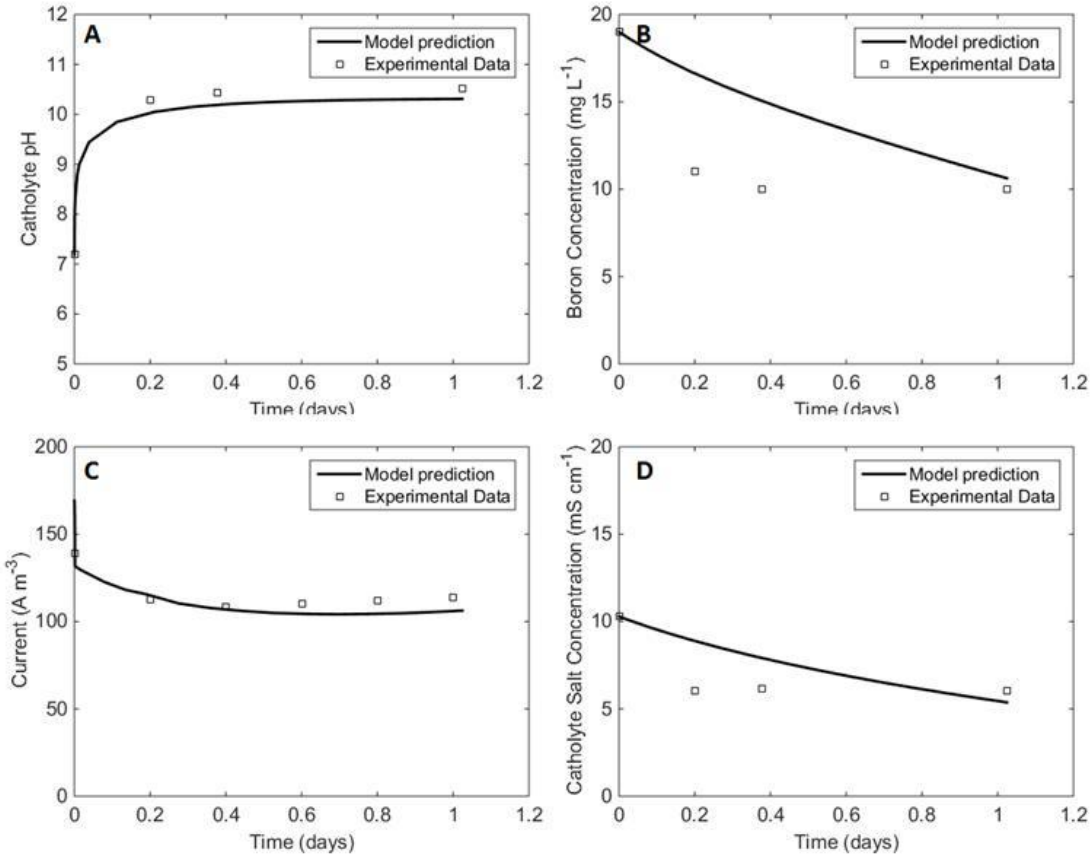

Figure 10.10 Model fitting of the MFC as pretreatment of brackish water. (A) MFC catholyte pH; (B) Boron concentration in the MFC catholyte; (C) Current generation; (D) MFC catholyte conductivity.

10.3.2. Model simulation

10.3.2.1. Boron removal in the MDC-DD system

The model has simulated multiple outputs as a function of time. Both the DD-pretreatment and DD-post-treatment modes were simulated at two flow rates of the salt solution, 0.17 and 0.12 L d^{-1} (Figure 10.11&10.12). It is unlikely that the system will reach absolutely steady state, due to

the recirculation between the MDC catholyte and the DD stripping solution that concentrates the salt in the system. Contradictory to our previous assumption that the accumulated anions in the DD stripping solution could outcompete the transport of hydroxide ions across the AEM and eventually diminish alkalization, leading to failure of boron removal, the simulated result indicates that the convective transport of boron owing to water osmosis from the feed into the stripping solution can effectively reduce boron concentration in the feed solution. In both the DD-pretreatment and DD-post-treatment modes, when the salt concentration in the stripping solution exceeds that of the feed solution around day 17 (Figure 10.11A&D) and day 5 (Figure 10.12A&D), a more rapid drop in boron concentration in DD-feed, and consequently more rapid increase of boron concentration in DD-strip are observed. Figure 10.11C&F and Figure 10.12C&F show the contribution of different driving forces, with the vertical span indicating the positive contribution to boron removal. It is observed that the contribution from osmosis-driven convective transport in the DD changes from negative to positive when the concentration difference reverses at day 17 in the DD-pretreatment system (Figure 10.11B&E) and at day 5 in the DD-post-treatment system (Figure 10.12B&E). The contribution by the DD-osmosis keeps increasing to 40~80% at day 20 in the DD-pretreatment system, and reaches more than 90% in the DD-post-treatment system within 5 days. The early region where the contribution by the DD-ion-exchange (indicated by blue color) spans from negative to positive values suggests that the DD-osmosis driven boron transport (indicated by black color) has negative contribution and is offset by the DD-ion-exchange (Figure 10.11C&F and Figure 10.12C&F).

Current-driven transport of borate ions has very little influence on boron removal when the salt solution is operated at a flow rate of 0.17 L d^{-1} (Figure 10.11C), while increasing the HRT by reducing the flow rate to 0.12 L d^{-1} enhances the current-driven removal of borate ions (indicated by green color) due to alleviated competition from other anions (Figure 10.11F). In the MDC with DD-pretreatment system, although a faster flow rate of 0.17 L d^{-1} of salt solution in the MDC guarantees short HRT and maintains the pH above 10 (hydroxide ions are not removed in the desalination process) (Figure 10.13A), borate ions have little chance to be removed from the solution due to the high concentrations of other anions (salt solution conductivity above 3 mS cm^{-1} (Figure 10.11A). Longer HRT (at a slower salt flow rate of 0.12 L d^{-1}) can slightly improve boron removal in both pretreatment and post-treatment operations. The DD-post-treatment system is able to reduce boron concentration to around 1 mg L^{-1} at a salt flow rate of 0.12 L d^{-1} (Figure 10.12D).

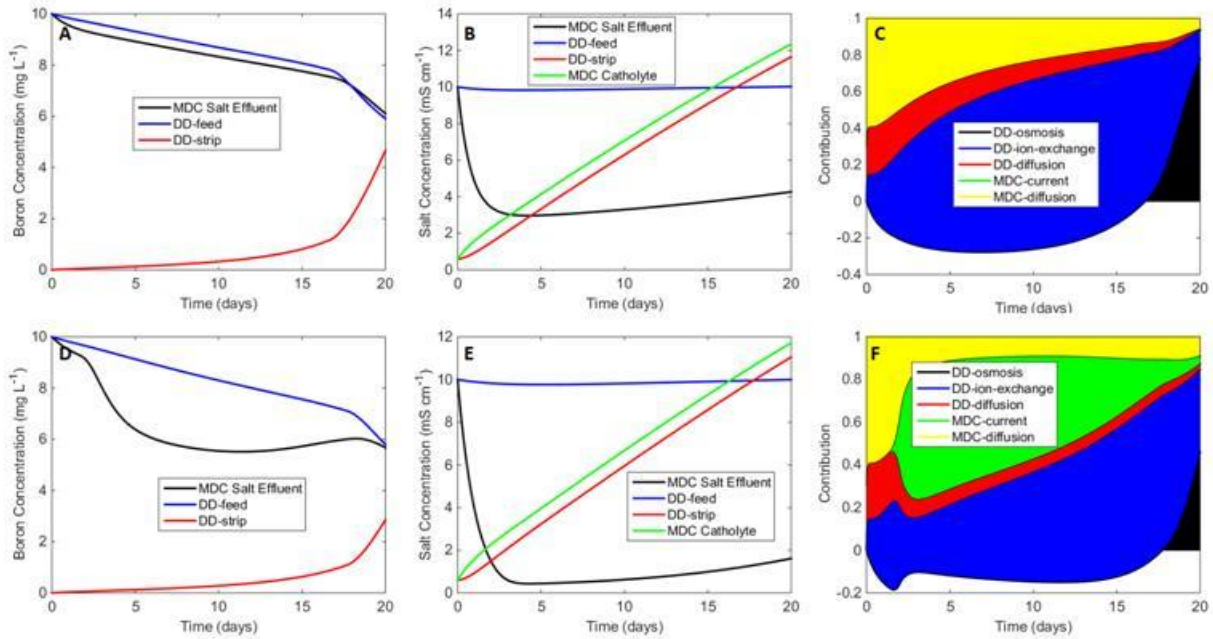

Figure 10.11 Simulation of the MDC with DD-pretreatment system at a salt flow rate of 0.17 L d^{-1} (A-C) and 0.12 L d^{-1} (D-F): (A) boron concentration; (B) conductivity; (C) contribution of different driving forces to the boron removal; (D) boron concentration; (E) conductivity; and (F) contribution of different driving forces to the boron removal.

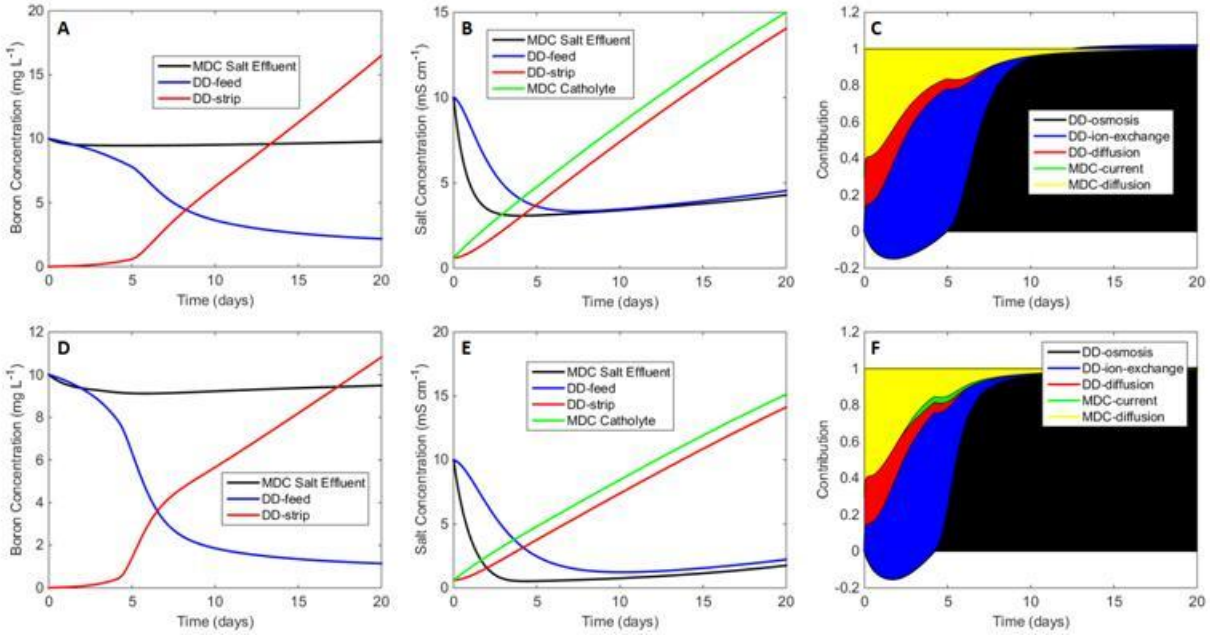

Figure 10.12 Simulation of MDC with DD-post-treatment system at salt flow rate at 0.17 L d^{-1} (A-C) and 0.12 L d-1 (D-F): (A) Boron concentration; (B) Conductivity; (C) Contribution of different driving forces to the boron removal; (D) Boron concentration; (E) Conductivity; (F) Contribution of different driving forces to the boron removal.

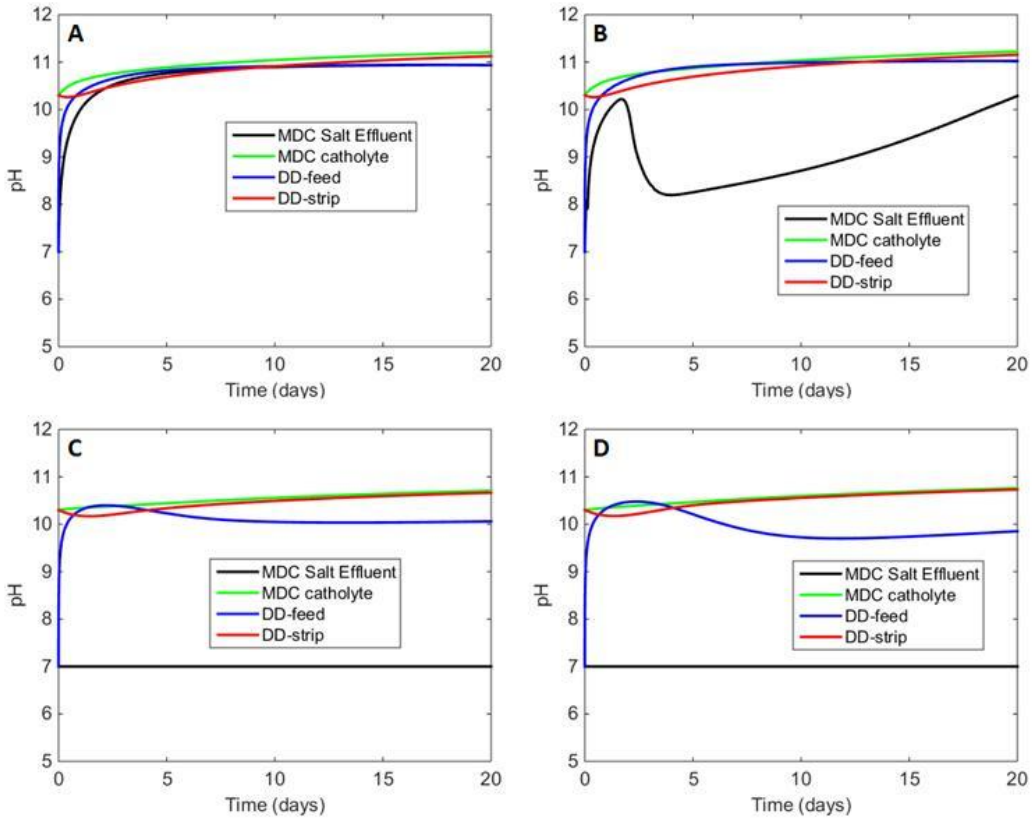

Figure 10.13 Simulation of pH of solutions in MDC-DD system: (A) DD as pretreatment at salt solution flow rate of 0.17 L d^{-1}; (B) DD as pretreatment at salt solution flow rate of 0.12 L d^{-1}; (C) DD as post-treatment at salt solution flow rate of 0.17 L d^{-1}; (D) DD as post-treatment at salt solution flow rate of 0.12 L d^{-1}.

10.3.2.2 Boron removal in the MFC system

Unlike the MDC-DD system, the continuous operation of the MFC system can reach a steady state (e.g. MFC as post-treatment in Figure 10.14). Thus the simulation of the MFC system was performed for the steady state performance under varied conditions. The synergistic effects of catholyte flow rate, anolyte flow rate, as well as initial boron concentration on the boron removal

in the catholyte and the boron accumulation in the anolyte were studied. In the MFC post-treatment system, the initial boron concentration is varied from 0 to 40 mg L^{-1} with the anolyte flow rate set at 1.44 L d^{-1} (Figure 10.14A&B). The simulation indicates that to achieve a boron concentration lower than 2 mg L^{-1}, the catholyte flow rate needs to be regulated accordingly and requires a slower flow rate (thus a longer HRT) for higher initial boron concentration in the catholyte. For example, the initial 10 mg L^{-1} B solution will need the catholyte flow rate to be slower than 0.20 L d^{-1}, while once the initial boron concentration drops below 5 mg L^{-1}, the treating capacity can be extensively improved with the flow rate greater than 0.70 L d^{-1} (Figure 10.14A). The resulted anolyte boron concentration in both cases is < 2 mg L^{-1} (Figure 10.14B).

The effects of catholyte flow rate and anolyte flow rate were then studied under the condition of a high boron concentration of 40 mg L^{-1} (Figure 10.14C&D). The anolyte flow rate does not have much impact on the catholyte boron concentration unless it drops to an extreme low rate (<0.10 L d^{-1}), which starves the anodophillic bacteria and stops current generation activity. The catholyte flow rate needs to be slower than 0.02 L d^{-1} to maintain a catholyte boron concentration lower than 2 mg L^{-1} (Figure 10.14C). The boron concentration in the anolyte is controlled by both anolyte and catholyte flow rates. A higher catholyte flow rate brings in more boron and needs correspondingly a higher anolyte flow rate to dilute the boron concentration in the anolyte. The ratio between the anolyte flow rate and the catholyte flow rate should be greater than 22.2 at the highest allowable catholyte flow rate of 0.02 L d^{-1} in order to achieve an anolyte boron concentration below 2 mg L^{-1}. With a slower catholyte flow rate, this boundary ratio needs to further increase and vice versa (due to a complex effect by boron migration driving forces). For

example, at 0.01 L d^{-1} catholyte flow rate, the ratio needs to reach 24.4 (Figure 10.14D). It is also observed that the catholyte pH is kept above 9.7 in the simulation range, and a slower anolyte (catholyte) flow rate will decrease (increase) the pH due to reduced current generation (a longer HRT for hydroxide ion production) (Figure 10.16).

Similar to the MDC-DD system, the osmosis-driven convection also plays an important role in the MFC system. In the MFC post-treatment system, at a catholyte flow rate of 0.02 L d^{-1} for treating 40 mg L^{-1} B solution, almost 80% of the boron removal is attributed to the osmosis-driven convection under the condition of weak current generation (higher external resistance) (Figure 10.14E). Lowering the external resistance to 30 Ω will improve current-driven boron migration, and reduce the catholyte boron concentration to less than 2.5 mg L^{-1} (~ 6 mg L^{-1} at 900 Ω) (Figure 10.14F). This results in current-driven contribution of 40% to boron removal with another 40% contributed by osmosis-driven convection (Figure 10.14E). At an external resistance of 900 Ω, current-driven contribution is less than 10%.

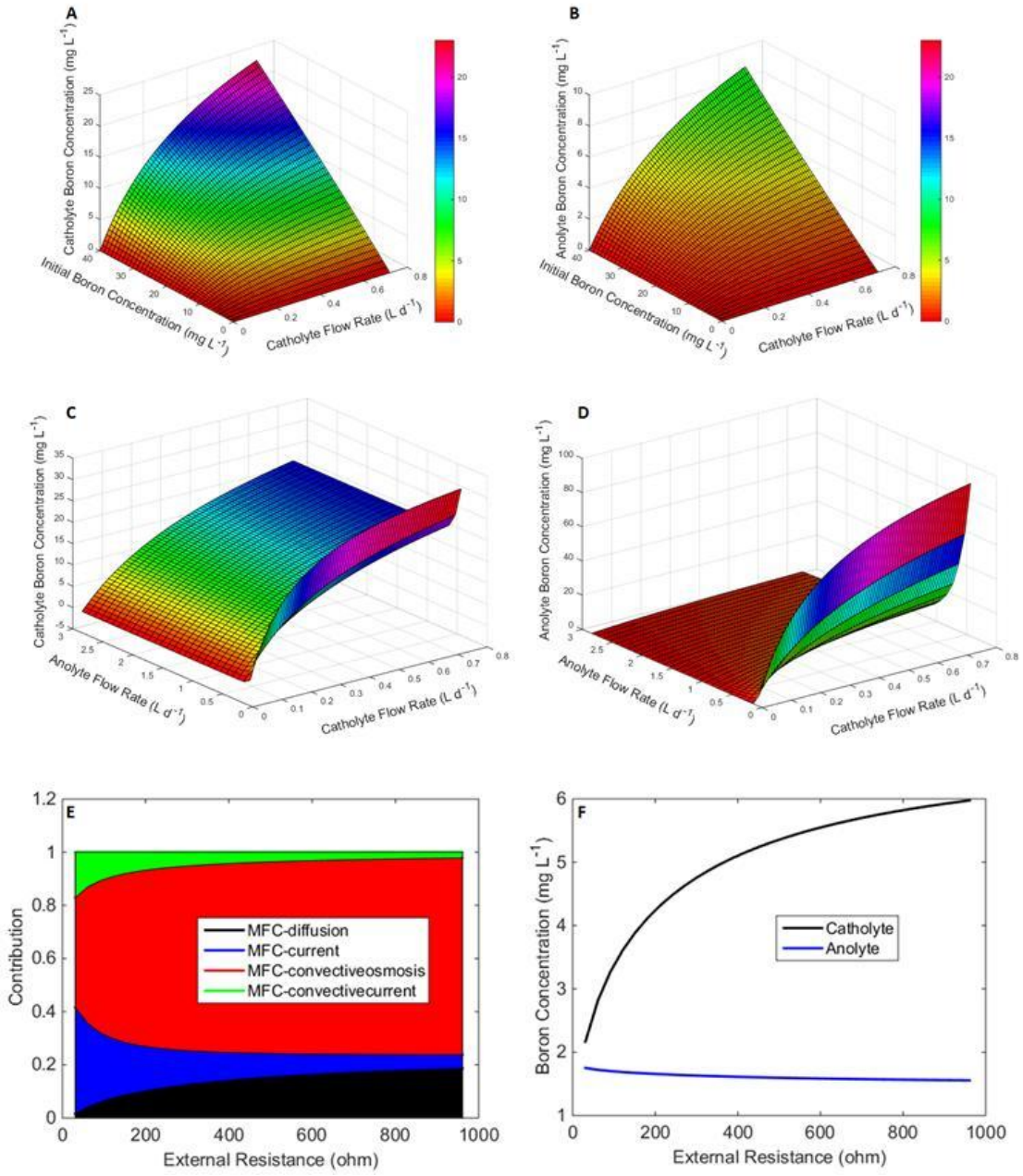

Figure 10.14 Simulation of the MFC post-treatment system: the variation of (A) catholyte boron concentration, and (B) anolyte boron concentration affected by different initial boron concentration and catholyte flow rates, at a constant anolyte flow rate of 1.44 L d^{-1}; the variation of (C) catholyte boron concentration, and (D) anolyte boron concentration affected by different anolyte and catholyte flow rates, at a constant initial boron

concentration of 40 mg L^{-1}; the variation of (E) contribution from different driving force to the boron removal from catholyte, and (F) boron concentration in anolyte and catholye affected by different external resistance. Color bar is inserted in A&B for better comparison.

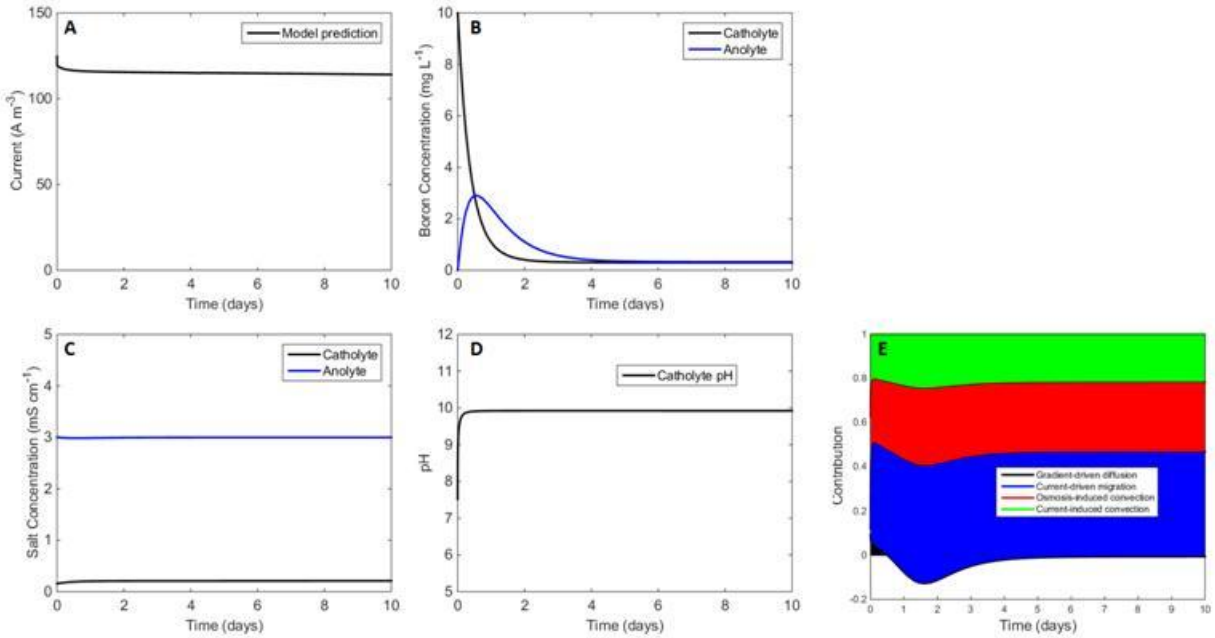

Figure 10.15 Simulation of continuous operation of MFC as post-treatment of brackish water.

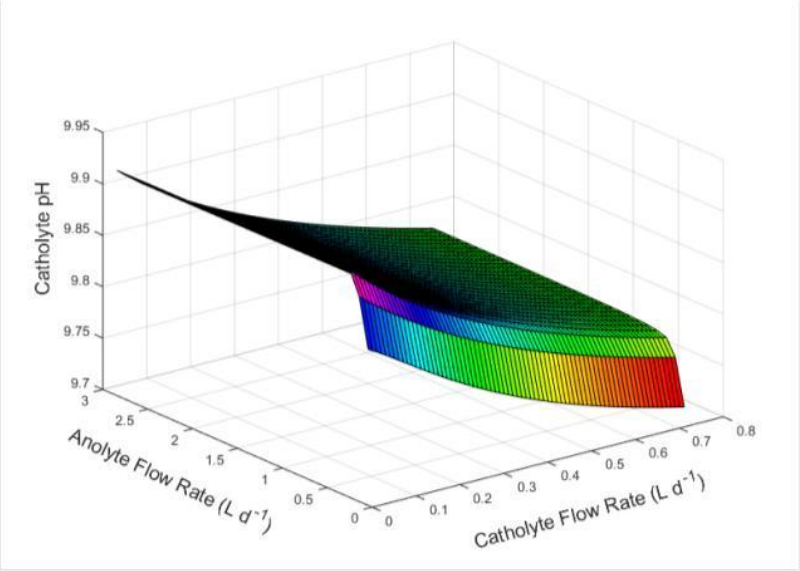

Figure 10.16 Simulation of pH variation affected by different anolyte and catholyte flow rates, at a constant initial boron concentration of 40 mg L^{-1} in MFC post-treatment system.

In the case of the MFC as pretreatment of seawater (salt concentration of 35 g L^{-1} and boron concentration of 5 mg L^{-1}), a unique issue is the inhibition of anodophillic bacteria due to transported salt from the catholyte. Thus the inhibition term $\frac{K_I}{K_I+(C_{salt,a}- C_{salt,a,0})}$ is simulated here with varied anolyte and catholyte flow rates. As expected, a faster anolyte flow rate ensures less inhibition of the bacteria, and the inhibition term can reach as close as to 1 (no inhibition effect). A faster catholyte flow rate has a negative impact on the inhibition, because it provides more salts being transported into the anolyte. At a slower anolyte flow rate, the inhibition is more severe with increasing catholyte flow rate, due to the slow transport of salt out of the anolyte. To keep the inhibition term above 90%, the catholyte flow rate needs to be below 0.02 L d^{-1}, with the anolyte flow rate limit of 3 L d^{-1} (Figure 10.17A). Both the catholyte boron concentration and salt concentration are reduced with a slower catholyte flow rate (longer HRT), but not affected

by the anolyte flow rate until the anolyte flow rate slows down to 0.14 L d^{-1} and the accumulated salt in anolyte reaches a high level (Figure 10.17B&C&D). For example, the anolyte salt concentration reaches 30.6 g L^{-1} at the anolyte and catholyte flow rates of 2.44 and 0.16 L d^{-1}, respectively, while the catholyte salt concentrations is lower at 21.4 g L^{-1} (Figure 10.17B&D). At this stage the salt diffusion from the catholyte to the anolyte is diminished and it may even cause diffusion of salt in opposite direction. The anodophilic bacteria could be extremely inhibited. A sharp decrease of the catholyte boron concentration is observed due to the osmotic water flux induced boron transport from the catholyte into the anolyte.

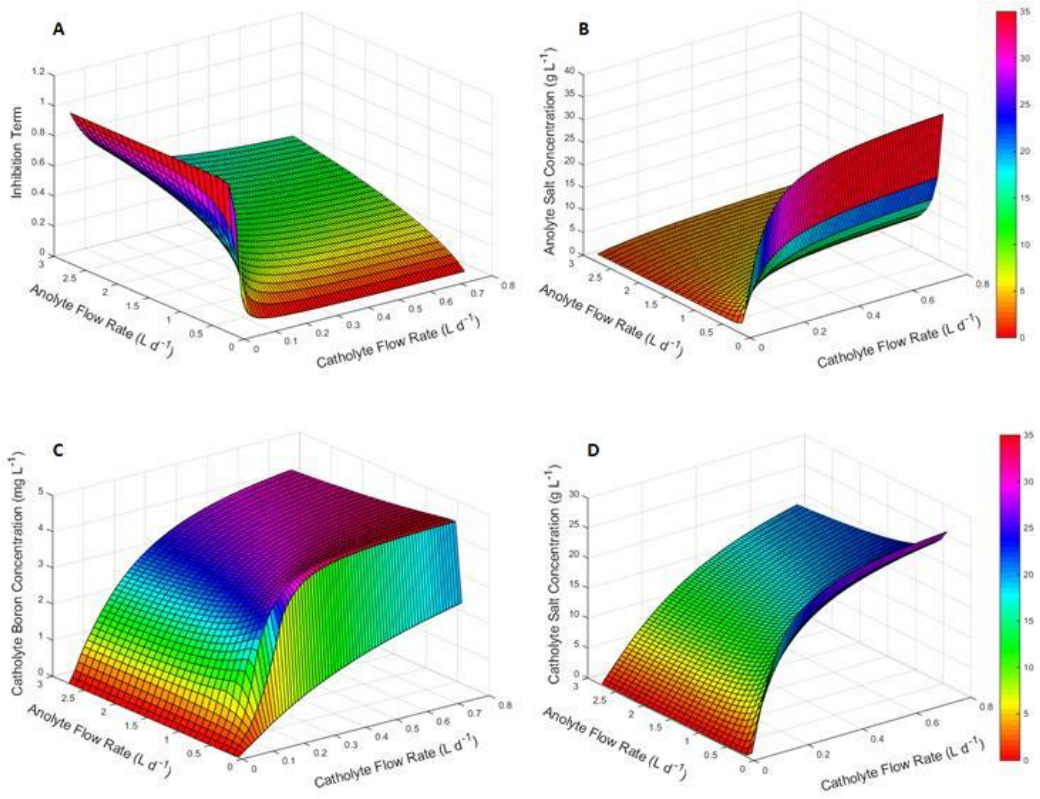

Figure 10.17 Simulation of the MFC pretreatment of seawater: the variation of (A) inhibition term; (B) anolyte salt concentration; (C) catholyte boron concentration; and (D) catholyte salt concentration affected by different anolyte and catholyte flow rates, at a

constant initial boron concentration of 5 mg L^{-1} and initial salt concentration of 35 g L^{-1}. Color bar is inserted in B&D for better comparison.

10.4 Conclusions

Mathematical modeling has been demonstrated as an effective tool to examine the mechanism of boron removal in BES. The driving forces of boron removal include electromigration induced by current generation and diffusion induced by concentration gradient. Convection transport induced by osmotic flux in the MFC and the DD plays a major role in boron removal. Additionally, current-induced convection in the MFC and ion-exchange in the DD also contribute to boron removal. The modeled results fit the experimental data well and provide valuable information for long term performance. In the MDC-DD system, although the boron concentration in salt solution can be reduced to meet WHO regulation with long operation time, the system cannot reach steady state and has potential risk of unsatisfied salt concentration in the effluent. The MFC can ensure effective boron removal, while the anolyte flow rate needs to be cautiously regulated in accordance to catholyte flow rate as well as salt concentration to avoid severe inhibition to current generation. Short anolyte HRT is required with high loading of salt in catholyte. Longer HRT of catholyte in MFC system can ensure a low salt concentration as well as boron concentration.

Chapter 11 Conclusions

MDC related technology has proved its capability to extract chemical energy stored in wastewater in the electricity form to drive desalination. The desalinated water product can achieve salinity level for both municipality and irrigation standards. It effectively removes multiple ions and non-dissociable compound boric acid. The removal rate of different ions largely depends on their concentrations as well as mobility. The special feature of alkalinity-generation-cathode successfully achieved pH elevation for boron removal, although a big portion of the boron is removed through convection transport of boric acid. Based on the energy consumption cost of MDC to remove 96% salt from 6g/L brackish water which is around 0.102$ per cubic meter of water, the benefit of pH amendment by the cathode of BES can save one third of operation cost (5 cents per cubic meter of salt solution) which otherwise will have to be amended by chemical addition of caustic soda. Despite the benefit of energy saving and the fact that the effluent quality in terms of salinity and other components can reach desirable concentration, however, MDC still has a long way to go before industrialization. The following will iterate on the several interrelated factors: water safety, desalination rate, configuration, modeling vs. reality and cost.

Concerns on water safety

First and foremost is the problem with contamination across the anion exchange membrane from the wastewater into the desalinated water product and causing biofouling on the AEM that faces the desalinated stream. The contamination problem might not be severe with domestic wastewater in the anode compartment as the feed, since the organic strength is very low and the excess organics migrated into the desalination compartment only contribute up to 7 mg L^{-1} TOC

in the desalinated water product. When industrial wastewater with high organic content was fed in the anode compartment, unfortunately, the risk of concentration-gradient-driven contamination becomes higher, especially with small size organics with molecular weight lower than 350 Da, Future research needs will be focused on either prevention of the back diffusion or further treatment of the desalinated product. The generated bioelectricity can generally alleviate the back diffusion issue, and the balance between organic content in wastewater and electricity inhibition to back diffusion needs to be carefully regulated. It is also critical to improve the membrane permselectivity that determines the back diffusion of cations through AEM. However this cannot be relied on environmental engineers alone. Thorough knowledge on the ion-exchange membrane material science is necessary to make this advancement. In terms of further polishing the water product, advanced oxidation coupled with UV is a promising approach by degrading small size organics and possible microorganism that grow in the water. The function of cathode that can generate hydrogen peroxide onsite with sufficient concentration around 10 mg L^{-1} shows promising potential for Advanced Oxidation Process to work. Given UV treatment is an effective disinfection polishing step for municipal wastewater treatment, it is convenient to link existing UV infrastructure to polish desalinated water product.

Slow desalination rate

Desalination rate in MDC with a weak anode can be several magnitudes lower than conventional desalination. The slow desalination rate is constricted by the slow metabolism of microorganisms that generate electrons to form current and drive desalination. Considering domestic wastewater might not be able to provide sufficient organic food to the anodophilic microorganisms in order to achieve maximal current generation which will impact the desalination capability, it is

reasonable to shift our attention to high organic content industrial wastewater source. However, we are faced with a dilemma that we want to boost the anode in MDC by providing high organic concentration, while we don't want to promote back-diffused contamination. Applying additional voltage to MDC that was not sufficient to cause water splitting reaction, the current generation in an MDC could be significantly improved. Due to improved efficiency, the energy consumption per unit of desalinated water produced can be even lowered with external voltage applied (Zhang and He 2015). It is also observed that with a long time external power boost, the current generation capability of the anodophilic microorganisms remained high even after the external power supply was removed. This gives us hope that through adaptation and acclimation of the microorganism community to the high demand of electron releasing, we will be able to further boost the anode performance.

Structure vs. efficiency

Desalination efficiency can vary with different configurations. Current common shapes of MDC are plate and tubular shapes, with aeration/ in-the-air diffusion cathode and in-the-air catholyte recirculation cathode respectively. It is believed when the cathode is in the air, the diffusion route delivers the oxygen to the cathode more efficiently due to much larger contacting area of the cathode to the air. Inter-membrane distance and HRT have complementary effects on desalination in the continuous mode, which results in comparable performance at larger inter-membrane distance. However, the desalination rate normalized by the volume of the reactor shows improvement with smaller inter-membrane distance. Decoupling the anode and the cathode in MDC can relieve the complexity of regular three-chamber configuration, at the sacrifice of performance to certain degree. Further evaluation on the land footage, construction

flexibility, operation and maintenance easiness, as well as desalination efficiency needs to be performed to further advance MDC technology.

Modeling vs. reality

Mathematical modeling has been a useful tool to analyze the MDC and provide predictions in a comprehensive way. Whether it is the configuration or the operation, the modeling tool can be applied to conduct optimization. Some limitation with the model needs to be considered and it is suggested that the model shall not be abused by not considering other realistic facts. For example, the model simulation may suggest that staged operation provides better desalination efficiency by treating incoming salt solution in a single stream. However, the simplified model might not be able to take into account the fact that smaller flow rate yields better condition for CSTR, while staged operation having all the salt solution in one stream might create a difficult situation for mixing in the reactor. Thus, experimental realization is essential when we adopt modeling results to real application.

Cost

Finally, the ultimate goal to advance MDC is to further reduce the construction cost, which mainly comes from the ion-exchange membrane (27% from AEM and 31% from CEM) and carbon brush (27%) and carbon cloth (13%) electrodes. The promising fact about MDC is the low operation and maintenance (O&M) cost compared with conventional treatment systems (conventional activated sludge and reverse osmosis), especially in the case of treating industrial wastewater (high organic loading) and brackish water (lower salinity) that can save up to 73% of O&M cost (Alammar 2015). Optimization of the circulation rate of the catholyte pump is critical

to further reduce the O&M cost. Further assessment on life span of MDC, and long term field experiments, as well as the reconstruction of infrastructure and relocation of the wastewater stream and salt water stream are needed to achieve a more realistic and convincing cost analysis.

Application niche

With the above challenges addressed, the MDC technology can be industrialized for energy efficiency and sustainable development purpose. The promising prospect will especially benefit coastal regions where a stream of seawater can be easily placed parallel with wastewater stream, or inland regions where there is abundant brackish water resources. However, it is necessary to determine how the two streams will be brought together. Considering we need large amount of wastewater to drive the desalination process and the source of wastewater is with close vicinity to human habitation, it will be easier and more cost effective to relocate brackish water or seawater for treatment. Navy ships can be benefited by MDC technology given the abundant salty water and limited fresh water and energy source (organic waste) on board. In the Mediterranean area, untreated sewage water is continuously discharged (eg. from Gaza Strip) to Mediterranean shores, and is causing considerable damage to marine life in the area. With the ongoing electricity and fuel shortage, introducing MDC also has the potential to solve the sea contamination problem without too much energy expense. The application niche of MDC also lies in treating high salinity wastewater for private industry and households, where a single stream of wastewater can be treated in MDC to achieve both salinity and organics removal so that wastewater can be recycled and reused.

Reference

Alammar, A. A. (2015) Cost Analysis of Microbial Desalination Cells Technology. A report submitted to the faculty of the Virginia Polytechnic Institute and State University.

Angenent, L.T. and Sung, S. (2001) Development of anaerobic migrating blanket reactor (AMBR), a novel anaerobic treatment system. Water Research 35(7), 1739-1747.

Ayres, R.S. and Westcot, D.W. (1985) Water Quality for Agriculture. FAO Irrigation & Drainage Paper, 29. Food and Agriculture Organization of the United Nations. Rome.

Bennett, A. (2013) 50th Anniversary: Desalination: 50 years of progress. Filtration & Separation 50(3), 32.

Berman, T., Mizrahi, R., and Dosoretz, C. G. (2011) Transparent exopolymer particles (TEP): A critical factor in aquatic biofilm initiation and fouling on filtration membranes. Desalination, 276, 184-190.

Brastad, K. and He, Z. (2013) Water softening using microbial desalination cell technology. Desalination 309, 32-37.

Cao, X., Huang, X., Liang, P., Xiao, K., Zhou, Y., Zhang, X. and Logan, B. (2009) A New Method for Water Desalination Using Microbial Desalination Cells. Environmental Science & Technology 43(18), 7148-7152.

Chen, S., Liu, G., Zhang, R., Qin, B. and Luo, Y. (2012b) Development of the Microbial Electrolysis Desalination and Chemical-Production Cell for Desalination as Well as Acid and Alkali Productions. Environmental Science & Technology 46(4), 2467-2472.

Chen, X., Sun, H., Liang, P., Zhang, X. and Huang, X. (2016) Optimization of membrane stack configuration in enlarged microbial desalination cells for efficient water desalination. Journal of Power Sources 324, 79-85.

Chen, X., Liang, P., Wei, Z.M., Zhang, X.Y. and Huang, X. (2012) Sustainable water desalination and electricity generation in a separator coupled stacked microbial desalination cell with buffer free electrolyte circulation. Bioresource Technology 119, 88-93.

Chen, X., Xia, X., Liang, P., Cao, X., Sun, H. and Huang, X. (2011) Stacked Microbial Desalination Cells to Enhance Water Desalination Efficiency. Environmental Science & Technology 45(6), 2465-2470.

Choi, M.-J., Chae, K.-J., Ajayi, F.F., Kim, K.-Y., Yu, H.-W., Kim, C.-w. and Kim, I.S. (2011) Effects of biofouling on ion transport through cation exchange membranes and microbial fuel cell performance. Bioresource Technology 102(1), 298-303.

Chu, J., Stabnikov, V. and Ivanov, V. (2012) Microbially Induced Calcium Carbonate Precipitation on Surface or in the Bulk of Soil. Geomicrobiology Journal 29(6), 544-549.

Cooley, H., & Ajami, N. (2012). Key Issues for Seawater Desalination in California: Cost and Financing: Pacific Institute for Studies in Development, Environment & Security.

Diblíková, L., Čurda, L. and Homolová, K. (2010) Electrodialysis in whey desalting process. Desalination and Water Treatment 14(1-3), 208-213.

Dlugolecki, P., Ogonowski, P., Metz, S.J., Saakes, M., Nijmeijer, K. and Wessling, M. (2010) On the resistances of membrane, diffusion boundary layer and double layer in ion exchange membrane transport. Journal of Membrane Science 349(1-2), 369-379.

Dydo, P. and Turek, M. (2013) Boron transport and removal using ion-exchange membranes: A critical review. Desalination 310, 2-8.

Fipps, G. (1996) Irrigation Water Quality Standards and Salinity Management Strategies. 7th Edition. Texas Agricultural Extension Service, Texas A & M University System.

Forrestal, C., Xu, P., Jenkins, P.E. and Ren, Z.Y. (2012) Microbial desalination cell with capacitive adsorption for ion migration control. Bioresource Technology 120, 332-336.

Garcia-Rodriguez, L. (2003) Renewable energy applications in desalination: state of the art. Solar Energy 75(5), 381–393.

Ge, Z. and He, Z. (2016) Long-term Performance of a 200-Liter Modularized Microbial Fuel Cell System Treating Municipal Wastewater: Treatment, Energy, and Cost. Environmental Science: Water Research & Technology.

Ge, Z., Dosoretz, C.G. and He, Z. (2014a) Effects of number of cell pairs on the performance of microbial desalination cells. Desalination 341, 101-106.

Ge, Z., Li, J., Xiao, L., Tong, Y. and He, Z. (2014b) Recovery of Electrical Energy in Microbial Fuel Cells. Environmental Science & Technology Letters 1(2), 137-141.

Gude, V.G. (2016) Desalination and sustainability - An appraisal and current perspective. Water Research 89, 87-106.

Guler, E., Ozakdag, D., Arda, M., Yuksel, M. and Kabay, N. (2010) Effect of temperature on seawater desalination-water quality analyses for desalinated seawater for its use as drinking and irrigation water. Environmental Geochemistry and Health 32(4), 335-339.

Guler, E., Kaya, C., Kabay, N. and Arda, M. (2015) Boron removal from seawater: State-of-the-art review. Desalination 356, 85-93.

Guler, E., Piekacz, J., Ozakdag, D., Kujawski, W., Arda, M., Yuksel, M. and Kabay, N. (2009) Influence of the chosen process parameters on the efficiency of seawater desalination: SWRO pilot plant results at Urla Bay seashore. Desalination and Water Treatment 5(1-3), 167-171.

Harnisch, F., Warmbier, R., Schneider, R. and Schroder, U. (2009) Modeling the ion transfer and polarization of ion exchange membranes in bioelectrochemical systems. Bioelectrochemistry 75(2), 136-141.

Huang, Z.Y., Chu, Y.F. and Hahn, J. (2010) Model simplification procedure for signal transduction pathway models: An application to IL-6 signaling. Chemical Engineering Science 65(6), 1964-1975.

Ivnitsky, H., Katz, I., Minz, D., Shimoni, E., Chen, Y., Tarchitzky, J. (2005) Characterization of membrane biofouling in nanofiltration processes of wastewater treatment, Desalination, 185, 55-268.

Jacobson, K.S., Drew, D.M. and He, Z. (2011a) Use of a Liter-Scale Microbial Desalination Cell As a Platform to Study Bioelectrochemical Desalination with Salt Solution or Artificial Seawater. Environmental Science & Technology 45(10), 4652-4657.

Jacobson, K.S., Drew, D. and He, Z. (2011b) Efficient salt removal in a continuously operated upflow microbial desalination cell with an air cathode. Bioresource Technology 102, 376-380.

Jing, G., Xing, L., Li, S. and Han, C. (2012) Reclaiming polymer-flooding produced water for beneficial use: Salt removal via electrodialysis. Desalination and Water Treatment 25(1-3), 71-77.

Kabay, N. and Bryjak, M. (2015) Boron Separation Processes, pp. 219-235, Elsevier, Amsterdam.

Kabay, N., Arar, O., Acar, F., Ghazal, A., Yuksel, U. and Yuksel, M. (2008) Removal of boron from water by electrodialysis: effect of feed characteristics and interfering ions. Desalination 223(1-3), 63-72.

Kaustubha Mohanty, Mihir K. Purkait. (2011) Membrane Technologies and Applications. CRC Press. Taylor &Francis Group. Boca Raton, FL

Kijanski, M., Bandura-Zalska, B., Dydo, P. and Turek, M. (2013) The concept of a system for electrodialytic boron removal into alkaline concentrate. Desalination 310, 75-80.

Kim, J.J., Yoon, H., Hong, J., Lee, T. and Wilf, M. (2013) Evaluation of new compact pretreatment system for high turbidity seawater: Fiber filter and ultrafiltration. Desalination 313, 28-35.

Kim, Y. and Logan, B.E. (2013) Microbial desalination cells for energy production and desalination. Desalination 308, 122–130.

Kim, Y. and Logan, B.E. (2011) Series Assembly of Microbial Desalination Cells Containing Stacked Electrodialysis Cells for Partial or Complete Seawater Desalination. Environmental Science & Technology 45(13), 5840-5845.

Kim, D., Jung, S., Sohn, J., Kim, H. and Lee, S. (2009) Biocide application for controlling biofouling of SWRO membranes - an overview. Desalination 238(1-3), 43-52.

Kim, J.R., Cheng, S., Oh, S.-E. and Logan, B.E. (2007) Power generation using different cation, anion, and ultrafiltration membranes in microbial fuel cells. Environmental Science & Technology 41(3), 1004-1009.

Kugel, A., Stafslien, S. and Chisholm, B.J. (2011) Antimicrobial coatings produced by "tethering" biocides to the coating matrix: A comprehensive review. Progress in Organic Coatings 72(3), 222-252.

Lee, H. S., Parameswaran, P., Marcus, A. K., Torres, C. I., Rittmann, B.E. (2008) Evaluation of energy-conversion efficiencies in microbial fuel cells (MFCs) utilizing fermentable and non-fermentable substrates. Water Res. 42, 1501-1510.

Levite, G. A., Moʻatsah ha-leʾumit le-meḥḳar ule-fituah. (1972) Utilization of brackish water. Proceeding of the ninth Israel symposium on desalination, bitan aharon. Jerusalem: National Council for Research and Development, Prime Minister's Office. Jerusalem, Israel.

Li, W.W., Yu, H.Q. and He, Z. (2014) Towards sustainable wastewater treatment by using microbial fuel cells-centered technologies. Energy & Environmental Science 7(3), 911-924.

Li, Y., Zhang, B., Cheng, M., Li, Y., Hao, L. and Guo, H. (2016) Spontaneous arsenic (III) oxidation with bioelectricity generation in single-chamber microbial fuel cells. J Hazard Mater 306, 8-12.

Liang, Y., Feng, H., Shen, D., Li, N., Long, Y., Zhou, Y., Gu, Y., Ying, X. and Dai, Q. (2016) A high-performance photo-microbial desalination cell. Electrochimica Acta 202, 197-202.

Liu, H., Cheng, S.A. and Logan, B.E. (2005) Power generation in fed-batch microbial fuel cells as a function of ionic strength, temperature, and reactor configuration. Environmental Science & Technology 39(14), 5488-5493.

Liu, H., Ramnarayanan, R. and Logan, B.E. (2004) Production of Electricity during Wastewater Treatment Using a Single Chamber Microbial Fuel Cell. Environmental Science & Technology 38(7), 2281-2285.

Logan, B.E. (2009) Exoelectrogenic bacteria that power microbial fuel cells. Nature Reviews Microbiology 7(5), 375-381.

Logan, B.E., Call, D., Cheng, S., Hamelers, H.V.M., Sleutels, T., Jeremiasse, A.W. and Rozendal, R.A. (2008) Microbial Electrolysis Cells for High Yield Hydrogen Gas Production from Organic Matter. Environmental Science & Technology 42(23), 8630-8640.

Logan, B. E., Hamelers, B., Rozendal, R. A., Schrorder, U., Keller, J., Fregui, S.. (2006) Microbial fuel cells: Methodology and technology. Environmental Science & Technology, 40, 5181-5192.

Lu, Y., Abu-Reesh, I.M. and He, Z. (2016) Treatment and desalination of domestic wastewater for water reuse in a four-chamber microbial desalination cell. Environmental Science and Pollution Research, 1-10.

Luo, S., Sun, H.Y., Ping, Q.Y., Jin, R. and He, Z. (2016) A Review of Modeling Bioelectrochemical Systems: Engineering and Statistical Aspects. Energies 9(2).

Luo, H., Xu, P., Roane, T., Jenkins, P. and Ren, Z. (2012a) Microbial desalination cells for improved performance in wastewater treatment, electricity production, and desalination. Bioresource Technology 105, 60-66.

Luo, H.P., Xu, P. and Ren, Z.Y. (2012b) Long-term performance and characterization of microbial desalination cells in treating domestic wastewater. Bioresource Technology 120, 187-193.

Luo, H.P., Xu, P., Jenkins, P.E. and Ren, Z.Y. (2012c) Ionic composition and transport mechanisms in microbial desalination cells. J. Membrane Sci. 409, 16-23.

Luo, H., Jenkins, P.E. and Ren, Z. (2011) Concurrent desalination and hydrogen generation using microbial electrolysis and desalination cells. Environmental Science & Technology 45(1), 340–344.

Marcus, A.K., Torres, C.I. and Rittmann, B.E. (2007) Conduction-based modeling of the biofilm anode of a microbial fuel cell. Biotechnology And Bioengineering 98(6), 1171-1182.

Mathioulakis, E., Belessiotis, V. and Delyannis, E. (2007) Desalination by using alternative energy: review and state-of-the-art. Desalination 203(1-3), 346–365.

McCarty, P.L., Bae, J. and Kim, J. (2011) Domestic Wastewater Treatment as a Net Energy Producer–Can This be Achieved? Environmental Science & Technology 45(17), 7100-7106.

Melnik, L., Vysotskaja, O. and Kornilovich, B. (1999) Boron behavior during desalination of sea and underground water by electrodialysis. Desalination 124(1-3), 125-130.

Mehanna, M., Saito, T., Yan, J., Hickner, M., Cao, X., Huang, X. and Logan, B. (2010a) Using microbial desalination cells to reduce water salinity prior to reverse osmosis. Energy & Environmental Science 3(8), 1114-1120.

Mehanna, M., Kiely, P.D., Call, D.F. and Logan, B.E. (2010b) A microbial electrodialysis cell for simultaneous water desalination and hydrogen gas production. Environmental Science & Technology 44(24), 9578–9583.

Miller, R. W., Gardiner, D. T. (2007) Soils in our environment. 9th Edition. Prentice Hall-Inc. Upper Sddle River, New Jersey.

Morel, A., Zuo, K., Xia, X., Wei, J., Luo, X., Liang, P. and Huang, X. (2012) Microbial desalination cells packed with ion-exchange resin to enhance water desalination rate. Bioresource Technology 118, 43–48.

National Research Council. (2008) Desalination: A National Perspective. National Academies Press. Washington, D.C.

Nikonenko, V.V., Pismenskaya, N.D., Belova, E.I., Sistat, P., Huguet, P., Pourcelly, G. and Larchet, C. (2010) Intensive current transfer in membrane systems: Modelling, mechanisms and application in electrodialysis. Advances in Colloid and Interface Science 160(1-2), 101-123.

Ofir, E., Brenner, A., Muuler, K. and Gitis, V. (2011) Boron removal from seawater by electro-chemical treatment as part of water desalination. Desalination and Water Treatment 31(1-3), 102-106.

Onda, K., LoBuglio, J. and Bartram, J. (2012) Global Access to Safe Water: Accounting for Water Quality and the Resulting Impact on MDG Progress. International Journal of Environmental Research and Public Health 9(3), 880-894.

Picioreanu, C., van Loosdrecht, M.C.M., Curtis, T.P. and Scott, K. (2010) Model based evaluation of the effect of pH and electrode geometry on microbial fuel cell performance. Bioelectrochemistry 78(1), 8-24.

Ping, Q., Porat, O., Dosoretz, C. and He, Z. (2016) Bioelectricity inhibits back diffusion from the anolyte into the desalinated streams in microbial desalination cells. Water Research 88, 266-273.

Ping, Q.Y., Huang, Z.Y., Dosoretz, C. and He, Z. (2015a) Integrated experimental investigation and mathematical modeling of brackish water desalination and wastewater treatment in microbial desalination cells. Water Research 77, 13-23.

Ping, Q., Abu-Reesh, I.M. and He, Z. (2015b) Boron removal from saline water by a microbial desalination cell integrated with donnan dialysis. Desalination 376, 55-61.

Ping, Q.Y., Zhang, C.Y., Chen, X.E., Zhang, B., Huang, Z.Y. and He, Z. (2014) Mathematical Model of Dynamic Behavior of Microbial Desalination Cells for Simultaneous Wastewater Treatment and Water Desalination. Environmental Science & Technology 48(21), 13010-13019.

Ping, Q. and He, Z. (2013a) Effects of inter-membrane distance and hydraulic retention time on the desalination performance of microbial desalination cells. Desalination and Water Treatment DOI: 10.1080/19443994.2013.789406.

Ping, Q.Y. and He, Z. (2013b) Improving the flexibility of microbial desalination cells through spatially decoupling anode and cathode. Bioresour Technol 144, 304-310.

Ping, Q.Y., Cohen, B., Dosoretz, C. and He, Z. (2013c) Long-term investigation of fouling of cation and anion exchange membranes in microbial desalination cells. Desalination 325, 48-55.

Pinto, R.P., Srinivasan, B., Escapa, A. and Tartakovsky, B. (2011) Multi-Population Model of a Microbial Electrolysis Cell. Environmental Science and Technology 45, 5039-5046.

Pinto, R.P., Srinivasan, B., Manuel, M.F. and Tartakovsky, B. (2010) A two-population bio-electrochemical model of a microbial fuel cell. Bioresource Technology 101(14), 5256-5265.

Popat, S.C., Ki, D., Rittmann, B.E. and Torres, C.I. (2012) Importance of OH- Transport from Cathodes in Microbial Fuel Cells. Chemsuschem 5(6), 1071-1079.

Qin, M., Ping, Q.Y., Lu, Y.B., Abu-Reesh, I.M. and He, Z. (2015) Understanding electricity generation in osmotic microbial fuel cells through integrated experimental investigation and mathematical modeling. Bioresource Technology 195, 194-201.

Qu, Y.P., Feng, Y.J., Wang, X., Liu, J., Lv, J.W., He, W.H. and Logan, B.E. (2012) Simultaneous water desalination and electricity generation in a microbial desalination cell with electrolyte recirculation for pH control. Bioresource Technology 106, 89-94.

Rabaey, K., Lissenns, G. and Verstraete, W. (2005). Microbial fuel cells: performances and perspectives. In Piet Lens, Peter Westermann, Marianne Haberbauer and Angelo Moreno (Ed.), Biofuels for Fuel Cells: Renewable Energy from Biomass Fermentation (pp. 377-399) London: IWA Publishing.

Rauschkolb, R.S., Rolston, D.E., Miller, R.J., Carlton, A. B., Burau, R.G. (1976) Applying Phosphorus Through Drip System. Calif. Agr. 8-10.

Rhoads, J.D., Kandiah, A., Maghali, A.M. (1992) The use of saline waters for crop production. FAO Irrigation & Drainage Paper, 48. Food and Agriculture Organization of the United Nations. Rome.

Rittmann, B.E. and McCarty, P. L. (2001) Environmental Biotechnology Principles and Applications. McGraw-Hill, New York.

Rivadeneyra Torres, A., Martinez-Toledo, M.V., Gonzalez-Martinez, A., Gonzalez-Lopez, J., Martin-Ramos, D. and Rivadeneyra, M.A. (2013) Precipitation of carbonates by bacteria isolated from wastewater samples collected in a conventional wastewater treatment plant. International Journal of Environmental Science and Technology 10(1), 141-150.

Rozendal, R.A., Hamelers, H.V.M., Rabaey, K., Keller, J. and Buisman, C.J.N. (2008) Towards practical implementation of bioelectrochemical wastewater treatment. Trends in Biotechnology 26(8), 450-459.

Saeed, H.M., Husseini, G.A., Yousef, S., Saif, J., Al-Asheh, S., Abu Fara, A., Azzam, S., Khawaga, R. and Aidan, A. (2015) Microbial desalination cell technology: A review and a case study. Desalination 359, 1-13.

Semiat, R. (2008) Energy Issues in Desalination Processes. Environmental Science and Technology 42(22), 8193–8201.

Sevda, S., Yuan, H., He, Z. and Abu-Reesh, I.M. (2015) Microbial desalination cells as a versatile technology: Functions, optimization and prospective. Desalination 371, 9-17.

Shatat, M, and Riffat, S.B. (2014) Water desalination technologies utilizing conventional and renewable energy sources. Int. J. Low-Carbon Tech. 9(1), 1-19.

Shiklomanov IA. (1993) World fresh water resources. Oxford University Press. Oxford, UK.

Stein, N.E., Hamelers, H.V.M. and Buisman, C.N.J. (2010) Stabilizing the baseline current of a microbial fuel cell-based biosensor through overpotential control under non-toxic conditions. Bioelectrochemistry 78(1), 87-91.

Strathmann, H. (2004) Ion-exchange Membrane Separation Processes. Elsevier B.V. Amsterdam.

Tak, H. I., Bakhtiyar, Y., Ahmad, F., Inam, A. (2012) Effluent Quality Parameters for Safe use in Agriculture. Water Quality, Soil and Managing Irrigation of Crops. In Tech.

Tong, Y. and He, Z. (2013) Nitrate removal from groundwater driven by electricity generation and heterotrophic denitrification in a bioelectrochemical system. J Hazard Mater 262, 614-619.

USBR (U.S. Bureau of Reclamation). (2003) Desalting Handbook for Planners, 3rd Edition. Washington, D.C.: USBR.

Vanysek,P. (2002) Ionic conductivity and diffusion at infinite dilution. In: CRC Handbook of Chemistry and Physics, 83rd Edition. CRC Press, Boca Raton.

Van der Bruggen, B. and Vandecasteele, C. (2002) Distillation vs. membrane filtration: overview of process evolutions in seawater desalination. Desalination 143(3), 207-218.

Venkidusamy, K., Megharaj, M., Marzorati, M., Lockington, R. and Naidu, R. (2016) Enhanced removal of petroleum hydrocarbons using a bioelectrochemical remediation system with pre-cultured anodes. Science of the Total Environment 539, 61-69.

Walker, W.S., Kim, Y., Lawler, D. F. (2014) Treatment of model inland brackish groundwater reverse osmosis concentrate with electrodialysis - Part II: Sensitivity to voltage application and membranes. Desalinatoin 345, 128-135.

Wang, Q., Yang, P. and Cong, W. (2011) Cation-exchange membrane fouling and cleaning in bipolar membrane electrodialysis of industrial glutamate production wastewater. Separation and Purification Technology 79(1), 103-113.

Wang, H. and Ren, Z.J. (2013) A comprehensive review of microbial electrochemical systems as a platform technology. Biotechnology Advances 31(8), 1796-1807.

Wang, X., Cheng, S., Zhang, X., Li, X.-y. and Logan, B.E. (2011) Impact of salinity on cathode catalyst performance in microbial fuel cells (MFCs). International Journal of Hydrogen Energy 36(21), 13900-13906.

Wen, Q.X., Zhang, H.C., Yang, H., Chen, Z.G., Nan, J. and Feng, Y.J. (2014) Improving desalination by coupling membrane capacitive deionization with microbial desalination cell. Desalination 354, 23-29.

Wen, Q., Zhang, H., Chen, Z., Li, Y., Nan, J. and Feng, Y. (2012) Using bacterial catalyst in the cathode of microbial desalination cell to improve wastewater treatment and desalination. Bioresource Technology 125, 108–113.

Wu, X., Tong, F., Yong, X., Zhou, J., Zhang, L., Jia, H. and Wei, P. (2016) Effect of NaX zeolite-modified graphite felts on hexavalent chromium removal in biocathode microbial fuel cells. J Hazard Mater 308, 303-311.

Xiao, L., Damien, J., Luo, J., Jang, H.D., Huang, J. and He, Z. (2012) Crumpled graphene particles for microbial fuel cell electrodes. Journal of Power Sources 208, 187-192.

Xu, J., Sheng, G.-P., Luo, H.-W., Li, W.-W., Wang, L.-F. and Yu, H.-Q. (2012) Fouling of proton exchange membrane (PEM) deteriorates the performance of microbial fuel cell. Water Research 46(6), 1817-1824.

Yuan, H.Y., Abu-Reesh, I.M. and He, Z. (2015) Enhancing desalination and wastewater treatment by coupling microbial desalination cells with forward osmosis. Chemical Engineering Journal 270, 437-443.

Yuan, Z., Pratt, S., Batstone, D.J. (2012) Phosphorus recovery from wastewater through microbial processes, Current Opinion in Biotechnology 23, 878–883.

Yang, Y., Xu, M., Guo, J. and Sun, G. (2012) Bacterial extracellular electron transfer in bioelectrochemical systems. Process Biochemistry 47(12), 1707-1714.

Zhang, B. and He, Z. (2012) Integrated salinity reduction and water recovery in an osmotic microbial desalination cell. Rsc Advances 2(8), 3265-3269.

Zhang, F. and He, Z. (2015) Scaling up microbial desalination cell system with a post-aerobic process for simultaneous wastewater treatment and seawater desalination. Desalination 360, 28-34.

Zhang, F., Ge, Z., Grimaud, J., Hurst, J. and He, Z. (2013) Long-Term Performance of Liter-Scale Microbial Fuel Cells Treating Primary Effluent Installed in a Municipal Wastewater Treatment Facility. Environmental Science & Technology 47(9), 4941-4948.

Zhang, F., Chen, M., Zhang, Y. and Zeng, R. (2012) Microbial desalination cells with ion exchange resin packed to enhance desalination at low salt concentration. Journal of Membrane Science 417, 28-33.

Zuo, K., Liu, F., Ren, S., Zhang, X., liang, p. and Huang, X. (2016a) A novel multi-stage microbial desalination cell for simultaneous desalination and enhanced organics and nitrogen removal from domestic wastewater. Environmental Science: Water Research & Technology.

Zuo, K., Wang, Z., Chen, X., Zhang, X., Zuo, J., Liang, P. and Huang, X. (2016b) Self-Driven Desalination and Advanced Treatment of Wastewater in a Modularized Filtration Air Cathode Microbial Desalination Cell. Environmental Science & Technology 50 (13), 7254–7262.

Zuo, K.C., Cai, J.X., Liang, S., Wu, S.J., Zhang, C.Y., Liang, P. and Huang, X. (2014) A Ten Liter Stacked Microbial Desalination Cell Packed With Mixed Ion-Exchange Resins for Secondary Effluent Desalination. Environmental Science & Technology 48(16), 9917-9924.

Zuo, K.C., Yuan, L.L., Wei, J.C., Liang, P. and Huang, X. (2013) Competitive migration behaviors of multiple ions and their impacts on ion-exchange resin packed microbial desalination cell. Bioresource Technology 146, 637-642.